

Identification and Functional Assessment  
of Novel Neuromuscular Disease-Causing Genes

Inaugural Dissertation

zur

Erlangung des Doktorgrades

Dr. nat. med.

der Medizinischen Fakultät

und

der Mathematisch-Naturwissenschaftlichen Fakultät

der Universität zu Köln

vorgelegt von

Andrea Delle Vedove

aus Cividale del Friuli, Italien

Hundt Druck GmbH, Köln

2023



Betreuerin: Prof. Dr. Brunhilde Wirth

Referenten: Prof. Dr. Andreas Beyer  
Prof. Dr. Kay Hofmann

Datum der mündlichen Prüfung: 20.12.2022



## Table of Contents

Table of Contents.....	V
List of Figures.....	VII
List of Tables.....	VIII
List of Abbreviations.....	IX
Abstract.....	XI
Zusammenfassung.....	XIII
Thesis Outline.....	XV
1 Introduction.....	1
1.1 Movement and Its Control.....	1
1.2 The Motor Unit.....	2
1.3 Neuromuscular Diseases.....	2
1.3.1 Acquired NMDs.....	3
1.3.2 Inherited NMDs.....	3
1.4 NMD diagnosis.....	3
1.4.1 Clinical assessment.....	4
1.4.2 Ancillary testing.....	4
1.4.3 Genetic testing.....	4
1.5 Overview of specific NMDs.....	7
1.5.1 Distal Arthrogyrosis.....	7
1.5.2 Congenital Myasthenic Syndromes.....	10
1.5.3 Hereditary Ataxias.....	15
1.6 NMDs Models.....	20
1.6.1 Animal Models.....	20
1.6.2 Induced Pluripotent Stem Cells.....	20
2 Aim.....	23
3 Main Publications.....	24
3.1 Biallelic Loss of <i>PIEZO2</i> causes Distal Arthrogyrosis.....	24
3.1.1 Description.....	24
3.1.2 Own Contributions.....	25
3.2 Biallelic Loss of <i>VAMP1</i> causes a Congenital Myasthenic Syndrome.....	25
3.2.1 Description.....	25
3.2.2 Own Contributions.....	26
3.3 <i>CAPRIN1</i> <sup>P512L</sup> causes early-onset ataxia, muscle weakness and.....	26
3.3.1 Description.....	26
3.3.2 Own Contributions.....	27
4 Discussion.....	28
4.1 <i>PIEZO2</i> & Distal Arthrogyrosis.....	28

4.2	<i>VAMP1</i> & Congenital Myasthenic Syndromes .....	33
4.3	<i>CAPRIN1</i> -related disorders .....	36
4.3.1	Open questions and possible future research directions .....	38
5	Additional Publications, Presentations & Scholarships .....	41
5.1	Additional Publications .....	41
5.1.1	Eisenberger T et al., 2018 .....	41
5.1.2	Karakaya M et al., 2018 .....	41
5.1.3	Janzen E et al., 2019 .....	41
5.1.4	Pavinato L et al., 2022 .....	41
5.1.5	Overhoff M et al, 2022 .....	42
5.2	Oral Presentations .....	43
5.3	Poster Presentations .....	43
5.4	Scholarships .....	44
6	References .....	45
7	Appendix .....	XVII
7.1	Appendix A.....	XVII
7.2	Appendix B.....	XXXVII
7.3	Appendix C.....	XLVII
8	Acknowledgements .....	LXXXIII
9	Curriculum Vitae .....	LXXXV
9.1	Personal Information .....	LXXXV
9.2	Education.....	LXXXV
9.3	Work Experience.....	LXXXV
10	Eidesstattliche Erklärung.....	LXXXVII

## List of Figures

Figure 1. The neural circuits involved in motor control .....	1
Figure 2. The motor unit .....	2
Figure 3. Suggested NMD diagnostic workflow .....	5
Figure 4. DA-associated mutations in sarcomeric proteins .....	8
Figure 5. Overview of the pathophysiology of CMS .....	13

## List of Tables

Table 1. Classification of inherited NMDs.....	3
Table 2. Single gene testing in NMDs.....	5
Table 3. Distal Arthrogryposis.....	9
Table 4. Congenital Myasthenic Syndromes.....	11
Table 5. Hereditary Ataxias (selection).....	17
Table 6. Overview of <i>PIEZO2</i> -related DAIPT cases.....	31
Table 7. Overview of <i>VAMP1</i> -related CMS cases .....	34
Table 8. Novel CMS-related genes .....	35
Table 9. Comparison of <i>CAPRIN1</i> -related disorders.....	37

## List of Abbreviations

ACh	AcetylCholine
AChE	AcetylCholine Esterase
AChR	AcetylCholine Receptor
AD	Autosomal Dominant
ADHD	Attention-Deficit/Hyperactivity Disorder
AFM	Atomic Force Microscopy
ALS	Amyothrophic Lateral Sclerosis
AMC	Arthrogyrosis Multiplex Congenita
AMPA	AminoMethylPhosphonic Acid ( $\alpha$ -amino-3-hydroxy-5-methyl-4-isoxazole propionate)
AR	Autosomal Recessive
ARSACS	Autosomal Recessive Spastic Ataxia of Charlevoix-Saguenay
ASD	Autism Spectrum Disorder
AT	Ataxia-Telangectasia
A $\beta$	$\beta$ -amyloid
CANVAS	Cerebellar ataxia, Neuropathy, Vestibular Areflexia Syndrome
ChAT	Choline AcetylTransferase
CK	Creatine Kinase
CMA	Chromosomal MicroArray
CMAP	Compound Muscle Action Potential
CMS	Congenital Myasthenic Syndrome
CMT1A	Charcot-Marie Tooth disease type 1A
CNV	Copy Number Variations
DA	Distal Arthrogyrosis
DAIPT	Distal Arthrogyrosis with Impaired Proprioception and Touch
DM	Myotonic Dystrophy
DRPLA	DentatoRubral-Pallidoluysian Atrophy
DTR	Deep Tendon Reflex
EAOH	Early-onset Ataxia with Oculomotor apraxia and Hypoalbuminemia
EC	Enteroendocrine Cells
EMG	ElectroMyoGraphy
ES	Exome Sequencing
FRAP	Fluorescence Recovery After Photobleaching
FRDA	Friedreich's Ataxia
FSHD	FacioScapuloHumeral muscular Dystrophy
FXS	Fragile X Syndrome
FXTAS	Fragile X-associated Tremor/Ataxia Syndrome
GS	Genome Sequencing
HA	Hereditary Ataxia

HNPP	Hereditary Neuropathy with Pressure Palsies
HPO	Human Phenotype Ontology
iNPC	induced Neural Progenitor Cells
iPSC	induced Pluripotent Stem Cells
KO	Knock-Out
LMN	Lower Motor Neuron
MLPA	Multiplex Ligation-dependent Probe Amplification
MN	Motor Neuron
MWS	Marden-Walker Syndrome
NCS	Nerve Conduction Studies
NGS	Next-Generation Sequencing
NMD	NeuroMuscular Disease
NMJ	NeuroMuscular Junction
NPC	Neural Progenitor Cell
OH	Orthostatic Hypotension
P10 / P15	Post-natal day 10 / 15
PEG	Percutaneous Endoscopic Gastrostomy
PrLD	Prion-Like Domain
RAN	Repeat-Associated Non-ATG-mediated
ROS	Reactive Oxygen Species
SCA	SpinoCerebellar Ataxia
SCAN2	SpinoCerebellar ataxia with Axonal Neuropathy 2
SCAR	SpinoCerebellar ataxia Autosomal Recessive
SMA	Spinal Muscular Atrophy
snRNP	small nuclear RiboNucleoProtein
SPAX	SPastix ATaxia
STR	Short Tandem Repeat
TGP	Targeted Gene Panel
TP-PCR	Triplet repeat Primed PCR
UMN	Upper Motor Neuron
VAcHT	Vesicular AcetylCholine Transporter
XL	X-linked
2D	two-Dimensional
3D	three-Dimensional

## Abstract

Inherited neuromuscular diseases comprise a highly heterogeneous group of disorders characterized by the impairment of the neural structures or motor unit components responsible for the generation of movement.

While as single gene-associated disorder the majority of them are rare, taken together their estimated prevalence reaches 1 – 3 cases / 1000 individuals. Due to their elevated morbidity and mortality, they represent a significant health burden for the affected individuals, their families, and the healthcare systems. Moreover, their clinical and genetic heterogeneity makes their diagnosis a long and complex process, which often requires specialized diagnostic procedures and poses a challenge in about half of the cases. However, thanks to decreasing costs and increased availability of next-generation sequencing technologies, the last years had witnessed a rise in the number of novel genes associated to neuromuscular disorders.

In this study, we identified three novel neuromuscular disease-causing genes: *PIEZO2*, whose biallelic loss-of-function mutations cause distal arthrogryposis with impaired proprioception and touch; *VAMP1*, whose biallelic loss-of-function mutations cause a novel presynaptic congenital myasthenic syndrome; *CAPRIN1*, whose specific p.Pro512Leu mutation causes a neurodegenerative disorder characterized by ataxia and muscle weakness.

For *PIEZO2*, we identified biallelic loss-of-function mutations using exome sequencing, SNPchip-based linkage analysis, DNA microarray, and Sanger sequencing in ten affected individuals of four independent families showing arthrogryposis, hypotonia, respiratory insufficiency at birth, scoliosis, and delayed motor development. This phenotype is clearly distinct from distal arthrogryposis with ocular anomalies which characterize the autosomal dominant distal arthrogryposis 3 (DA3), distal arthrogryposis 5 (DA5), and Marden-Walker syndrome (MWKS). While these disorders are caused by heterozygous gain-of-function mutations in *PIEZO2*, the novel reported mutations result in the loss of *PIEZO2*, since they lead to nonsense-mediated mRNA decay in patient-derived fibroblast cell lines. *PIEZO2* is a mechanosensitive ion channel playing a major role in light-touch sensation and proprioception. Mice ubiquitously depleted of *PIEZO2* die postnatally because of respiratory distress, while individuals lacking *PIEZO2* develop a neuromuscular disorder, likely due to the loss of proprioception inputs in muscles.

For *VAMP1*, we identified biallelic loss-of-function mutations using exome or genome sequencing in two pairs of siblings from two independent families affected by a novel congenital myasthenic syndrome. Electrodiagnostic examination showed severely low compound muscle action potentials and presynaptic impairment. The two described homozygous mutations are a frameshift and a missense mutation of a highly conserved residue, therefore are likely to result in the loss of *VAMP1* function. Indeed, the phenotype is resembled by *VAMP1<sup>lew/lew</sup>* mice, which carry a homozygous *VAMP1* truncating mutation and show neurophysiological features of presynaptic impairment.

For *CAPRIN1*, we identified the identical *de novo* c.1535C>T (p.Pro512Leu) missense variant using trio exome sequencing in two unrelated individuals displaying early-onset ataxia, dysarthria, cognitive decline and muscle weakness. This mutation causes the substitution of a highly conserved residue and

*in silico* tools predict an increase in the protein aggregation propensity. Overexpression of CAPRIN1<sup>P512L</sup> caused the formation of insoluble ubiquitinated aggregates, sequestering proteins associated with neurodegenerative disorders, such as ATXN2, GEMIN5, SNRNP200, and SNCA. Upon differentiation in cortical neurons of induced pluripotent stem cell (iPSC) lines where the CAPRIN1<sup>P512L</sup> was introduced via CRISPR/Cas9, reduced neuronal activity and altered stress granules dynamics were observed in the lines harboring the mutation. Moreover, nano-differential scanning fluorimetry revealed that CAPRIN1<sup>P512L</sup> adopts an extended conformation, and fluorescence microscopy demonstrated that RNA greatly enhances its aggregation *in vitro*.

Taken together, this study associates: (1) biallelic loss-of-function mutations in *PIEZO2* with the autosomal recessive distal arthrogryposis with impaired proprioception and touch; (2) biallelic loss-of-function mutations in *VAMP1* with an autosomal recessive presynaptic congenital myasthenic syndrome; (3) a recurrent *de novo* p.Pro512Leu mutation of *CAPRIN1* with a neurodegenerative disorder characterized by ataxia and muscle weakness.

## Zusammenfassung

Erbliche neuromuskuläre Erkrankungen umfassen eine sehr heterogene Gruppe von Krankheiten, welche durch eine Beeinträchtigung der neuronalen Strukturen oder der Komponenten der motorischen Einheiten, die für die Erzeugung von Bewegungen verantwortlich sind, charakterisiert sind.

Während die meisten von ihnen als gen-assoziierte Einzelerkrankungen selten sind, liegt die geschätzte Prävalenz der gesamten Krankheitsgruppe bei 1 - 3 Fällen / 1000 Menschen. Aufgrund ihrer hohen Morbidität und Mortalität stellen sie eine erhebliche gesundheitliche Belastung für die betroffenen Personen, ihre Familien und die Gesundheitssysteme dar. Darüber hinaus macht ihre klinische und genetische Heterogenität die Diagnosestellung zu einem langwierigen und komplexen Prozess, der häufig spezielle Diagnoseverfahren erfordert und in etwa der Hälfte der Fälle immer noch eine Herausforderung darstellt. Dank sinkender Kosten und der zunehmenden Verfügbarkeit von „next-generation“ Sequenzierungstechnologien konnte in den letzten Jahren jedoch ein Anstieg neuer Gene verzeichnet werden, die mit neuromuskulären Störungen in Verbindung gebracht werden konnten.

In dieser Studie haben wir drei neue Gene, die neuromuskuläre Erkrankungen verursachen, identifiziert: *PIEZO2*, dessen biallelische Loss-of-function-Mutationen eine distale Arthrogrypose mit beeinträchtigter Propriozeption und Tastsinn verursachen; *VAMP1*, dessen biallelische Loss-of-function-Mutationen ein neuartiges präsynaptisches kongenitales myasthenisches Syndrom verursachen; und *CAPRIN1*, dessen spezifische p.Pro512Leu-Mutation eine neurodegenerative Störung verursacht, die durch Ataxie und Muskelschwäche gekennzeichnet ist.

Für *PIEZO2* identifizierten wir biallelische Loss-of-function-Mutationen mittels Exom-Sequenzierung, SNPchip-basierter Kopplungsanalyse, DNA-Microarray und Sanger-Sequenzierung bei zehn betroffenen Individuen aus vier unabhängigen Familien. Die Betroffenen weisen Arthrogrypose, Hypotonie, respiratorische Insuffizienz bei der Geburt, Skoliose und verzögerte motorische Entwicklung auf. Dieser Phänotyp unterscheidet sich deutlich von der distalen Arthrogrypose mit Augenanomalien, die autosomal dominante distale Arthrogrypose 3 (DA3), distale Arthrogrypose 5 (DA5) und dem Marden-Walker-Syndrom (MWKS) kennzeichnen. Während diese Erkrankungen durch heterozygote Gain-of-function-Mutationen in *PIEZO2* verursacht werden, führen die hier neu beschriebenen Mutationen zum Verlust von *PIEZO2*, da sie in von Patienten abgeleiteten Fibroblasten-Zelllinien zu einem Nonsense-mediated mRNA Decay führen. *PIEZO2* ist ein mechanosensitiver Ionenkanal, der eine wichtige Rolle bei der Wahrnehmung von leichten Berührungen und der Propriozeption spielt. Mäuse, denen *PIEZO2* ubiquitär fehlt, sterben postnatal an Atemnot, während Individuen, denen *PIEZO2* fehlt, eine neuromuskuläre Störung entwickeln, die wahrscheinlich auf den Verlust der Propriozeption in den Muskeln zurückzuführen ist.

Für *VAMP1* haben wir mittels Exom- oder Genomsequenzierung bei zwei Geschwisterpaaren aus zwei unabhängigen Familien, die von einem neuartigen kongenitalen myasthenischen Syndrom betroffen sind, biallelische Loss-of-function-Mutationen identifiziert. Die elektrodiagnostische Untersuchung ergab stark erniedrigte zusammengesetzte Muskelaktionspotenziale und präsynaptische Beeinträchtigungen. Bei den beiden beschriebenen homozygoten Mutationen handelt es sich um eine

Frameshift-Mutation und eine missense Mutation einer hochkonservierten Aminosäure, die wahrscheinlich zu einem Verlust der Funktion von VAMP1 führen. Der Phänotyp ähnelt dem der *VAMP1<sup>lew/lew</sup>*-Mäuse, die eine homozygote *VAMP1* trunkierende Mutation tragen und neurophysiologische Merkmale einer präsynaptischen Beeinträchtigung aufweisen.

Für *CAPRIN1* identifizierten wir die identische *de novo* c.1535C>T (p.Pro512Leu) missense Variante mit Hilfe der Trio-Exom-Sequenzierung bei zwei nicht verwandten Personen, die eine früh einsetzende Ataxie, Dysarthrie, kognitiven Abbau und Muskelschwäche aufweisen. Diese Mutation führt zur Substitution einer hochkonservierten Aminosäure und *in silico*-Tools sagen eine erhöhte Aggregationsneigung des Proteins voraus. Die Überexpression von *CAPRIN1<sup>P512L</sup>* führte zur Bildung unlöslicher ubiquitiniertes Aggregate, die Proteine sequestrieren, die mit neurodegenerativen Erkrankungen in Verbindung gebracht werden, wie *ATXN2*, *GEMIN5*, *SNRNP200* und *SNCA*. Nach der Differenzierung in kortikale Neuronen von induzierten pluripotenten Stammzellen (iPSC), in denen die *CAPRIN1<sup>P512L</sup>* Mutation mittels CRISPR/Cas9 eingeführt wurde, wurde in diesen Linien eine verringerte neuronale Aktivität und eine veränderte Dynamik der Stressgranula beobachtet. Darüber hinaus ergab die Nano-Differential-Scanning-Fluorimetrie, dass *CAPRIN1<sup>P512L</sup>* eine verlängerte Konformation annimmt, und die Fluoreszenzmikroskopie zeigte, dass die RNA seine Aggregation *in vitro* stark fördert. Insgesamt assoziiert diese Studie: (1) biallelische Loss-of-function-Mutationen in *PIEZO2* mit der autosomal rezessiven distalen Arthrogrypose mit beeinträchtigter Propriozeption und Tastsinn; (2) biallelische Loss-of-function-Mutationen in *VAMP1* mit einem autosomal rezessiven präsynaptischen kongenitalen myasthenischen Syndrom; (3) eine wiederkehrende *de novo* p. Pro512Leu-Mutation von *CAPRIN1* mit einer neurodegenerativen Störung, die durch Ataxie und Muskelschwäche gekennzeichnet ist.

## Thesis Outline

This PhD thesis describes the identification of three novel neuromuscular disease-causing genes and is structured in 10 chapters organized as follows.

The "Introduction" briefly summarizes the neural structures responsible for the generation of movement ("Movement and Its Control", "The Motor Unit"), which represent the systems affected by neuromuscular diseases. A general overview of the classification of these disorders and the workflow of their diagnosis follows ("Neuromuscular Diseases", "NMD diagnosis"). The chapter ends with a more detailed synopsis of the specific NMDs that are reported in this work ("Overview of specific NMDs") and an overview of the NMD models, focusing on induced pluripotent stem cells ("NMDs Models").

Afterwards, the research aim is outlined in "Aim", followed by an overview of the main publications and relative contributions ("Main Publications"), which are appended in the chapter "Appendix".

The "Discussion" section contains a summary of the novel cases affected by the NMDs described in this thesis and reported after the publication and an update of the knowledge about the associated gene.



# 1 Introduction

## 1.1 Movement and Its Control

Movement is by definition a change of position. It is one of the key features of an organism, accounting not only for its ability to interact with the surrounding environment, but also for basal autonomic functions in complex organisms (Purves, 2018).

While a movement itself is the result of a biochemical process happening in the muscle, its control is the result of the interaction between four circuits (Figure 1) (Purves, 2018). The neural structure in direct connection with the skeletal muscle is represented by the motor neurons (MNs) localized in the brainstem or in the spinal cord (lower MNs, LMNs), which receive most of their inputs from local circuit neurons (Kandel, 2013). These interneurons perform an integration of the inputs received by sensory neurons and by other descending systems (Purves, 2018). These higher pathways comprise the axons of neurons localized in the motor cortex and in other brainstem centers (upper MNs, UMNs) which are responsible for initiating and guiding the execution of movements, and regulating muscle tone and orienting eyes, head, and body according to the information received from vestibular, somatic, auditory and visual clues (Purves, 2018). The last two circuits are the basal ganglia and the cerebellum, which have essential functions in the indirect modulation of movements: the former prevents UMNs from starting unwanted movements while the latter coordinates ongoing movements reducing the errors between intended and performed actions (Purves, 2018).

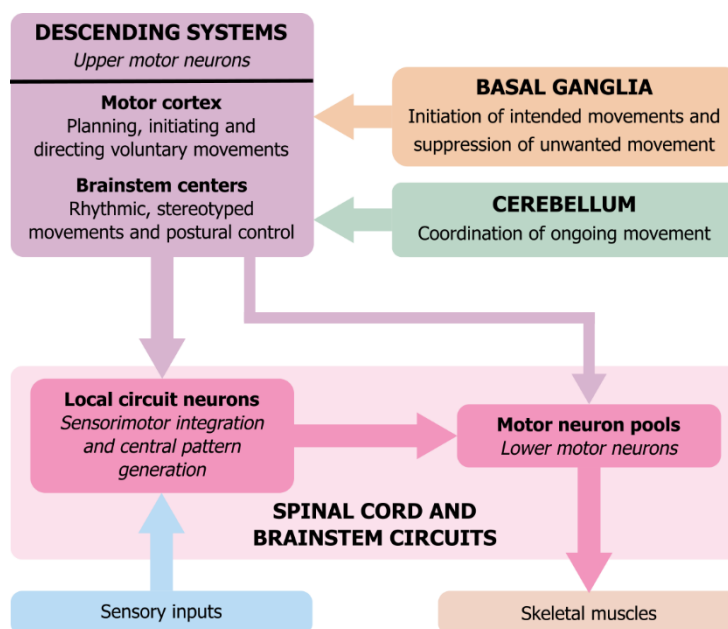


Figure 1. The neural circuits involved in motor control

Four systems – spinal and brainstem circuits, descending systems in the cerebral cortex and brainstem, basal ganglia and cerebellum – control the execution of movements. Adapted from Purves (2018).

## 1.2 The Motor Unit

While each one of these circuits is fundamental for the proper execution of a movement, their activity converges on a motor unit. This element is formed by a single  $\alpha$ -MN, a LMN having a large body size, and the extrafusal muscle fibers it innervates through a synaptic connection, the neuromuscular junction (NMJ). These muscle fibers are responsible for generating the force required for a movement and owe their name to the fact that they do not belong to muscle fuses (or muscle spindles) (Figure 2). These structures are stretch receptors formed by encapsulated intrafusal muscle fibers receiving afferent innervation by sensory neurons that form synapses with LMNs and interneurons and are responsible for the stretch reflexes (or deep tendon reflexes, DTRs). They also receive efferent innervation from  $\gamma$ -MNs, smaller LMNs that regulate their excitability. Their function is to detect changes in the muscle length and regulate dynamically the stretch of the muscle. Moreover, they are responsible for the basal level of tension in the muscle, the muscle tone.

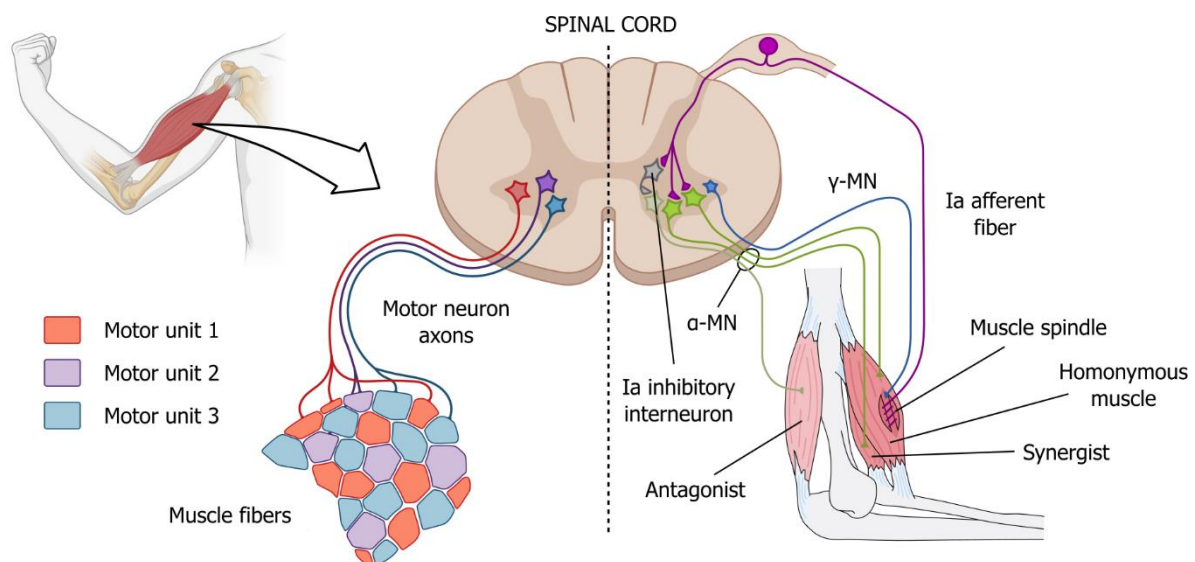


Figure 2. The motor unit

A motor unit is formed by a  $\alpha$ -MN and the muscle fibers it innervates.  $\alpha$ -MNs receive excitatory innervation from agonists' muscle spindles, which send inhibitory signals to the antagonists'  $\alpha$ -MNs through inhibitory interneurons.  $\gamma$ -MNs innervate intrafusal muscle fibers and regulate their excitability. Adapted from Pearson Education, Inc. and Kandel (2013). Created with BioRender.com.

## 1.3 Neuromuscular Diseases

The impairment of one or more neural structures or motor unit components responsible for the generation of movement results in a neuromuscular disease (NMD).

This is an umbrella term encompassing a heterogeneous group of disorders with an estimated prevalence of 1 – 3 cases / 1000 individuals (Deenen et al., 2015). They are characterized by elevated morbidity and mortality, representing therefore a significant health burden for the society (Laing et al., 2021; Ryder et al., 2017). The great variety of structures that can be affected and the multiplicity of pathomechanisms involved make the establishment of a systematic classification of the disorders difficult. For the purposes of this work, NMDs will be divided into acquired and inherited.

### 1.3.1 Acquired NMDs

Acquired NMDs are disorders affecting the neuromuscular system that develop after birth and are not congenital or hereditary. Metabolic diseases, such as diabetes, can cause symmetric polyneuropathies. Inflammatory diseases can involve directly nerves (Guillain-Barré Syndrome) or muscles (idiopathic inflammatory myopathies). Viruses (HIV, VZV) or bacteria (*Borrelia* genus, *T. pallidum*) can cause infections neuropathies. Vitamin deficiencies (cobalamin, pyridoxine, thiamine deficiencies) or exposure to toxic substances (drugs, industrial agents, metals) can cause neuropathies. The NMJs can also be affected in myasthenia gravis, Lambert-Eaton myasthenic syndrome, snake-venom, and botulism poisoning (Feldman, 2021).

### 1.3.2 Inherited NMDs

The other group of NMDs has a genetic origin. Thanks to next-generation sequencing (NGS) technologies, the number of genes linked to NMDs is continuously increasing. An updated list is published every year on *Neuromuscular Disorders* or is available online (Cohen et al., 2021; *GeneTable of Neuromuscular Disorders*). Due to the high genetic and phenotypic heterogeneity of NMDs, the current 641 genes are associated with 1037 different phenotypes, classified into 16 groups (Table 1). For example, mutations in *ATXN2* are linked to two different NMD phenotypes: a hereditary ataxia (spinocerebellar ataxia 2, SCA2) and a MN disease (amyotrophic lateral sclerosis, ALS).

**Table 1. Classification of inherited NMDs**

NMD group	NMD number
1. Muscular Dystrophies	66
2. Congenital Muscular Dystrophies	53
3. Congenital Myopathies	68
4. Distal Myopathies	28
5. Other Myopathies	39
6. Myotonic Syndromes	9
7. Ion Channel Muscle Diseases	13
8. Malignant Hyperthermias	6
9. Metabolic Myopathies	30
10. Hereditary Cardiomyopathies	176
a. Non-Arrhythmogenic	102
b. Arrhythmogenic	74
11. Congenital Myasthenic Syndromes	42
12. Motor Neuron Diseases	105
13. Hereditary Ataxias	102
14. Hereditary Motor and Sensory Neuropathies	130
15. Hereditary Paraplegias	83
16. Other Neuromuscular Disorders	87
	1037

From *GeneTable of Neuromuscular Disorders*

## 1.4 NMD diagnosis

Due to the rarity and the great complexity of these disorders, reaching the correct diagnosis is a long and painstaking process, requiring a high level of medical specialization and a broad range of diagnostics procedures (Barp et al., 2021).

### 1.4.1 Clinical assessment

The first step in the evaluation of an individual with neuromuscular symptoms is a comprehensive clinical assessment (Thompson et al., 2020; Yubero et al., 2021). This phase is crucial because it allows clinicians to discriminate between an acquired or an inherited NMD. It includes an exhaustive personal and familial clinical history and a thorough neurological examination, gathering information about the age of onset and the progression of the symptoms, the degree and localization of the affected muscle groups and the presence of extramuscular manifestations (Feldman, 2021). Common NMD features are muscle weakness, contractures, pain and spasticity (Barbosa-Gouveia et al., 2022). Elements supporting a genetic cause are: familiarity, early onset, progression, association with musculoskeletal abnormalities (pes cavus, scoliosis, contractures) (Barp et al., 2021). These characteristics are fundamental not only to establish the following workup, but also to guide the diagnosis when an inherited NMD is suspected. Indeed, the introduction of a phenotypic annotation system based on Human Phenotype Ontology (HPO) terms allowed the development of bioinformatics tools that aid in finding the correct diagnosis between thousands of rare phenotypes (Kohler et al., 2021). Examples are the Phenomizer, a web-based application allowing clinicians to rank diagnoses of genetic diseases based on observed phenotypic similarities (Kohler et al., 2009), and the Exomiser, a program prioritizing likely causative variants obtained from NGS technologies according to a set of phenotypes encoded by HPO terms (Kohler et al., 2019; Smedley et al., 2015; Thompson, Papakonstantinou Ntalis, et al., 2019).

### 1.4.2 Ancillary testing

Ancillary tests are often used as second step to exclude acquired pathologies and narrow down the candidate list (Barp et al., 2021). These tests include a wide range of investigations, such as blood tests (serum CK, autoantibodies, vitamins), imaging techniques (cardiac ultrasound, muscle magnetic resonance imaging (MRI)), neurophysiological studies (electromyography (EMG), nerve conduction studies (NCS)), lumbar puncture, and muscle/nerve biopsies. These examinations encompass non-invasive techniques, such as MRI, to very invasive ones, such as muscle or nerve biopsies. Moreover, they usually are time-consuming, require high expertise, and dedicated facilities. Therefore, their role is increasingly challenged by genetic testing (Thompson et al., 2020).

### 1.4.3 Genetic testing

Genetic testing represents a fundamental step in the diagnosis of inherited NMDs. Even if a detailed clinical assessment and additional testing can exclude some disorders and orient the diagnosis toward others, the constantly increasing genetic heterogeneity of NMDs makes almost impossible to pinpoint with these elements alone the causing mutation.

In the traditional approach to NMDs, a single-gene diagnostic test represented the last step of the diagnostic workflow. This strategy was revolutionized by NGS, which allowed multiple genes to be sequenced in parallel. In just more than a decade, the number of genes more than doubled, passing from 290 in 2010 to 643 in 2021 (Cohen et al., 2021; Thompson et al., 2020). In the last few years, its decreasing costs and increasing availability prompted its use as a first-tier test in the diagnostic

workflow (Thompson et al., 2020; Yubero et al., 2021). However, ancillary tests are often conducted in parallel providing useful diagnostic information, while single-gene testing still represents a first-line procedure for some NMDs (Barp et al., 2021; Thompson et al., 2020; Yubero et al., 2021).

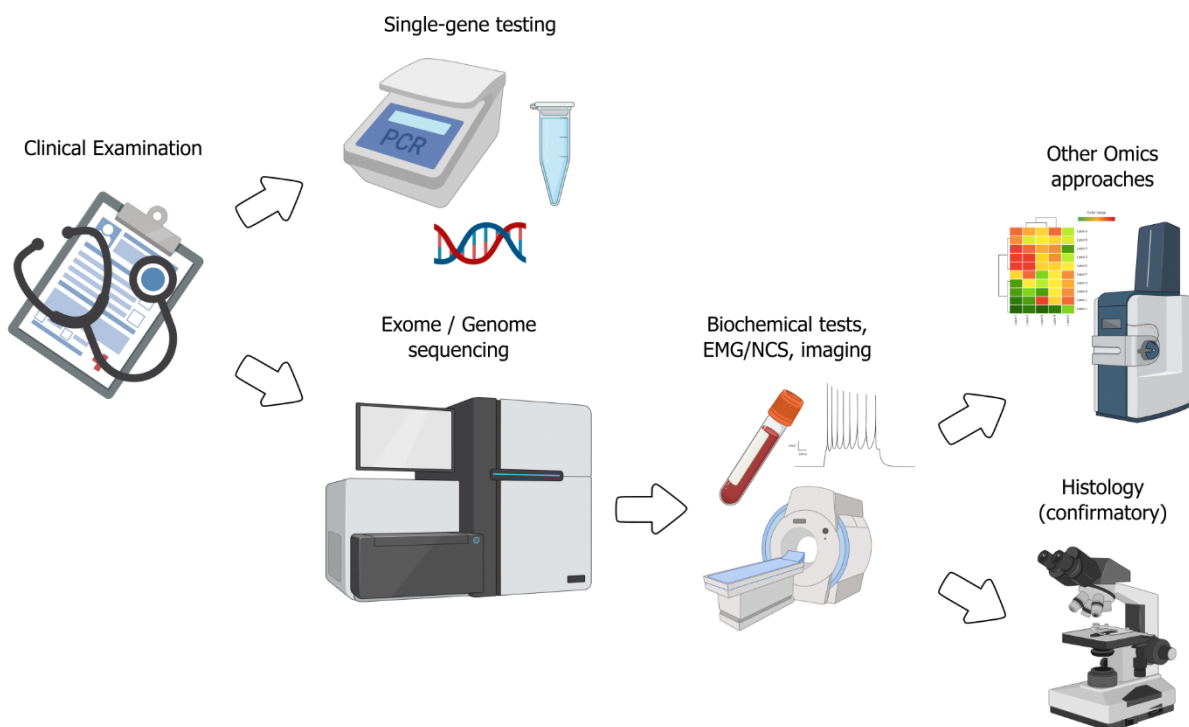


Figure 3. Suggested NMD diagnostic workflow

In the suggested diagnostic workflow for NMDs by Thompson et al. (2020), the first step is a detailed clinical investigation. If the clinical findings point to a specific diagnosis, a single-gene testing follows. Otherwise, exome or genome sequencing should be carried out to identify the disease-causing mutation. Additional biochemical, electrophysiological or histological tests can be used to confirm the diagnosis. Other Omics approaches (such as transcriptomics or proteomics) help define the impact of the NGS-discovered variant. Adapted from Thompson et al. (2020). Created with BioRender.com.

1.4.3.1 Single-gene testing

Single-gene testing is recommended for several NMDs when there is a strong suspicion of a specific cause and/or NGS is not appropriate for the diagnosis (Table 2).

**Table 2. Single gene testing in NMDs**

	MLPA	CMA	NGS	TP-PCR	Sanger	Southern Blotting	Long-Range PCR
Dystrophinopathies	1	-	2	-	3	-	-
5q-SMA	1	-	-	-	2	-	-
DM1 / DM2	-	-	-	1	-	2	-
FSHD1 / FSHD2	-	-	-	-	2	1	-
CMT1A dup / HNPP del	1	1	-	-	-	-	-
FRDA	-	-	-	1	2	3	3

The number indicates the test's tier. MLPA: Multiplex Ligation-dependent Probe Amplification; CMA: Chromosomal MicroArray; NGS: Next-Generation Sequencing; TP-PCR: Triplet repeat Primed PCR; SMA: Spinal Muscular Atrophy; DM: Myotonic Dystrophy; FSHD: FacioScapuloHumeral muscular Dystrophy; CMT1A: Charcot-Marie Tooth disease type 1A; HNPP: Hereditary Neuropathy with Pressure Palsies; FRDA: Friedrich's Ataxia.

Adapted from Yubero et al. (2021)

For example, Karakaya et al. (2018) screened for mutations in *SMN1* a cohort of more than 3400 individuals showing clinical signs of a LMN disorder, due to the high prevalence and the broad age of onset and clinical severity of spinal muscular atrophy (SMA) and reached a diagnosis in 51.6% of the cases.

#### 1.4.3.2 Targeted Gene Panel Testing

Targeted gene panels (TGPs) are NGS tests where the exons of a certain number of genes are sequenced in parallel. They are often used as first-tier diagnostic test when the clinical examination did not lead to a specific diagnostic hypothesis (Barp et al., 2021). Most often they are custom-made and have the advantage to be cheaper than other NGS techniques, requiring less resources for data processing, analysis and storage, and the avoidance of incidental findings (Barp et al., 2021). However, their major drawbacks are: (1) their design, which has to be carefully planned in order to maximize the diagnostic yield and minimize costs, (2) and the need of periodical updates in order to include the latest findings (Barp et al., 2021). Therefore, their diagnostic yield is very variable. The use of a gene panel covering 479 NMD-related genes in a cohort of 65 individuals provided the diagnosis in 33% of the cases (Karakaya et al., 2018).

#### 1.4.3.3 Exome Sequencing

Exome sequencing (ES) is a technique that allows the sequencing of the exons of the human genome. This represents ~ 2% of the genome (Gilissen et al., 2012), and is believed to be its most informative part, harboring roughly 85% of the known genetic causes for Mendelian disorders (Gilissen et al., 2012). ES is often performed when a TGP fails to identify the causative mutation or there is no other reasonable diagnostic hypothesis (Barp et al., 2021). Therefore, it allows the analysis of the already known disease-causing genes, but also the identification of novel ones. Due to its decreasing costs, ES has the potential of replacing TGP: *in silico* gene panels, that is the analysis of a subset of genes from ES data, can be carried out with rapid turnaround time. Moreover, these panels can be easily updated upon the discovery of novel genes. If these *in silico* panels are negative, the remaining ES data can be analyzed and novel disease-causing genes can be found. Between the different strategies to perform an ES analysis (Gilissen et al., 2012), trio-based ES, namely sequencing the proband and the parents, is one of the most successful and enables the direct identification of *de novo* variants (de Ligt et al., 2012; Deciphering Developmental Disorders, 2015). For neurodevelopmental disorders, this approach led to a 40% diagnostic rate, with a 12% increase in comparison to the proband-only ES (Wright et al., 2018). Moreover, in the case of a negative result, ES data can be re-analyzed subsequently, focusing on the latest findings. If the suspected disease-causing variant is not described, due to the rarity of these disorders it is often critical to find other individuals having the same phenotype and carrying a variant in the same gene. Nowadays, this "matching" process is facilitated by online databases, such as GeneMatcher (Sobreira et al., 2015).

#### 1.4.3.4 Genome Sequencing

Genome sequencing (GS) represents the following step in the diagnostic workflow. Due to the lack of capture enrichment, it provides a more uniform coverage in comparison to ES, especially for exon 1 and GC-rich regions, and allows a more reliable detection of copy number variations (CNVs). Moreover,

it spans deep intronic and regulatory regions, which are missed by ES (Barp et al., 2021; Thompson et al., 2020; Yubero et al., 2021). Despite these advantages, the use of GS led to a very modest increase in the diagnostic rate (Wright et al., 2018), and is burdened by challenges in the interpretation of the variants, and higher costs and storage requirements (Barp et al., 2021).

#### 1.4.3.5 Further Analyses

Even though the NMD field experienced tremendous advances, unfortunately about half of the patients remains without a genetic diagnosis (Thompson et al., 2020). New technologies, such as long-read sequencing compensate for the shortcomings of short-read techniques, enabling not only the detection of structural variations, such as repeat expansions and large indels, but also direct haplotype phasing and methylation studies (Barp et al., 2021; Marwaha et al., 2022). For example, nanopore sequencing was able to identify the *D4Z4* repeat contraction in affected individuals suffering from facioscapulohumeral dystrophy 1 (Mitsuhashi et al., 2017).

Even if GS is able to cover deep intronic sequences, often the interpretation of variants in these regions is difficult, in particular concerning the effects on splicing events (Thompson et al., 2020). A complementary approach can be RNA sequencing, which can provide information about expression outliers, splice-disrupting mutations, allele-specific expression and transcriptomic structural variants (Marwaha et al., 2022; Thompson et al., 2020). While this approach can increase the diagnosis rate (Cummings et al., 2017), tissue selection assumes particular consideration because of the tissue-specific gene expression (Gonorazky et al., 2019).

Lastly, proteomics from patient-derived muscle tissue allow the study of post-translational modifications and protein networks (Thompson et al., 2020), and are useful to identify prognostic markers or targets for therapeutic intervention (Yubero et al., 2021).

## 1.5 Overview of specific NMDs

In this thesis, three genes were associated to novel neuromuscular disorders:

- *PIEZO2* to a novel type of distal arthrogryposis;
- *VAMP1* to a novel congenital myasthenic syndrome;
- *CAPRIN1* to a novel neurodegenerative disorder characterized by early-onset ataxia and muscle weakness.

Therefore, a short introduction about these NMDs will follow.

### 1.5.1 Distal Arthrogryposis

Distal Arthrogryposis (DA) belongs to the spectrum of arthrogryposis multiplex congenita (AMC), a group of disorders characterized by contractures in more than two joints and at multiple body areas at birth. The incidence of AMC is 1 to 3000 – 5000 live births (Ma & Yu, 2017). DA is characterized by congenital non progressive contractures of the distal joints. The hands usually show clenched fists, ulnar deviation of fingers and camptodactyly, while the feet have deformities (Kimber, 2015). The other joints are variably involved. No associated visceral anomalies are described, and intelligence is normal (Desai et al., 2020).

Bamshad et al. (2009) classified DA in 10 different types (Table 3). They are usually transmitted with an autosomal dominant pattern and are associated to gain-of-function mutations in several sarcomeric proteins and PIEZO2 (Figure 4, Table 3) (Desai et al., 2020).

#### 1.5.1.1 Pathophysiology

The common pathophysiological mechanism of AMC is the reduction in the movements during the fetal life (Kimber, 2015), which leads to the formation of extra connective tissue around the joints. Therefore, DA can be caused by disorders of the central nervous system, of the neuromuscular junction, of muscle or connective tissue, but also compromised space in utero or drugs (Kimber, 2015).

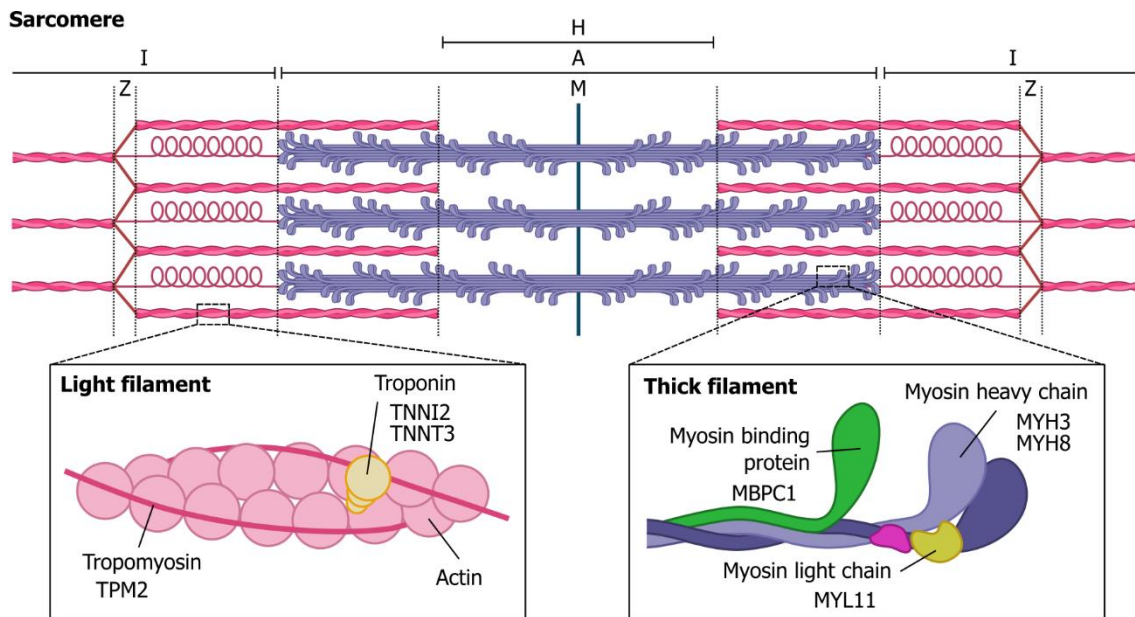


Figure 4. DA-associated mutations in sarcomeric proteins

The majority of DA are caused by mutations in sarcomeric proteins, such as tropomyosin, troponin and myosin chains. The sarcomere is the functional unit of the muscle and it is comprised between two Z-lines. These lines are located in the I-band, occupied by light filaments. Between these bands, A-bands are present and contain both light and thick filaments. Within the A-band is present the H-zone, formed only by thick filaments. The M-line occupies the middle of the H-zone. Adapted from Desai et al. (2020). Created with BioRender.com.

**Table 3. Distal Arthrogryposis**

Disorder	Inheritance	Chromosome	Gene	Protein function	Clinical presentation
<b>DA1</b>					
DA1A1	AD	9p13	<i>TPM2</i>	Structural and Ca <sup>2+</sup> -dependent regulation of striated muscle contraction	Camptodactyly, ulnar deviation of the fingers, finger overlap, clubfoot, triangular face with prominent nasolabial folds, downward-slanting palpebral fissures
DA1B	AD	12q23	<i>MYBPC1</i>	Stabilization of actomyosin cross-bridges	
DA1C	AD/AR	16p11	<i>MYL11</i>	Maintainment of muscle integrity during development	
<b>DA2</b>					
DA2A	AD	17p13	<i>MYH3</i>	Striated muscle contraction (myosin heavy chain)	Camptodactyly, clubfoot, flatfoot, calcaneovarus deformities, kyphoscoliosis, "whistling face"
DA2B1	AD	11p15	<i>TNNI2</i>	Ca <sup>2+</sup> -mediated regulation of striated muscle contraction	
DA2B2	AD	11p15	<i>TNNT3</i>	Ca <sup>2+</sup> -mediated regulation of striated muscle contraction	
DA2B3	AD	17p13	<i>MYH3</i>	Striated muscle contraction (myosin heavy chain)	
DA3	AD	18p11	<i>PIEZO2</i>	Mechanosensation	Camptodactyly, clubfoot, low stature, palatoschisis
DA4	na	na	na		Contractures, severe scoliosis
DA5	AD	18p11	<i>PIEZO2</i>	Mechanosensation	Contractures, ptosis, strabismus, firm muscle tone, restrictive lung disease
DA6	na	na	na		Contractures, sensorineural hearing loss
DA7	AD	17p13.1	<i>MYH8</i>	Striated muscle contraction (myosin heavy chain)	Trismus, pseudocamptodactyly
DA8	AD	17p13	<i>MYH3</i>	Striated muscle contraction (myosin heavy chain)	Contractures, short stature, pterygia involving neck, axilla, elbows and knees, shortened hamstring muscles
DA9	AD	5q23	<i>FBN2</i>	Assembly of elastic fibers	Contractures, Marfan-like syndrome, but without cardiovascular anomalies
DA10	AD	2q	na		Plantar flexion contractures

DA: Distal Arthrogryposis; AD: Autosomal Dominant; AR: Autosomal Recessive; na: not available.

Adapted from Desai et al. (2020); Ma and Yu (2017); *Online Mendelian Inheritance in Man, OMIM®*. MIM Number: #108120.

### 1.5.2 Congenital Myasthenic Syndromes

Congenital myasthenic syndromes (CMSs) are inherited disorders affecting the function of the NMJ. Their prevalence is likely underestimated and varies considerably among countries and studies, spanning around 9.2 - 22.2 / 1000000 (Finsterer, 2020).

The onset is usually at birth or in early childhood, rarely later in life (Engel et al., 2015). Their clinical features vary broadly, but generally comprises transient/permanent muscle fatigability/weakness affecting extraocular, facial, bulbar, truncal, respiratory, or limb muscles (Finsterer, 2019). The severity ranges from mild, phasic weakness to early lethality (Finsterer, 2019).

Blood tests may be carried out to exclude the presence of antibodies anti-AChR, anti-MuSK and anti-LRP4, or to test serum creatine kinase (CK) levels.

Electromyography with low-frequency repetitive nerve stimulation (2 – 5 Hz) shows a compound muscle action potential (CMAP) decrement > 10% and single fiber electromyography shows increased jitter or blockings. High-frequency repetitive nerve stimulation (20 – 50 Hz) may show a CMAP increment in some presynaptic subtypes (*PREPL*- and vesicle exocytosis-related) (Abicht et al., 2003). Muscle biopsy is generally normal, but can show tubular aggregates in some CMS linked to protein glycosylation (Abicht et al., 2003; Finsterer, 2019).

A common classification of CMSs defines four CMS categories based on the location of the affected protein or of the functional impairment: presynaptic, synaptic, postsynaptic and pre- and post-synaptic (Table 4, adapted from Abicht et al. (2003)).

**Table 4. Congenital Myasthenic Syndromes**

Localization of the defect	Prevalence (%)	Gene	Inheritance	Clinical presentation	AChE inhibitors response
<b>Presynaptic</b>					
Axonal transport	< 1	<i>MYO9A</i>	AR	Early onset, ptosis, ophthalmoplegia, moderate global weakness, bulbar involvement, respiratory crises. ID or learning difficulties, nystagmus, oculomotor apraxia	Improvement
Mitochondrial metabolism	< 1	<i>SLC25A1</i>	AR	Relatively mild phenotype, ID, subtle mitochondrial abnormalities	-
Acetylcholine synthesis and recycling	< 5	<i>CHAT</i>	AR	Hypotonia, respiratory failure at birth, episodic apnea, improvement with age	Improvement
	< 1	<i>SLC18A3</i>	AR	Early onset, arthrogryposis/joint contractures, apneic crisis at birth, marked ptosis, ophthalmoplegia, muscle fatigability. Sometimes learning difficulties	Some improvement
	< 1	<i>PREPL</i>	AR	Congenital hypotonia, feeding difficulties, ptosis, proximal muscle weakness	Some improvement
	< 1	<i>UNC13A</i>	AR	Hypotonia, feeding difficulties, respiratory insufficiency, microcephaly, facial dysmorphism	Some improvement
Vesicle exocytosis	< 1	<i>SNAP25</i>	AD	Epileptic encephalopathy of infancy, severe ID, cerebellar ataxia, brain atrophy	Ineffective
	< 1	<i>SYT2</i>	AD / AR	AD: slowly progressive distal motor neuropathy, hypotonia, weakness AR: severe congenital hypotonia and weakness	Some improvement
	<b>Synaptic</b>				
Basal lamina / NMJ development	< 5	<i>COL13A1</i>	AR	At birth, respiratory distress and dysphagia. Recurrent apnea triggered by infections. In adulthood, bilateral non fatigable ptosis and marked axial weakness	Likely ineffective
Anchoring of acetylcholinesterase	10 - 15	<i>COLQ</i>	AR	Often severe. General muscle weakness, more severe of axial muscles. Extraocular muscles are spared.	Deterioration or ineffective
Basal lamina defects	< 1	<i>LAMA5</i>	AR	Muscle weakness, myopia, facial tics	Improvement
	< 1	<i>LAMB2</i>	AR	Pierson syndrome (microcoria and nephrotic syndrome), respiratory distress, ptosis	Deterioration

*continues* →

→ Table 4 (continued)

Localization of the defect	Prev. (%)	Gene	Inh.	Clinical presentation	AChE inhibitors response
Postsynaptic	70 - 75				
AChR deficiency	40 - 50				
Primary AChR deficiency	30 - 35	<i>CHRNA1, CHRNB1, CHRND, CHRNE</i>	AR	Early onset. Mild to severe. Ptosis, EOP, bulbar and limb weakness	Improvement
Slow-channel CMS	5 - 10	<i>CHRNA1, CHRNB1, CHRND, CHRNE</i>	AD	Childhood to adult onset. Selective severe cervical, wrist, finger extensor weakness. Progressive respiratory insufficiency	Deterioration
Fast-channel CMS	10 - 15	<i>CHRNA1, CHRNB1, CHRND, CHRNE</i>	AR	Early childhood. Mild to severe phenotype	Improvement
γ-subunit mutations	< 1	<i>CHRNA1</i>	AR	Syndromic phenotype (lethal multiple pterygia syndrome or Escobar syndrome)	-
	< 1	<i>AGRN</i>	AR	Early-onset or late-onset phenotype. If late onset: distal muscle weakness and wasting in addition to myasthenia	Deterioration
	< 1	<i>LRP4</i>	AR	Respiratory failure and feeding difficulties at birth, delayed motor milestones, ptosis, ophthalmoparesis, limb weakness	Deterioration or ineffective
	< 1	<i>MUSK</i>	AR	Broad phenotype. Early onset with ptosis, respiratory failure and proximal muscle weakness. Late-onset with limb girdle weakness	Deterioration or ineffective
Endplate development and maintenance	< 1	<i>MUSK</i>	AR	Limb-girdle pattern of predominantly proximal weakness, waddling gait and ptosis. No EOP	Deterioration or ineffective
	10 - 15	<i>DOK7</i>	AR	Early onset: mild to severe hypotonia, respiratory failure at birth, episodic apnea, arthrogryposis multiplex congenita	Improvement
	15 - 20	<i>RAPSN</i>	AR	Late onset: limb weakness in adolescence or adulthood	Improvement
Intermediate filaments linking	< 1	<i>PLEC</i>	AR	Childhood to adulthood onset: fatigable proximal myopathy and ptosis, with or without epidermolysis bullosa	Improvement
Muscle action potential	< 1	<i>SCN4A</i>	AR	Early-onset hypotonia, dysphagia, periodic paralysis, myotonia, myopathy	Some improvement
Pre- and post-synaptic	1 - 5				
Protein glycosylation	< 5	<i>GFPT1</i>	AR	Limb-girdle pattern of weakness. No ptosis or EOP. In some muscle biopsies tubular aggregates are present. ID was reported with DPAGT1 mutations. High CK and muscular dystrophy with GMPPB mutations.	Improvement
	< 1	<i>DPAGT1</i>	AR		
	< 1	<i>GMPPB</i>	AR		
	< 1	<i>ALG2</i>	AR		
	< 1	<i>ALG14</i>	AR		

Prev.: Prevalence; Inh.: Inheritance; AChE: AcetylCholinEsterase; AD: Autosomal Dominant; AR: Autosomal Recessive; ID: Intellectual Disability; EOP = External Ophthalmoplegia; CMS: Congenital Myasthenic Syndrome; CK: Creatine Kinase; -: no data.

Adapted from Abicht et al. (2003); Finsterer (2019)

1.5.2.1 Pathophysiology

CMSs arise from defects of the NMJ function. NMJs are the interface between MN axons and muscle fibers. They are composed by three elements: (1) the presynaptic MN terminal, (2) the synaptic cleft and (3) the postsynaptic muscle membrane (Figure 5).

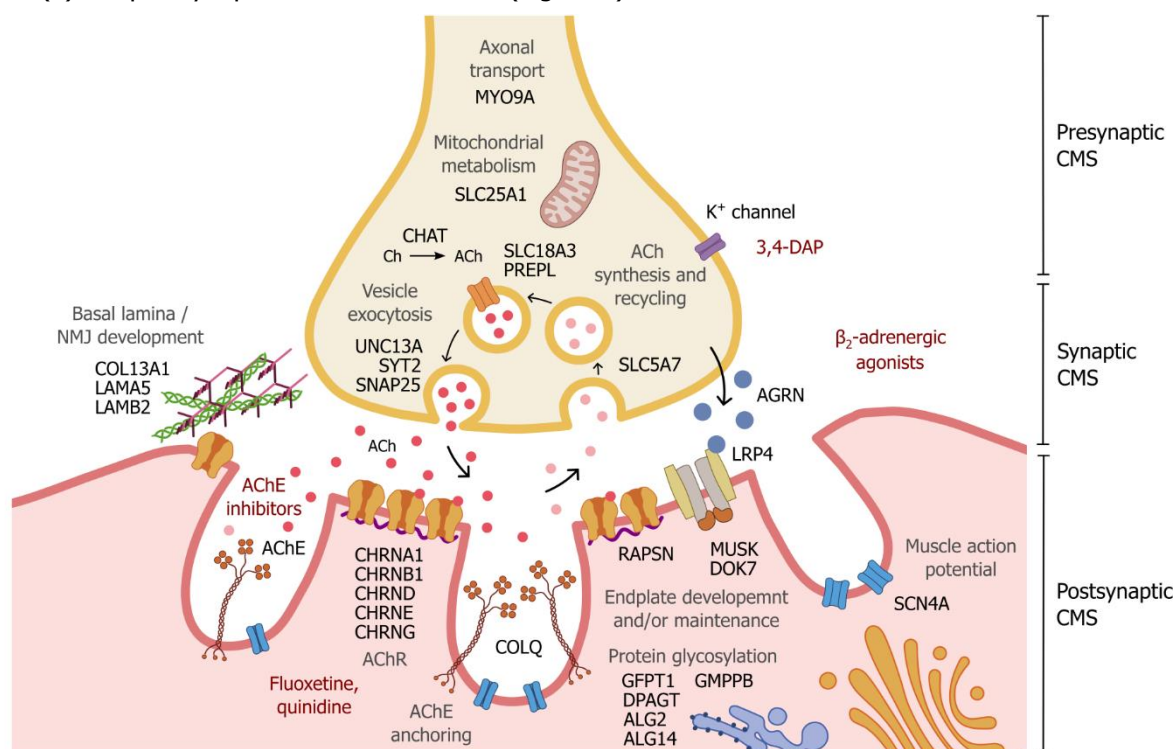


Figure 5. Overview of the pathophysiology of CMS

CMSs are caused by defects in the NMJ function. They can be divided in: (1) presynaptic, if they affect the MN terminal, (2) synaptic, if they affect the NMJ / basal lamina development, or the AChE anchoring, (3) postsynaptic, if they affect the muscle endplate. Protein glycosylation defects are considered both pre- and post-synaptic. The cellular processes impaired in CMSs are displayed in grey, with the related proteins in black. Drugs that can be used to treat the disorders are highlighted in dark red. Adapted from Ramdas and Beeson (2021); Thompson, Bonne, et al. (2019). Created with BioRender.com.

The presynaptic terminal is a specialized axonal ending of the MN, which enlarges in a synaptic bouton filled with vesicles containing the neurotransmitter acetylcholine (ACh) (Rodriguez Cruz et al., 2020). Its correct branching and guidance are likely to rely on MYO9A (Ramdas & Beeson, 2021). ACh is synthesized by the enzyme choline acetyltransferase (ChAT / *CHAT* gene) and loaded into the synaptic vesicles by the vesicular acetylcholine transporter (VACht / *SLC18A3* gene) (Rodriguez Cruz et al., 2020). The trafficking of this transporter between vesicles and cytoplasm depends on AP-1, whose membrane binding is regulated by PREPL (Finsterer, 2019). The release of these vesicles is mediated by the soluble N-ethylmaleimide-sensitive factor attachment protein receptor (SNARE) complex, formed by the vesicle SNARE (v-SNARE), the target membrane SNARE (t-SNARE) and SNAP25 (Ramdas & Beeson, 2021). This process involves (1) docking, the contact of the synaptic vesicle and the plasma membrane, (2) priming, the maturation process necessary for vesicle (3) fusion with the plasma membrane (Finsterer, 2019). UNC13A mediates the docking-priming phases, bringing in close proximity the components of the SNARE complex (Finsterer, 2019). This allows the v-SNARE VAMP1 to form a ternary complex with the t-SNARE syntaxin and SNAP25 (Ramdas & Beeson, 2021). Upon

action potential, voltage-gated calcium channels (VGCC) open and the increase in  $\text{Ca}^{2+}$  is sensed by the  $\text{Ca}^{2+}$  sensor SYT2, which binds the SNARE complex favoring fusion and ACh release (Ramdas & Beeson, 2021; Rodriguez Cruz et al., 2020). Mutations of *UNC13A*, *SNAP25* and *SYT2* are associated with presynaptic CMS.

In the synaptic cleft, ACh binds its two binding sites on the ACh receptor (AChR) (Engel et al., 2015). The AChR is clustered on the crests of the junctional folds and is formed by 5 subunits,  $\alpha_2\beta\delta\gamma$  in the fetus or  $\alpha_2\beta\delta\epsilon$  in the adult, encoded by the genes *CHRNA1*, *CHRNA2*, *CHRNB*, *CHRND*, *CHRNA3* and *CHRNE* (Winterthun et al., 2005). AChR deficiency on the postsynaptic membrane is commonly due to *CHRNE* mutations, whose severity is partially reduced by low expression of the fetal *CHRNA3* (Ramdas & Beeson, 2021). Mutations of this subunit are linked to lethal multiple pterigia syndrome or its non-lethal Escobar variant (Finsterer, 2019). AChR mutations affecting its kinetics can lead to a slow-channel CMS, caused by a secondary endplate myopathy due to prolonged channel opening, or rapid-channel CMS, caused by the reduction of muscle fiber depolarization due to its shortened opening time. The correct AChR clustering and NMJ stability depends on the AGRN-LRP4-MUSK-DOK7 pathway (Ramdas & Beeson, 2021). AGRN is released by the nerve terminal and binds LRP4, activating the dimerization of MUSK and its autophosphorylation. This is amplified by DOK7, which leads to RAPSN clustering and AChR anchoring (Ramdas & Beeson, 2021). Mutations in the AGRN-LRP4-MUSK-DOK7 pathway are responsible for an impaired NMJ formation/maintenance and AChR clustering. At the junctional folds is present PLEC, an intermediate filament-linking protein important for junctional folds maintenance, whose mutations are also associated with CMS (Engel et al., 2015). Fundamental for correct AChR assembly and transport, but also NMJ integrity, is protein glycosylation by enzymes like GFPT1, DPAGT1, GMPPB, ALG2 and ALG14 (Ramdas & Beeson, 2021). Even if ubiquitously expressed, the glycosylation defects affect primarily the NMJ, which can show structural changes like the presence of tubular aggregation.

ACh binding to its receptor triggers the short opening of the channel pore. Then, ACh dissociates and is hydrolyzed by acetylcholinesterase (AChE) in choline and acetate (Purves, 2018). Choline can then be recycled in the presynaptic terminal by the  $\text{Na}^+$ -dependent high-affinity choline transporter 1 (ChT / *SLC5A7* gene) (Finsterer, 2019). The AChE is anchored to the basal lamina by COLQ, a triple-stranded collagen-like tail (Finsterer & Stollberger, 1999). COLQ mutations lead to lack of AChE, prolonged ACh stimulation of the muscle fiber and endplate myopathy. Other components of the basal lamina important for the NMJ stability are LAMA5, LAMB2 and COL13A1 (Ramdas & Beeson, 2021). Mutations of some of these components often cause syndromic phenotypes. The cation influx due to the depolarization of the endplate potential (EPP) has to reach the threshold needed to activate the  $\text{Na}_v1.4$  channels (*SCN4A*) of the postsynaptic membrane in order to generate a sustained action potential. This difference is the margin of safety, which allows the NMJ to function under physiological or stress conditions (Rodriguez Cruz et al., 2020). *SCN4A* mutations are a rare cause of CMS and are linked to channelopathies, such as hyperkalemic and hypokalemic periodic paralysis, paramyotonia congenital and sodium channel myotonia (Ramdas & Beeson, 2021).

### 1.5.2.2 Therapy

The rarity and the phenotypic variability of the CMSs hinders the development of standardized treatments (Ramdas & Beeson, 2021). However, several drugs are often used off-label as symptomatic measure. Importantly, reaching a genetic diagnosis is crucial, since drugs that improve symptoms in some CMSs subtypes may worsen them in others (Ramdas & Beeson, 2021).

An AChE inhibitor (Pyridostigmine) is the most commonly used drug. It acts increasing the availability of ACh in the synaptic cleft. It worsens the *COLQ*-, *LAMB2*-, *LRP4*-, *MUSK*- and *DOK7*-related CMS (Finsterer, 2019).

3,4-diaminopyridine (3,4-DAP) prolongs the presynaptic action potential and increases the amount of ACh. It can be given in combination with AChE inhibitors, and not only in presynaptic syndromes (Finsterer, 2019).

$\beta_2$ -adrenergic agonists (Salbutamol, Albuterol, Ephedrine) are effective for CMSs caused by mutations in genes related to synaptic and endplate developments and maintenance CMSs. Their exact mechanism of action is not known and they need a prolonged administration in order to observe a response (Finsterer, 2019).

Fluoxetine and quinidine are used in slow channels CMSs (Ramdas & Beeson, 2021).

Beside drug treatments, physiotherapy, speech and occupational therapies are required. Orthoses, walkers, wheel chairs allow mobility (Finsterer, 2019).

More invasive measures like intubation and mechanical ventilation, or percutaneous endoscopic gastrostomy (PEG) are sometimes necessary (Finsterer, 2019).

### 1.5.3 Hereditary Ataxias

Hereditary Ataxias (HAs) comprise a heterogeneous group of NMDs and include 102 phenotypes in the last version of *GeneTable of Neuromuscular Disorders*. There is a great uncertainty in the epidemiology of HA, not only due to the variety of the disorders, but also due to the differences between the populations' genetic background and the availability of diagnostic testing (Klockgether et al., 2019). Nevertheless, HA prevalence should range between 5 – 10 / 100000 (Haj Salem et al., 2021; Ruano et al., 2014).

Ataxia means "lack of order" and denotes the lack of coordination of the affected individuals. This disease hallmark is evident as unsteady gait, unexpected falls and often occurs together with slurred speech (dysarthria) (Klockgether et al., 2019). The onset of HAs is usually mid-adulthood, but they can occur in childhood or old age too. In general, if an ataxia has an age of onset before 25 years (early-onset ataxia), there is a high likelihood that its cause is genetic or metabolic (Witek et al., 2021). The diagnosis of these cases is complicated by their heterogeneity and the fact that ataxia could be a sign of a more complex phenotype, like congenital hindbrain abnormalities (Joubert syndrome), metabolic (glucose transporter type 1 deficiency syndrome) or mitochondrial (neuropathy, ataxia, retinitis pigmentosa (NARP)) disorders (Krygier & Mazurkiewicz-Beldzinska, 2021).

In the diagnostic approach to early-onset ataxias, the first step is the exclusion of conditions resembling HAs, such as "ataxia mimics", like vestibular dysfunction, sensory ataxia or myopathies, or

acquired ataxias, due to toxins, inflammation or nutrient deficiencies (Witek et al., 2021). Afterwards, a brain MRI should be acquired in order to reveal cerebellar atrophy, structural defects, vascular malformations and leukodystrophy. Moreover, imaging can give important diagnostic clues if characteristic brain abnormalities are present, such as the “molar tooth sign” of Joubert syndrome or the superior vermian atrophy and pontine striations of the Charlevoix-Saguenay syndrome. Electrophysiological studies may uncover a polyneuropathy, which is axonal in Friedreich’s ataxia and demyelinating in the Charlevoix-Saguenay syndrome. According to the anomalies detected, a complete blood count and vitamin E or  $\alpha$ -fetoprotein levels measurements can address the diagnosis to specific ataxic phenotypes.

HAs are classified according to their inheritance mode in autosomal dominant ataxias (or spinocerebellar ataxias, SCAs), autosomal recessive cerebellar ataxias (ARCAs) or X-linked ataxias (Table 5).

**Table 5. Hereditary Ataxias (selection)**

Disorder	Inheritance	Gene	Mutation		Protein function	Clinical presentation
Repeat expansion mutations						
SCA1	AD	<i>ATXN1</i>	CAG	c	Chromatin-binding factor	Ataxia, spasticity, ophtalmoplegia, early bulbar symptoms, pyramidal signs, peripheral neuropathy; occasional cognitive decline
SCA2	AD	<i>ATXN2</i>	CAG	c	RNA binding protein	Ataxia, slow saccads, peripheral neuropathy, chorea, dementia
SCA3	AD	<i>ATXN3</i>	CAG	c	Deubiquitinating enzyme	Ataxia, ophtalmoplegia, fasciculations, amyotrophy, sensory loss; pyramidal/extrapyrmidal signs
SCA6	AD	<i>CACNA1A</i>	CAG	c	$\alpha_{1A}$ subunit of the P/Q type $Ca^{2+}$ channel	Late-onset ataxia, very slow progression; onset may be episodic; normal life span
SCA7	AD	<i>ATXN7</i>	CAG	c	Histone acetyltransferase complex subunit	Ataxia, spasticity, visual loss with retinopathy; often rapidly progressive
SCA8	AD	<i>ATXN8</i> <i>ATXN8OS</i>	CAG CTG	c nc	Unknown	Slowly progressive ataxia, spasticity; rarely, cognitive impairment in persons with earlier onset
SCA10	AD	<i>ATXN10</i>	ATTCT	nc	Unknown	Ataxia, seizures in certain families
SCA12	AD	<i>PPP2R2B</i>	CAG	nc	Brain-specific regulatory subunit of protein phosphatase 2A	Ataxia, action tremor in the 4 <sup>th</sup> decade, cognitive/psychiatric disorders (dementia, hyperreflexia, subtle parkinsonism)
SCA17	AD	<i>TBP</i>	CAG / CAA	c	TATA-box-binding protein	Ataxia, mental deterioration; occasional chorea, dystonia, myoclonus, epilepsy
SCA31	AD	<i>BEAN1</i>	TGGAA	nc	Brain-expressed protein binding NEDD4 homologue	Late-onset ataxia, slow progression with normal sensation
SCA36	AD	<i>NOP56</i>	GGCCTG	nc	Nucleolar protein 56 involved in RNA maturation	Ataxia, hyperreflexia, muscle fasciculations, tongue atrophy, hearing loss
DRPLA	AD	<i>ATN1</i>	CAG	c	Transcriptional corepressor	Ataxia, chorea, dementia, myoclonus, seizures; mimics Huntington's disease
FRDA	AR	<i>FXN</i>	GAA	nc	Mitochondrial protein regulating iron transport and respiration	Childhood-onset, slowly progressive ataxia, absent tendon reflexes, Babinski reflex, posterior column sensory loss, cardiomyopathy, scoliosis, pes cavus, diabetes; in some: onset $\geq$ 25 years, slower progression and retained reflexes
CANVAS	AR	<i>RFC1</i>	AAGGG	nc	Subunit of the replication factor C involved in DNA replication and repair	Spectrum ranging from cerebellar ataxia, neuropathy, vestibular areflexia syndrome (CANVAS), to cerebellar, sensory, vestibular impairment, or phenotypes involving predominantly or exclusively one of the systems involved in balance control
FXTAS	XL	<i>FMR1</i>	CGG	nc	Polyribosome-associated RNA-binding protein	Late-onset ataxia, mental deterioration; occasional chorea, dystonia, myoclonus, epilepsy

*continues* →

→ Table 5 (continued)

Disorder	Inheritance	Gene	Mutation	Protein function	Clinical presentation
Non-repeat mutations					
Episodic ataxia type 2	AD	<i>CACNA1A</i>	del / ns / mis	$\alpha_{1A}$ subunit of the P/Q type $Ca^{2+}$ channel	Early-onset episodic ataxia, often progressive
SCA13	AD	<i>KCNC3</i>	missense	$K_v3.3$ subunit	Slowly progressive ataxia with adult onset. Non-progressive congenital ataxia
SCA14	AD	<i>PRKCG</i>	missense	Protein kinase C $\gamma$	Ataxia, often slow progressive, slight hyperreflexia
SCA15/16	AD	<i>ITPR1</i>	del / mis	Channel mediating $Ca^{2+}$ release from the endoplasmic reticulum	Adult onset, slowly progressive ataxia
SCA29	AD	<i>ITPR1</i>	mis		Non-progressive congenital ataxia, intellectual disability
SCA19/22	AD	<i>KCND3</i>	del / mis	$K_v4.3$ subunit	Ataxia, cognitive impairment, myoclonus
SCA28	AD	<i>AFG3L2</i>	del / mis	ATP-dependent protease in the inner mitochondrial membrane	Ataxia, spasticity, ophthalmoparesis, slow saccades, ptosis
SPAX5	AR	<i>AFG3L2</i>	mis		Ataxia, spasticity, myoclonic epilepsy
SCA5	AD		del / mis	Cytoskeletal protein that stabilizes membrane proteins, including glutamate receptors	Ataxia with variable disease onset
SCAR14	AR	<i>SPTBN2</i>	ns / mis		Severe early-onset ataxia, intellectual disability
AT	AR	<i>ATM</i>	ns / mis	Serine/threonine protein kinase activating checkpoint signaling	Early-onset ataxia, oculomotor apraxia, choreoathetosis, telangiectasias of the conjunctiva, immunodeficiency, cancer risk, $\uparrow$ alpha-fetoprotein
ARSACS	AR	<i>SACS</i>	ns / mis	Co-chaperone regulating Hsp70	Early-onset ataxia with spastic paraparesis and axonal/demyelinating sensorimotor neuropathy; hypointense pontine stripes on T2-weighted MRI
SCAR8	AR	<i>SYNE1</i>	ns / mis	LINC (LInker of Nucleoskeleton and Cytoskeleton) complex component	Ataxia with variable spasticity, further multisystemic disorder with impaired intellectual development
SCAR10	AR	<i>ANO10</i>	ns / mis	$Cl^-$ channel and phospholipid scrambler	Early-onset ataxia with spasticity, downbeat nystagmus, fasciculations
EAOH	AR	<i>APTX</i>	ns / mis	DNA-binding protein involved in DNA repair	Early-onset ataxia, oculomotor apraxia, extrapyramidal features, sensorimotor neuropathy, hypoalbuminemia; secondary coenzyme Q10 deficiency
SCAN2	AR	<i>SETX</i>	ns / mis	Probable RNA/DNA helicase	Early-onset ataxia, oculomotor apraxia, sensorimotor neuropathy, $\uparrow$ alpha-fetoprotein
Spastic Paraplegia 7	AR	<i>SPG7</i>	del / ns	ATP-dependent zinc metalloprotease	Progressive ataxia with spasticity and ophthalmoplegia

SCA: Spinocerebellar Ataxia; DRPLA: DentatoRubral-Pallidoluyisian Atrophy; FRDA: Friedreich's Ataxia; CANVAS: Cerebellar ataxia, Neuropathy, Vestibular Areflexia Syndrome; FXTAS: Fragile X-associated Tremor/Ataxia Syndrome; SPAX: SPastix ATaxia; SCAR: Spinocerebellar ataxia Autosomal Recessive; AT: Ataxia-Telangiectasia; ARSACS: Autosomal Recessive Spastic Ataxia of Charlevoix-Saguenay; EAOH: Early-onset Ataxia with Oculomotor apraxia and Hypoalbuminemia; SCAN2: Spinocerebellar ataxia with Axonal Neuropathy 2; AD: Autosomal Dominant; AR: Autosomal Recessive; XL: X-linked; c: coding; nc: non-coding; del: deletion; ns: nonsense; mis: missense; DTR: Deep tendon Reflex

Adapted from Perlman (1998), Klockgether et al. (2019) and Krygier and Mazurkiewicz-Beldzinska (2021)

### 1.5.3.1 Pathophysiology

The most common pathomechanism of HAs is the presence of short tandem repeat (STR) expansions (Perlman, 1998). These consist in the repetition of 1 – 6 nucleotide and can be inherited in an AD, AR or X-linked pattern (Perlman, 1998). SCAs caused by repeat expansions are characterized by anticipation: the disease occurs earlier and with a more severe phenotype in subsequent generations as a result of the expansion of the repeat size during transmission (Klockgether et al., 2019). The repeats can belong to the coding sequence or be localized in intronic or untranslated regions (UTR). Six SCAs (SCA1, SCA2, SCA3, SCA6, SCA7 and SCA17) and the dentatorubral-pallidoluysian atrophy (DRPA) are caused by pathological CAG expansions in the coding sequence, which result in the translation of polyglutamine (polyQ) stretches within the disease-causative proteins (Klockgether et al., 2019). These disorders are thus referred as poliQ disorders, along with other neurodegenerative disorders like Huntington disease (Klockgether et al., 2019). A common hallmark of these disorders is the accumulation and aggregation of cellular deposits, through a process starting from the formation of oligomers and ending with the constitution of sedimentable aggregates. While the role of these different species is still under debate, the correlation between the repeat length, protein aggregation and disease anticipation suggests an important role of protein misfolding in the disease pathogenesis (Klockgether et al., 2019). Moreover, these aggregates could sequester important protein quality control components, like molecular chaperones or the proteasome. PolyQ expansions may influence protein-protein interactions, altering protein function or localization within the cell (Klockgether et al., 2019). These mechanisms are not unique to poliQ SCAs: missense variants in *PRKCG* increase amyloid fibril formation of protein kinase C $\gamma$  and mutations in *SPTBN2* alter the stability of glutamate receptors in Purkinje cells (Klockgether et al., 2019). Although polyQ toxicity is a well-recognized SCA pathomechanism, the evidence of repeat-associated non-ATG-mediated (RAN) translation and consequent homopolymeric production in Huntington disease indicates their possible role in these disorders too (Klockgether et al., 2019).

The repeat expansions of other SCAs (SCA10, SCA31, SCA36) are instead localized in not-coding regions. In contrast to the coding expansions, which are usually shorter than 100 repeats, these may comprise hundreds of repeats. The expanded repeat-containing transcripts accumulate in RNA foci, sequestering RNA-binding proteins and altering RNA-dependent processes (Klockgether et al., 2019). While repeat expansion mutations account for a substantial number of HAs, many ataxias are caused by non-repeat mutations. Examples of these disorders are SCAs associated to variants in genes encoding ion channels (*CACNA1A*, *KCNC3*, *KCND3*, *ITPR1*). These proteins are responsible for the regulation of the autonomous firing of Purkinje cells or of their neuronal inputs, therefore their dysfunction is believed to result in impaired Ca<sup>2+</sup> homeostasis and neuronal degeneration (Klockgether et al., 2019) (Muller, 2021).

Other pathological mechanisms include impaired bioenergetics due to mitochondrial dysfunction (SPAX5), deficits in DNA integrity (ataxia-telangiectasia, early-onset ataxia with oculomotor apraxia and hypoalbuminemia, spinocerebellar ataxia with axonal neuropathy 2) or changes in gene expression (SCA7).

## 1.6 NMDs Models

Due to the high heterogeneity of NMDs, several *in vitro* and *in vivo* models have been adopted in order to understand their pathophysiology (Fralish et al., 2021). Traditionally, these investigations start with the collection of samples from the affected tissue and their direct observation or their further processing to establish cell lines harboring the disease-causing mutation (Sen & Thummer, 2022). However, in many NMDs, the affected cell types are difficult to access and ethical issues hinder their availability (Logan et al., 2019). Therefore, the acquisition of primary samples is limited to post-mortem tissues, which, however, represent the end stage of the disease (Sen & Thummer, 2022).

In order to circumvent these hurdles, different models have been introduced to investigate the pathophysiology of these conditions.

### 1.6.1 Animal Models

Several organisms have been used to model NMDs and investigate possible treatments (Fralish et al., 2021): *Caenorhabditis elegans* (Sleigh & Sattelle, 2010), zebrafish (Babin et al., 2014), *Drosophila melanogaster* (Shields et al., 2017), and mice (Burgess et al., 2016). Nevertheless, rodents are the most commonly used species, due to their deep genetic characterization, short life span, and easy genetic manipulation (Gama Sosa et al., 2012). Animal models allow scientists to study the effects of a mutation in a complex organism, investigating differences at macro- and microscopic level, and give the opportunity to study phenotypes like behavioral changes. However, they present several drawbacks: their brain anatomy and physiology differ considerably from the human ones, and their shorter life expectancy hinders the development of ageing-related phenotypes (Sen & Thummer, 2022). These shortcomings can lead to the inability to recapitulate phenotypes caused by human variants and are responsible for the discordance between the efficacy of drug in preclinical animal trials and their failure in clinical human ones (Logan et al., 2019). For example, for neurodegenerative disorders, the overexpression of a mutant protein or of a protein carrying several mutations is often required in order to observe a phenotype in a mouse model (Gama Sosa et al., 2012). This is probably necessary because of the long time needed in order to see a phenotype, but makes it difficult to separate the effects of the mutation from the ones of the overexpression of the protein, especially if the study lacks an appropriate control overexpressing the wild-type protein at similar levels (Logan et al., 2019).

### 1.6.2 Induced Pluripotent Stem Cells

The introduction of induced pluripotent stem cells (iPSCs) as a disease model represented a turning point in the field of NMDs, and in particular neurodegenerative disorders. Human iPSCs have key advantages in comparison to animal models: (1) their self-renewal ability supplies a virtually unlimited source of experimental material, (2) their human origin grants the identical genomic organization of the affected organism, (3) the possibility of reprogramming patient-derived cells provides the peculiar genetic background of the affected individual, (4) the availability of cell-type specific protocols allows their differentiation in the most disease-relevant cell types (Logan et al., 2019).

In order to study a specific disease-associated variant, two approaches are possible:

1. reprogramming patient-derived cells into iPSCs

This method requires patient-derived cells, whose collection can sometimes be problematic. However, while the first protocols generated iPSCs from fibroblasts and thus required a skin biopsy, novel ones reprogram other cell types using blood or urine (Loh et al., 2009; Xue et al., 2013). Direct reprogramming has the advantage to preserve the genetic background of the affected individual, but a thorough characterization (morphological evaluation, pluripotency marker expression, karyotyping) of the newly established iPSC line is required (Steege et al., 2021).

2. genome editing of an established iPSC line

The introduction of the desired variant in a wild-type cell line has the advantage of rendering superfluous the use of patient-derived material. Genome editing can be achieved using several tools, such as zinc-finger nucleases (ZFN), Transcription Activator-Like Effector Nuclease (TALEN), CRISPR/Cas9 or base editing (McTague et al., 2021). In particular, the versatility and ease of the CRISPR/Cas9 technology made it the method of choice for genome editing (McTague et al., 2021). This approach requires the screening of potential off-target sites of the tool used, but it proves less laborious and presents a fundamental advantage: the generation of isogenic lines, which just differ for the introduced mutation. Therefore, the observed experimental differences can be reliably attributed to the genetic modification and confounding effects of the genetic background or reprogramming strategies can be minimized (McTague et al., 2021). Moreover, genome editing can also be alternatively applied to correct the disease-causing variant in iPSCs reprogrammed from patient-derived cells, in order to test the reversal of the mutation-related phenotypes (McTague et al., 2021).

iPSC can be then differentiated into:

- two-dimensional (2D) cultures

These represent the most commonly used modelling systems (Logan et al., 2019). Using different protocols, iPSCs can be differentiated into different subtypes of neural cells, obtaining a homogeneous culture in relatively short time and in a fairly reproducible way, thus allowing the analysis of cell-type specific physiology and cell morphology with high resolution (Logan et al., 2019). However, the short differentiation time and the lack of complex organization and interaction between different cell types produces immature cells (McTague et al., 2021).

- three-dimensional (3D) organoids

Organoids represent a more complex model, since they are composed by multiple cell types and are able to recapitulate to some extent the brain architecture and function (Logan et al., 2019; McTague et al., 2021). Due to their longer generation time, they resemble more mature cells and allow for complex neuronal network formation (McTague et al., 2021). However, the diffusion of nutrients and oxygen to their core limits their growth and long-term culture (Logan et al., 2019). Therefore, novel strategies to provide support are currently under investigation,

like alternative scaffolds or methods to induce their vasculature development (McTague et al., 2021). Unfortunately, due to the technical challenges, the reproducibility of cerebral organoids is low, with high batch-to-batch variability and their generation requires longer time and higher money investments (McTague et al., 2021).

Both 2D cultures and 3D organoids produce immature cells resembling neural populations of the human fetal nervous system (McTague et al., 2021). For this reason, phenotypes commonly seen in neurodegenerative disorders might not be observed in these models (Logan et al., 2019). For example, a common pathological finding in these disorders is protein aggregation: Alzheimer's disease is characterized by the presence of extracellular senile plaques of  $\beta$  amyloid and intracellular neurofibrillary tangles (Hampel et al., 2021), Parkinson's disease displays Lewy bodies as pathological hallmark (Spillantini et al., 1997), Huntington's disease presents intraneuronal inclusions of huntingtin (DiFiglia et al., 1997), and ALS MNs show TARDBP-positive inclusions (Neumann et al., 2006). However, the majority of the studies that used iPSCs to model these disorders did not address or report the presence of protein aggregation, whose lack is likely attributed to their immaturity (Logan et al., 2019).

Therefore, strategies to boost cellular maturation have been investigated (Logan et al., 2019). For example, the use of high-passage iPSCs has been proposed, due to the induction of ageing marks (Petrini et al., 2017). However, this method is unpractical because of the long waiting time and the increased risk of the chromosomal abnormalities occurrence in the cell line. Other published approaches have been the expression of progerin or the treatment with telomerase-inhibitors of the iPSC cultures (Miller et al., 2013; Vera et al., 2016).

As an alternative to these iPSC-ageing strategies, methods for the direct reprogramming of somatic cells into neural cells were developed (Mertens et al., 2015; Tang et al., 2017). Even if these techniques allow the retention of ageing hallmarks, they have major limitations: (1) the derived neurons cannot be further expanded, resulting in a reduction of experimental material available; (2) each reprogramming event is independent from the others, introducing higher batch-to-batch differences and decreasing the reproducibility of the results (Logan et al., 2019). In order to overcome these drawbacks, several protocols have been developed to generate proliferating induced neural progenitor cells (iNPCs) and differentiate them in neural subtypes (Hou et al., 2017; Meyer et al., 2014; Mirakhori et al., 2015). However, it is not clear if iNPCs-derived cultures mimic better than the iPSC-derived ones the disease phenotypes (Logan et al., 2019).

## 2 Aim

The aim of the study performed in this PhD thesis was to identify novel genes underlying neuromuscular diseases and to provide insights in their pathomechanisms.

This work started in the frame of the "Workpackage 2" of the EU-funded Horizon 2020 NeurOmics project, whose goal was the identification of novel NMD genes. To achieve this goal, the workflow reported by Karakaya et al. (2018) was followed. Briefly:

1. Individuals showing signs compatible with LMN disease, such as muscle weakness, hypotonia or muscle atrophy were enrolled and clinically characterized based on a questionnaire including patient and family history, neuromuscular clinical alterations, biochemical testing, electrophysiological and imaging studies;
2. Deletions or mutations in *SMN1* were tested by MLPA and long-range PCR and sequencing of *SMN1* genomic region;
3. If negative, a targeted Gene Panel Testing, covering 62 - 479 genes, was performed and analyzed;
4. If negative, exome / genome sequencing were carried out and analyzed;
5. In the presence of a candidate gene for the NMD, further functional studies were implemented.

These investigations depend on the pathophysiological hypothesis. For example, in presence of variants predicted to lead to altered gene expression, control and patient-derived fibroblasts or lymphoblastoid lines can be established and reverse transcription PCR can be carried out. Alternatively, especially if a gain-of-function mechanism is suspected, wild-type or mutant constructs can be designed and expressed in cellular models, such as HEK293T and SH-SY5Y cell lines. The effect of a variant can also be investigated in more sophisticated systems, as iPSCs, which can be genetically engineered to introduce the studied mutation and subsequently differentiated in the affected cell type. Furthermore, animal models carrying mutations comparable to the affected individuals' can be examined, in particular when complex phenotypes involving the interaction between different tissues or organs need to be researched.

## 3 Main Publications

### 3.1 Biallelic Loss of *PIEZO2* causes Distal Arthrogryposis

**Delle Vedove A\***, Storbeck M\*, Heller R, Hölker I, Hebbar M, Shukla A, Magnusson O, Cirak S, Girisha KM, O'Driscoll M, Loeys B, Wirth B. Biallelic Loss of Proprioception-Related *PIEZO2* Causes Muscular Atrophy with Perinatal Respiratory Distress, Arthrogryposis, and Scoliosis. *Am J Hum Genet.* 2016 Nov 3;99(5):1206-1216. doi: 10.1016/j.ajhg.2016.09.019. Epub 2016 Oct 27. Erratum in: *Am J Hum Genet.* 2016 Dec 1;99(6):1406-1408. PMID: 27843126; PMCID: PMC5097934.

\* The authors contributed equally to this work

#### 3.1.1 Description

Biallelic loss-of-function mutations in *PIEZO2* (GenBank: NM\_022068) were identified in ten affected individuals from four independent families showing distal arthrogryposis (congenital talipes equinovarus, hands camptodactyly), transient respiratory distress at birth, hypotonia, delayed motor milestones, absent deep tendon reflexes, muscle weakness, and scoliosis. After negative *SMN1* testing, the index patient from one family and two affected individuals from another family underwent ES with the respective unaffected parents. Due to the consanguinity of the families, an autosomal recessive mode of inheritance was assumed and homozygous variants were prioritized in the affected individuals. This allowed the identification of the homozygous c.5621del and c.1550\_1552delinsCGAA variants in *PIEZO2*. In a third family, three individuals showing a similar phenotype were first investigated by homozygosity mapping, which detected a 13 Mb region containing *PIEZO2*. Therefore, *PIEZO2* exons harboring the dominant variants causing distal arthrogryposis type 3 (DA3), distal arthrogryposis type 5 (DA5) and Marden-Walker Syndrome (MWS) (exons 15, 20, 43, 45, 52) (Coste et al., 2013; McMillin et al., 2014; Okubo et al., 2015) were sequenced by Sanger sequencing, which led to the identification of the c.3019\_3029del variant. An additional individual belonging to a fourth family and displaying similar clinical features underwent microarray analysis, which revealed a homozygous deletion of ~63 kb containing *PIEZO2* exons 6 and 7. Available additional family members were Sanger sequenced for their relatives' specific variants for the segregation analysis, which confirmed an autosomal recessive pattern of inheritance. Since three variants were frameshift and the out-of-frame deletion of two exons was likely to result in the loss of *PIEZO2* due to nonsense-mediated mRNA decay, we established fibroblast cell lines from several individuals of the first two families in order to verify changes in *PIEZO2* expression. Indeed, cell lines of affected individuals showed reduced gene expression, which could be partially rescued using nonsense-mediated mRNA decay inhibitors, such as emetine and cycloheximide. Moreover, we investigated the possible effects of the variants on splicing, and discovered the expression of a  $\Delta 13$  isoform in the individuals harboring a variant in exon 13 of *PIEZO2*.

### 3.1.2 Own Contributions

I analyzed the exome sequencing data of family A together with the postdoc Dr. Markus Storbeck and we identified the variant in *PIEZO2*. I analyzed the exome sequencing data from family C and identified the corresponding *PIEZO2* variant. I designed, carried out and analyzed the Sanger sequencing from families A, B and C. Together with Dr. Raoul Heller, I collected clinical information from families A and C during the affected individuals' examination. I kept in culture fibroblasts from families A and C, and performed the reverse-transcription PCR experiments. I wrote the "Supplemental Case Reports" in the "Supplemental Data and the Considerations for differential diagnosis" with Dr. Raoul Heller. I drew Figure 1 with Dr. Markus Storbeck. I compiled Table 1 together with Dr. Markus Storbeck and Dr. Raoul Heller. I reviewed the draft of the manuscript.

## 3.2 Biallelic Loss of *VAMP1* causes a Congenital Myasthenic Syndrome

Salpietro V\*, Lin W\*, **Delle Vedove A\***, Storbeck M, Liu Y, Efthymiou S, Manole A, Wiethoff S, Ye Q, Sagar A, McElreavey K, Krishnakumar SS; SYNAPS Study Group, Pitt M, Bello OD, Rothman JE, Basel-Vanagaite L, Hubshman MW, Aharoni S, Manzur AY, Wirth B, Houlden H. Homozygous mutations in *VAMP1* cause a presynaptic congenital myasthenic syndrome. *Ann Neurol*. 2017 Apr;81(4):597-603. doi: 10.1002/ana.24905. Epub 2017 Mar 29. PMID: 28253535; PMCID: PMC5413866.

\* The authors contributed equally to this work

### 3.2.1 Description

Biallelic loss-of-function mutations in *VAMP1* (GenBank: NM\_014231) were identified in four affected individuals from two independent families showing severe hypotonia, muscle weakness, feeding difficulties, and delayed motor milestones. The index patient from the first family tested negatively for *SMN1* deletions and for pathological variants in 62 NMD-causing genes present in a targeted gene panel (Karakaya et al., 2018). Therefore, together with his affected sister and their unaffected parents, he underwent genome sequencing, which allowed the identification of the homozygous c.146G>C variant in *VAMP1*. A second family with two individuals showing a similar phenotype was examined independently and the trio-based ES of the index patient and the unaffected parents identified the homozygous variant c.51\_64del. Sanger sequencing confirmed the segregation of the variants in other affected individuals. *Vamp1* is expressed at the mouse presynaptic MN terminal (Liu et al., 2011), and mice carrying a homozygous nonsense variant in *Vamp1* (*Vamp1<sup>lew/lew</sup>*) display the lethal-wasting phenotype characterized by immobility by post-natal day 10 (P10) and death around P15 (Nystuen et al., 2007). Therefore, affected individuals underwent EMG and NCS, which detected electrophysiological alterations compatible with a presynaptic congenital myasthenic syndrome. Indeed, treating the affected individuals with acetylcholinesterase inhibitors improved the symptoms. Electrophysiological evaluation of *Vamp1<sup>lew/lew</sup>* mice confirmed a reduction of the amplitude of endplate potentials (EPP) and synaptic facilitation upon low-frequency (10 Hz) repetitive nerve stimulation, compatible with a presynaptic CMS.

### 3.2.2 Own Contributions

I analyzed the genome sequencing data of family 2 (B) together with the postdoc Dr. Markus Storbeck. I wrote the draft of the clinical part of the manuscript and compiled the Table 1 part about family 2 (B). I drew parts of Figure 1 and reviewed the manuscript draft.

### 3.3 CAPRIN1<sup>P512L</sup> causes early-onset ataxia, muscle weakness and

**Delle Vedove A**, Natarajan J, Zanni G, Eckenweiler M, Muiños-Bühl A, Storbeck M, Guillén Boixet J, Barresi S, Pizzi S, Hölker I, Körber F, Franzmann TM, Bertini ES, Kirschner J, Alberti S, Tartaglia M, Wirth B. CAPRIN1<sup>P512L</sup> causes aberrant protein aggregation and associates with early-onset ataxia. *Cell Mol Life Sci*. 2022 Sep 22;79(10):526. doi: 10.1007/s00018-022-04544-3. PMID: 36136249; PMCID: PMC9499908.

#### 3.3.1 Description

The identical *de novo* c.1535C>T variant in *CAPRIN1* (GenBank: NM\_005898) was identified in two affected individuals from two independent families showing early-onset ataxia, muscle weakness, cognitive delay with cerebellar atrophy on MRI. The first individual developed of gait abnormalities and predominantly proximal muscle weakness at 10 years of age. In the following years, her symptoms worsened with ataxia, increased muscle weakness and cognitive decline, which made her bedridden. A second individual from an independent family showed dysarthria at 4 years of age, ataxia and learning difficulties at 7 years of age and ataxia and muscle weakness around 12 years of age. The first individual tested negative for *SMN1* deletions or pathological variants in a targeted gene panel containing 62 NMD-causing genes (Karakaya, 2018). Both affected individual-parents trios underwent ES, which identified the identical CAPRIN1 p.Pro512Leu mutation (CAPRIN1<sup>P512L</sup>). A third 14-year-old individual with ataxia, cerebellar atrophy and axonal neuropathy, carrying the same *de novo* variant was identified through GeneMatcher just after the approval of the manuscript and was added as a note edit in proof (Sobreira et al., 2015). Since CAPRIN1 is a RNA-binding protein harboring a prion-like domain (PrLD) and PrLD-containing proteins are associated to neurodegenerative disorders through increased protein aggregation, we hypothesized an analogous mechanism for CAPRIN1<sup>P512L</sup>. Indeed, *in silico* analyses uncovered an increased aggregation propensity of the mutant protein and overexpression of CAPRIN1<sup>P512L</sup> in HEK293T cells demonstrated a reduction of its solubility. CAPRIN1<sup>P512L</sup> overexpression in SH-SY5Y cells led to the formation of ubiquitinated aggregates, which sequestered other proteins associated with neurodegenerative disorders (ATXN2, GEMIN5, SNRNP200 and SNCA). To investigate the mutant effects in neurons, we generated a heterozygous CAPRIN1<sup>WT/P512L</sup> and a homozygous CAPRIN1<sup>P512L/P512L</sup> iPSC lines by CRISPR/Cas9 gene editing. iPSC-derived cortical neurons harboring the CAPRIN1<sup>P512L</sup> mutation displayed reduced neuronal activity and altered stress granule dynamics. To further study the P512L effects on the protein, we used nano-differential scanning fluorimetry and fluorescence correlation spectroscopy, which revealed that CAPRIN1<sup>P512L</sup> adopts an extended conformation. Moreover, fluorescence anisotropy measurements detected a decrease in the RNA-binding affinity of CAPRIN1<sup>P512L</sup>, and fluorescence microscopy uncovered a dramatic increase in protein aggregation upon RNA addition.

### 3.3.2 Own Contributions

I analyzed the exome sequencing data of the first family together with the postdoc Dr. Markus Storbeck. I carried out the *in silico* modeling of the effects of CAPRIN1<sup>P512L</sup>, performed the overexpression experiments in HEK293T and SH-SY5Y cells. I performed the solubility analysis of CAPRIN1. I carried out the immunofluorescence experiments in SH-SY5Y cells, acquired the images and quantified the aggregates' parameters. I generated isogenic CAPRIN1<sup>WT/P512L</sup> and CAPRIN1<sup>P512L/P512L</sup> iPSC lines from the CAPRIN1<sup>WT/WT</sup> one using CRISPR/Cas9 gene editing and differentiated them into cortical neurons. I performed the NaAsO<sub>2</sub> treatment and compiled a macro to analyze the images. I recorded the spontaneous neuronal activity using a microelectrode array system and analyzed the data. I wrote the manuscript and drew the figures.

## 4 Discussion

This work confirms the extreme clinical and genetic heterogeneity of NMDs and the use of high-throughput sequencing as valuable tool to reach a diagnosis.

In addition to the discussion in the specific paper, this section provides an update about the knowledge regarding the identified genes that was attained after their publication.

### 4.1 *PIEZO2* & Distal Arthrogryposis

Other classifications of DA have been suggested in addition to the one of Bamshad et al. (2009) (Hall et al., 2019), which still remains useful as clinical classification, because of the unique features that aid in making a diagnosis. Recently, Griffet et al. (2021) classified DA into disorders caused by mutations in sarcomeric proteins and *PIEZO2*. He identifies some clinical features shared by the individuals carrying mutations of the sarcomeric proteins, such as ulnar deviation of the fingers, finger overlap, camptodactyly, foot deformities, while he recognizes blepharophimosis, restrictive lung disease, and muscle hypertonicity as characteristics of the individuals carrying *PIEZO2* mutations.

Since the publication of Delle Vedove et al. (2016), several articles and/or reports presented other individuals carrying biallelic mutations in *PIEZO2* and displaying a phenotype now known as distal arthrogryposis with impaired proprioception and touch (DAIPT, MIM: #617146) (Behunova et al., 2019; Chesler et al., 2016; Haliloglu et al., 2017; Klaniewska et al., 2021; Mahmud et al., 2017; Masingue et al., 2019; Oakley-Hannibal et al., 2020; Yamaguchi et al., 2019). Other affected individuals are reported in other works, but their detailed clinical description is lacking (Marshall et al., 2020; Szczot et al., 2018). The summary of the main phenotypes of these individuals is summarized in Table 6. Most of them are born from consanguineous parents and carry homozygous loss-of-function *PIEZO2* variants, often causing a frameshift or disrupting splicing. The main clinical characteristics are the presence of DA, hypotonia at birth and motor development delay. Very common at birth is the presence of respiratory insufficiency, and/or feeding difficulties. Spine deformities, such as scoliosis or kyphosis, often develop during infancy and childhood. When investigated, light touch sensation and proprioception are compromised, while there are no alterations in the perception of pain. Cognitive impairment was reported only in few individuals and is not a main feature of the affected individuals. Many progresses regarding *PIEZO2* were done after the publication of Delle Vedove et al. (2016). Due to the large size of the protein, the presence of multiple transmembrane domains and the formation of oligomers, uncovering its structural features has been particularly challenging. While it was clear that *PIEZO* channel pore properties were dictated by the C-terminal region (Coste et al., 2015), cryo-electron microscopy allowed the resolution of the channel structure just recently (Saotome et al., 2018; Wang et al., 2019; Zhao et al., 2018). *PIEZO2* is a three-bladed, propeller-like trimer, forming a nano-dome with an extracellular cap-like structure and a intracellular beam. Each protomer contains 36 transmembrane segments organized in 9 units of four transmembrane helices (THU) and 2 transmembrane segments enclosing the central pore (Wang et al., 2019). Interestingly, Delle Vedove et al. (2016) observed exon 13 skipping in patient-derived fibroblast cell lines harboring a homozygous frameshift mutation in this exon. While *PIEZO2* expression in these cell lines is clearly reduced, the

presence of this alternative isoform is not sufficient to counteract the lack of the full-length PIEZO2. Indeed, a  $\Delta 13$  isoform would lack the residues 510-586, leading to the deletion of the transmembrane segments TM10 and TM11 of the THU3, therefore probably altering PIEZO2 activation properties.

Moreover, over the past years the knowledge about the role of *PIEZO2* in several physiological processes was deepened. In particular, many of the phenotypes presented by the individuals carrying biallelic loss-of-function mutations in *PIEZO2* were mirrored in mouse models (Szczot et al., 2021).

A good percentage of the individuals lacking *PIEZO2* displayed respiratory insufficiency and feeding difficulties after birth. While it was already reported that constitutive *Piezo2* knock-out (KO) in mice leads to perinatal death (Dubin et al., 2012), Nonomura et al. (2017) was able to pinpoint the fundamental *PIEZO2* role in airway stretch sensation: constitutive *Piezo2* KO mice show signs of respiratory distress and fail to suckle, they display a lower respiratory frequency and O<sub>2</sub> blood saturation (Nonomura et al., 2017), without defects in embryonic lung development. *Piezo2* conditional KO in sensory neurons demonstrated that the respiratory deficits depend on the lack of airway stretch sensing by these neuronal population.

Due to the difficulties in a reliable assessment of light-touch sensation and proprioception, their alterations were investigated only in a subset of affected individuals (Case et al., 2021; Chesler et al., 2016), where they were found compromised. Comparably, mice lacking *PIEZO2* in Merkel cells and sensory neurons showed a reduction in the neuronal firing rate upon skin stimulation and in the sensitivity to von Frey filaments stimulation (Ranade et al., 2014; Woo et al., 2014). *PIEZO2* loss in Merkel cells was also linked to a reduction in inhibitory signals in pruriceptive pathways, leading to the development of alopecia, the sensation of itch upon innocuous mechanical stimuli (Feng et al., 2018). However, this condition was not reported by any affected individual. A possible justification is that alopecia is a condition associated with ageing and the individuals lacking *PIEZO2* might not have developed it, since they have generally a young age. Moreover, it was recently demonstrated the important role of *PIEZO1* in pruriception (Hill et al., 2022). When investigated, individuals lacking *PIEZO2* showed proprioceptive deficits, compatible with sensory ataxia (Chesler et al., 2016). These features are recapitulated by selective *Piezo2* KO in sensory neurons, which led to a dramatic reduction in muscle spindles firing upon stretch and abnormal limb positioning compatible with proprioceptive deficits (Woo et al., 2015). Moreover, proprioceptive deficits are the likely underlying pathomechanism of the spinal and hip deformities found in several individuals: indeed, *Piezo2* conditional KO in osteoblasts and chondrocytes does not lead to the development of any skeletal abnormality. On the contrary, *Piezo2* KO in sensory neurons leads to alterations of the hip and the development of spinal scoliosis and/or kyphosis (Assaraf et al., 2020).

Urinary symptoms represent another subtle phenotype: a small cohort of 8 affected individuals reported several complains, such as a reduction of the voiding frequency, sudden urge incontinence, or feeling of incomplete voiding (Marshall et al., 2020). *Piezo2* was found to be expressed in the urothelium and in the sensory neurons innervating the urinary bladder. Mice carrying a conditional *Piezo2* KO in these cell types showed impaired bladder-stretch sensing and bladder control (Marshall et al., 2020).

Moreover, PIEZO2 was detected in the outer hairy cells of the mouse inner ear (Wu et al., 2017), whose function is the regulation of the sensitivity of the inner hairy cells to the auditory stimuli. *Piezo2* conditional KO in these cells leads to an increase in the acoustic brain response (ABR) threshold for frequencies higher than 32 kHz. No changes in the auditory system of the PIEZO2 affected individuals was reported. This is in agreement with the fact that the human ear is only able to perceive frequencies in the range comprised between 20 and 20000 Hz (Purves, 2018).

PIEZO2 was also detected in the baroreceptors innervating the aorta and the carotid sinus (Zeng et al., 2018). Ablation of PIEZO1 and PIEZO2 in the nodose and petrosal sensory ganglia neurons leads to the abolition of the baroreflex, a physiological decrease in the heart rate upon blood pressure increase (Zeng et al., 2018). Furthermore, the ablation PIEZO2 in vagal and glossopharyngeal aortic baroreceptors eliminated the baroreceptor reflex, pinpointing PIEZO2 as the main mechanoreceptor for blood pressure sensation (Min et al., 2019). However, neither complains of orthostatic hypotension (OH) were expressly made by affected individuals, nor alterations in the baroreflex were reported. This could be related to the relatively young age of the affected individuals, while it is known OH prevalence increases with age (From the American Association of Neurological Surgeons et al., 2018), or the existence of compensatory mechanisms, owing to the PIEZO1 expression.

*Piezo2* is expressed in enteroendocrine cells (EC), where it regulates neurotransmitter release upon mechanical stretch (Alcaino et al., 2018). However, there is no reported phenotype in individuals carrying biallelic PIEZO2 loss-of-function mutations.

**Table 6. Overview of *PIEZO2*-related DAIPT cases**

Study	Delle Vedove et al. (2016)										Chesler et al. (2016)		Mahmud et al. (2017)		Haliloglu et al. (2017)		Masingue Behunova et al. (2019)		Yamaguchi et al. (2019)		Oakley-Hannibal et al. (2020)		Klaniewska et al. (2021)			Tot.																
	TR		IN		LY		PK		BD		EU/JP		BD		TR		TN		AT		JP		IQ		PL		PL	PL														
Nationality	TR		IN		LY		PK		BD		EU/JP		BD		TR		TN		AT		JP		IQ		PL	PL	PL	9/15														
Parental consanguinity	+		+		+		+		-		-		+		+		-		+		+		-	-	-																	
Gender	M	M	F	M	F	M	M	F	F	M	F	F	M	F	F	M	F	F	M	F	F	F	F	F	F		M															
Age	9	23	12	17	10	27	6	5	25	25	19	10	30	23	14	18	20	24	3	12	9	1	2	3																		
Zygosity	hom		hom		hom		hom		hom		CHZ	CHZ	hom	hom	hom	hom	hom	hom	CHZ	hom	hom	CHZ	CHZ	CHZ																		
cDNA change	c.5621del		c.3019_3029del		c.1550_1552del insCGAA		del exons 6-7		c.4723C>T		c.5053C>T		c.5053C>T		c.5054G>C		c.2708C>G		c.1384C>T		c.3241C>T		c.76C>T		c.1528-1G>T		c.4171_4174del		c.1895_1896del		c.1080+1G>A		c.4092+1G>T		c.6175_6191del		c.6355+1G>T		c.6088C>T		c.7613+1G>A	
Protein alteration	p.L1874Rfs*5		p.P1007Lfs*3		p.S517Tfs*48		p.?		p.R1575*		p.R1685*		p.R1685*		p.R1685P		p.S903*		p.R462*		p.R1051*		p.R26*		p.?		p.V1391Kfs*39		p.Q632Rfs*32		p.?		p.?		p.S2059Efs*73		p.?		p.R2030*		p.?	
Consequence	fs		fs		fs		sp		fs		fs		fs		fs		fs		fs		sp		fs		fs		fs		sp		sp		fs		sp		fs		sp			
Short stature	-	+	+	+	+	+	+	na	+	+	na	na	+	+	+	+	na	na	-	+	-	+	+	+	+	+	-	na	na	na	na	na	na	na	na	na	na	na	na	13/16		
Feeding difficulties	-	na	+	na	na	na	+	na	na	+	+	+	na	na	na	+	-	-	+	+	+	+	+	+	+	+	+	+	+	+	+	+	+	+	+	+	+	+	+	+	12/15	
Perinatal respiratory distress	+	+	+	+	+	na	+	na	na	na	na	na	na	na	na	-	+	+	+	+	-	-	+	-	+	-	+	-	+	-	+	-	+	-	+	-	+	-	+	11/15		
Hypotonia	+	+	+	+	+	na	+	+	na	+	+	+	+	+	+	+	+	+	+	+	+	+	+	+	+	+	+	+	+	+	+	+	+	+	+	+	+	+	+	+	22/22	
Motor delay	+	+	+	+	+	+	+	+	+	+	+	+	+	+	+	+	+	+	+	+	+	+	+	+	+	+	+	+	+	+	+	+	+	+	+	+	+	+	+	+	24/24	

*continues* →

→ Table 6 (continued)

Study	Delle Vedove et al. (2016)										Chesler et al. (2016)					Mahmud et al. (2017)					Haliloglu Masingue Behunova Yamaguchi Hannibal et al. (2017) et al. (2019) et al. (2019)			Oakley-Klaniewska et al. (2020) (2021)			Tot
	na	+	+	na	+	+	+	+	+	na	na	na	na	+	na	na	na	na	na	na							
Touch impairment	na	+	+	na	+	+	+	+	+	na	na	na	na	+	na	na	na	na	8/8								
Vibration impairment	na	+	na	+	+	na	na	na	-	na	na	na	+	na	na	na	na	4/5									
Proprioception impairment	na	na	na	na	na	na	na	na	na	na	+	+	+	+	+	+	+	na	+	na	na	na	na	na	9/9		
Pain impairment	na	na	na	na	na	na	na	na	na	na	-	-	+	+	+	-	na	na	na	na	na	na	-	na	3/7		
Absent DTR	+	+	+	+	+	+	+	+	+	na	+	+	+	+	+	na	+	+	+	+	-	+	+	+	21/22		
DA hand foot	+	+	+	+	+	+	+	+	+	+	+	+	+	+	+	+	+	+	+	+	+	+	+	+	24/24		
Thumb deformity	+	+	-	+	-	+	+	+	na	+	+	-	+	+	+	+	na	na	-	+	-	na	-	+	14/20		
Spinal deformity	+	+	+	+	-	+	+	+	+	+	+	+	+	+	+	+	+	+	+	+	+	+	-	+	22/24		
Urinary symptoms	+	na	+	+	na	na	na	na	na	na	na	na	na	na	na	na	3/3										
Cognitive impairment	-	-	-	-	-	-	+	+	-	+	-	-	-	-	-	-	-	-	-	-	na	-	-	+	4/23		

TR: Turkey; IN: India; LY: Libya; PK: Pakistan; BD: Bangladesh; EU/JP: Europe/Japan; TN: Tunisia; AT: Austria; JP: Japan; IQ: Iraq; PL: Poland; +: present; -: absent; na: not available; M: male; F: female; hom: homozygous; CHZ: compound heterozygous; fs: frameshift; sp: splicing; mis: missense

## 4.2 *VAMP1* & Congenital Myasthenic Syndromes

Since our work associating *VAMP1* biallelic variants with CMS, additional cases of *VAMP1*-associated CMS were described (Table 7) (Monies et al., 2017; Nair et al., 2018; Polavarapu et al., 2021; Shen et al., 2017). The affected individuals mostly belong to consanguineous families and carry homozygous *VAMP1* frameshift variants. They present congenital severe hypotonia, feeding difficulties and/or respiratory distress, muscle weakness with delayed motor milestones. If administered, AChE inhibitors improved the symptoms.

Moreover, variants in novel genes have been associated with CMS (Table 8).

**Table 7. Overview of *VAMP1*-related CMS cases**

Study	Shen et al. (2017)	Salpietro et al. (2017)			Monies et al. (2017)		Nair et al. (2018)	Polavarapu et al. (2021)			Total	
	Brazilian	Kuwaiti	Israeli	Saudi Arabian		Lebanese	Indian					
Nationality	Brazilian	Kuwaiti	Israeli	Saudi Arabian		Lebanese	Indian					
Parental consanguinity	+	+	+	+	+	-	na	+	+	+	+	9/11
Gender	F	F	M	M	F	F	M	na	F	F	F	
Zygoty	hom	hom	hom	hom	hom	hom	hom	hom	hom	hom	hom	
cDNA change	c.340del	c.51_64del	c.146G>C	c.129+1G>A	c.128_129del	c.97C>T	c.66del	c.202C>T	c.97C>T			
Protein alteration	p.Ile114Serfs*72	p.Gly18Trpfs*5	p.Arg49Pro	p.?	p.Glu43Glyfs*24	p.Arg33*	p.Gly23Alafs*6	p.Arg68*	p.Arg33*			
Onset	birth	birth	birth	PN	birth	birth	birth	na	birth	birth	birth	
Hypotonia	+	+	+	+	+	+	+	na	+	+	+	10/10
Feeding difficulties / respiratory distress	+	+	+	+	+	na	na	na	+	+	+	8/8
Muscle weakness	+	+	+	+	+	+	+	na	+	+	+	10/10
Delayed motor milestones	+	+	+	+	+	na	+	na	+	+	+	9/9
Ophtalmoplegia	+	+	+	+	+	na	na	na	+	-	na	6/7
CMAP		↓	↓	↓	na	na	na	na	na	na	na	
Low freq. RNS	↓	na	na	na	na	na	na	na	na	na	na	
High freq. RNS	↑	↑	↑	na	na	na	na	na	na	na	na	
Muscle biopsy	Type 2 fiber atrophy	na	Myopathic features	na	na	na	na	na	Fiber size variation	na	Fiber size variation	
AChE inhibitors response	+	+	+	+	+	na	na	na	+	+	na	7/7

CMAP: Compound Muscle Action Potential; RNS: Repetitive Nerve Stimulation; AChE: Acetylcholinesterase; +: present; -: absent; na: not available; F: female; M: male; hom: homozygous; PN: prenatal

**Table 8. Novel CMS-related genes**

Localization of the defect	Prevalence (%)	Gene	Inheritance	Clinical presentation	Response to AChE inhibitors
Presynaptic	5 – 10				
Acetylcholine synthesis and recycling	< 1	<i>SLC5A7</i>	AR	Early onset, arthrogryposis/joint contractures, apneic crisis at birth, marked ptosis, ophthalmoplegia, muscle fatigability. Sometimes learning difficulties	Some improvement
Synaptic	15 - 20				
Basal lamina defects	< 1	<i>LAMA5</i>	AR	Muscle weakness, myopia, facial tics	Improvement

AChE: Acetylcholinesterase; AR: autosomal recessive

### 4.3 *CAPRIN1*-related disorders

As shortly stated in the paper, just after the acceptance for publication of the article, a third 14-years-old female individual affected by ataxia with cerebellar atrophy and axonal neuropathy, harboring the identical *de novo* c.1535C>T variant in *CAPRIN1* was reported through GeneMatcher by S. Donkervoort and C. G. Bönnemann at the National Institute of Neurological Disorders and Stroke (NINDS) of the National Institutes of Health. This unexpected finding represents additional evidence of the causality of the *CAPRIN1*<sup>P512L</sup> mutation, which was identified as likely causative by three independent research groups.

Importantly, the phenotype described in these individuals allows the discrimination with other early-onset hereditary ataxias caused by repeat expansion mutations, which cannot be identified by short-read sequencing technologies. In particular, Friedreich's Ataxia (FRDA), which represents the most common autosomal recessive ataxia (Pandolfo, 2008), could be considered in the differential diagnosis because of the following features: (1) the affected individuals have unaffected parents and this could be compatible with an autosomal recessive inheritance pattern; (2) the disorder has an early onset (<25 years of age); (3) presence of progressive limb ataxia with muscle weakness, dysarthria, absent deep tendon reflexes, scoliosis and sensorimotor neuropathy (Pandolfo, 2008). However, FRDA individuals show mostly subtentorial white matter atrophy with no obvious cerebellar atrophy at MRI imaging (Pandolfo, 2008), while individuals harboring the *CAPRIN1*<sup>P512L</sup> mutation show both cerebellar and cerebral atrophy. Besides, the latter results in intellectual disability, which is absent in FRDA individuals (Pandolfo, 2008). Moreover, most FRDA individuals develop hypertrophic cardiomyopathy and visual deficits late in the disease course (Pandolfo, 2008), which were not described in individuals with the *CAPRIN1*<sup>P512L</sup> mutation.

The other autosomal recessive HA due to repeat expansion mutations is cerebellar ataxia, neuropathy, vestibular areflexia syndrome (CANVAS). However, the age of onset of this disorder is after 35 years (Cortese et al., 2020), and it can reasonably be excluded.

The remaining repeat expansion-related HAs have an autosomal dominant pattern, which is not compatible with the pedigrees of the affected individuals. Even if highly unlikely, the possibility of *de novo* occurrence of the mutations or anticipation cannot exclude completely these diagnosis (Brandsma et al., 2019), which can be discarded because of their clinical features: SCA2 shows parkinsonism; SCA6 has a late-onset and a slow progression; SCA8 displays spasticity; SCA10 and SCA12 are characterized by epilepsy; SCA17 exhibits psychiatric features and chorea (Brandsma et al., 2019).

Of note is the recently reported neurodevelopmental disorder associated with *CAPRIN1* haploinsufficiency by Pavinato et al. (2022). While there have been sporadic reports associating *CAPRIN1* and autism spectrum disorder (ASD) (Du et al., 2020; Jiang et al., 2013), this work presents a cohort of 12 individuals from 10 independent families showing language impairment, intellectual disability, attention-deficit/hyperactivity disorder (ADHD), and ASD as main features. These subjects carry heterozygous loss-of-function variants in *CAPRIN1*. Except for two cases where the variant was inherited by a parent, the others are *de novo* variants, as in previous reports (Du et al., 2020; Jiang

et al., 2013). Indeed, *CAPRIN1* is predicted to be intolerant to loss-of-function variants (pLI = 0.97, gnomAD) and haploinsufficient *CAPRIN1*<sup>+/-</sup> mice exhibited ASD-like phenotypes, such as a reduction in sociality, response to novelty and flexibility in learning (Ohashi et al., 2016). Moreover, *CAPRIN1*<sup>-/-</sup> cultured neurons show an alteration in the dendritic localization of synaptic mRNAs and proteins and alterations in the development of neuronal networks (Ohashi et al., 2016; Shiina et al., 2010). *CAPRIN1*<sup>+/-</sup> iPSC-derived cortical neurons display a reduction in neurite length, electrical activity, and overall survival (Pavinato et al., 2022). The latter could be associated to Ca<sup>2+</sup> overload and increased oxidative stress (Pavinato et al., 2022).

Therefore, mutations in *CAPRIN1* can be associated with two distinct disorders: the *CAPRIN1*<sup>P512L</sup> mutation causes an early-onset neurodegenerative disorder characterized by ataxia, muscle weakness, and mild intellectual disability, while *CAPRIN1* haploinsufficiency causes a neurodevelopmental disorder characterized by language impairment, intellectual disability, ADHD and ASD (Table 9).

**Table 9. Comparison of *CAPRIN1*-related disorders**

	<i>CAPRIN1</i> <sup>P512L</sup>	<i>CAPRIN1</i> haploinsufficiency
Clinical features	Muscle weakness, ataxia, intellectual disability	Language impairment, intellectual disability, ADHD, and ASD
Onset	Childhood	Childhood
Genetic alteration	P.Pro512Leu mutation	<i>CAPRIN1</i> heterozygous loss-of-function mutations
Inheritance	<i>de novo</i>	<i>de novo</i> / AD
iPSC-derived neurons phenotypes	↓ electric activity ↑ SG <sup>+</sup> cells ratio ↑ SG duration	↓ electric activity ↓ survival ↑ Ca <sup>2+</sup> flow ↑ ROS ↑ global translation ↓ dendritic translation
Additional features	↑ aggregation upon overexpression ↑ aggregation upon RNA binding <i>in vitro</i> ↓ RNA affinity <i>in vitro</i>	na
Mouse model	na	↓ sociality ↓ response to novelty ↓ flexibility in learning (from Ohashi et al. (2016))

AD: Autosomal Dominant; ROS: reactive oxygen species; na: not available.

The differences between these phenotypes reflect the distinct pathomechanism of the disorders: *CAPRIN1* is an RNA-binding protein present in dendritic RNA transport granules (Shiina et al., 2005), therefore its haploinsufficiency likely causes an alteration in the neurodevelopment. In neuronal cultures from *Caprin1*<sup>-/-</sup> mice, there was a reduction in the dendritic localization of Na<sup>+</sup>/K<sup>+</sup> ATPase subunits and a poor neuronal network development, or a reduction in the distribution of the GRIA1 subunit of the alpha-amino-3-hydroxy-5-methyl-4-isoxazole propionate (AMPA) receptors (Ohashi et al., 2016; Shiina et al., 2010). On the contrary, individuals carrying the *CAPRIN1*<sup>P512L</sup> mutation showed a normal development until they presented cerebellar signs, muscle weakness and intellectual disability. Therefore, a distinct pathomechanism is likely to be the cause of this disorder.

Our hypothesis is that protein misfolding and aggregation play an important role in the pathophysiology of this disorder. Indeed, a broadly recognized mechanism for several

neurodegenerative disorders, such as ALS or Parkinson's Disease, is protein misfolding (Sprunger & Jackrel, 2021). These diseases are often driven by mutations that decrease the protein solubility and increase their aggregation propensity (Sprunger & Jackrel, 2021). Interestingly, many of these disease-causing mutations affect proteins containing a prion-like domain (PrLD) (Sprunger & Jackrel, 2021). PrLD-containing proteins mainly comprise RNA-binding proteins and have unique properties that allow them to form transient condensates with RNAs and other proteins through a process called liquid-liquid phase separation (LLPS) (Sprunger & Jackrel, 2021). Pathological mutations impair this dynamic and transient process, leading to the formation of gel-like or insoluble condensates, which cause cell toxicity and neuronal degeneration (Sprunger & Jackrel, 2021). Therefore, it is reasonable to hypothesize a similar mechanism for the CAPRIN1<sup>P512L</sup> mutation. Several *in silico* models (PLAAC, ZipperDB, CamSol) predict an increase in CAPRIN1 aggregation (Goldschmidt et al., 2010; Lancaster et al., 2014; Sormanni et al., 2015). Importantly, these algorithms use different strategies to predict the aggregation propensity: the prion aggregation prediction algorithm (PAPA) score from the PLAAC tool is exclusively based on the aminoacid composition (Lancaster et al., 2014; Toombs et al., 2012), while the ZipperDB uses a structure-based approach for its modeling (Goldschmidt et al., 2010). These *in silico* predictions are confirmed by: (1) the biochemical assays proving a reduction of CAPRIN1<sup>P512L</sup> solubility, (2) the presence of aggregates upon its overexpression and (3) the in-depth biochemical studies of the protein.

#### 4.3.1 Open questions and possible future research directions

While this study has provided evidence of an association between the CAPRIN1<sup>P512L</sup> mutation and a novel neurodegenerative disorder, several points can be further investigated:

- the exact role of protein misfolding and aggregation

While several lines of evidence point in the direction of an increased CAPRIN1<sup>P512L</sup> misfolding, this mechanism can be definitively demonstrated just in specimens of the affected tissue. Since all the affected individuals are alive, and there are obvious limitations in accessing brain tissues, this approach was not pursued. An alternative option would be the study of protein aggregation from other patient samples. In other neurodegenerative disorders, such as Parkinson's disease or Alzheimer's disease, several assays have been developed to identify protein aggregation from cerebrospinal fluid or blood serum (Leuzy et al., 2021; Lobanova et al., 2022; Park et al., 2011; Tokuda et al., 2010). For example, Lobanova et al. (2022) recently detected an increase in aggregates' size using phase-controlled and high resolution atomic force microscopy (AFM) on Parkinson's disease serum and cerebrospinal fluid samples. This method could be used to test the presence of aggregates of increased size in the individuals harboring the CAPRIN1<sup>P512L</sup> compared to controls, but cannot identify if they are specifically due to CAPRIN1 aggregation. However, the post-mortem analysis of the tissues would be fundamental to confirm this theory. Moreover, neurodegenerative disease-related proteins undergo misfolding and often organize in amyloid (Soto & Pritzkow, 2018), highly ordered aggregates that can be stained with specific dyes, such as thioflavin T and Congo red (Yakupova et al., 2019). The presence of CAPRIN1 aggregation and amyloidosis could be verified in histopathological sections of these specimens.

Additionally, samples could be fractionated using sarkosyl (Tarutani et al., 2022), and processed with novel methods such as cryo-electron microscopy (Arseni et al., 2022; Yang et al., 2022). Increasing evidence shows that the real toxic species responsible for neuronal degeneration are misfolded oligomers (Soto & Pritzkow, 2018). While fluorescence correlation spectroscopy analysis shows that in absence of RNA CAPRIN1<sup>P512L</sup> association properties do not change, they could be tested with AFM and biochemical methods in iPSC-derived neurons, or fluorescence recovery after photobleaching (FRAP) experiments in cells overexpressing the mutant protein (Chetri et al., 2022).

iPSC-derived neurons harboring the CAPRIN1<sup>P512L</sup> mutation do not show overt protein aggregation, but do show signs of reduced electrical activity. This finding is in line with the majority of the studies that used iPSC-derived neurons to model neurodegenerative disorders, which did not report overt protein aggregation (Logan et al., 2019). However, this prompts the search for other phenotypes, such as impaired neurite length, increased oxidative stress, or mitochondrial dysfunction (Logan et al., 2019). Moreover, since CAPRIN1 is involved in dendritic RNA transport (El Fatimy et al., 2012; Shiina et al., 2005; Shiina et al., 2010), and fluorescence anisotropy measurements show a reduction in RNA-binding affinity, changes in global or local translation can be investigated.

- the relationship between CAPRIN1 and FMR1

CAPRIN1 is an interacting partner of FMR1 (El Fatimy et al., 2012). Interestingly, loss-of-function mutations of both genes are associated to a phenotype characterized by language impairment, ADHD and ASD: *CAPRIN1* haploinsufficiency causes the novel neurodevelopmental disorder described by Pavinato et al. (2022), while trinucleotide repeat expansions > 200 units leading to *FMR1* methylation and silencing cause Fragile X syndrome (FXS) (Hagerman et al., 2017; Pavinato et al., 2022). On the other side, CAPRIN1<sup>P512L</sup> causes a neurodegenerative disorder while shorter trinucleotide repeat expansions (55 – 200 units) of *FRM1* cause FXTAS. Both phenotypes present ataxia and intellectual disability (Hagerman & Hagerman, 2021). However, these disorders differ for (1) the age of onset, which is childhood for the CAPRIN1<sup>P512L</sup>-related disorder and > 50 years for FXTAS (Jacquemont et al., 2003); (2) the MRI findings, which is cerebellar and cerebral atrophy for CAPRIN1<sup>P512L</sup>-related disorder and white matter T2 hyperintensities at MRI at the middle cerebellar peduncles for FXTAS (Hagerman & Hagerman, 2021). Of note, many individuals with FXTAS present parkinsonism and 10% of them Lewy bodies in the substantia nigra upon post-mortem examination (Salcedo-Arellano et al., 2020). This is particularly interesting since in several disorders characterized by protein misfolding cross-seeding, namely the incorporation of distinct aggregation-prone proteins, has been described (Soto & Pritzkow, 2018). Therefore, it is possible that other proteins with prion characteristics, such as ATX2 or  $\alpha$ -synuclein could be found in these aggregates (Jan et al., 2021; March et al., 2016). Moreover, Asamitsu et al. (2021) recently demonstrated that the *FMR1* CGG repeat expansion produces via RAN translation a toxic FMRpolyG protein with prion-

like properties that undergoes phase transition upon the binding of CGG quadruplexes. Therefore, the presence of FMR1 can be studied in CAPRIN1<sup>P512L</sup> aggregates.

- the relationship between CAPRIN1 and GEMIN5

GEMIN5 biallelic loss-of-function mutations have recently been associated to a more severe neurodevelopmental disorder characterized by neurodevelopmental delay and cerebellar atrophy due to disruption of the small ribonuclear proteins (snRNPs) complex or RNA translation (Francisco-Velilla et al., 2022; Kour et al., 2021). Since CAPRIN1 binds GEMIN5 (Vu et al., 2021), its sequestration in CAPRIN1<sup>P512L</sup> aggregates could cause a reduction in GEMIN5 levels. Since GEMIN5 biallelic mutations result in altered GEMIN5 and GEMIN2 localization in iPSC-derived neurons (Kour et al., 2021), these can be directly investigated in CAPRIN1<sup>P512L</sup> iPSC-derived neurons. Moreover, alterations in translation can be studied, since GEMIN5 mutants impair GEMIN5 binding to polysomes for specific mRNAs and CAPRIN1 is also involved with translation regulation (El Fatimy et al., 2012; Francisco-Velilla et al., 2022).

## 5 Additional Publications, Presentations & Scholarships

### 5.1 Additional Publications

#### 5.1.1 Eisenberger T et al., 2018

Eisenberger T, Di Donato N, Decker C, **Delle Vedove A**, Neuhaus C, Nürnberg G, Toliat M, Nürnberg P, Mürbe D, Bolz HJ. A C-terminal nonsense mutation links PTPRQ with autosomal-dominant hearing loss, DFNA73. *Genet Med*. 2018 Jun;20(6):614-621. doi: 10.1038/gim.2017.155. Epub 2017 Oct 12. PMID: 29309402; PMCID: PMC5993672.

##### 5.1.1.1 Own contributions

I cultured control and patient-derived fibroblasts and performed the semiquantitative reverse transcription PCR experiment in Figure 4.

#### 5.1.2 Karakaya M et al., 2018

Karakaya M, Storbeck M, Strathmann EA, **Delle Vedove A**, Hölker I, Altmueller J, Naghiyeva L, Schmitz-Steinkrüger L, Vezyroglou K, Motameny S, Alawbathani S, Thiele H, Polat AI, Okur D, Boostani R, Karimiani EG, Wunderlich G, Ardikli D, Topaloglu H, Kirschner J, Schrank B, Maroofian R, Magnusson O, Yis U, Nürnberg P, Heller R, Wirth B. Targeted sequencing with expanded gene profile enables high diagnostic yield in non-5q-spinal muscular atrophies. *Hum Mutat*. 2018 Sep;39(9):1284-1298. doi: 10.1002/humu.23560. Epub 2018 Jul 25. PMID: 29858556.

##### 5.1.2.1 Own contributions

I analyzed the ES/GS data of some of the individuals reported in the publication. I reviewed the draft of the manuscript.

#### 5.1.3 Janzen E et al., 2019

Janzen E, Wolff L, Mendoza-Ferreira N, Hupperich K, **Delle Vedove A**, Hosseinibarkooie S, Kye MJ, Wirth B. *PLS3* Overexpression Delays Ataxia in *Chp1* Mutant Mice. *Front Neurosci*. 2019 Sep 19;13:993. doi: 10.3389/fnins.2019.00993. PMID: 31607845; PMCID: PMC6761326.

##### 5.1.3.1 Own contributions

I compiled the Fiji macro for the analysis of the image set in Figure 3A.

#### 5.1.4 Pavinato L et al., 2022

Pavinato L, **Delle Vedove A**, Carli D, Ferrero M, Carestiato S, Howe JL, Agolini E, Coviello DA, van de Laar I, Au PYB, Di Gregorio E, Fabbiani A, Croci S, Mencarelli MA, Bruno LP, Renieri A, Veltra D, Sofocleous C, Faivre L, Mazel B, Safrrou H, Denommé-Pichon AS, van Slegtenhorst MA, Giesbertz N, van Jaarsveld RH, Childers A, Rogers RC, Novelli A, De Rubeis S, Buxbaum JD, Scherer SW, Ferrero GB, Wirth B, Brusco A. *CAPRIN1* haploinsufficiency causes a neurodevelopmental disorder with language impairment, ADHD and ASD. *Brain*. 2022 Jul 27:awac278. doi: 10.1093/brain/awac278. Epub ahead of print. PMID: 35979925.

#### 5.1.4.1 Own contributions

I generated the isogenic *CAPRIN1*<sup>+/-</sup> iPSC line by CRISPR/Cas9 genome editing. I reviewed the draft of the manuscript.

#### 5.1.5 Overhoff M et al, 2022

Overhoff M, Tellkamp F, Hess S, Tolve M, Tutas J, Faerfers M, Ickert L, Mohammadi M, De Bruyckere E, Kallergi E, **Delle Vedove A**, Nikolettou V, Wirth B, Isensee J, Hucho T, Puchkov D, Isbrandt D, Krueger M, Kloppenburg P, Kononenko NL. Autophagy regulates neuronal excitability by controlling cAMP/protein kinase A signaling at the synapse. *EMBO J*. 2022 Oct 11:e110963. doi: 10.15252/embj.2022110963. Epub ahead of print. PMID: 36217825.

#### 5.1.5.1 Own contributions

I assisted with the microelectrode array experiment setup and analysis.

## 5.2 Oral Presentations

- 2022.07.25 – 28      **Mechanotransduction, Muscle Spindles and Proprioception**  
Physiological Institute – Munich (Germany)  
„Biallelic loss of *PIEZO2* in humans causes arthrogyriposis and proprioceptive deficits“
- 2022.06.22 – 23      **IPMM Days 2022**  
Center for Molecular Medicine Cologne (CMMC) – Cologne (Germany)  
„A recurrent *de novo* *CAPRIN1* variant causes progressive early onset ataxia“
- 2022.03.16 – 18      **Gesellschaft für Humangenetik Tagung 2022**  
Congress Centrum Würzburg – Würzburg (Germany)  
„A recurrent *de novo* *CAPRIN1* mutation causes a novel progressive early onset neurodegenerative disorder“
- 2021.11.12            **Symposium of the Institute of Human Genetics**  
Institute of Human Genetics, University of Cologne – Cologne (Germany)  
„A recurrent *de novo* *CAPRIN1* mutation causes a novel progressive early onset neurodegenerative disorder“
- 2021.05.04            **Research Track**  
University of Cologne – Cologne (Germany)  
„Gene hunting: finding a needle in a haystack“
- 2019.04.09 – 10      **IPMM Days 2019**  
Center for Molecular Medicine Cologne (CMMC) – Cologne (Germany)  
„A *de novo* mutation of *CAPRIN1* causes a novel progressive NMD“
- 2017.03.15 – 16      **IPMM Days 2017**  
Center for Molecular Medicine Cologne (CMMC) – Cologne (Germany)  
„*PIEZO2* homozygous frameshift mutations cause muscle atrophy with arthrogyriposis, perinatal respiratory distress and scoliosis“

## 5.3 Poster Presentations

- 2021.10.18 – 22      **American Society of Human Genetics Annual Meeting 2021**  
Virtual Meeting  
„A recurrent *de novo* *CAPRIN1* mutation causes a novel progressive early onset neurodegenerative disorder“
- 2021.06.15 – 16      **IPMM Days 2021**  
Center for Molecular Medicine Cologne (CMMC) – Cologne (Germany)  
„*CAPRIN1*: how a recurrent *de novo* mutation causes a progressive early onset neurodegenerative disorder in a prion-like domain-harboring protein“

- 2020.06.06 – 09      **European Society of Human Genetics Conference 2020**  
Virtual Conference  
„A recurrent *de novo* CAPRIN1 mutation causes a novel progressive early onset neurodegenerative disorder“
- 2019.06.15 – 18      **European Society of Human Genetics Conference 2019**  
Swedish Exhibition and Congress Centre – Gothenburg (Sweden)  
„A *de novo* mutation of the stress granules-associated CAPRIN1 causes a novel progressive neurodegenerative disorder“
- 2018.11.15            **Symposium of the Institute of Human Genetics**  
Institute of Human Genetics, University of Cologne – Cologne (Germany)  
„A *de novo* mutation of the stress granules-associated CAPRIN1 causes a novel progressive neurodegenerative disorder“
- 2018.03.28 – 29      **IPMM Days 2018**  
Center for Molecular Medicine Cologne (CMMC) – Cologne (Germany)  
„Homozygous Mutations in *VAMP1* Cause a Presynaptic Congenital Myasthenic Syndrome“
- 2017.03.17            **1<sup>st</sup> Neuroscience Day**  
MIT Lecture Hall Building, University of Cologne – Cologne (Germany)  
„*PIEZO2* homozygous frameshift mutations cause a novel autosomal recessive neuromuscular disorder“
- 2016.02.25 – 26      **IPMM Days 2016**  
Center for Molecular Medicine Cologne (CMMC) – Cologne (Germany)  
„Identification and functional assessment of novel neuromuscular disease-causing genes“
- 2016.03.07 – 09      **NeurOmics Annual Meeting**  
Autonomous University of Barcelona – Bellaterra, Barcelona (Spain)  
„*PIEZO2* homozygous frameshift mutations cause a novel autosomal recessive neuromuscular disorder“

## 5.4 Scholarships

- 2017                    **“IPaK – Promoting International Doctorates at the University of Cologne”**  
University of Cologne – Cologne (Germany)  
Mobility Grant for travel expenses for the „Clinical Genomics and NGS“ course taking place from the 30<sup>th</sup> April to the 5<sup>th</sup> May 2017 in Bertinoro (Italy)

## 6 References

- Abicht, A., Müller, J. S., & Lochmüller, H. (2003, December 23, 2021). *Congenital Myasthenic Syndromes Overview*. Retrieved September 4 from <https://www.ncbi.nlm.nih.gov/books/NBK1168/>
- Alcaino, C., Knutson, K. R., Treichel, A. J., Yildiz, G., Strege, P. R., Linden, D. R., Li, J. H., Leiter, A. B., Szurszewski, J. H., Farrugia, G., & Beyder, A. (2018). A population of gut epithelial enterochromaffin cells is mechanosensitive and requires Piezo2 to convert force into serotonin release. *Proc Natl Acad Sci U S A*, *115*(32), E7632-E7641. <https://doi.org/10.1073/pnas.1804938115>
- Arseni, D., Hasegawa, M., Murzin, A. G., Kametani, F., Arai, M., Yoshida, M., & Ryskeldi-Falcon, B. (2022). Structure of pathological TDP-43 filaments from ALS with FTL. *Nature*, *601*(7891), 139-143. <https://doi.org/10.1038/s41586-021-04199-3>
- Asamitsu, S., Yabuki, Y., Ikenoshita, S., Kawakubo, K., Kawasaki, M., Usuki, S., Nakayama, Y., Adachi, K., Kugoh, H., Ishii, K., Matsuura, T., Nanba, E., Sugiyama, H., Fukunaga, K., & Shioda, N. (2021). CGG repeat RNA G-quadruplexes interact with FMRpolyG to cause neuronal dysfunction in fragile X-related tremor/ataxia syndrome. *Sci Adv*, *7*(3). <https://doi.org/10.1126/sciadv.abd9440>
- Assaraf, E., Blecher, R., Heinemann-Yerushalmi, L., Krief, S., Carmel Vinestock, R., Biton, I. E., Brumfeld, V., Rotkopf, R., Avisar, E., Agar, G., & Zelzer, E. (2020). Piezo2 expressed in proprioceptive neurons is essential for skeletal integrity. *Nat Commun*, *11*(1), 3168. <https://doi.org/10.1038/s41467-020-16971-6>
- Babin, P. J., Goizet, C., & Raldua, D. (2014). Zebrafish models of human motor neuron diseases: advantages and limitations. *Prog Neurobiol*, *118*, 36-58. <https://doi.org/10.1016/j.pneurobio.2014.03.001>
- Bamshad, M., Van Heest, A. E., & Pleasure, D. (2009). Arthrogyrosis: a review and update. *J Bone Joint Surg Am*, *91 Suppl 4*, 40-46. <https://doi.org/10.2106/JBJS.I.00281>
- Barbosa-Gouveia, S., Vazquez-Mosquera, M. E., Gonzalez-Vioque, E., Hermida-Ameijeiras, A., Sanchez-Pintos, P., de Castro, M. J., Leon, S. R., Gil-Fournier, B., Dominguez-Gonzalez, C., Camacho Salas, A., Negrão, L., Fineza, I., Laranjeira, F., & Couce, M. L. (2022). Rapid Molecular Diagnosis of Genetically Inherited Neuromuscular Disorders Using Next-Generation Sequencing Technologies. *J Clin Med*, *11*(10). <https://doi.org/10.3390/jcm11102750>
- Barp, A., Mosca, L., & Sansone, V. A. (2021). Facilitations and Hurdles of Genetic Testing in Neuromuscular Disorders. *Diagnostics (Basel)*, *11*(4). <https://doi.org/10.3390/diagnostics11040701>
- Behunova, J., Gerykova Bujalkova, M., Gras, G., Taylor, T., Ihm, U., Kircher, S., Rehder, H., & Laccone, F. (2019). Distal Arthrogyrosis with Impaired Proprioception and Touch: Description of an Early Phenotype in a Boy with Compound Heterozygosity of PIEZO2 Mutations and Review of the Literature. *Mol Syndromol*, *9*(6), 287-294. <https://doi.org/10.1159/000494451>
- Brandsma, R., Verschuuren-Bemelmans, C. C., Amrom, D., Barisic, N., Baxter, P., Bertini, E., Blumkin, L., Brankovic-Sreckovic, V., Brouwer, O. F., Burk, K., Catsman-Berrepoets, C. E., Craiu, D., de Co, I. F. M., Gburek, J., Kennedy, C., de Koning, T. J., Kremer, H. P. H., Kumar, R., Macaya, A., . . . Sival, D. A. (2019). A clinical diagnostic algorithm for early onset cerebellar ataxia. *Eur J Paediatr Neurol*, *23*(5), 692-706. <https://doi.org/10.1016/j.ejpn.2019.08.004>
- Burgess, R. W., Cox, G. A., & Seburn, K. L. (2016). Neuromuscular Disease Models and Analysis. *Methods Mol Biol*, *1438*, 349-394. [https://doi.org/10.1007/978-1-4939-3661-8\\_19](https://doi.org/10.1007/978-1-4939-3661-8_19)
- Case, L. K., Liljencrantz, J., Madian, N., Necaie, A., Tubbs, J., McCall, M., Bradson, M. L., Szczot, M., Pitcher, M. H., Ghitani, N., Frangos, E., Cole, J., Bharucha-Goebel, D., Saade, D., Ogata, T., Donkervoort, S., Foley, A. R., Bonnemann, C. G., Olausson, H., . . . Chesler, A. T. (2021). Innocuous pressure sensation requires A-type afferents but not functional PIEZO2 channels in humans. *Nat Commun*, *12*(1), 657. <https://doi.org/10.1038/s41467-021-20939-5>
- Chesler, A. T., Szczot, M., Bharucha-Goebel, D., Ceko, M., Donkervoort, S., Laubacher, C., Hayes, L. H., Alter, K., Zampieri, C., Stanley, C., Innes, A. M., Mah, J. K., Grosman, C. M., Bradley, N., Nguyen, D., Foley, A. R., Le Pichon, C. E., & Bonnemann, C. G. (2016). The Role of PIEZO2 in Human Mechanosensation. *N Engl J Med*, *375*(14), 1355-1364. <https://doi.org/10.1056/NEJMoa1602812>

- Chetri, P. B., Khan, H., & Tripathi, T. (2022). Chapter 5 - Methods to determine the oligomeric structure of proteins. In T. Tripathi & V. K. Dubey (Eds.), *Advances in Protein Molecular and Structural Biology Methods* (pp. 49-76). Academic Press. <https://doi.org/https://doi.org/10.1016/B978-0-323-90264-9.00005-2>
- Cohen, E., Bonne, G., Rivier, F., & Hamroun, D. (2021). The 2022 version of the gene table of neuromuscular disorders (nuclear genome). *Neuromuscul Disord*, *31*(12), 1313-1357. <https://doi.org/10.1016/j.nmd.2021.11.004>
- Cortese, A., Reilly, M. M., & Houlden, H. (2020). *RFC1* CANVAS / Spectrum Disorder. In M. P. Adam, D. B. Everman, & G. M. Mirzaa (Eds.), *GeneReviews*(R). <https://www.ncbi.nlm.nih.gov/books/NBK564656/>
- Coste, B., Houge, G., Murray, M. F., Stitzel, N., Bandell, M., Giovanni, M. A., Philippakis, A., Hoischen, A., Riemer, G., Steen, U., Steen, V. M., Mathur, J., Cox, J., Lebo, M., Rehm, H., Weiss, S. T., Wood, J. N., Maas, R. L., Sunyaev, S. R., & Patapoutian, A. (2013). Gain-of-function mutations in the mechanically activated ion channel PIEZO2 cause a subtype of Distal Arthrogryposis. *Proc Natl Acad Sci U S A*, *110*(12), 4667-4672. <https://doi.org/10.1073/pnas.1221400110>
- Coste, B., Murthy, S. E., Mathur, J., Schmidt, M., Mechoukhi, Y., Delmas, P., & Patapoutian, A. (2015). Piezo1 ion channel pore properties are dictated by C-terminal region. *Nat Commun*, *6*, 7223. <https://doi.org/10.1038/ncomms8223>
- Cummings, B. B., Marshall, J. L., Tukiainen, T., Lek, M., Donkervoort, S., Foley, A. R., Bolduc, V., Waddell, L. B., Sandaradura, S. A., O'Grady, G. L., Estrella, E., Reddy, H. M., Zhao, F., Weisburd, B., Karczewski, K. J., O'Donnell-Luria, A. H., Birnbaum, D., Sarkozy, A., Hu, Y., . . . MacArthur, D. G. (2017). Improving genetic diagnosis in Mendelian disease with transcriptome sequencing. *Sci Transl Med*, *9*(386). <https://doi.org/10.1126/scitranslmed.aal5209>
- de Ligt, J., Willemsen, M. H., van Bon, B. W., Kleefstra, T., Yntema, H. G., Kroes, T., Vulto-van Silfhout, A. T., Koolen, D. A., de Vries, P., Gilissen, C., del Rosario, M., Hoischen, A., Scheffer, H., de Vries, B. B., Brunner, H. G., Veltman, J. A., & Vissers, L. E. (2012). Diagnostic exome sequencing in persons with severe intellectual disability. *N Engl J Med*, *367*(20), 1921-1929. <https://doi.org/10.1056/NEJMoa1206524>
- Deciphering Developmental Disorders, S. (2015). Large-scale discovery of novel genetic causes of developmental disorders. *Nature*, *519*(7542), 223-228. <https://doi.org/10.1038/nature14135>
- Deenen, J. C., Horlings, C. G., Verschuuren, J. J., Verbeek, A. L., & van Engelen, B. G. (2015). The Epidemiology of Neuromuscular Disorders: A Comprehensive Overview of the Literature. *J Neuromuscul Dis*, *2*(1), 73-85. <http://www.ncbi.nlm.nih.gov/pubmed/28198707>
- Delle Vedove, A., Storbeck, M., Heller, R., Holker, I., Hebbar, M., Shukla, A., Magnusson, O., Cirak, S., Girisha, K. M., O'Driscoll, M., Loeys, B., & Wirth, B. (2016). Biallelic Loss of Proprioception-Related PIEZO2 Causes Muscular Atrophy with Perinatal Respiratory Distress, Arthrogryposis, and Scoliosis. *Am J Hum Genet*, *99*(6), 1406-1408. <https://doi.org/10.1016/j.ajhg.2016.11.009>
- Desai, D., Stiene, D., Song, T., & Sadayappan, S. (2020). Distal Arthrogryposis and Lethal Congenital Contracture Syndrome - An Overview. *Front Physiol*, *11*, 689. <https://doi.org/10.3389/fphys.2020.00689>
- DiFiglia, M., Sapp, E., Chase, K. O., Davies, S. W., Bates, G. P., Vonsattel, J. P., & Aronin, N. (1997). Aggregation of huntingtin in neuronal intranuclear inclusions and dystrophic neurites in brain. *Science*, *277*(5334), 1990-1993. <https://doi.org/10.1126/science.277.5334.1990>
- Du, Y., Li, Z., Liu, Z., Zhang, N., Wang, R., Li, F., Zhang, T., Jiang, Y., Zhi, X., Wang, Z., & Wu, J. (2020). Nonrandom occurrence of multiple de novo coding variants in a proband indicates the existence of an oligogenic model in autism. *Genet Med*, *22*(1), 170-180. <https://doi.org/10.1038/s41436-019-0610-2>
- Dubin, A. E., Schmidt, M., Mathur, J., Petrus, M. J., Xiao, B., Coste, B., & Patapoutian, A. (2012). Inflammatory signals enhance piezo2-mediated mechanosensitive currents. *Cell Rep*, *2*(3), 511-517. <https://doi.org/10.1016/j.celrep.2012.07.014>
- El Fatimy, R., Tremblay, S., Dury, A. Y., Solomon, S., De Koninck, P., Schrader, J. W., & Khandjian, E. W. (2012). Fragile X mental retardation protein interacts with the RNA-binding protein Caprin1 in

- neuronal RiboNucleoProtein complexes [corrected]. *PLoS One*, 7(6), e39338. <https://doi.org/10.1371/journal.pone.0039338>
- Engel, A. G., Shen, X. M., Selcen, D., & Sine, S. M. (2015). Congenital myasthenic syndromes: pathogenesis, diagnosis, and treatment. *Lancet Neurol*, 14(4), 420-434. [https://doi.org/10.1016/S1474-4422\(14\)70201-7](https://doi.org/10.1016/S1474-4422(14)70201-7)
- Feldman, E. L. (2021). *Atlas of Neuromuscular Diseases* (3 ed.). Springer. <https://doi.org/https://doi.org/10.1007/978-3-030-63449-0>
- Feng, J., Luo, J., Yang, P., Du, J., Kim, B. S., & Hu, H. (2018). Piezo2 channel-Merkel cell signaling modulates the conversion of touch to itch. *Science*, 360(6388), 530-533. <https://doi.org/10.1126/science.aar5703>
- Finsterer, J. (2019). Congenital myasthenic syndromes. *Orphanet J Rare Dis*, 14(1), 57. <https://doi.org/10.1186/s13023-019-1025-5>
- Finsterer, J. (2020). Prevalence in congenital myasthenic syndrome. *Eur J Paediatr Neurol*, 26, 5-6. <https://doi.org/10.1016/j.ejpn.2020.04.011>
- Finsterer, J., & Stollberger, C. (1999). Cardiac involvement in Werdnig-Hoffmann's spinal muscular atrophy. *Cardiology*, 92(3), 178-182. <https://doi.org/6968>
- Fralish, Z., Lotz, E. M., Chavez, T., Khodabukus, A., & Bursac, N. (2021). Neuromuscular Development and Disease: Learning From in vitro and in vivo Models. *Front Cell Dev Biol*, 9, 764732. <https://doi.org/10.3389/fcell.2021.764732>
- Francisco-Velilla, R., Embarc-Buh, A., Del Cano-Ochoa, F., Abellan, S., Vilar, M., Alvarez, S., Fernandez-Jaen, A., Kour, S., Rajan, D. S., Pandey, U. B., Ramon-Maiques, S., & Martinez-Salas, E. (2022). Functional and structural deficiencies of Gemin5 variants associated with neurological disorders. *Life Sci Alliance*, 5(7). <https://doi.org/10.26508/lsa.202201403>
- From the American Association of Neurological Surgeons, A. S. o. N. C., Interventional Radiology Society of Europe, C. I. R. A. C. o. N. S. E. S. o. M. I. N. T. E. S. o. N. E. S. O. S. f. C. A., Interventions, S. o. I. R. S. o. N. S., World Stroke, O., Sacks, D., Baxter, B., Campbell, B. C. V., Carpenter, J. S., Cognard, C., Dippel, D., Eesa, M., Fischer, U., Hausegger, K., Hirsch, J. A., Shazam Hussain, M., Jansen, O., Jayaraman, M. V., Khalessi, A. A., Kluck, B. W., . . . Vorwerk, D. (2018). Multisociety Consensus Quality Improvement Revised Consensus Statement for Endovascular Therapy of Acute Ischemic Stroke. *Int J Stroke*, 13(6), 612-632. <https://doi.org/10.1177/1747493018778713>
- Gama Sosa, M. A., De Gasperi, R., & Elder, G. A. (2012). Modeling human neurodegenerative diseases in transgenic systems. *Hum Genet*, 131(4), 535-563. <https://doi.org/10.1007/s00439-011-1119-1>
- GeneTable of Neuromuscular Disorders*. Retrieved 22 August 2022 from <https://www.musclegenetable.fr/>
- Gilissen, C., Hoischen, A., Brunner, H. G., & Veltman, J. A. (2012). Disease gene identification strategies for exome sequencing. *Eur J Hum Genet*, 20(5), 490-497. <https://doi.org/10.1038/ejhg.2011.258>
- Goldschmidt, L., Teng, P. K., Riek, R., & Eisenberg, D. (2010). Identifying the amyloids, proteins capable of forming amyloid-like fibrils. *Proc Natl Acad Sci U S A*, 107(8), 3487-3492. <https://doi.org/10.1073/pnas.0915166107>
- Gonorazky, H. D., Naumenko, S., Ramani, A. K., Nelakuditi, V., Mashouri, P., Wang, P., Kao, D., Ohri, K., Viththiyapaskaran, S., Tarnopolsky, M. A., Mathews, K. D., Moore, S. A., Osorio, A. N., Villanova, D., Kemaladewi, D. U., Cohn, R. D., Brudno, M., & Dowling, J. J. (2019). Expanding the Boundaries of RNA Sequencing as a Diagnostic Tool for Rare Mendelian Disease. *Am J Hum Genet*, 104(3), 466-483. <https://doi.org/10.1016/j.ajhg.2019.01.012>
- Griffet, J., Dieterich, K., Bourg, V., & Bourgeois, E. (2021). Amyoplasia and distal arthrogryposis. *Orthop Traumatol Surg Res*, 107(1S), 102781. <https://doi.org/10.1016/j.otsr.2020.102781>
- Hagerman, R., & Hagerman, P. (2021). Fragile X-associated tremor/ataxia syndrome: pathophysiology and management. *Curr Opin Neurol*, 34(4), 541-546. <https://doi.org/10.1097/WCO.0000000000000954>
- Hagerman, R. J., Berry-Kravis, E., Hazlett, H. C., Bailey, D. B., Jr., Moine, H., Kooy, R. F., Tassone, F., Gantois, I., Sonenberg, N., Mandel, J. L., & Hagerman, P. J. (2017). Fragile X syndrome. *Nat Rev Dis Primers*, 3, 17065. <https://doi.org/10.1038/nrdp.2017.65>

- Haj Salem, I., Beaudin, M., Stumpf, M., Estiar, M. A., Cote, P. O., Brunet, F., Gamache, P. L., Rouleau, G. A., Mourabit-Amari, K., Gan-Or, Z., & Dupre, N. (2021). Genetic and Epidemiological Study of Adult Ataxia and Spastic Paraplegia in Eastern Quebec. *Can J Neurol Sci*, 48(5), 655-665. <https://doi.org/10.1017/cjn.2020.277>
- Haliloglu, G., Becker, K., Temucin, C., Talim, B., Kucuksahin, N., Pergande, M., Motameny, S., Nurnberg, P., Aydingoz, U., Topaloglu, H., & Cirak, S. (2017). Recessive PIEZO2 stop mutation causes distal arthrogyriposis with distal muscle weakness, scoliosis and proprioception defects. *J Hum Genet*, 62(4), 497-501. <https://doi.org/10.1038/jhg.2016.153>
- Hall, J. G., Kimber, E., & Dieterich, K. (2019). Classification of arthrogyriposis. *Am J Med Genet C Semin Med Genet*, 181(3), 300-303. <https://doi.org/10.1002/ajmg.c.31716>
- Hampel, H., Hardy, J., Blennow, K., Chen, C., Perry, G., Kim, S. H., Villemagne, V. L., Aisen, P., Vendruscolo, M., Iwatsubo, T., Masters, C. L., Cho, M., Lannfelt, L., Cummings, J. L., & Vergallo, A. (2021). The Amyloid-beta Pathway in Alzheimer's Disease. *Mol Psychiatry*, 26(10), 5481-5503. <https://doi.org/10.1038/s41380-021-01249-0>
- Hill, R. Z., Loud, M. C., Dubin, A. E., Peet, B., & Patapoutian, A. (2022). PIEZO1 transduces mechanical itch in mice. *Nature*, 607(7917), 104-110. <https://doi.org/10.1038/s41586-022-04860-5>
- Hou, P. S., Chuang, C. Y., Yeh, C. H., Chiang, W., Liu, H. J., Lin, T. N., & Kuo, H. C. (2017). Direct Conversion of Human Fibroblasts into Neural Progenitors Using Transcription Factors Enriched in Human ESC-Derived Neural Progenitors. *Stem Cell Reports*, 8(1), 54-68. <https://doi.org/10.1016/j.stemcr.2016.11.006>
- Jacquemont, S., Hagerman, R. J., Leehey, M., Grigsby, J., Zhang, L., Brunberg, J. A., Greco, C., Des Portes, V., Jardini, T., Levine, R., Berry-Kravis, E., Brown, W. T., Schaeffer, S., Kissel, J., Tassone, F., & Hagerman, P. J. (2003). Fragile X premutation tremor/ataxia syndrome: molecular, clinical, and neuroimaging correlates. *Am J Hum Genet*, 72(4), 869-878. <https://doi.org/10.1086/374321>
- Jan, A., Goncalves, N. P., Vaegter, C. B., Jensen, P. H., & Ferreira, N. (2021). The Prion-Like Spreading of Alpha-Synuclein in Parkinson's Disease: Update on Models and Hypotheses. *Int J Mol Sci*, 22(15). <https://doi.org/10.3390/ijms22158338>
- Jiang, Y. H., Yuen, R. K., Jin, X., Wang, M., Chen, N., Wu, X., Ju, J., Mei, J., Shi, Y., He, M., Wang, G., Liang, J., Wang, Z., Cao, D., Carter, M. T., Chrysler, C., Drmic, I. E., Howe, J. L., Lau, L., . . . Scherer, S. W. (2013). Detection of clinically relevant genetic variants in autism spectrum disorder by whole-genome sequencing. *Am J Hum Genet*, 93(2), 249-263. <https://doi.org/10.1016/j.ajhg.2013.06.012>
- Kandel, E. R. (2013). *Principles of Neural Science* (5th ed.). McGraw Hill.
- Karakaya, M. (2018). *Identification and characterization of neuromuscular disease-causing genes by next-generation sequencing technology* University of Cologne].
- Karakaya, M., Storbeck, M., Strathmann, E. A., Delle Vedove, A., Holker, I., Altmueller, J., Naghiyeva, L., Schmitz-Steinkruger, L., Vezyroglou, K., Motameny, S., Alawbathani, S., Thiele, H., Polat, A. I., Okur, D., Boostani, R., Karimiani, E. G., Wunderlich, G., Ardicli, D., Topaloglu, H., . . . Wirth, B. (2018). Targeted sequencing with expanded gene profile enables high diagnostic yield in non-5q-spinal muscular atrophies. *Hum Mutat*, 39(9), 1284-1298. <https://doi.org/10.1002/humu.23560>
- Kimber, E. (2015). AMC: amyoplasia and distal arthrogyriposis. *J Child Orthop*, 9(6), 427-432. <https://doi.org/10.1007/s11832-015-0689-1>
- Klaniewska, M., Jedrzejowska, M., Rydzanicz, M., Paprocka, J., Biela, M., Wolanska, E., Pollak, A., Debek, E., Sasiadek, M., Ploski, R., Gos, M., & Smigiel, R. (2021). Case Report: Further Delineation of Neurological Symptoms in Young Children Caused by Compound Heterozygous Mutation in the PIEZO2 Gene. *Front Genet*, 12, 620752. <https://doi.org/10.3389/fgene.2021.620752>
- Klockgether, T., Mariotti, C., & Paulson, H. L. (2019). Spinocerebellar ataxia. *Nat Rev Dis Primers*, 5(1), 24. <https://doi.org/10.1038/s41572-019-0074-3>
- Kohler, S., Gargano, M., Matentzoglou, N., Carmody, L. C., Lewis-Smith, D., Vasilevsky, N. A., Danis, D., Balagura, G., Baynam, G., Brower, A. M., Callahan, T. J., Chute, C. G., Est, J. L., Galer, P. D., Ganesan, S., Griese, M., Haimel, M., Pazmandi, J., Hanauer, M., . . . Robinson, P. N. (2021). The Human Phenotype Ontology in 2021. *Nucleic Acids Res*, 49(D1), D1207-D1217. <https://doi.org/10.1093/nar/gkaa1043>

- Kohler, S., Oien, N. C., Buske, O. J., Groza, T., Jacobsen, J. O. B., McNamara, C., Vasilevsky, N., Carmody, L. C., Gourdine, J. P., Gargano, M., McMurphy, J. A., Danis, D., Mungall, C. J., Smedley, D., Haendel, M., & Robinson, P. N. (2019). Encoding Clinical Data with the Human Phenotype Ontology for Computational Differential Diagnostics. *Curr Protoc Hum Genet*, 103(1), e92. <https://doi.org/10.1002/cphg.92>
- Kohler, S., Schulz, M. H., Krawitz, P., Bauer, S., Dolken, S., Ott, C. E., Mundlos, C., Horn, D., Mundlos, S., & Robinson, P. N. (2009). Clinical diagnostics in human genetics with semantic similarity searches in ontologies. *Am J Hum Genet*, 85(4), 457-464. <https://doi.org/10.1016/j.ajhg.2009.09.003>
- Kour, S., Rajan, D. S., Fortuna, T. R., Anderson, E. N., Ward, C., Lee, Y., Lee, S., Shin, Y. B., Chae, J. H., Choi, M., Siquier, K., Cantagrel, V., Amiel, J., Stolerman, E. S., Barnett, S. S., Cousin, M. A., Castro, D., McDonald, K., Kirmse, B., . . . Pandey, U. B. (2021). Loss of function mutations in GEMIN5 cause a neurodevelopmental disorder. *Nat Commun*, 12(1), 2558. <https://doi.org/10.1038/s41467-021-22627-w>
- Krygier, M., & Mazurkiewicz-Beldzinska, M. (2021). Milestones in genetics of cerebellar ataxias. *Neurogenetics*, 22(4), 225-234. <https://doi.org/10.1007/s10048-021-00656-3>
- Laing, N. G., Ong, R. W., & Ravenscroft, G. (2021). Genetic neuromuscular disorders: what is the best that we can do? *Neuromuscul Disord*, 31(10), 1081-1089. <https://doi.org/10.1016/j.nmd.2021.07.007>
- Lancaster, A. K., Nutter-Upham, A., Lindquist, S., & King, O. D. (2014). PLAAC: a web and command-line application to identify proteins with prion-like amino acid composition. *Bioinformatics*, 30(17), 2501-2502. <https://doi.org/10.1093/bioinformatics/btu310>
- Leuzy, A., Cullen, N. C., Mattsson-Carlgrén, N., & Hansson, O. (2021). Current advances in plasma and cerebrospinal fluid biomarkers in Alzheimer's disease. *Curr Opin Neurol*, 34(2), 266-274. <https://doi.org/10.1097/WCO.0000000000000904>
- Liu, Y., Sugiura, Y., & Lin, W. (2011). The role of synaptobrevin1/VAMP1 in Ca<sup>2+</sup>-triggered neurotransmitter release at the mouse neuromuscular junction. *J Physiol*, 589(Pt 7), 1603-1618. <https://doi.org/10.1113/jphysiol.2010.201939>
- Lobanova, E., Whiten, D., Ruggeri, F. S., Taylor, C. G., Kouli, A., Xia, Z., Emin, D., Zhang, Y. P., Lam, J. Y. L., Williams-Gray, C. H., & Klenerman, D. (2022). Imaging protein aggregates in the serum and cerebrospinal fluid in Parkinson's disease. *Brain*, 145(2), 632-643. <https://doi.org/10.1093/brain/awab306>
- Logan, S., Arzua, T., Canfield, S. G., Seminary, E. R., Sison, S. L., Ebert, A. D., & Bai, X. (2019). Studying Human Neurological Disorders Using Induced Pluripotent Stem Cells: From 2D Monolayer to 3D Organoid and Blood Brain Barrier Models. *Compr Physiol*, 9(2), 565-611. <https://doi.org/10.1002/cphy.c180025>
- Loh, Y. H., Agarwal, S., Park, I. H., Urbach, A., Huo, H., Heffner, G. C., Kim, K., Miller, J. D., Ng, K., & Daley, G. Q. (2009). Generation of induced pluripotent stem cells from human blood. *Blood*, 113(22), 5476-5479. <https://doi.org/10.1182/blood-2009-02-204800>
- Ma, L., & Yu, X. (2017). Arthrogryposis multiplex congenita: classification, diagnosis, perioperative care, and anesthesia. *Front Med*, 11(1), 48-52. <https://doi.org/10.1007/s11684-017-0500-4>
- Mahmud, A. A., Nahid, N. A., Nassif, C., Sayeed, M. S., Ahmed, M. U., Parveen, M., Khalil, M. I., Islam, M. M., Nahar, Z., Rypens, F., Hamdan, F. F., Rouleau, G. A., Hasnat, A., & Michaud, J. L. (2017). Loss of the proprioception and touch sensation channel PIEZO2 in siblings with a progressive form of contractures. *Clin Genet*, 91(3), 470-475. <https://doi.org/10.1111/cge.12850>
- March, Z. M., King, O. D., & Shorter, J. (2016). Prion-like domains as epigenetic regulators, scaffolds for subcellular organization, and drivers of neurodegenerative disease. *Brain Res*, 1647, 9-18. <https://doi.org/10.1016/j.brainres.2016.02.037>
- Marshall, K. L., Saade, D., Ghitani, N., Coombs, A. M., Szczot, M., Keller, J., Ogata, T., Daou, I., Stowers, L. T., Bonnemann, C. G., Chesler, A. T., & Patapoutian, A. (2020). PIEZO2 in sensory neurons and urothelial cells coordinates urination. *Nature*, 588(7837), 290-295. <https://doi.org/10.1038/s41586-020-2830-7>
- Marwaha, S., Knowles, J. W., & Ashley, E. A. (2022). A guide for the diagnosis of rare and undiagnosed disease: beyond the exome. *Genome Med*, 14(1), 23. <https://doi.org/10.1186/s13073-022-01026-w>

- Masingue, M., Faure, J., Sole, G., Stojkovic, T., & Leonard-Louis, S. (2019). A novel nonsense PIEZO2 mutation in a family with scoliosis and proprioceptive defect. *Neuromuscul Disord*, *29*(1), 75-79. <https://doi.org/10.1016/j.nmd.2018.10.005>
- McMillin, M. J., Beck, A. E., Chong, J. X., Shively, K. M., Buckingham, K. J., Gildersleeve, H. I., Aracena, M. I., Aylsworth, A. S., Bitoun, P., Carey, J. C., Clericuzio, C. L., Crow, Y. J., Curry, C. J., Devriendt, K., Everman, D. B., Fryer, A., Gibson, K., Giovannucci Uzielli, M. L., Graham, J. M., Jr., . . . Bamshad, M. J. (2014). Mutations in PIEZO2 cause Gordon syndrome, Marden-Walker syndrome, and distal arthrogryposis type 5. *Am J Hum Genet*, *94*(5), 734-744. <https://doi.org/10.1016/j.ajhg.2014.03.015>
- McTague, A., Rossignoli, G., Ferrini, A., Barral, S., & Kurian, M. A. (2021). Genome Editing in iPSC-Based Neural Systems: From Disease Models to Future Therapeutic Strategies. *Front Genome Ed*, *3*, 630600. <https://doi.org/10.3389/fgeed.2021.630600>
- Mertens, J., Paquola, A. C. M., Ku, M., Hatch, E., Bohnke, L., Ladjevardi, S., McGrath, S., Campbell, B., Lee, H., Herdy, J. R., Goncalves, J. T., Toda, T., Kim, Y., Winkler, J., Yao, J., Hetzer, M. W., & Gage, F. H. (2015). Directly Reprogrammed Human Neurons Retain Aging-Associated Transcriptomic Signatures and Reveal Age-Related Nucleocytoplasmic Defects. *Cell Stem Cell*, *17*(6), 705-718. <https://doi.org/10.1016/j.stem.2015.09.001>
- Meyer, K., Ferraiuolo, L., Miranda, C. J., Likhite, S., McElroy, S., Rensch, S., Ditsworth, D., Lagier-Tourenne, C., Smith, R. A., Ravits, J., Burghes, A. H., Shaw, P. J., Cleveland, D. W., Kolb, S. J., & Kaspar, B. K. (2014). Direct conversion of patient fibroblasts demonstrates non-cell autonomous toxicity of astrocytes to motor neurons in familial and sporadic ALS. *Proc Natl Acad Sci U S A*, *111*(2), 829-832. <https://doi.org/10.1073/pnas.1314085111>
- Miller, J. D., Ganat, Y. M., Kishinevsky, S., Bowman, R. L., Liu, B., Tu, E. Y., Mandal, P. K., Vera, E., Shim, J. W., Kriks, S., Taldone, T., Fusaki, N., Tomishima, M. J., Krainc, D., Milner, T. A., Rossi, D. J., & Studer, L. (2013). Human iPSC-based modeling of late-onset disease via progerin-induced aging. *Cell Stem Cell*, *13*(6), 691-705. <https://doi.org/10.1016/j.stem.2013.11.006>
- Min, S., Chang, R. B., Prescott, S. L., Beeler, B., Joshi, N. R., Strohlic, D. E., & Liberles, S. D. (2019). Arterial Baroreceptors Sense Blood Pressure through Decorated Aortic Claws. *Cell Rep*, *29*(8), 2192-2201 e2193. <https://doi.org/10.1016/j.celrep.2019.10.040>
- Mirakhori, F., Zeynali, B., Rassouli, H., Salekdeh, G. H., & Baharvand, H. (2015). Direct conversion of human fibroblasts into dopaminergic neural progenitor-like cells using TAT-mediated protein transduction of recombinant factors. *Biochem Biophys Res Commun*, *459*(4), 655-661. <https://doi.org/10.1016/j.bbrc.2015.02.166>
- Mitsuhashi, S., Nakagawa, S., Takahashi Ueda, M., Imanishi, T., Frith, M. C., & Mitsuhashi, H. (2017). Nanopore-based single molecule sequencing of the D4Z4 array responsible for facioscapulohumeral muscular dystrophy. *Sci Rep*, *7*(1), 14789. <https://doi.org/10.1038/s41598-017-13712-6>
- Monies, D., Abouelhoda, M., AlSayed, M., Alhasnani, Z., Alotaibi, M., Kayyali, H., Al-Owain, M., Shah, A., Rahbeeni, Z., Al-Muhaizea, M. A., Alzaidan, H. I., Cupler, E., Bohlega, S., Faqeh, E., Faden, M., Alyounes, B., Jaroudi, D., Goljan, E., Elbardisy, H., . . . Alkuraya, F. S. (2017). The landscape of genetic diseases in Saudi Arabia based on the first 1000 diagnostic panels and exomes. *Hum Genet*, *136*(8), 921-939. <https://doi.org/10.1007/s00439-017-1821-8>
- Muller, U. (2021). Spinocerebellar ataxias (SCAs) caused by common mutations. *Neurogenetics*, *22*(4), 235-250. <https://doi.org/10.1007/s10048-021-00662-5>
- Nair, P., Sabbagh, S., Mansour, H., Fawaz, A., Hmameess, G., Noun, P., Dagher, R., Megarbane, H., Hana, S., Alame, S., Lamaa, M., Hasbini, D., Farah, R., Rajab, M., Stora, S., El-Tourjuman, O., Abou Jaoude, P., Chalouhi, G., Sayad, R., . . . Megarbane, A. (2018). Contribution of next generation sequencing in pediatric practice in Lebanon. A Study on 213 cases. *Mol Genet Genomic Med*, *6*(6), 1041-1052. <https://doi.org/10.1002/mgg3.480>
- Neumann, M., Sampathu, D. M., Kwong, L. K., Truax, A. C., Micsenyi, M. C., Chou, T. T., Bruce, J., Schuck, T., Grossman, M., Clark, C. M., McCluskey, L. F., Miller, B. L., Masliah, E., Mackenzie, I. R., Feldman, H., Feiden, W., Kretschmar, H. A., Trojanowski, J. Q., & Lee, V. M. (2006). Ubiquitinated TDP-43 in frontotemporal lobar degeneration and amyotrophic lateral sclerosis. *Science*, *314*(5796), 130-133. <https://doi.org/10.1126/science.1134108>

- Nonomura, K., Woo, S. H., Chang, R. B., Gillich, A., Qiu, Z., Francisco, A. G., Ranade, S. S., Liberles, S. D., & Patapoutian, A. (2017). Piezo2 senses airway stretch and mediates lung inflation-induced apnoea. *Nature*, *541*(7636), 176-181. <https://doi.org/10.1038/nature20793>
- Nystuen, A. M., Schwendinger, J. K., Sachs, A. J., Yang, A. W., & Haider, N. B. (2007). A null mutation in VAMP1/synaptobrevin is associated with neurological defects and prewean mortality in the lethal-wasting mouse mutant. *Neurogenetics*, *8*(1), 1-10. <https://doi.org/10.1007/s10048-006-0068-7>
- Oakley-Hannibal, E., Ghali, N., Pope, F. M., De Franco, E., Ellard, S., van Dijk, F. S., & Brady, A. F. (2020). A neuromuscular disorder with homozygosity for PIEZO2 gene variants: an important differential diagnosis for kyphoscoliotic Ehlers-Danlos Syndrome. *Clin Dysmorphol*, *29*(1), 69-72. <https://doi.org/10.1097/MCD.0000000000000304>
- Ohashi, R., Takao, K., Miyakawa, T., & Shiina, N. (2016). Comprehensive behavioral analysis of RNG105 (Caprin1) heterozygous mice: Reduced social interaction and attenuated response to novelty. *Sci Rep*, *6*, 20775. <https://doi.org/10.1038/srep20775>
- Okubo, M., Fujita, A., Saito, Y., Komaki, H., Ishiyama, A., Takeshita, E., Kojima, E., Koichihara, R., Saito, T., Nakagawa, E., Sugai, K., Yamazaki, H., Kusaka, K., Tanaka, H., Miyake, N., Matsumoto, N., & Sasaki, M. (2015). A family of distal arthrogyrosis type 5 due to a novel PIEZO2 mutation. *Am J Med Genet A*, *167A*(5), 1100-1106. <https://doi.org/10.1002/ajmg.a.36881>
- Online Mendelian Inheritance in Man, OMIM®. MIM Number: #108120. Retrieved 1 September 2022 from <https://www.omim.org/entry/108120>
- Pandolfo, M. (2008). Friedreich ataxia. *Arch Neurol*, *65*(10), 1296-1303. <https://doi.org/10.1001/archneur.65.10.1296>
- Park, M. J., Cheon, S. M., Bae, H. R., Kim, S. H., & Kim, J. W. (2011). Elevated levels of alpha-synuclein oligomer in the cerebrospinal fluid of drug-naive patients with Parkinson's disease. *J Clin Neurol*, *7*(4), 215-222. <https://doi.org/10.3988/jcn.2011.7.4.215>
- Pavinato, L., Delle Vedove, A., Carli, D., Ferrero, M., Carestiatto, S., Howe, J. L., Agolini, E., Coviello, D. A., van de Laar, I., Au, P. Y. B., Di Gregorio, E., Fabbiani, A., Croci, S., Mencarelli, M. A., Bruno, L. P., Renieri, A., Veltra, D., Sofocleous, C., Faivre, L., . . . Brusco, A. (2022). CAPRIN1 haploinsufficiency causes a neurodevelopmental disorder with language impairment, ADHD and ASD. *Brain*. <https://doi.org/10.1093/brain/awac278>
- Perlman, S. (1998). Hereditary Ataxia Overview. In M. P. Adam, D. B. Everman, & G. M. Mirzaa (Eds.), *GeneReviews*(R). <https://www.ncbi.nlm.nih.gov/books/NBK1138/>
- Petrini, S., Borghi, R., D'Oria, V., Restaldi, F., Moreno, S., Novelli, A., Bertini, E., & Compagnucci, C. (2017). Aged induced pluripotent stem cell (iPSCs) as a new cellular model for studying premature aging. *Aging (Albany NY)*, *9*(5), 1453-1469. <https://doi.org/10.18632/aging.101248>
- Polavarapu, K., Vengalil, S., Preethish-Kumar, V., Arunachal, G., Nashi, S., Mohan, D., Chawla, T., Bardhan, M., Nandeesh, B., Gupta, P., Gowda, V. K., Lochmuller, H., & Nalini, A. (2021). Recessive VAMP1 mutations associated with severe congenital myasthenic syndromes - A recognizable clinical phenotype. *Eur J Paediatr Neurol*, *31*, 54-60. <https://doi.org/10.1016/j.ejpn.2021.02.005>
- Purves, D. (2018). *Neuroscience* (6th ed.). Sinauer Associates.
- Ramdas, S., & Beeson, D. (2021). Congenital myasthenic syndromes: where do we go from here? *Neuromuscul Disord*, *31*(10), 943-954. <https://doi.org/10.1016/j.nmd.2021.07.400>
- Ranade, S. S., Woo, S. H., Dubin, A. E., Moshourab, R. A., Wetzell, C., Petrus, M., Mathur, J., Begay, V., Coste, B., Mainquist, J., Wilson, A. J., Francisco, A. G., Reddy, K., Qiu, Z., Wood, J. N., Lewin, G. R., & Patapoutian, A. (2014). Piezo2 is the major transducer of mechanical forces for touch sensation in mice. *Nature*, *516*(7529), 121-125. <https://doi.org/10.1038/nature13980>
- Rodriguez Cruz, P. M., Cossins, J., Beeson, D., & Vincent, A. (2020). The Neuromuscular Junction in Health and Disease: Molecular Mechanisms Governing Synaptic Formation and Homeostasis. *Front Mol Neurosci*, *13*, 610964. <https://doi.org/10.3389/fnmol.2020.610964>
- Ruano, L., Melo, C., Silva, M. C., & Coutinho, P. (2014). The global epidemiology of hereditary ataxia and spastic paraplegia: a systematic review of prevalence studies. *Neuroepidemiology*, *42*(3), 174-183. <https://doi.org/10.1159/000358801>

- Ryder, S., Leadley, R. M., Armstrong, N., Westwood, M., de Kock, S., Butt, T., Jain, M., & Kleijnen, J. (2017). The burden, epidemiology, costs and treatment for Duchenne muscular dystrophy: an evidence review. *Orphanet J Rare Dis*, *12*(1), 79. <https://doi.org/10.1186/s13023-017-0631-3>
- Salcedo-Arellano, M. J., Wolf-Ochoa, M. W., Hong, T., Amina, S., Tassone, F., Lechpammer, M., Hagerman, R., & Martinez-Cerdeno, V. (2020). Parkinsonism Versus Concomitant Parkinson's Disease in Fragile X-Associated Tremor/Ataxia Syndrome. *Mov Disord Clin Pract*, *7*(4), 413-418. <https://doi.org/10.1002/mdc3.12942>
- Salpietro, V., Lin, W., Delle Vedove, A., Storbeck, M., Liu, Y., Efthymiou, S., Manole, A., Wiethoff, S., Ye, Q., Saggari, A., McElreavey, K., Krishnakumar, S., Pitt, M., Bello, O., Rothman, J. E., Basel-Vanagaite, L., Hubshman, M. W., Aharoni, S., Manzur, A. Y., . . . Houlden, H. (2017). Homozygous mutations in VAMP1 cause a presynaptic congenital myasthenic syndrome. *Ann Neurol*. <https://doi.org/10.1002/ana.24905>
- Saotome, K., Murthy, S. E., Kefauver, J. M., Whitwam, T., Patapoutian, A., & Ward, A. B. (2018). Structure of the mechanically activated ion channel Piezo1. *Nature*, *554*(7693), 481-486. <https://doi.org/10.1038/nature25453>
- Sen, T., & Thummer, R. P. (2022). CRISPR and iPSCs: Recent Developments and Future Perspectives in Neurodegenerative Disease Modelling, Research, and Therapeutics. *Neurotox Res*, *40*(5), 1597-1623. <https://doi.org/10.1007/s12640-022-00564-w>
- Shen, X. M., Scola, R. H., Lorenzoni, P. J., Kay, C. S., Werneck, L. C., Brengman, J., Selcen, D., & Engel, A. G. (2017). Novel synaptobrevin-1 mutation causes fatal congenital myasthenic syndrome. *Ann Clin Transl Neurol*, *4*(2), 130-138. <https://doi.org/10.1002/acn3.387>
- Shields, M. C., Bowers, M. R., Fulcer, M. M., Bollig, M. K., Rock, P. J., Sutton, B. R., Vrtilas-Mortimer, A. D., Lochmuller, H., Whittaker, R. G., Horvath, R., & Reist, N. E. (2017). Drosophila studies support a role for a presynaptic synaptotagmin mutation in a human congenital myasthenic syndrome. *PLoS One*, *12*(9), e0184817. <https://doi.org/10.1371/journal.pone.0184817>
- Shiina, N., Shinkura, K., & Tokunaga, M. (2005). A novel RNA-binding protein in neuronal RNA granules: regulatory machinery for local translation. *J Neurosci*, *25*(17), 4420-4434. <https://doi.org/10.1523/JNEUROSCI.0382-05.2005>
- Shiina, N., Yamaguchi, K., & Tokunaga, M. (2010). RNG105 deficiency impairs the dendritic localization of mRNAs for Na<sup>+</sup>/K<sup>+</sup> ATPase subunit isoforms and leads to the degeneration of neuronal networks. *J Neurosci*, *30*(38), 12816-12830. <https://doi.org/10.1523/JNEUROSCI.6386-09.2010>
- Sleigh, J., & Sattelle, D. (2010). C. elegans models of neuromuscular diseases expedite translational research. *Translational Neuroscience*, *1*(3), 214-227. <https://doi.org/doi:10.2478/v10134-010-0032-9>
- Smedley, D., Jacobsen, J. O., Jager, M., Kohler, S., Holtgrewe, M., Schubach, M., Siragusa, E., Zemojtel, T., Buske, O. J., Washington, N. L., Bone, W. P., Haendel, M. A., & Robinson, P. N. (2015). Next-generation diagnostics and disease-gene discovery with the Exomiser. *Nat Protoc*, *10*(12), 2004-2015. <https://doi.org/10.1038/nprot.2015.124>
- Sobreira, N., Schiettecatte, F., Valle, D., & Hamosh, A. (2015). GeneMatcher: a matching tool for connecting investigators with an interest in the same gene. *Hum Mutat*, *36*(10), 928-930. <https://doi.org/10.1002/humu.22844>
- Sormanni, P., Aprile, F. A., & Vendruscolo, M. (2015). The CamSol method of rational design of protein mutants with enhanced solubility. *J Mol Biol*, *427*(2), 478-490. <https://doi.org/10.1016/j.jmb.2014.09.026>
- Soto, C., & Pritzkow, S. (2018). Protein misfolding, aggregation, and conformational strains in neurodegenerative diseases. *Nat Neurosci*, *21*(10), 1332-1340. <https://doi.org/10.1038/s41593-018-0235-9>
- Spillantini, M. G., Schmidt, M. L., Lee, V. M., Trojanowski, J. Q., Jakes, R., & Goedert, M. (1997). Alpha-synuclein in Lewy bodies. *Nature*, *388*(6645), 839-840. <https://doi.org/10.1038/42166>
- Sprunger, M. L., & Jackrel, M. E. (2021). Prion-Like Proteins in Phase Separation and Their Link to Disease. *Biomolecules*, *11*(7). <https://doi.org/10.3390/biom11071014>
- Steeg, R., Mueller, S. C., Mah, N., Holst, B., Cabrera-Socorro, A., Stacey, G. N., De Sousa, P. A., Courtney, A., & Zimmermann, H. (2021). EBISC best practice: How to ensure optimal generation,

- qualification, and distribution of iPSC lines. *Stem Cell Reports*, 16(8), 1853-1867. <https://doi.org/10.1016/j.stemcr.2021.07.009>
- Szczot, M., Liljencrantz, J., Ghitani, N., Barik, A., Lam, R., Thompson, J. H., Bharucha-Goebel, D., Saade, D., Necaie, A., Donkervoort, S., Foley, A. R., Gordon, T., Case, L., Bushnell, M. C., Bonnemann, C. G., & Chesler, A. T. (2018). PIEZO2 mediates injury-induced tactile pain in mice and humans. *Sci Transl Med*, 10(462). <https://doi.org/10.1126/scitranslmed.aat9892>
- Szczot, M., Nickolls, A. R., Lam, R. M., & Chesler, A. T. (2021). The Form and Function of PIEZO2. *Annu Rev Biochem*, 90, 507-534. <https://doi.org/10.1146/annurev-biochem-081720-023244>
- Tang, Y., Liu, M. L., Zang, T., & Zhang, C. L. (2017). Direct Reprogramming Rather than iPSC-Based Reprogramming Maintains Aging Hallmarks in Human Motor Neurons. *Front Mol Neurosci*, 10, 359. <https://doi.org/10.3389/fnmol.2017.00359>
- Tarutani, A., Adachi, T., Akatsu, H., Hashizume, Y., Hasegawa, K., Saito, Y., Robinson, A. C., Mann, D. M. A., Yoshida, M., Murayama, S., & Hasegawa, M. (2022). Ultrastructural and biochemical classification of pathogenic tau, alpha-synuclein and TDP-43. *Acta Neuropathol*, 143(6), 613-640. <https://doi.org/10.1007/s00401-022-02426-3>
- Thompson, R., Bonne, G., Missier, P., & Lochmuller, H. (2019). Targeted therapies for congenital myasthenic syndromes: systematic review and steps towards a treataboloome. *Emerg Top Life Sci*, 3(1), 19-37. <https://doi.org/10.1042/ETLS20180100>
- Thompson, R., Papakonstantinou Ntalis, A., Beltran, S., Topf, A., de Paula Estephan, E., Polavarapu, K., t Hoen, P. A. C., Missier, P., & Lochmuller, H. (2019). Increasing phenotypic annotation improves the diagnostic rate of exome sequencing in a rare neuromuscular disorder. *Hum Mutat*, 40(10), 1797-1812. <https://doi.org/10.1002/humu.23792>
- Thompson, R., Spendiff, S., Roos, A., Bourque, P. R., Warman Chardon, J., Kirschner, J., Horvath, R., & Lochmuller, H. (2020). Advances in the diagnosis of inherited neuromuscular diseases and implications for therapy development. *Lancet Neurol*, 19(6), 522-532. [https://doi.org/10.1016/S1474-4422\(20\)30028-4](https://doi.org/10.1016/S1474-4422(20)30028-4)
- Tokuda, T., Qureshi, M. M., Ardah, M. T., Varghese, S., Shehab, S. A., Kasai, T., Ishigami, N., Tamaoka, A., Nakagawa, M., & El-Agnaf, O. M. (2010). Detection of elevated levels of alpha-synuclein oligomers in CSF from patients with Parkinson disease. *Neurology*, 75(20), 1766-1772. <https://doi.org/10.1212/WNL.0b013e3181fd613b>
- Toombs, J. A., Petri, M., Paul, K. R., Kan, G. Y., Ben-Hur, A., & Ross, E. D. (2012). De novo design of synthetic prion domains. *Proc Natl Acad Sci U S A*, 109(17), 6519-6524. <https://doi.org/10.1073/pnas.1119366109>
- Vera, E., Bosco, N., & Studer, L. (2016). Generating Late-Onset Human iPSC-Based Disease Models by Inducing Neuronal Age-Related Phenotypes through Telomerase Manipulation. *Cell Rep*, 17(4), 1184-1192. <https://doi.org/10.1016/j.celrep.2016.09.062>
- Vu, L., Ghosh, A., Tran, C., Tebung, W. A., Sidibe, H., Garcia-Mansfield, K., David-Dirgo, V., Sharma, R., Pirrotte, P., Bowser, R., & Vande Velde, C. (2021). Defining the Caprin-1 Interactome in Unstressed and Stressed Conditions. *J Proteome Res*, 20(6), 3165-3178. <https://doi.org/10.1021/acs.jproteome.1c00016>
- Wang, L., Zhou, H., Zhang, M., Liu, W., Deng, T., Zhao, Q., Li, Y., Lei, J., Li, X., & Xiao, B. (2019). Structure and mechanogating of the mammalian tactile channel PIEZO2. *Nature*, 573(7773), 225-229. <https://doi.org/10.1038/s41586-019-1505-8>
- Winterthun, S., Ferrari, G., He, L., Taylor, R. W., Zeviani, M., Turnbull, D. M., Engelsens, B. A., Moen, G., & Bindoff, L. A. (2005). Autosomal recessive mitochondrial ataxic syndrome due to mitochondrial polymerase gamma mutations. *Neurology*, 64(7), 1204-1208. <https://doi.org/10.1212/01.WNL.0000156516.77696.5A>
- Witek, N., Hawkins, J., & Hall, D. (2021). Genetic ataxias: update on classification and diagnostic approaches. *Curr Neurol Neurosci Rep*, 21(3), 13. <https://doi.org/10.1007/s11910-021-01092-4>
- Woo, S. H., Lukacs, V., de Nooij, J. C., Zaytseva, D., Criddle, C. R., Francisco, A., Jessell, T. M., Wilkinson, K. A., & Patapoutian, A. (2015). Piezo2 is the principal mechanotransduction channel for proprioception. *Nat Neurosci*, 18(12), 1756-1762. <https://doi.org/10.1038/nn.4162>

- Woo, S. H., Ranade, S., Weyer, A. D., Dubin, A. E., Baba, Y., Qiu, Z., Petrus, M., Miyamoto, T., Reddy, K., Lumpkin, E. A., Stucky, C. L., & Patapoutian, A. (2014). Piezo2 is required for Merkel-cell mechanotransduction. *Nature*, *509*(7502), 622-626. <https://doi.org/10.1038/nature13251>
- Wright, C. F., FitzPatrick, D. R., & Firth, H. V. (2018). Paediatric genomics: diagnosing rare disease in children. *Nat Rev Genet*, *19*(5), 253-268. <https://doi.org/10.1038/nrg.2017.116>
- Wu, Z., Grillet, N., Zhao, B., Cunningham, C., Harkins-Perry, S., Coste, B., Ranade, S., Zebbarjadi, N., Beurg, M., Fettiplace, R., Patapoutian, A., & Mueller, U. (2017). Mechanosensory hair cells express two molecularly distinct mechanotransduction channels. *Nat Neurosci*, *20*(1), 24-33. <https://doi.org/10.1038/nn.4449>
- Xue, Y., Cai, X., Wang, L., Liao, B., Zhang, H., Shan, Y., Chen, Q., Zhou, T., Li, X., Hou, J., Chen, S., Luo, R., Qin, D., Pei, D., & Pan, G. (2013). Generating a non-integrating human induced pluripotent stem cell bank from urine-derived cells. *PLoS One*, *8*(8), e70573. <https://doi.org/10.1371/journal.pone.0070573>
- Yakupova, E. I., Bobyleva, L. G., Vikhlyantsev, I. M., & Bobylev, A. G. (2019). Congo Red and amyloids: history and relationship. *Biosci Rep*, *39*(1). <https://doi.org/10.1042/BSR20181415>
- Yamaguchi, T., Takano, K., Inaba, Y., Morikawa, M., Motobayashi, M., Kawamura, R., Wakui, K., Nishi, E., Hirabayashi, S. I., Fukushima, Y., Kato, H., Takahashi, J., & Kosho, T. (2019). PIEZO2 deficiency is a recognizable arthrogyrosis syndrome: A new case and literature review. *Am J Med Genet A*, *179*(6), 948-957. <https://doi.org/10.1002/ajmg.a.61142>
- Yang, Y., Shi, Y., Schweighauser, M., Zhang, X., Kotecha, A., Murzin, A. G., Garringer, H. J., Cullinane, P. W., Saito, Y., Foroud, T., Warner, T. T., Hasegawa, K., Vidal, R., Murayama, S., Revesz, T., Ghetti, B., Hasegawa, M., Lashley, T., Scheres, S. H. W., & Goedert, M. (2022). Structures of alpha-synuclein filaments from human brains with Lewy pathology. *Nature*. <https://doi.org/10.1038/s41586-022-05319-3>
- Yubero, D., Natera-de Benito, D., Pijuan, J., Armstrong, J., Martorell, L., Fernandez, G., Maynou, J., Jou, C., Roldan, M., Ortez, C., Nascimento, A., Hoenicka, J., & Palau, F. (2021). The Increasing Impact of Translational Research in the Molecular Diagnostics of Neuromuscular Diseases. *Int J Mol Sci*, *22*(8). <https://doi.org/10.3390/ijms22084274>
- Zeng, W. Z., Marshall, K. L., Min, S., Daou, I., Chapleau, M. W., Abboud, F. M., Liberles, S. D., & Patapoutian, A. (2018). PIEZOs mediate neuronal sensing of blood pressure and the baroreceptor reflex. *Science*, *362*(6413), 464-467. <https://doi.org/10.1126/science.aau6324>
- Zhao, Q., Zhou, H., Chi, S., Wang, Y., Wang, J., Geng, J., Wu, K., Liu, W., Zhang, T., Dong, M. Q., Wang, J., Li, X., & Xiao, B. (2018). Structure and mechanogating mechanism of the Piezo1 channel. *Nature*, *554*(7693), 487-492. <https://doi.org/10.1038/nature25743>

## 7 Appendix

The main results of this thesis were published in these works and follow appended.

### 7.1 Appendix A

**Delle Vedove A\***, Storbeck M\*, Heller R, Hölker I, Hebbar M, Shukla A, Magnusson O, Cirak S, Girisha KM, O'Driscoll M, Loeys B, Wirth B. Biallelic Loss of Proprioception-Related PIEZO2 Causes Muscular Atrophy with Perinatal Respiratory Distress, Arthrogyryposis, and Scoliosis. *Am J Hum Genet.* 2016 Nov 3;99(5):1206-1216. doi: 10.1016/j.ajhg.2016.09.019. Epub 2016 Oct 27. Erratum in: *Am J Hum Genet.* 2016 Dec 1;99(6):1406-1408. PMID: 27843126; PMCID: PMC5097934.

\* The authors contributed equally to this work

This work was published by Elsevier Inc. and is appended under the Publisher's permission.



# Biallelic Loss of Proprioception-Related PIEZO2 Causes Muscular Atrophy with Perinatal Respiratory Distress, Arthrogryposis, and Scoliosis

Andrea Delle Vedove,<sup>1,2,3,9</sup> Markus Storbeck,<sup>1,2,3,9</sup> Raoul Heller,<sup>1</sup> Irmgard Hölker,<sup>1,2,3</sup> Malavika Hebbar,<sup>4</sup> Anju Shukla,<sup>4</sup> Olafur Magnusson,<sup>5</sup> Sebahattin Cirak,<sup>1,2,6</sup> Katta M. Girisha,<sup>4</sup> Mary O'Driscoll,<sup>7</sup> Bart Loeys,<sup>8</sup> and Brunhilde Wirth<sup>1,2,3,\*</sup>

We report ten individuals of four independent consanguineous families from Turkey, India, Libya, and Pakistan with a variable clinical phenotype that comprises arthrogryposis, spontaneously resolving respiratory insufficiency at birth, muscular atrophy predominantly of the distal lower limbs, scoliosis, and mild distal sensory involvement. Using whole-exome sequencing, SNPchip-based linkage analysis, DNA microarray, and Sanger sequencing, we identified three independent homozygous frameshift mutations and a homozygous deletion of two exons in *PIEZO2* that segregated in all affected individuals of the respective family. The mutations are localized in the N-terminal and central region of the gene, leading to nonsense-mediated transcript decay and consequently to lack of PIEZO2 protein. In contrast, heterozygous gain-of-function missense mutations, mainly localized at the C terminus, cause dominant distal arthrogryposis 3 (DA3), distal arthrogryposis 5 (DA5), or Marden-Walker syndrome (MWKS), which encompass contractures of hands and feet, scoliosis, ophthalmoplegia, and ptosis. *PIEZO2* encodes a mechanosensitive ion channel that plays a major role in light-touch mechanosensation and has recently been identified as the principal mechanotransduction channel for proprioception. Mice ubiquitously depleted of PIEZO2 are postnatally lethal. However, individuals lacking PIEZO2 develop a not life-threatening, slowly progressive disorder, which is likely due to loss of PIEZO2 protein in afferent neurons leading to disturbed proprioception causing aberrant muscle development and function. Here we report a recessively inherited *PIEZO2*-related disease and demonstrate that depending on the type of mutation and the mode of inheritance, *PIEZO2* causes clinically distinguishable phenotypes.

Mechanotransduction describes various mechanisms to convert mechanical stimuli into biological signals. It is important for several biological processes including sensory perception like pain,<sup>1</sup> touch,<sup>2</sup> hearing,<sup>3</sup> and proprioception,<sup>4</sup> but also for embryonic development of tissues and organs.<sup>5</sup> Proprioception is the sensing of body part positioning and muscle stretch, which is mediated by mechanosensation in proprioceptors like muscle spindles in striated muscles or the Golgi tendon organs (GTOs) in tendons.<sup>4</sup> These structures sense mechanical forces like stretch or pressure upon their cell membranes via mechanically activated ion channels, and they propagate proprioceptive information via afferent nerve fibers. Activity of mechanosensitive ion channels has been widely reported in a variety of cell types including dorsal root ganglia sensory neurons,<sup>6,7</sup> skeletal myotubes,<sup>8,9</sup> and others.<sup>10</sup> In 2010, Coste and colleagues identified Piezo channels as essential components of mechanically activated cation channels<sup>11</sup> and later demonstrated that Piezo proteins themselves are the pore-forming subunits of mechanically activated channels.<sup>12</sup> Piezo channels are non-selective cation channels and there are two Piezo genes in mammals, *PIEZO1* (GenBank: NG\_042229.1, MIM: 611184) and *PIEZO2* (GenBank: NG\_034005.1, MIM: 613629). These encode

proteins with respective sizes of up to 2,521 aa and 2,777 aa that share approximately 50% of sequence identity.<sup>13</sup> Both *PIEZO* genes are strongly expressed in the urinary bladder and lung, *PIEZO1* is expressed in kidney and skin, and *PIEZO2* is specifically expressed in dorsal root ganglia<sup>11</sup> and in Merkel cells in the skin.<sup>14</sup> There are multiple mRNA isoforms described for *PIEZO1* and *PIEZO2* in human and mouse, but it is unknown whether they are translated into proteins or have diverse functionality.<sup>13</sup>

Dominant gain-of-function mutations in *PIEZO2* have been shown to cause Gordon syndrome/distal arthrogryposis 3 (DA3 [MIM: 114300]), distal arthrogryposis 5 (DA5 [MIM: 108145]), and Marden-Walker syndrome (MWKS [MIM: 248700]).<sup>15–17</sup> In view of their phenotypic overlap, DA3, DA5, and MWKS have been proposed to be etiologically related and probably have a common developmental mechanism.<sup>18,19</sup> All three syndromes typically involve congenital contractures of hands and feet. Features of the dominant *PIEZO2* phenotypic spectrum include cleft palate, ophthalmoplegia, ptosis, and cerebellar malformations. Some cases present with pulmonary hypertension secondary to restrictive chest disease.<sup>18,20</sup>

Here we describe ten individuals from four independent consanguineous families with autosomal-recessive

<sup>1</sup>Institute of Human Genetics, University of Cologne, 50931 Cologne, Germany; <sup>2</sup>Center for Molecular Medicine Cologne, University of Cologne, 50931 Cologne, Germany; <sup>3</sup>Institute for Genetics, University of Cologne, 50674 Cologne, Germany; <sup>4</sup>Department of Medical Genetics, Kasturba Medical College, Manipal University, Manipal, Karnataka 576104, India; <sup>5</sup>deCODE genetics, 101 Reykjavik, Iceland; <sup>6</sup>Children's Hospital, University Hospital of Cologne, 50931 Cologne, Germany; <sup>7</sup>Birmingham Women's NHS Foundation Trust, Birmingham T15 2TH, UK; <sup>8</sup>Antwerp University Hospital, 2650 Edegem, Belgium

<sup>9</sup>These authors contributed equally to this work

\*Correspondence: [brunhilde.wirth@uk-koeln.de](mailto:brunhilde.wirth@uk-koeln.de)

<http://dx.doi.org/10.1016/j.ajhg.2016.09.019>

© 2016 American Society of Human Genetics.

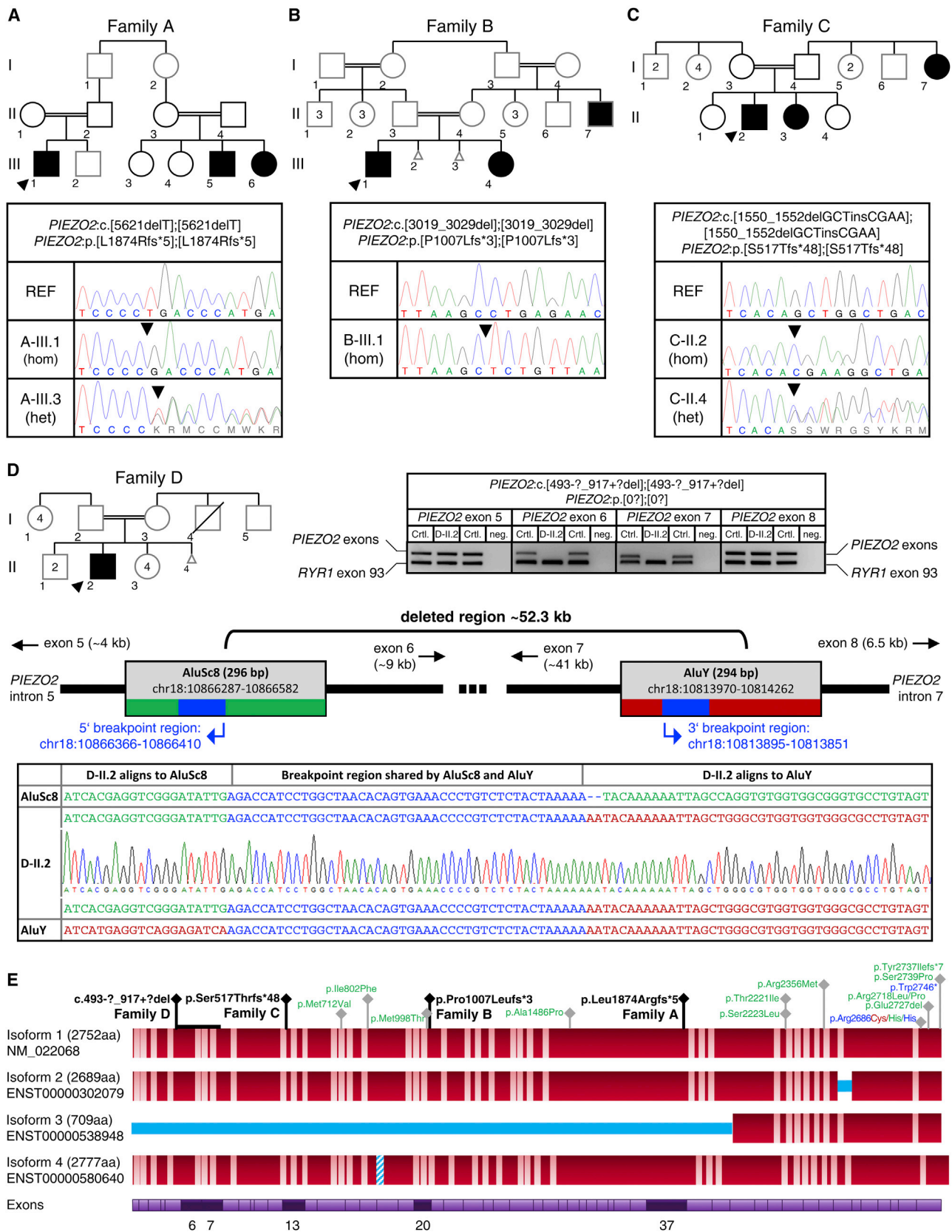


**Figure 1. Identification of Homozygous Frameshift Variants in *PIEZO2* in Ten Affected Individuals of Four Independent Families** (A–D) Pedigrees and Sanger sequencing results of four independent families with homozygous frameshift mutations (A–C) or homozygous exon deletions (D) in *PIEZO2*. DNA was not available for individuals with gray outline. The unequivocal individual identifier is assembled of family, generation, and individual (e.g., A-III.1). Deletion of a genomic region comprising the *PIEZO2* exons 6 and 7 in individual D-II.2 (D) was confirmed by PCR analysis and by identification of the breakpoint region. *PIEZO2* exons 5, 6, 7, and 8 were (legend continued on next page)

inheritance of *PIEZO2* alterations (Figure 1, Table 1, Supplemental Data) from Turkey, India, Libya, and Pakistan. Written informed consent for study participation, analyses of proband material, the generation of individual-derived primary fibroblasts, and publication of anonymized data was obtained from affected individuals, parents, and close relatives. The study was approved by the ethical committee of the University of Cologne. Affected individuals variably presented with congenital contractures, spontaneously resolving postnatal respiratory distress for a few days after birth, scoliosis, slowly progressive muscular weakness and hypotonia, absent deep tendon reflexes, and short stature (Figure 2). Congenital contractures of the feet were always present (e.g., congenital talipes equinovarus), and additionally claw toes, varus or valgus deformities, and ankle contractures were observed (Figure 2B). Contractures of the wrist or hands presenting as camptodactyly, arachnodactyly, or bilateral duck bill deformity of the thumb were present in the majority of affected individuals (Figure 2C). The extent of muscle weakness and atrophy affected mostly the distal extremities and showed interfamilial variability: whereas some individuals have difficulties sitting without assistance, others are able to practice wheelchair sports. In some individuals, proximal and truncal muscle involvement caused reduced shoulder girdle strength, severe scoliosis, and delayed or reduced head control. Muscular weakness and atrophy caused strongly delayed motor development and some individuals were non-ambulatory at the age of 10. Three of seven examined individuals presented with hypomimia. One individual (A-III.1) presented bladder dysfunction with bilateral hydronephrosis. However, since his two affected cousins did not, this is most likely an unrelated finding. CK levels were normal in the majority of case subjects or were just slightly elevated. Two out of four affected individuals who underwent EMG and NCS showed a sensory neuropathy. When performed, brain or spine MRI or CT did not show any abnormality (Supplemental Data).

In an effort to identify the genetic etiology of the disease, whole-exome sequencing (WES) was conducted for the affected son of family A (A-III.1), both of his unaffected parents (A-II.1, A-II.2), and both affected siblings of family C (C-II.2, C-II.3) (Figures 1A and 1C). DNA samples were prepared for WES using the Nextera Exome Enrichment method from Illumina. In short, 50 ng of gDNA was “tagmented” using the Nextera transposome complex, generating adaptor-ligated DNA fragments ready for enrichment. All samples were barcode/index-labelled as a part of the tagmentation process. Samples were quantified using Picogreen measurements and the quality of each

sample was assessed using the Agilent BioAnalyzer. Up to 12 samples were pooled together in equal quantities before capture. A bait library of >340,000, 95-mer biotinylated probes was used to enrich a 62 Mb region of the genome containing 201,121 coding exons (20,794 genes), UTRs, and ncRNA regions. The biotinylated probes were used to hybridize to the target sequences, followed by capture using streptavidin beads. The captured DNA was further amplified by PCR and the quality of the pooled, enriched sequencing libraries was determined on the BioAnalyzer. Further, quality control was done by sequencing each 12-sample pool on the Illumina MiSeq instrument, assessing optimal cluster densities, distribution of reads from each sample within the pool, and other quality metrics such as insert size and duplications. WES samples were sequenced on Illumina HiSeq 2500 instruments (four lanes per pool), using TruSeq v4 cluster and SBS kits, respectively. Variants were analyzed using the Clinical Sequence Miner application (DeCODE Genetics, Iceland). Low-quality variants, variants with call ratios of less than 20%, and variants with global allele frequencies higher than 0.01 were excluded from analysis. Variants were analyzed under the assumption of being present or homozygous in all affected individuals and absent or heterozygous in all unaffected individuals. We detected the homozygous frameshift variants c.5621\_5621delT (p.Leu1874Argfs\*5) (GenBank: NM\_022068, exon 37) in affected individual A-III.1 and c.1550\_1552delGCTinsCGAA (p.Ser517Thrfs\*48) (exon 13) in both affected siblings C-II.2 and C-II.3 in *PIEZO2*. Homozygosity mapping was performed for affected individuals of family B (B-II.7, B-III.1, B-III.4) using an Illumina Cyto-SNP12v2 array, resulting in a 13 Mb-linked region on chromosome 18 including *PIEZO2*. In an effort to identify possible variants in the affected individual B-III.1, we Sanger sequenced *PIEZO2* exons for which dominant mutations had been found in individuals affected by DA3, DA5, or MWKS (exons 15, 20, 43, 45, 52).<sup>16</sup> We identified the homozygous frameshift variant c.3019\_3029del (p.Pro1007Leufs\*3) (exon 20), which was also present in the other affected individuals of family B. All identified homozygous frameshift variants were validated by Sanger sequencing and were present in the homozygous state in all affected individuals of the families A, B, and C, but not in tested unaffected members of the respective family (Figure S1). As expected, all parents were heterozygous carriers of the respective variant, and available unaffected siblings were either heterozygous or did not carry the mutated variant (Figures 1A–1C). Neither of the detected frameshift variants was listed in the ExAC database (Exome Aggregation Consortium [ExAC], Cambridge, MA, 05/02/2016),

---

amplified in multiplex with *RYR1* exon 93 as PCR-positive control. Breakpoint regions were identified by Sanger sequencing of a long-range PCR product amplified from the genomic region between exon 5 and exon 8.

(E) *PIEZO2* protein structure and mutations identified: homozygous loss-of-function mutations (black) and dominant gain-of-function mutations for DA3 (blue), DA5 (green), and MWKS (red) are given. Protein isoforms refer to UniProt entry Q9H5I5. Bright regions indicate putative transmembrane domains (approximated scale); blue regions indicate missing or inserted regions in different isoforms. The bottom line shows exons in which homozygous frameshift mutations were identified.

**Table 1. Phenotypical Characterization of Affected Individuals with Homozygous *PIEZO2* LoF Variants**

Family - Individual	A-III.1	A-III.5	A-III.6	B-III.1	B-III.4	B-II.7	C-II.2	C-II.3	C-I.7	D-II.2	Dominant disease
Origin	Turkey			India			Libya	Pakistan			
Sex	M	M	F	M	F	M	M	F	F	M	
Age at exam (current age) [year]	5 (9)	23 (23)	12 (12)	15 (17)	7 (10)	27 (27)	6 (6)	4 (5)	25 (26)	25 (25)	
Exon	exon 37			exon 20			exon 13			del exons 6-7	variable
Zygoty	hom			hom			hom			hom	het
cDNA change	c.5621delT			c.3019_3029del			c.1550_1552delGCTinsCGAA			c.493-?_917+?del	variable
Protein alteration	p.Leu1874Argfs*5			p.Pro1007Leufs*3			p.Ser517Thrfs*48			p.0?	variable
<b>Birth to Infancy</b>											
Congenital respir. insuff.	+	+	+	+	+	NA	+	NA	NA	NA	NA
Neonatal hypotonia	+	+	+	+	+	NA	+	+	NA	+	NA
Delayed motor milestones	+	+	+	+	+	+	+	+	+	+	NA
Cognitive delay	-	-	-	-	-	-	+	+	NA	+	3/67
<b>Phenotypical Findings</b>											
Short stature	-	+	+	+	+	+	+	+	NA	+	33/63
UL weakness	P	-	D > P	NA	-	-	D	D	NA	D	NA
LL weakness	D > P	D	D > P	NA	D	-	D	D	NA	D	NA
Absent deep tendon reflexes	+	+	+	+	+	+	+	+	NA	+	NA
Mild dysarthria	+	+	+	+	+	+	NA	NA	NA	+	NA
Other	-	reduced sensitivity	reduced sensitivity	(L)RTI, GER	-	-	feeding difficulties	-	-	(L)RTI, GER, feeding difficulties	-
<b>Musculoskeletal</b>											
Scoliosis	+	+	+	+	-	+	+	+	+	+	21/60
Arachnodactyly	-	-	-	+	+	+	-	-	NA	+	NA
Camptodactyly	-	-	-	+	+	+	+	+	NA	+	7/7
Duck bill deformity of the thumb	+	+	-	+	-	+	+	+	NA	+	NA

(Continued on next page)

Table 1. Continued											
Family - Individual	A-III.1	A-III.5	A-III.6	B-III.1	B-III.4	B-III.7	C-II.2	C-II.3	C-I.7	D-II.2	Dominant disease
<b>Feet Abnormalities</b>											
Bilateral CTEV	+	-	+	+	+	+	+	NA	NA	+	+
Bilateral pes planus	-	+	+	+	-	+	-	+	NA	-	NA
Sandal gap deformity	-	+	+	+	+	+	+	+	NA	-	NA
Orofacial hypotonia/hypomimia	NA	-	+	-	-	+	+	+	-	NA	3/7
Elevated CK	NA	+	-	-	-	NA	NA	NA	NA	-	NA

Clinical characteristics of the affected individuals. Relative frequency of clinical features in dominant *PIEZO2*-related disease<sup>15-17</sup> are given in the right column, if applicable. Abbreviations are as follows: M, male; F, female; year, age in years; UL, upper limb; LL, lower limb; P, proximal; D, distal; CTEV, congenital talipes equinovarus; NA, information not available; +, feature is present; -, feature is absent; het, heterozygous; hom, homozygous; (L)RTI, recurrent (lower) respiratory tract infection; GER, gastro-esophageal reflux; CK, creatine kinase.

which provides datasets of 60,706 unrelated individuals. Strikingly, for the whole *PIEZO2* gene, only 15 loss-of-function (LoF) variants with an average allele count of 1.2 were reported at ExAC, while none of these variants was found in the homozygous state. This supports the probably detrimental nature of homozygous LoF variants in *PIEZO2*. For the affected individual II.2 of family D, microarray analysis was performed. Analysis revealed a homozygous deletion of ~42 kb of chromosome 18 (p11.22) containing exon 6 (ENSE00001018194) and exon 7 (ENSE00001111048) of *PIEZO2* and a homozygous deletion of ~63 kb of chromosome 15 (q15.3), which contains *CATSPER2*, *STRC*, and part of *CKMT1B*. Homozygous deletions of *STRC* are associated with non-syndromic sensorineural hearing loss<sup>21</sup> and indeed individual D-II.2 shows hearing loss, most likely caused by this deletion. Other individuals with mutations of *STRC* do not present with any of the neuromuscular features present in individual D-II.2 and thus, it is unlikely that the *STRC* deletion accounts for his full phenotype. To validate the genomic deletion of *PIEZO2* exons, we carried out exon-specific PCR on DNA of individual D-II.2 and on DNA of healthy control individuals. PCR was carried out as multiplex PCR, amplifying the exons 5, 6, 7, and 8 each together with an independent genomic region (here, *RYR1* exon 93) as control. While control DNAs allowed amplification of *PIEZO2* exons, DNA of individual D-II.2 failed to yield PCR products for exons 6 and 7, while the multiplexed independent genomic region was successfully amplified (Figure 1D). Likewise, the neighboring exons 5 and 8 were successfully amplified from D-II.2 and control DNA. This suggests that indeed the *PIEZO2* exons 6 and 7 are homozygously deleted in the affected individual D-II.2. Detection of exons 5 and 8 indicates that the deletion breakpoints must localize within intron 5 and intron 7, respectively. To determine the exact deletion breakpoints, long-range PCR was carried out using the KOD FX Neo polymerase (Toyobo Life Science). Using a touchdown PCR protocol, we amplified an approximately 65 kb genomic region of *PIEZO2* ranging from exon 5 to exon 8 using the oligonucleotides 5'-TAGCTTAAAGGGAGCTGATGCTG-3' (fw) and 5'-TGTGTTGGAATAGAGTATCGATTAGTCAG-3' (rev). Due to the assumed ~42 kb deletion in individual D-II.2, the PCR yielded a product exceeding 10 kb. The respective band was extracted from an agarose gel using the QiaExII gel extraction protocol (Qiagen) for large DNA fragments. Sanger sequencing was carried out on the PCR product targeting intron 5 in the forward direction, while approaching exon 6 in 1 kb intervals. Breakpoint regions were detected within Alu elements mapping to chr18: 10,866,287–10,866,582 (AluSc8) and chr18: 10,813,970–10,814,262 (AluY), respectively (Figure 1D). Due to high sequence similarity of both Alu elements, it was not possible to determine the exact deletion breakpoint. However, Sanger sequencing indicated that the breakpoint must localize within a 44 bp region that both Alu elements have in common. These regions correspond



**Figure 2. Phenotypic Characteristics of Affected Individuals with Homozygous LoF Variants in *PIEZO2***

Photographs of individuals with homozygous frameshift variants/exon deletions in *PIEZO2*.

(A) Frontal photographs. Facial muscle weakness was present in some of the examined affected individuals. Note weak facial expression/hypomimia in individual B-III.4 and C-II.2.

(B) Foot deformities were present in all examined affected individuals including congenital bilateral talipes equinovarus, pes planus, sandal gap deformity, and other valgus and varus deformities.

(C) Common hand abnormalities included arachnodactyly and camptodactyly. Note the characteristic hyperextension of the proximal interphalangeal joint with flexion of the metacarpophalangeal joint of the thumb (duck bill deformity) that was present in the majority of case subjects.

(D) Spinal skeletal deformities were present in all affected individuals and have been in part surgically corrected. Affected individuals have a short stature (e.g., A-III.5).

to the chromosomal coordinates chr18: 10,866,366–10,866,410 in *PIEZO2* intron 5 and chr18: 10,813,895–10,813,851 in intron 7, respectively (Figure 1D). Thus, a region of ~52.3 kb is deleted in the affected individual D-II.2. The fused intronic sequence between the exons 5 and 8 comprises ~4.75 kb of intron 5 and ~6.9 kb of intron 7, which makes a splicing aberration of exons 5 and 8 to appear unlikely. With exon lengths of 211 bp (exon 6) and 214 bp (exon 7), respectively, deletion of both exons would result in disruption of the reading frame and thus in loss of *PIEZO2* protein function. Whether absence of exons 6 and 7 causes downstream missplicing events cannot be answered with certainty, because we do not

have access to RNA from the proband. The position of all newly identified homozygous variants in *PIEZO2* and previously reported dominant heterozygous mutations for DA3, DA5, and MWKS are depicted in Figure 1E.

Both frameshift mutations and out-of-frame exon skipping will cause termination of protein synthesis via premature termination codons (PTCs). Disregarding some known exceptions, transcripts that carry PTCs at least 50 to 55 bp upstream of the most 3' coding exon-exon boundary undergo nonsense-mediated decay (NMD) and are not translated into functional proteins.<sup>22,23</sup> To validate our hypothesis that the homozygous presence of PTCs in *PIEZO2* transcripts leads to NMD in affected individuals, we

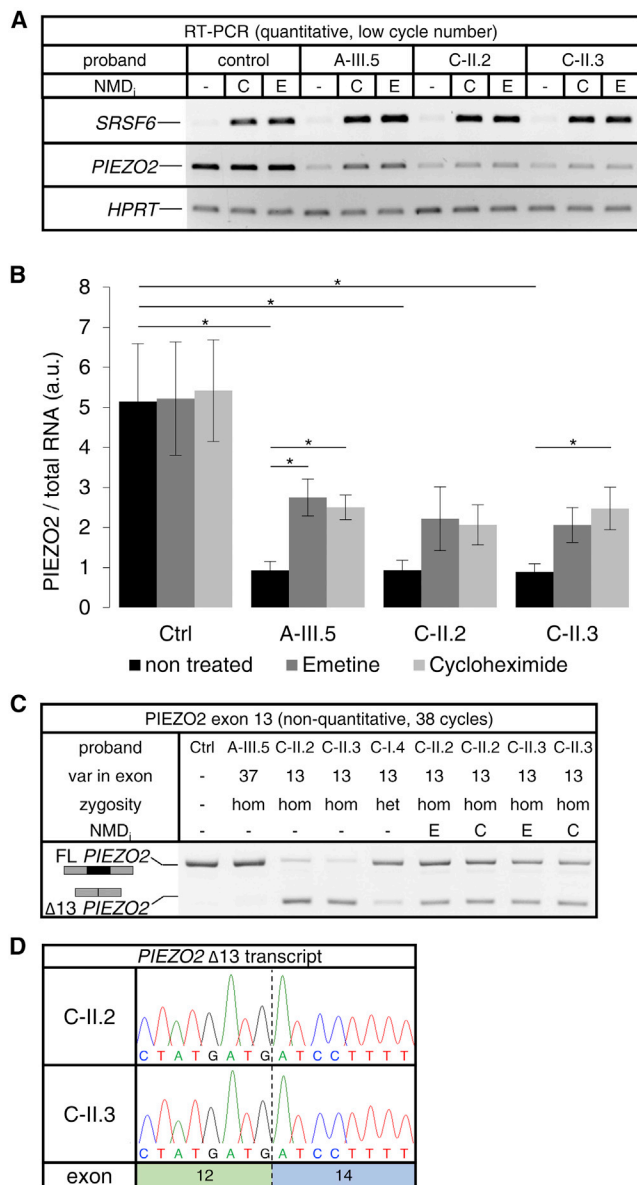


### Figure 3. Homozygous Frameshift Variants in *PIEZO2* Cause Nonsense-Mediated Decay of *PIEZO2* Transcripts

Determination of *PIEZO2* transcript levels by semiquantitative PCR. RNA was isolated from control and affected individual-derived fibroblasts that were either treated or non-treated with an NMD-inhibiting agent. 300 ng of RNA was reversely transcribed into cDNA.

(A) RT-PCR of *SRSF6* and *PIEZO2*. *SRSF6* (PCR product size: 253 bp) is a physiological target of NMD used as control. A region spanning exons 51 and 52 of *PIEZO2* (28 cycles; PCR product size: 306 bp) was amplified. Both cycloheximide (C) and emetine (E) treatment efficiently inhibited NMD. *HPRT1* was amplified as loading control (product size: 168 bp).

(B) Quantification of *PIEZO2* transcripts. Bars show the mean and standard errors of triplicate NMD inhibition experiments. Asterisks indicate statistical significance ( $p < 0.05$ ).

(C) Oligonucleotides in *PIEZO2* exons 12 and 14 were used to coordinately amplify transcripts containing (FL) or lacking ( $\Delta 13$ ) exon 13 (38 cycles; FL-PCR product size: 430 bp;  $\Delta 13$ -PCR product size: 199 bp).

(D)  $\Delta 13$  PCR products were Sanger sequenced demonstrating skipping of *PIEZO2* exon 13 in presence of the variant c.1550\_1552delGCTinsCGAA.

analyzed RNA isolated from affected individual-derived primary fibroblasts by RT-PCR. Fibroblast cell lines derived from skin biopsies of affected and unaffected family members were cultured in either normal DMEM containing 10% FCS, penicillin-streptomycin, and amphotericin B or treated in medium containing 1.0 mg/mL cycloheximide or 10  $\mu$ g/mL emetine for 8 hr to inhibit NMD. RNA was isolated with the QIAGEN RNeasy Mini Kit and 300 ng of total RNA were reversely transcribed to cDNA using the QIAGEN QuantiTect Reverse Transcription Kit. Successful inhibition of the NMD mechanism was assayed by PCR amplifying *SRSF6* (*SRP55*) transcripts (fw, 5'-GCTA CGGAAGCCGCATGACCAATGG-3' and rev, 5'-GGCCA CAAAACACGCAAGGTAACAG-3'), which is a well-known NMD target under physiological conditions.<sup>24</sup> *SRSF6* PCR products were visualized on EtBr-stained agarose gels. *SRSF6* transcripts were weakly detectable in untreated control and affected individuals' fibroblasts but were markedly increased in cycloheximide- or emetine-treated cells (Figure 3A). This suggests that NMD is inhibited effectively under the applied condition.

*PIEZO2* has four annotated transcripts that are translated into proteins (Figure 1E, UniProt): three encode a full-length protein with some alternative exons, and one transcript (ENST00000538948) encodes a shorter protein mapping to the C-terminal end of *PIEZO2*. To detect *PIEZO2* transcripts, oligonucleotides were designed mapping to the terminal exons 51 and 52 of *PIEZO2* (fw, 5'-AACTCT CAGGCCCTGGAAGTGGT-3' and rev, 5'-TTTGATCATTG TCTCTGGTGAGCGA-3'). *PIEZO2* transcripts were PCR amplified and PCR products were visualized on EtBr-stained agarose gels. *HPRT1* (GenBank: NG\_012329.1) was amplified as loading control (fw, 5'-GCTATTGTAAT GACCAGTCAACAGGGGAC-3' and rev, 5'-CCTTGACCA TCTTTGGATTATACTGCC-3').

Semiquantitative RT-PCR (low cycle number) specifically showed a prominent band of *PIEZO2* transcripts in untreated control cell lines, while *PIEZO2* transcripts were strongly and significantly diminished or absent in affected individuals with homozygous frameshift variants supporting the LoF nature of these variants (Figure 3A). To check whether the strong downregulation of *PIEZO2* transcripts is based on NMD, *PIEZO2* RNA levels in fibroblast derived from affected individuals were compared between untreated and cycloheximide- or emetine-treated samples, respectively. *PIEZO2* transcripts were easily detectable in RNA derived from cycloheximide- or emetine-treated fibroblasts but only minimally in untreated cells (Figure 3A), suggesting that large portions of *PIEZO2* transcripts indeed undergo NMD in individuals carrying homozygous frameshift variants. NMD inhibition experiments were carried out in triplicate and results were statistically analyzed using Student's t test (Figure 3B). Interestingly,

Abbreviations are as follows: C, cycloheximide; E, emetine; hom, homozygous; het, heterozygous; FL, full-length;  $\Delta 13$ , delta exon 13 (exon skipping).

NMD-related transcript decay was significant and somewhat stronger in individual A-III.5 compared to both tested affected individuals of family C. *PIEZO2* levels in affected individuals C-II.2 and C-II.3 were also increased upon NMD inhibition, but the effect was weaker and not significant in most cases. During routine splicing analysis (Human Splicing Finder 3), the variant c.1550\_1552delGCTinsCGAA of family C generated a 100% binding site match for the SR-rich splice factor SF2/ASF in *PIEZO2* exon 13. SF2 may have both a positive or negative effect on exon inclusion by regulating U1 snRNP and U2AF interaction with splice sites.<sup>25–27</sup> To test whether the homozygous frameshift variant in family C altered the splicing of *PIEZO2* exon 13, RT-PCR was carried out. Oligonucleotides were designed for *PIEZO2* exon 12 and exon 14 to generate differently sized PCR products for respective transcripts containing (430 bp, FL = full-length) or lacking (199 bp,  $\Delta$ 13) exon 13 (fw, 5'-GCGAGAGGAGGAAGAGGAAGAGAA-3' and rev, 5'-TTGCTCTGTGAGGTGCTGCCTC-3'). A 38 cycle RT-PCR specifically showed strong expression of FL transcripts in control cells and slightly diminished expression in fibroblasts of affected individual A-III.5 (variant in exon 37) (Figure 3C). FL transcripts were strongly diminished in affected individuals C-II.2 and C-II.3, instead replaced by  $\Delta$ 13 transcripts. Strikingly, FL transcripts were detectable in affected individuals of family C after NMD inhibition. Sanger sequencing of PCR products confirmed the identity of  $\Delta$ 13 transcripts (Figure 3D). The *PIEZO2* exon 13 is 231-bp long and is thus an in-frame exon encoding exactly 77 amino acids. These data suggest that skipping of exon 13 due to the identified indel variant does not disrupt the reading frame in *PIEZO2*  $\Delta$ 13 transcripts. Thus, they escape NMD and are detectable under physiological conditions. In contrast, FL transcripts undergo NMD and are detectable solely after NMD inhibition. Therefore, weaker NMD of *PIEZO2* transcripts in affected individuals of family C, as compared to family A, is probably attributable to the partial escape of transcripts from NMD by restoration of the reading-frame due to exon skipping. The affected individuals C-II.2 and C-II.3 have a phenotype comparable to affected individuals from other families described here, so it appears unlikely that restored *PIEZO2*  $\Delta$ 13 transcripts can sufficiently restore protein function to ameliorate the disease. Functional implications of protein domains encoded by exon 13 are not available at present. Neither did skipping of exon 13 cause the downstream exons 14 to 17 to be aberrantly spliced, as investigated by exon-specific RT-PCRs (data not shown). Indeed, affected individuals of family C showed trace levels of *PIEZO2* transcript expression (assay for exon 52) under low cycle quantitative conditions, which were absent in A-III.5 (Figure 3A). This supports our hypothesis that exon 13 skipping in part protects *PIEZO2* transcripts from NMD, but also underlines that frame-correcting exon skipping occurs in only a small fraction of transcripts. In silico splicing analysis of the frameshift variant in *PIEZO2* exon 37 (family A), for which we had fibroblasts available, did

not predict any alteration in splicing inclusion of exon 37. Neither did RT-PCR demonstrate expression of *PIEZO2* transcripts lacking exon 37 under normal or NMD-inhibiting conditions (data not shown).

NMD of *PIEZO2* transcripts based on homozygous frameshift mutations should lead to strongly diminished or absent *PIEZO2* protein levels. To validate this hypothesis, we performed SDS-PAGE and western blotting of protein isolated from affected individual-derived fibroblasts. We sought to optimize immunological detection of *PIEZO2* by using three commercially available antibodies for *PIEZO2*. Neither of the employed antibodies allowed specific detection of *PIEZO2* bands. None of the two expected protein sizes (~700 aa and ~2,700 aa) were specifically detectable in fibroblasts derived from affected or unaffected individuals or in HEK293T cells. This might be due to absence or low abundance of *PIEZO2* proteins in these cell types. Even though *PIEZO2* is expressed in skin, its expression is thought to be restricted to Merkel cells. Most likely, *PIEZO2* protein levels in the tested cell lines are insufficient for specific detection by western blotting and thus we rely on reduced expression levels and NMD detected in previous RNA expression analyses.

In conclusion, we present a clinical entity related to homozygous LoF mutations in *PIEZO2*. This phenotype differs from the autosomal dominant for several reasons. First of all, although almost all individuals affected by recessive *PIEZO2*-related disease show spine deformities like kyphoscoliosis, only about a third of individuals affected by dominant *PIEZO2*-related disease present this feature.<sup>15–17</sup> Furthermore, in contrast to the individuals affected by the dominant disease spectrum, who show ophthalmoplegia or ptosis in 53 of 70 and in 48 of 68 case subjects, respectively,<sup>15–17</sup> the individuals carrying *PIEZO2* homozygous LoF variations display no specific ocular phenotype. Several authors reported pulmonary disease with dominant *PIEZO2* disorders (18 of 72 case subjects), particularly in individuals affected by DAS<sup>15–17</sup> due to restrictive chest disease,<sup>18,20</sup> as a consequence of increased resting muscle tone that occurs in later life. Respiratory involvement in the individuals reported here is mainly represented by neonatal respiratory insufficiency, which fully recovered during the first days of life, which is in contrast to other conditions, such as SMARD, where permanent assisted ventilation is required.<sup>28,29</sup> This suggests a distinct functional etiology of neonatal respiratory distress in recessive *PIEZO2*-related disease, and this phenotype may serve as a hallmark to clinically distinguish dominant from recessive types of *PIEZO2*-related disease. DA3 or MWKS may also present with cerebellar malformations.<sup>16</sup> In the present study, the few affected individuals that underwent brain and spinal MRI did not show any cerebellar or spinal abnormalities. A mild dysarthria is another feature shared by some of the affected individuals with homozygous *PIEZO2* variants that has not been reported for the autosomal-dominant disease. A delayed cognitive development and/or reduced communication skills were present in three of the

examined affected individuals. All the heterozygous carriers of the LoF mutations in the four families were fully asymptomatic and did not show any of the main features of the disorder reported here, such as spine deformities, congenital talipes equinovarus, respiratory distress at birth, short stature, dysarthria, or delayed motor milestones.

DA3, DA5, and MWKS are caused by dominant mutations that are mainly localized at the C-terminal end of PIEZO2<sup>16</sup> (Figure 1E). Dominant disease-causing PIEZO2 mutations change the biophysical properties of PIEZO2 channels which inactivate slower and/or recover faster from inactivation.<sup>15</sup> This leads to increased channel activity and is functionally in agreement with the gain-of-function (GoF) nature of mutations that cause dominantly inherited PIEZO2-related diseases. LoF variants identified here were distributed across the PIEZO2 gene and do not map to any hotspots as is the case for dominant GoF variants. Interestingly, the only heterozygous nonsense mutation p.Trp2746\* associated with dominant DA3 is localized in the last exon of PIEZO2 and thus transcripts carrying that mutation are expected to escape NMD.<sup>22,23</sup> Accordingly, heterozygous absence of the terminal amino acids causing a phenotype fully matching DA3 argues for a GoF effect of this mutation but not for haploinsufficiency as the cause of disease. Indeed, the C-terminal region of PIEZO2 has been previously speculated to fulfill regulatory roles for this ion channel,<sup>15</sup> which is supportive of a GoF mechanism. The frameshift mutations (families A, B, C) and exon deletions (family D) described here are LoF mutations, as expression levels of PIEZO2 transcripts were markedly reduced in the tested individuals (Figure 3A). The distinct clinical manifestations of the AD PIEZO2-related spectrum and the recessive PIEZO2-related disease suggests that GoF and LoF variants in PIEZO2 have different effects on muscle development and disease pathophysiology. Thus, depending on their nature and their position, PIEZO2 variants may lead to distinct clinical phenotypes. Similar distinguishable phenotypes caused by different type of mutations have been reported for other genes.<sup>30–32</sup>

PIEZO2, but not PIEZO1, is expressed in murine dorsal root ganglia,<sup>11</sup> which relay somatosensory information like mechanical, thermal, noxious, and chemical stimuli. We hypothesize that loss of PIEZO2 channels in dorsal root ganglia leads to dysregulation of muscle proprioceptive function and thus to impaired muscle development in humans. Due to its low mRNA level, it is highly unlikely that PIEZO1 is relevant for mechanically activated (MA) currents in dorsal root ganglia. In contrast, PIEZO2 has been demonstrated to be sufficient to evoke large MA currents in various cell types upon heterologous expression.<sup>11</sup> Moreover, dorsal root ganglia, as PIEZO2-expressing tissue, have been implicated in normal muscle development.<sup>33</sup> Nikolaou and colleagues have demonstrated that upon motor denervation, maintaining the innervation of afferent fibers to the muscle was effectively counteracting arthrogryposis.<sup>33</sup> This suggests that sensory input and intact afferent connectivity play important roles during

muscle development and regeneration. Indeed, reduced fetal movement, regardless of its etiology, is associated with impaired muscle development. Whether the lack of fetal movement (i.e., muscle contraction) or the lack of sensing/coordinating this muscle contraction (i.e., deficient afferent innervation leading to failure in contractile feedback) finally result in the same consequences (e.g., arthrogryposis) is still unclear. However, Woo and colleagues clearly demonstrated that *Piezo2* is mainly expressed in proprioceptive neurons but not in skeletal muscle and that PIEZO2 MA-currents are necessary for normal muscle development in the mouse.<sup>34</sup> Indeed, mice depleted of *Piezo2* in proprioceptive neurons fail to show rapidly adapting MA currents in dorsal root ganglia (DRG) with no obvious quantitative or structural changes observable upon *Piezo2* conditional knock-out (cKO). cKO mice are born normally but develop limb coordination abnormalities and gait instability at P7. Moreover, *Piezo2*-deficient proprioceptive neurons were mechanically unresponsive to induced muscle stretch.<sup>34</sup> To our knowledge there is no published data demonstrating the expression of PIEZO2 in human proprioceptive neurons. PIEZO2 ion channels with dominant GoF mutations are hyperactive due to decelerated channel inactivation but accelerated channel regeneration, so mutated channels induce stronger firing upon mechanical stimulation.<sup>15</sup> Thus, in PIEZO2-related human disease, there is either increased afferent firing upon mechanical stimulation (GoF in dominant disease) or failure in afferent responsiveness to mechanical stimuli (LoF in recessive disease). Indeed, nerve conduction studies performed on affected individuals A-III.6 and D-II.2 showed clearly diminished sensory nerve conduction velocities. The expression pattern of PIEZO2 in Merkel cells of the skin and in dorsal root ganglia sensory neurons is in good concordance with sensory conduction deficits in the two tested individuals. We propose that homozygous frameshift variants in PIEZO2 lead to the loss of PIEZO2 protein and thus to reduced rapidly adapting MA currents in dorsal root ganglia afferents. Interestingly, Woo and colleagues have demonstrated an increase of intermediately adapting (IA) MA currents and hyperexcitability in *Piezo2*-deficient proprioceptive neurons.<sup>34</sup> Increased IA currents and a decreased tolerance to evoke action potentials might result in neuronal activity that is independent of mechanical stimuli. Each of these mechanisms may cause aberrant feedback of muscle stretch and muscle contraction, and as a developmental consequence, disturbed muscle morphology and function.

The muscle-related phenotype observed in individuals carrying PIEZO2 homozygous LoF variations is in line with observations in *Piezo2* cKO mice.<sup>34</sup> Homozygous frameshift mutations are expected to cause the loss of PIEZO2 protein in all cell types. However, mice ubiquitously depleted of PIEZO2 were reported to die shortly after birth,<sup>35</sup> whereas individuals with homozygous LoF mutations survive until adulthood and currently there is no sign of a reduced life expectancy. Strikingly, most of the

affected individuals that we have included in this report presented with postnatal respiratory distress, which was spontaneously resolving. Even though the reason for early postnatal lethality of ubiquitous *Piezo2*-depleted mice was not disclosed by the authors, we speculate that respiratory insufficiency might have equally occurred in mice.

We speculate whether there is another entity that makes the human phenotype milder compared to ubiquitous *Piezo2*-KO mice: there are four annotated protein-coding isoforms for human *PIEZO2* (Figure 1E). However, all reading-frame-disrupting variants and aberrations identified here occur in the N-terminal and central region of *PIEZO2*. The short isoform 3 (709 aa) uses an alternative initial exon (i.e., exon 39b, ENSE00002321328) that is not used by any other annotated *PIEZO2* isoform. Thus, isoform 3 should not be affected, as all identified LoF mutations were located upstream of exon 39. To our knowledge, there is no literature providing data about the function or expression patterns of this C-terminal isoform. Our attempts to identify isoform 3 in human control fibroblasts and in fibroblasts derived from affected individuals using multiple primer sets targeting exon 39b and downstream exons were unsuccessful (data not shown), indicating that this isoform is probably not expressed in human fibroblasts. However, despite the lack of functional implications of this isoform and lack of expression in fibroblasts, we cannot rule out a possible compensatory effect evoked by isoform 3 in neurons and other cell types. Furthermore, we demonstrated that the frameshift variant c.1550\_1552delGCTinsCGAA in exon 13 of *PIEZO2* causes skipping of exon 13, while the immediate downstream exons were not affected by this missplicing event. Interestingly, all exons harboring homozygous frameshift mutations (exons 13, 20, and 37) are in-frame exons. Possible skipping of these exons would remove frameshift variants from transcripts, restore the reading frame, and allow transcripts to escape from NMD. Indeed, we demonstrated that  $\Delta 13$  transcripts escaped NMD, while transcripts containing exon 13 with frameshift variants were detectable only under NMD inhibition (Figure 3C). For testing, we had fibroblast cell lines harboring homozygous mutations only in exon 13 and exon 37 and we did not identify transcripts lacking exon 37. Still, it could be postulated that frame-corrected transcripts may encode (partly) functional *PIEZO2* protein, which might in turn explain the relatively mild phenotype in these affected individuals as compared to ubiquitous *Piezo2* KO mice.<sup>35</sup>

In conclusion, we identified homozygous LoF variants in *PIEZO2* as the underlying cause for an autosomal-recessive distal muscular atrophy with arthrogryposis, kyphoscoliosis, and neonatal respiratory insufficiency distinct from previously described dominant *PIEZO2* diseases. We speculate that loss of *PIEZO2* proteins in afferent neurons cause aberrant muscle development and function, probably due to impaired proprioceptive feedback. Although *PIEZO2* in mice is physiologically highly expressed in dorsal root ganglia, further molecular and

electrophysiological functional studies will be required to validate afferent neurons as the disease-causing, *PIEZO2*-deficient tissue leading to disturbed muscular function and development.

### Accession Numbers

Whole-exome sequencing data were deposited at the European Genome-phenome Archive (EGA) under the accession number EGAD00001002694.

### Supplemental Data

Supplemental Data include case reports and one figure and can be found with this article online at <http://dx.doi.org/10.1016/j.ajhg.2016.09.019>.

### Acknowledgments

We are grateful to Dr. Spier and Dr. Lyding from the University Hospital Bonn and to Dr. Herkenrath from the University Hospital of Cologne for referral of affected individuals, and to Dr. Wunderlich for electrophysiological examination. The research leading to these results has received funding from the European Community's Seventh Framework Programme (FP7/2007-2013) under grant agreement no. 2012-305121 "Integrated European -omics research project for diagnosis and therapy in rare neuromuscular and neurodegenerative diseases (NEUROMICS)." The work was also partially funded by The Department of Science and Technology, India, through the project titled "Application of autozygosity mapping and exome sequencing to identify genetic basis of disorders of skeletal development" (SB/SO/HS/005/2014).

Received: July 13, 2016

Accepted: September 26, 2016

Published: October 27, 2016

### Web Resources

Ensembl Genome Browser, <http://www.ensembl.org/index.html>  
European Genome-phenome Archive (EGA), <https://www.ebi.ac.uk/ega>

ExAC Browser, <http://exac.broadinstitute.org/>

GenBank, <http://www.ncbi.nlm.nih.gov/genbank/>

GeneCards, <http://www.genecards.org>

HGMD Professional, <http://www.hgmd.cf.ac.uk/ac/index.php>

Human Splicing Finder, <http://www.umd.be/HSF3/HSF.html>

NCBI, <http://www.ncbi.nlm.nih.gov/>

OMIM, <http://www.omim.org/>

UCSC Genome Browser, <http://genome.ucsc.edu>

UniProt, <http://www.uniprot.org/>

### References

1. Viana, F. (2016). TRPA1 channels: molecular sentinels of cellular stress and tissue damage. *J. Physiol.* 594, 4151–4169.
2. Zimmerman, A., Bai, L., and Ginty, D.D. (2014). The gentle touch receptors of mammalian skin. *Science* 346, 950–954.
3. Goutman, J.D., Elgoyhen, A.B., and Gómez-Casati, M.E. (2015). Cochlear hair cells: The sound-sensing machines. *FEBS Lett.* 589, 3354–3361.

4. Proske, U., and Gandevia, S.C. (2012). The proprioceptive senses: their roles in signaling body shape, body position and movement, and muscle force. *Physiol. Rev.* *92*, 1651–1697.
5. Haack, T., and Abdelilah-Seyfried, S. (2016). The force within: endocardial development, mechanotransduction and signalling during cardiac morphogenesis. *Development* *143*, 373–386.
6. Delmas, P., Hao, J., and Rodat-Despoix, L. (2011). Molecular mechanisms of mechanotransduction in mammalian sensory neurons. *Nat. Rev. Neurosci.* *12*, 139–153.
7. McCarter, G.C., Reichling, D.B., and Levine, J.D. (1999). Mechanical transduction by rat dorsal root ganglion neurons in vitro. *Neurosci. Lett.* *273*, 179–182.
8. Franco, A., Jr., and Lansman, J.B. (1990). Calcium entry through stretch-inactivated ion channels in mdx myotubes. *Nature* *344*, 670–673.
9. McBride, D.W., Jr., and Hamill, O.P. (1992). Pressure-clamp: a method for rapid step perturbation of mechanosensitive channels. *Pflügers Arch.* *421*, 606–612.
10. Volkens, L., Mechoukhi, Y., and Coste, B. (2015). Piezo channels: from structure to function. *Pflügers Arch.* *467*, 95–99.
11. Coste, B., Mathur, J., Schmidt, M., Earley, T.J., Ranade, S., Petrus, M.J., Dubin, A.E., and Patapoutian, A. (2010). Piezo1 and Piezo2 are essential components of distinct mechanically activated cation channels. *Science* *330*, 55–60.
12. Coste, B., Xiao, B., Santos, J.S., Syeda, R., Grandl, J., Spencer, K.S., Kim, S.E., Schmidt, M., Mathur, J., Dubin, A.E., et al. (2012). Piezo proteins are pore-forming subunits of mechanically activated channels. *Nature* *483*, 176–181.
13. Bagriantsev, S.N., Gracheva, E.O., and Gallagher, P.G. (2014). Piezo proteins: regulators of mechanosensation and other cellular processes. *J. Biol. Chem.* *289*, 31673–31681.
14. Woo, S.H., Ranade, S., Weyer, A.D., Dubin, A.E., Baba, Y., Qiu, Z., Petrus, M., Miyamoto, T., Reddy, K., Lumpkin, E.A., et al. (2014). Piezo2 is required for Merkel-cell mechanotransduction. *Nature* *509*, 622–626.
15. Coste, B., Houge, G., Murray, M.F., Stitzel, N., Bandell, M., Giovanni, M.A., Philippakis, A., Hoischen, A., Riemer, G., Steen, U., et al. (2013). Gain-of-function mutations in the mechanically activated ion channel PIEZO2 cause a subtype of distal arthrogyposis. *Proc. Natl. Acad. Sci. USA* *110*, 4667–4672.
16. McMillin, M.J., Beck, A.E., Chong, J.X., Shively, K.M., Buckingham, K.J., Gildersleeve, H.I., Aracena, M.I., Aylsworth, A.S., Bitoun, P., Carey, J.C., et al.; University of Washington Center for Mendelian Genomics (2014). Mutations in PIEZO2 cause Gordon syndrome, Marden-Walker syndrome, and distal arthrogyposis type 5. *Am. J. Hum. Genet.* *94*, 734–744.
17. Okubo, M., Fujita, A., Saito, Y., Komaki, H., Ishiyama, A., Take-shita, E., Kojima, E., Koichihara, R., Saito, T., Nakagawa, E., et al. (2015). A family of distal arthrogyposis type 5 due to a novel PIEZO2 mutation. *Am. J. Med. Genet. A.* *167A*, 1100–1106.
18. Bamshad, M., Jorde, L.B., and Carey, J.C. (1996). A revised and extended classification of the distal arthrogyposes. *Am. J. Med. Genet.* *65*, 277–281.
19. Fryns, J.P., Willekens, D., Van Schoubroeck, D., and Moerman, P. (1998). Marden-Walker syndrome versus isolated distal arthrogyposis: evidence that both conditions may be variable manifestations of the same mutated gene. *Clin. Genet.* *54*, 86–89.
20. Williams, M.S., Elliott, C.G., and Bamshad, M.J. (2007). Pulmonary disease is a component of distal arthrogyposis type 5. *Am. J. Med. Genet. A.* *143A*, 752–756.
21. Francey, L.J., Conlin, L.K., Kadesch, H.E., Clark, D., Berrodin, D., Sun, Y., Glessner, J., Hakonarson, H., Jalas, C., Landau, C., et al. (2012). Genome-wide SNP genotyping identifies the Stereocilin (STRC) gene as a major contributor to pediatric bilateral sensorineural hearing impairment. *Am. J. Med. Genet. A.* *158A*, 298–308.
22. Fatscher, T., Boehm, V., and Gehring, N.H. (2015). Mechanism, factors, and physiological role of nonsense-mediated mRNA decay. *Cell. Mol. Life Sci.* *72*, 4523–4544.
23. Nagy, E., and Maquat, L.E. (1998). A rule for termination-codon position within intron-containing genes: when nonsense affects RNA abundance. *Trends Biochem. Sci.* *23*, 198–199.
24. Lareau, L.F., Inada, M., Green, R.E., Wengrod, J.C., and Brenner, S.E. (2007). Unproductive splicing of SR genes associated with highly conserved and ultraconserved DNA elements. *Nature* *446*, 926–929.
25. Jamison, S.F., Pasman, Z., Wang, J., Will, C., Lüthmann, R., Manley, J.L., and Garcia-Blanco, M.A. (1995). U1 snRNP-ASF/SF2 interaction and 5' splice site recognition: characterization of required elements. *Nucleic Acids Res.* *23*, 3260–3267.
26. Kohtz, J.D., Jamison, S.F., Will, C.L., Zuo, P., Lüthmann, R., Garcia-Blanco, M.A., and Manley, J.L. (1994). Protein-protein interactions and 5'-splice-site recognition in mammalian mRNA precursors. *Nature* *368*, 119–124.
27. Dauksaite, V., and Akusjärvi, G. (2002). Human splicing factor ASF/SF2 encodes for a repressor domain required for its inhibitory activity on pre-mRNA splicing. *J. Biol. Chem.* *277*, 12579–12586.
28. Grohmann, K., Schuelke, M., Diers, A., Hoffmann, K., Lucke, B., Adams, C., Bertini, E., Leonhardt-Horti, H., Muntoni, F., Ouvrier, R., et al. (2001). Mutations in the gene encoding immunoglobulin mu-binding protein 2 cause spinal muscular atrophy with respiratory distress type 1. *Nat. Genet.* *29*, 75–77.
29. Grohmann, K., Varon, R., Stolz, P., Schuelke, M., Janetzki, C., Bertini, E., Bushby, K., Muntoni, F., Ouvrier, R., Van Maldergem, L., et al. (2003). Infantile spinal muscular atrophy with respiratory distress type 1 (SMARD1). *Ann. Neurol.* *54*, 719–724.
30. Inoue, K., Khajavi, M., Ohyama, T., Hirabayashi, S., Wilson, J., Reggin, J.D., Mancias, P., Butler, I.J., Wilkinson, M.F., Wegner, M., and Lupski, J.R. (2004). Molecular mechanism for distinct neurological phenotypes conveyed by allelic truncating mutations. *Nat. Genet.* *36*, 361–369.
31. Warner, L.E., Hilz, M.J., Appel, S.H., Killian, J.M., Kolodry, E.H., Karpati, G., Carpenter, S., Watters, G.V., Wheeler, C., Witt, D., et al. (1996). Clinical phenotypes of different MPZ (P0) mutations may include Charcot-Marie-Tooth type 1B, Dejerine-Sottas, and congenital hypomyelination. *Neuron* *17*, 451–460.
32. Elsayed, S.M., Heller, R., Thoenes, M., Zaki, M.S., Swan, D., El-sobky, E., Zühlke, C., Ebermann, I., Nürnberg, G., Nürnberg, P., and Bolz, H.J. (2014). Autosomal dominant SCA5 and autosomal recessive infantile SCA are allelic conditions resulting from SPTBN2 mutations. *Eur. J. Hum. Genet.* *22*, 286–288.
33. Nikolaou, S., Hu, L., and Cornwall, R. (2015). Afferent innervation, muscle spindles, and contractures following neonatal brachial plexus injury in a mouse model. *J. Hand Surg. Am.* *40*, 2007–2016.
34. Woo, S.H., Lukacs, V., de Nooij, J.C., Zaytseva, D., Criddle, C.R., Francisco, A., Jessell, T.M., Wilkinson, K.A., and Patapoutian, A. (2015). Piezo2 is the principal mechanotransduction channel for proprioception. *Nat. Neurosci.* *18*, 1756–1762.
35. Dubin, A.E., Schmidt, M., Mathur, J., Petrus, M.J., Xiao, B., Coste, B., and Patapoutian, A. (2012). Inflammatory signals enhance piezo2-mediated mechanosensitive currents. *Cell Rep.* *2*, 511–517.

**The American Journal of Human Genetics, Volume 99**

**Supplemental Data**

**Biallelic Loss of Proprioception-Related PIEZO2**

**Causes Muscular Atrophy with Perinatal Respiratory**

**Distress, Arthrogryposis, and Scoliosis**

**Andrea Delle Vedove, Markus Storbeck, Raoul Heller, Irmgard Hölker, Malavika Hebbar, Anju Shukla, Olafur Magnusson, Sebahattin Cirak, Katta M. Girisha, Mary O'Driscoll, Bart Loeys, and Brunhilde Wirth**

## Supplemental case reports:

### A-III.1

9-year-old male, son of consanguineous parents of Turkish ancestry. Prenatal USS diagnosis of bilateral CTEV and bilateral hydronephrosis, but good foetal activity. Born at term, floppy and cyanotic infant (APGAR: 6/8/9). After initial CPAP ventilation, oxygen administration needed no longer but residual inspiratory stridor in the first days. Good facial grimacing. CK: 266 U/L. A muscular biopsy at 3 years of age (y.o.a.) yielded unspecific findings: mild calibre variation of the muscular fibres with atrophy and hypertrophy of individual type I as well as type II fibres.

On examination at 5 years of age he could stand and walk a few steps only with support. He presented with generalized hypotonia, distal symmetrical muscular atrophy of the legs, mild muscular atrophy of upper limb girdle and kyphoscoliosis. Absent or weak deep tendon reflexes. The large joints were slightly hypermobile. Intelligence was normal.

### A-III.5

23-year-old male, son of consanguineous Turkish parents, first cousin of A-III.1. Born at term, APGAR 9/9/10, even though he showed signs of laboured respiration and inspiratory stridor within the first 48 hours. Postnatally and during early childhood generalized hypotonia and absent deep tendon reflexes. Mildly elevated CK at 2 years of age (118 U/l, reference 15-90 U/l). Delayed motor milestones (sitting: 2 years 1 month; standing: 2 years 5 months, walking: approx. 5 years). Ocular motor findings and restrictive or other pulmonary disease were excluded. EMG and NCS, EEG and evoked potentials, cranial MRI all performed around 1 y.o.a. were reported as normal. At 11 y.o.a. pulmonary function tests excluded an obstructive/restrictive lung disease.

On examination at 23 y.o.a. his height was 163 cm, and there was symmetrical distal muscular atrophy of lower limbs with bilateral pes planovalgus and bilateral hallux valgus. He wore ankle splints. Scoliosis (29° Cobb) was treated with Cheneau bracing. He had an athletic upper body, but sloping shoulders, and early fatigue limited the elevation of his arms. He nevertheless played wheelchair basketball. Hyperextended proximal interphalangeal joint (PIP) with flexion of metacarpophalangeal joint (MCP) of thumb bilaterally (so called duck bill or 90° angle deformity). Absent deep tendon reflexes. Mildly reduced light touch sensitivity, markedly impaired sensation of vibration. Normal intelligence, speech therapy for marked dysarthria.

### A-III.6

12-year-old female, sister of A-III-5. Born at term, CTEV, floppy infant and respiratory distress (APGAR 4/7/8) necessitating intubation for the first three postnatal days. Partially tube-fed during the 1<sup>st</sup> year due to weak uncoordinated suck. Initially more marked reduction of motor activity in upper than lower limbs. During childhood, she presented a generalized hypotonia and motor delay (sitting: 2 years 1, month; standing: 2 years 6 months). CTEV was surgically corrected, but she developed a bilateral pes planus and pes transversoplanus. Scoliosis (40° Cobb) at 4 years of age required brace treatment.

On examination at 12 y.o.a. she had symmetrical distal and proximal muscular weakness with lowest scores of 3/6 points for flexor and extensor hallucis longus and abductor pollicis as well as for neck flexor and extensors, but also involvement of upper limb girdle with sloping shoulders. Abduction of arms not possible beyond 150°. Absent deep tendon reflexes. Bilateral pes planovalgus. 26/34 points in the North Star Ambulatory assessment. She still wore a brace. No oculomotor anomalies. CK values were normal. N. tibialis derived motor nerve conduction velocity and muscle action potential were within normal range, whilst n. suralis derived sensory conduction velocities (37 m/s) and sensory nerve action potentials (6 µV) were bilaterally reduced. These findings were compatible with an axonal-demyelinating sensory neuropathy. Normal intelligence, hypomimic face and dysarthria for which she received speech therapy.

#### B-III.1

17-year-old male, son of consanguineous parents of Indian ancestry. At birth he presented with CTEV and respiratory insufficiency with cyanosis in the first days of life were reported. During childhood he showed hypotonia and he was frequently admitted to the hospital due to recurrent episodes of LRTI. Febrile and tonic-clonic seizures were also reported. Delayed motor milestones (head control: 7 months; sitting: 1 year 7 months; standing without support: 5 years; walking: 6 years). Kyphoscoliosis and lumbar lordosis are documented at 10 y.o.a. and were surgically corrected at 12 y.o.a.

On examination at 15 y.o.a. his height was 149 cm, and he had pectus carinatum, wide nipples, a small umbilical hernia, long neck with drooping shoulders. He showed a long face with long nose, wide nasal bridge, thin upper lip, high arched palate and small chin. Contractures at the wrist joints, arachnodactyly and a bilateral single palmar crease are reported. Bilateral duck bill deformity of the thumb. Absent deep tendon reflexes. Bilateral hallux valgus. Normal intelligence with mild dysarthria. CK levels were reported as normal. No abnormalities at ENMG and EEG were reported. Brain and spine CT, spine MRI were also normal.

#### B-III.4

10-year-old female, sister of B-III.1. At birth bilateral CTEV and asphyxia. During childhood she showed hypotonia and febrile seizures. Motor milestones were delayed (head control: 6 months; sitting: 18 months; standing: 4 years; walking: 5 years).

On examination at 7 y.o.a. she was 107 cm tall and showed similar facial features as her brother. She presented hand (arachnodactyly and camptodactyly) and foot deformities (valgus deformity of the right foot and varus deformity of the left foot, bilateral hallux valgus). Absent deep tendon reflexes. No scoliosis. Intelligence was normal with mild dysarthria. CK levels were normal (240 UI/L).

#### B-II.7

27-year-old male, son of consanguineous parents, uncle of B-III.1 and B-III.4. At birth CTEV. Delayed motor milestones. Arachnodactyly and camptodactyly.

On examination at 27 y.o.a., he showed severe kyphoscoliosis and lordosis. Wide nasal bridge, prominent nose, long philtrum and thin upper lip were also present. Bilateral pes varus and hallux valgus. Bilateral duck bill deformity of the thumb. Normal intelligence with mild dysarthria.

#### C-II.2

6-year-old male, son of consanguineous parents of Libyan origin. During pregnancy normal fetal activity was reported. At birth pocket-knife position of the lower limbs. Postnatally non-invasive oxygen supplementation for 8 days, weak suck, but tube feeding was not necessary. He suffered from recurrent upper respiratory tract infections. Symmetrical hypotonia, more marked at the lower extremities, scoliosis. Motor milestones (sitting: 2 years, 5 months) but also global development are delayed, probably partly because of the difficult socioeconomic background of refugee family.

On examination at 6 y.o.a. he showed short stature, myopathic facies with ptosis, reduced head control, marked distal symmetrical limb weakness (1/6) and truncal hypotonia, resulting in inability to stand unsupportedly and severe kyphoscoliosis (47° Cobb). Managed a few seconds of supported upright position with genu recurvatum. Absent deep tendon reflexes. He used a wheelchair.

### C-II.3

6-year-old female, sister of C-II.2. During pregnancy reported normal foetal activity. Born at term. She achieved unsupported sitting at 2 years of age. Generalized hypotonia, including orofacial hypomimia. At 3 years and 11 months she showed bilateral pes valgus.

On examination at 4 y.o.a., myopathic facies with ptosis, reduced head control, marked distal symmetrical limb weakness (2/6 on MRC scale) and truncal hypotonia, resulting in inability to stand unsupportedly and severe kyphoscoliosis (43° Cobb). Managed to pull herself for a few seconds into supported upright position with genu recurvatum. Bilateral duck bill deformity of the thumb. Absent deep tendon reflexes. Mild developmental delay, but difficult socioeconomic background of refugee family

### C-I.7

26-year-old affected female, paternal aunt of C-II.2 and C-II.3. who reportedly started walking at 8 y.o.a. and shows pronounced scoliosis. No further details were available for this individual.

### D-II.2

25-year-old male, son of consanguineous parents of Pakistani ancestry. He showed bilateral CTEV, severe hypotonia, frequent infections, feeding problems and stridor during infancy. He was developmentally delayed (walked at 5-6 years of age) and had short stature (Ht/Wt < 0,4<sup>th</sup> centile) and reduced head circumference. GER, hepatosplenomegaly with normal USS of the abdomen and liver biopsy and a large umbilical hernia were reported. Hands were notable for arachno- and camptodactyly. Bilateral duck bill deformity of the thumb. He underwent surgery to correct his scoliosis. Urine organic acids and plasma aminoacids were normal. CK > 700 UI/L (1990), subsequently normal. Electrophysiological studies showed an axonal neuropathy. Brain MRI was normal. Congenital fibre type disproportion was described in the muscle biopsy.

On examination at 25 y.o.a, he showed plagiocephaly, myopia, hearing loss, prominent nose, short philtrum, thin upper lip and underbite. Absent deep tendon reflexes. A mild/borderline learning disability is also reported.

**Considerations for differential diagnosis:**

The key features that define the core phenotype are the combination of transitional neonatal respiratory distress, symmetrical distal lower limb muscle atrophy of variable severity with hallux valgus and pes planovalgus, only mild upper limb involvement with duckbill deformity of thumbs, mild upper limb girdle weakness with sloping shoulders and neck weakness, truncal hypotonia with potentially severe kyphoscoliosis, and mild distal sensory involvement.

The recessive *PIEZO2*-associated phenotype described here is not associated with increased early lethality, and does not appear to be primarily progressive. Initial hypotonia improves with age and the major complication is progressive scoliosis.

CK may initially be mildly elevated, but normal later on, the findings on muscle biopsy were unspecific (fibre type disproportion) where performed.

This phenotype excludes disorders with early high lethality like DSMA1 (MIM 604320), SMAX2 (MIM 301830), CFTD/NEM3 (MIM 255310/161800), lethal congenital contracture syndromes (PS253310). It is also incompatible with those congenital arthrogryposis syndromes that are regularly associated with pterygia, increased bone fragility, structural brain anomalies and microcephaly, persistent dysphagia, or ocular involvement as in DA5 (MIM 108145) and Marden-Walker syndrome (MIM 248700). Distal arthrogryposis type 2 (MIM 193700 and 601680, respectively) and type 9 (MIM 121050) can be distinguished by the absence of characteristic perioral contractures and marfanoid habitus, cardiac involvement and crumpled ears, respectively.

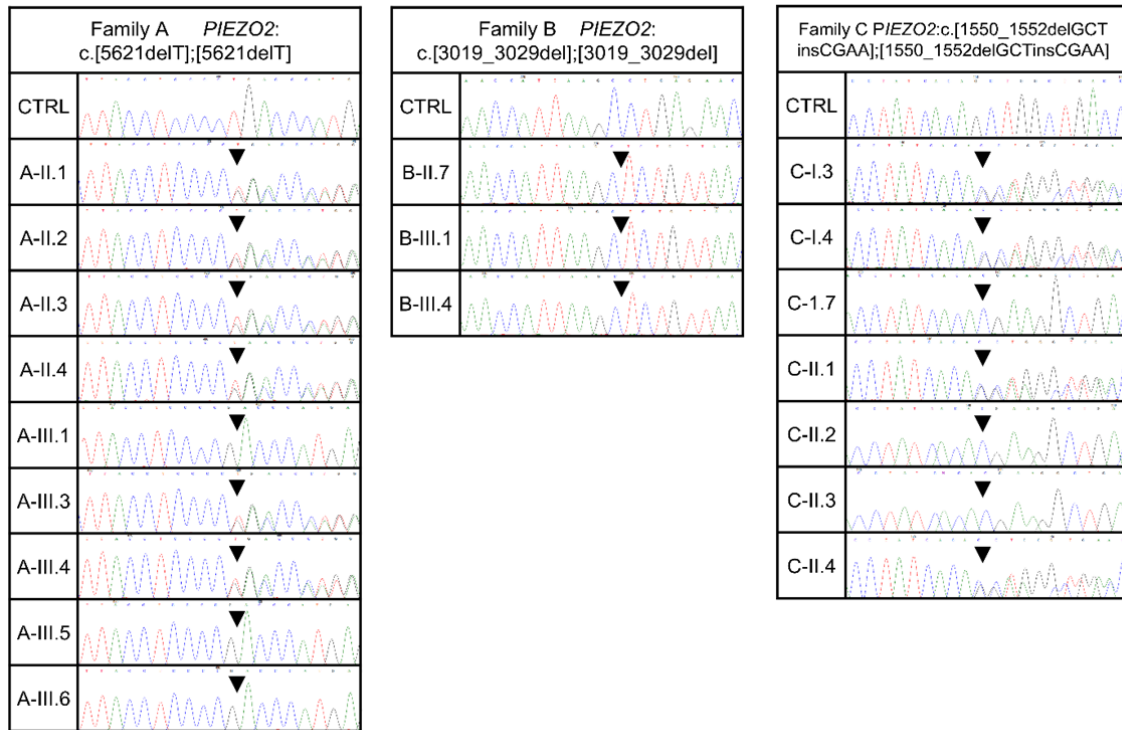


**Figure S1: Sanger sequencing and segregation analysis in affected and unaffected individuals.** Sanger sequencing results of all available individuals of families A, B and C. Homozygous frameshift variants are present in all affected individuals. Available unaffected family members were heterozygous carriers of the indicated variant.



## 7.2 Appendix B

Salpietro V\*, Lin W\*, **Delle Vedove A\***, Storbeck M, Liu Y, Efthymiou S, Manole A, Wiethoff S, Ye Q, Sagar A, McElreavey K, Krishnakumar SS; SYNAPS Study Group, Pitt M, Bello OD, Rothman JE, Basel-Vanagaite L, Hubshman MW, Aharoni S, Manzur AY, Wirth B, Houlden H. Homozygous mutations in VAMP1 cause a presynaptic congenital myasthenic syndrome. *Ann Neurol*. 2017 Apr;81(4):597-603. doi: 10.1002/ana.24905. Epub 2017 Mar 29. PMID: 28253535; PMCID: PMC5413866.

\* The authors contributed equally to this work

This work was published by Wiley Inc. and is appended under the Publisher's permission.



# Homozygous Mutations in *VAMP1* Cause a Presynaptic Congenital Myasthenic Syndrome

Vincenzo Salpietro, MD,<sup>1\*</sup>  
 Weichun Lin, PhD,<sup>2\*</sup>  
 Andrea Delle Vedove, MD,<sup>3,4\*</sup>  
 Markus Storbeck, PhD,<sup>3,4</sup> Yun Liu, PhD,<sup>2</sup>  
 Stephanie Efthymiou, MSc,<sup>1</sup>  
 Andreea Manole, BSc,<sup>1</sup>  
 Sarah Wiethoff, MD, PhD,<sup>1</sup>  
 Qiaohong Ye, BSc,<sup>2</sup> Anand Saggarr, MD,<sup>5</sup>  
 Kenneth McElreavey, PhD,<sup>6</sup>  
 Shyam S. Krishnakumar, PhD,<sup>7,8</sup>  
 SYNAPS Study Group,  
 Matthew Pitt, MD,<sup>9</sup>  
 Oscar D. Bello, PhD,<sup>7,8</sup>  
 James E. Rothman, PhD,<sup>7,8</sup>  
 Lina Basel-Vanagaite, MD, PhD,<sup>10,11,12</sup>  
 Monika Weisz Hubshman, MD, PhD,<sup>10,11,12</sup>  
 Sharon Aharoni, MD,<sup>12,13</sup>  
 Adnan Y. Manzur, MD,<sup>14</sup>  
 Brunhilde Wirth, PhD,<sup>3</sup> and  
 Henry Houlden, MD, PhD<sup>1</sup>

We report 2 families with undiagnosed recessive presynaptic congenital myasthenic syndrome (CMS). Whole exome or genome sequencing identified segregating homozygous variants in *VAMP1*: c.51\_64delAGGTGGGGTCCCC in a Kuwaiti family and c.146G>C in an Israeli family. *VAMP1* is crucial for vesicle fusion at presynaptic neuromuscular junction (NMJ). Electrodiagnostic examination showed severely low compound muscle action potentials and presynaptic impairment. We assessed the effect of the nonsense mutation on mRNA levels and evaluated the NMJ transmission in *VAMP1*<sup>lew/lew</sup> mice, observing neurophysiological features of presynaptic impairment, similar to the patients. Taken together, our findings highlight *VAMP1* homozygous mutations as a cause of presynaptic CMS.

ANN NEUROL 2017;81:597–603

The congenital myasthenic syndromes (CMSs) are a heterogeneous group of inherited diseases of the neuromuscular junction (NMJ), with fatigable muscle weakness as the clinical hallmark.<sup>1</sup> Several molecular causes

can be implicated in CMS pathophysiology, including mutations in genes encoding proteins associated with the muscle nicotinic acetylcholine receptor and the synaptic basal lamina, or (more rarely) involved in the NMJ presynaptic transmission.<sup>2–6</sup>

We describe 2 families from Kuwait and Israel where 2 of the siblings in each family presented clinical and neurophysiological features typical of a presynaptic CMS. Whole exome sequencing (WES) or whole genome sequencing (WGS) followed by Sanger sequencing unraveled either a homozygous frameshift or missense variants in *VAMP1* segregating with the phenotype in the 2 families. Screening a cohort of 63 undiagnosed CMS individuals failed to show any further causative variant in *VAMP1*.

## Materials and Methods

### Subjects

This study was approved by the institutional review boards of the participating centers. Informed consent was obtained from the families. Clinical details were obtained from medical

From the <sup>1</sup>Department of Molecular Neuroscience, Institute of Neurology, University College London Institute of Neurology, London, United Kingdom; <sup>2</sup>Department of Neuroscience, University of Texas Southwestern Medical Center, Dallas, TX; <sup>3</sup>Institute of Human Genetics, Center for Molecular Medicine Cologne, Cologne, Germany; <sup>4</sup>Institute for Genetics, University of Cologne, Cologne, Germany; <sup>5</sup>St George's Hospital, National Health Service Foundation Trust, London, United Kingdom; <sup>6</sup>Human Developmental Genetics, Pasteur Institute, Paris, France; <sup>7</sup>Department of Cell Biology, Yale School of Medicine, New Haven, CT; <sup>8</sup>Department of Clinical and Experimental Epilepsy, University College London Institute of Neurology, London, United Kingdom; <sup>9</sup>Department of Clinical Neurophysiology, Great Ormond Street Hospital for Children, National Health Service Foundation Trust, London, United Kingdom; <sup>10</sup>Pediatric Genetics Unit, Schneider Children's Medical Center of Israel, Petach Tikva, Israel; <sup>11</sup>Raphael Recanati Genetic Institute, Rabin Medical Center, Petach Tikva, Israel; <sup>12</sup>Sackler Faculty of Medicine, Tel Aviv University, Tel Aviv, Israel; <sup>13</sup>Institute of Child Neurology, Schneider Children's Medical Center of Israel, Petach Tikva, Israel; and <sup>14</sup>Department of Pediatric Neurology, Dubowitz Neuromuscular Centre, Great Ormond Street Hospital for Children National Health Service Foundation Trust, London, United Kingdom

Address correspondence to Dr Houlden, Department of Molecular Neuroscience, UCL Institute of Neurology, London WC1N 3BG, United Kingdom, E-mail: h.houlden@ucl.ac.uk or Dr Wirth, Institute of Human Genetics, University of Cologne, Cologne 50931, Germany, E-mail: brunhilde.wirth@uk-koeln.de.

\*V.S., W.L., and A.D.V. contributed equally to the present work.

Additional supporting information can be found in the online version of this article.

Received Dec 9, 2016, and in revised form Feb 24, 2017. Accepted for publication Feb 24, 2017.

View this article online at [wileyonlinelibrary.com](http://wileyonlinelibrary.com). DOI: 10.1002/ana.24905

records. Neurophysiological studies were performed according to standard procedures.<sup>7,8</sup>

### Genetic Studies

Before WES, the Kuwaiti probands (Family 1) underwent extensive molecular investigations that included sequencing of *AGRN*, mitochondrial DNA (mtDNA) sequencing, and deletion/duplication analysis and array comparative genome hybridization, which were all negative. Clinical trio-based WES of Family 1 and WGS of the Israeli probands and their parents (Family 2) were performed as previously described.<sup>9,10</sup> Immortalized lymphoblastoid cell lines were used for RNA extraction, reverse transcription polymerase chain reaction (RT-PCR) analysis, and semiquantitative RT-PCR assay. Sanger sequencing was performed to analyze segregation of the variants identified by WES/WGS.

### *Vamp1*<sup>lew/lew</sup> Mice

Breeder pairs of *Vamp1*<sup>+lew</sup> mice (C3H/HeDiSnJ-*Vamp1*<sup>lew</sup>/GrSj, stock # 004626) were obtained from the Jackson Laboratory (Bar Harbor, ME) and mated to generate homozygous mutant (*Vamp1*<sup>lew/lew</sup>) mice. Electrophysiological and morphological analyses of the NMJ in the *Vamp1*<sup>lew/lew</sup> mice were performed as previously reported.<sup>11,12</sup> All experimental protocols were approved by the University of Texas Southwestern Medical Center institutional animal care and use committee.

## Results

### Clinical and Neurophysiological Characteristics

**FAMILY 1.** Both affected individuals A.II-1 and A.II-3 (Fig 1A) presented shortly after birth with hypotonia and muscular weakness. Feeding difficulties requiring gavage feeding, delayed motor development, and ophthalmoparesis characterized the disease course. A.II-3 also presented joint contractures. Creatine kinase and plasma lactate were normal in the 2 children. On initial evaluation of Patient A.II-3, muscle biopsy showed myopathic features and borderline low complex IV activity (0.011; normal range = 0.014–0.034), but congenital myopathy gene panel and mtDNA analysis were negative. Although hypotonia slightly improved in Patient A.II-1, at the age of 3 years she still had difficulties standing upright and was unable to walk without support. Electrodiagnostic examination (EDX) in the 2 individuals showed similar findings (Table), with marked reduction in the amplitude of the compound muscle action potentials (CMAPs) and an increase in the amplitude to >200% of baseline on repetitive nerve stimulation (RNS) to 20Hz, indicating presynaptic impairment of NMJ transmission. The children's weakness slightly ameliorated under pyridostigmine treatment.

**FAMILY 2.** The affected individuals of this family (B.II-2 and B.II-3; see Fig 1B) showed severe hypotonia and muscle weakness since birth. Both siblings had

feeding difficulties and required percutaneous endoscopic gastrostomy. They presented severe impairment of developmental milestones. B.II-1 also showed joint laxity and kyphoscoliosis. B.II-3 presented knee contractures and breathing difficulties. During disease course, both children showed markedly reduced ability to generate anti-gravity posture and movements. B.II-2 never reached autonomous walk; his EDX showed severely low CMAPs and increased neuromuscular jitter, indicating NMJ transmission abnormalities (see Table 1). In both siblings, pyridostigmine treatment improved symptoms.

### Identification of the *VAMP1* Mutation

Trio-based WES of Family 1 (A.I-1, A.I-2, A.II-1; see Fig 1A) indicated in the index case 3 genes (Supplementary Table 1) carrying homozygous exonic variants predicted to have a possible pathogenic effect on protein function, based on the guidelines for variant classification.<sup>13</sup> Full Sanger-based segregation analysis of the candidate variants reduced the gene list to only 1 mutation in *VAMP1* (NM\_014231: c.51\_64delAGGTGGGG GTCCCC; p.Gly18TrpfsTer5\*), which was found to be homozygous in the affected individuals and heterozygous in their healthy sister and in the unaffected parents (see Fig 1C; data shown for the index case and her parents).

WGS of the 4 members of Family 2 (B.I-2, B.I-3, B.II-2, B.II-3; see Fig 1B) identified 6 genes carrying rare (likely) damaging variants (Supplementary Table 2), which were homozygous in the affected individuals and heterozygous in the parents.<sup>12</sup> Among these 6 variants, a homozygous missense mutation in *VAMP1* (NM\_014231: c.146G>C; p.Arg49Pro; see Fig 1D) emerged as the most likely explanation for the disease pathogenesis, as supported by protein function (the mutation affects a conserved amino acid within the active domain of the protein),<sup>14,15</sup> expression and role of this gene in the NMJ,<sup>12,16</sup> and the homozygous mutation identified in the patients from Family 1 presenting the same phenotype (see Fig 1C–G).

RT-PCR assay (performed to analyze possible nonsense-mediated decay associated with the *VAMP1* truncating variant in Family 1) found a mild reduction of mutant cDNA expression in the index case compared to the heterozygous carriers and the wild-type control (see Fig 1E, F).

### Impairments of the Neuromuscular Junction in *Vamp1*<sup>lew/lew</sup> Mice

To further investigate whether a biallelic null mutation in *VAMP1* in animal models may cause presynaptic NMJ

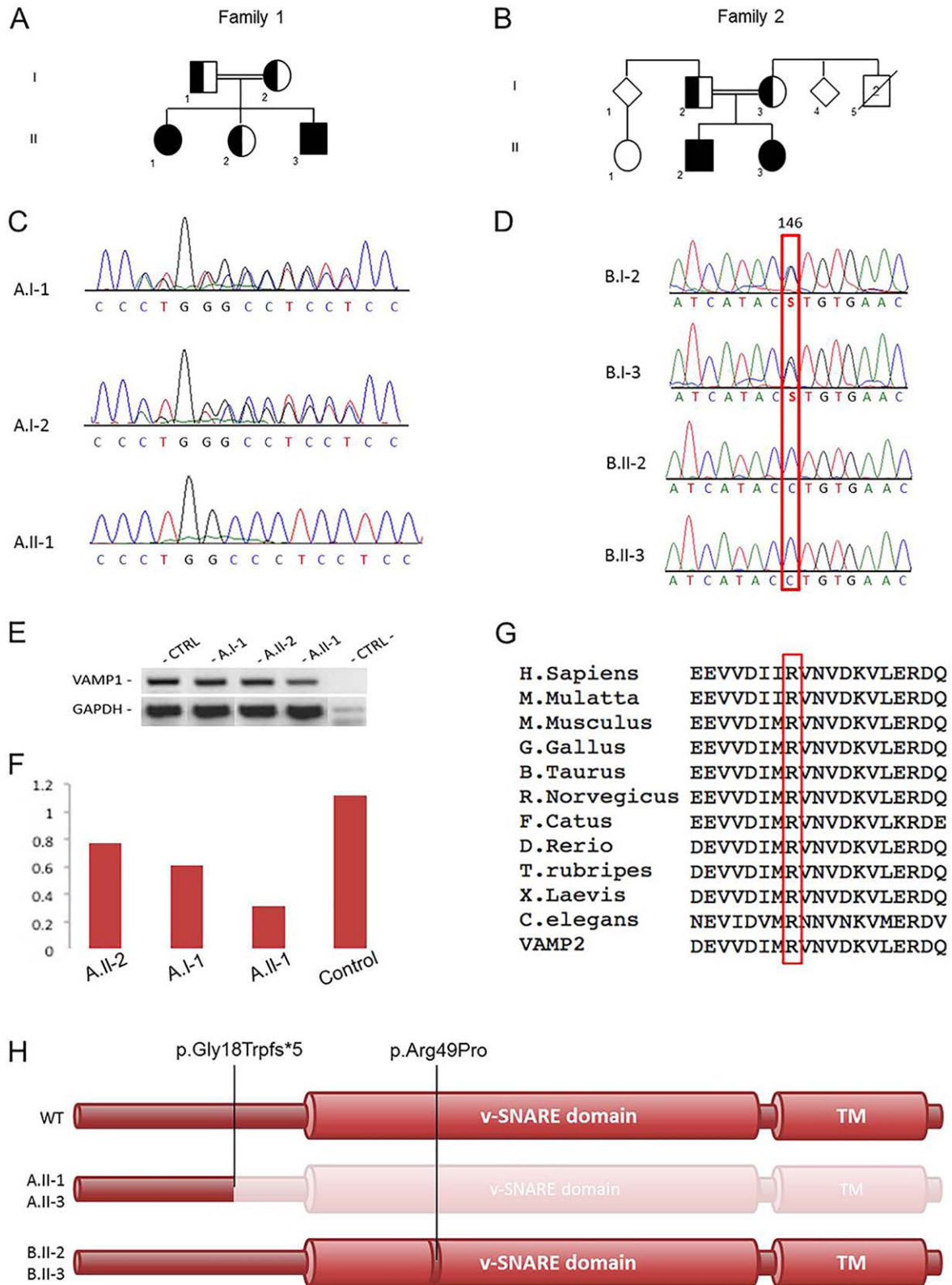


**FIGURE 1: Family trees, Sanger sequencing, and VAMP1 mutation analysis.** (A) Pedigree from Family 1. (B) Pedigree from Family 2. (C) Electropherograms of carrier parents and index case with the c.51\_64delAGGTGGGGGTCCCC variant. (D) Electropherograms of carrier parents and the 2 patients with the c.146G>C variant. (E) Reverse transcription polymerase chain reaction (PCR) amplifying the mutant cDNA transcript from mRNA extracted from the immortalized lymphoblastoid cell lines of the index case, her father, and her healthy sister (both carriers of the heterozygous deletion), and a wild-type control (CTRL). (F) Analysis of the semiquantitative PCR using the densitometry software ImageJ after normalization relative to a housekeeping gene (*GAPDH*) and calculation using a relative relationship method. (G) Multiple-sequence alignment showing complete conservation of protein sequence across species and SNARE homolog *VAMP2* in the v-SNARE coiled coil homology, in which the disease-segregating mutation p.Arg49Pro was found. (H) *VAMP1* protein representative. The c.51\_64delAGGTGGGGGTCCCC deletion causes a nonsense mutation, putatively producing a truncated protein lacking the v-SNARE and the transmembrane (TM) domains, whereas the p.Arg49Pro mutation affects an active site of the conserved v-SNARE domain.

**TABLE 1. Clinical and Neurophysiological Features of VAMP1-Associated Congenital Myasthenic Syndrome in Our Families**

Feature	A.II-1	A.II-3	B.II-1	B.II-2
Parental consanguinity	+	+	+	+
Onset	Birth	Birth	Antenatal, DFM	Birth
Muscle weakness	++	++	++	++
Developmental delay	++	++	++	++
Feeding difficulties	++	++	++	++
Ophthalmological abnormalities	Strabismus, mild ophthalmoplegia	Mild ophthalmoplegia	Strabismus	Strabismus
GI abnormalities	–	GERD	Dysphagia	Dysphagia
Skeletal joint abnormalities	–	Joint contractures	Joint laxity, kyphoscoliosis	Joint contractures
Chest infections, aspiration	+	+	+	+
Response to pyridostigmine	+	+	+	+
Sensory studies	Normal	Normal	Normal	NT
Motor studies	AH CMAP ↓↓	AH CMAP ↓↓	ACL CMAP ↓↓	NT
EMG	Myopathic	Myopathic	Myopathic	NT
Repetitive stimulation	AH: 3Hz, + 32.8%; 20Hz, + 640%	AH: 3Hz, + 60%; 20Hz, + 207%	NA	NT
Jitter	EDC, no twitch	Orb oculi, no twitch	↑↑ mean MCD = 74.3 μs	NT

ACL = accessorius motor left; AH = abductor pollicis; CMAP = compound muscle action potential; DFM = decreased fetal movements; EDC = extensor digitorum communis; EMG = electromyogram; GERD = gastroesophageal reflux disease; GI = gastrointestinal; MCD = mean consecutive difference; NA = not available; NT = not tested; Orb oculi = orbicularis oculi.

abnormalities similarly to affected individuals, we re-examined *Vamp1*<sup>lew/lew</sup> mutant mice that were previously described.<sup>11,12</sup> The endplates were localized along the central regions of the muscle in both control and *Vamp1*<sup>lew/lew</sup> mice (Fig 2). Individual neuromuscular synapses were found markedly smaller in *Vamp1*<sup>lew/lew</sup> mice compared with control, and a severe reduction in endplate potentials (EPPs) was also observed in the mutant mice. Importantly, a low-frequency, repetitive stimulation (10Hz) led to a run-down of EPPs in control mice, but synaptic facilitation in *Vamp1*<sup>lew/lew</sup> mice, indicating presynaptic defects.

## Discussion

Here, we report 4 children from 2 consanguineous families who presented with typical clinical and neurophysiological features of presynaptic CMS associated with homozygous mutations in *VAMP1*.

The protein encoded by this gene is a member of the synaptobrevin family.<sup>14</sup> Synaptobrevins (eg,

Vamp1, Vamp2), syntaxins, and the synaptosomal-associated protein Snap25 represent the main components of the SNARE (soluble N-ethylmaleimide-sensitive factor attachment protein receptors) complex, which is involved in docking and fusion of synaptic vesicles with the presynaptic membrane at the central and the neuromuscular synapses.<sup>15,16</sup> Proteins belonging to this complex are involved in vesicle docking through the evolutionarily conserved active v-SNARE coiled coil homology domain and present high sequence similarity across the different SNAREs.<sup>17–19</sup>

Notably, the c.51\_64delAGGTGGGGGTCCCC frameshift deletion identified in Family 1 leads to a change in the gene reading frame with the generation of a premature stop codon 5 amino acids downstream (see Fig 1H). The result is a putative *VAMP1* product of only 21 amino acids, with a resulting function that is highly likely to be disrupted due to the absence of the downstream v-SNARE domain (amino acids 33–93). The

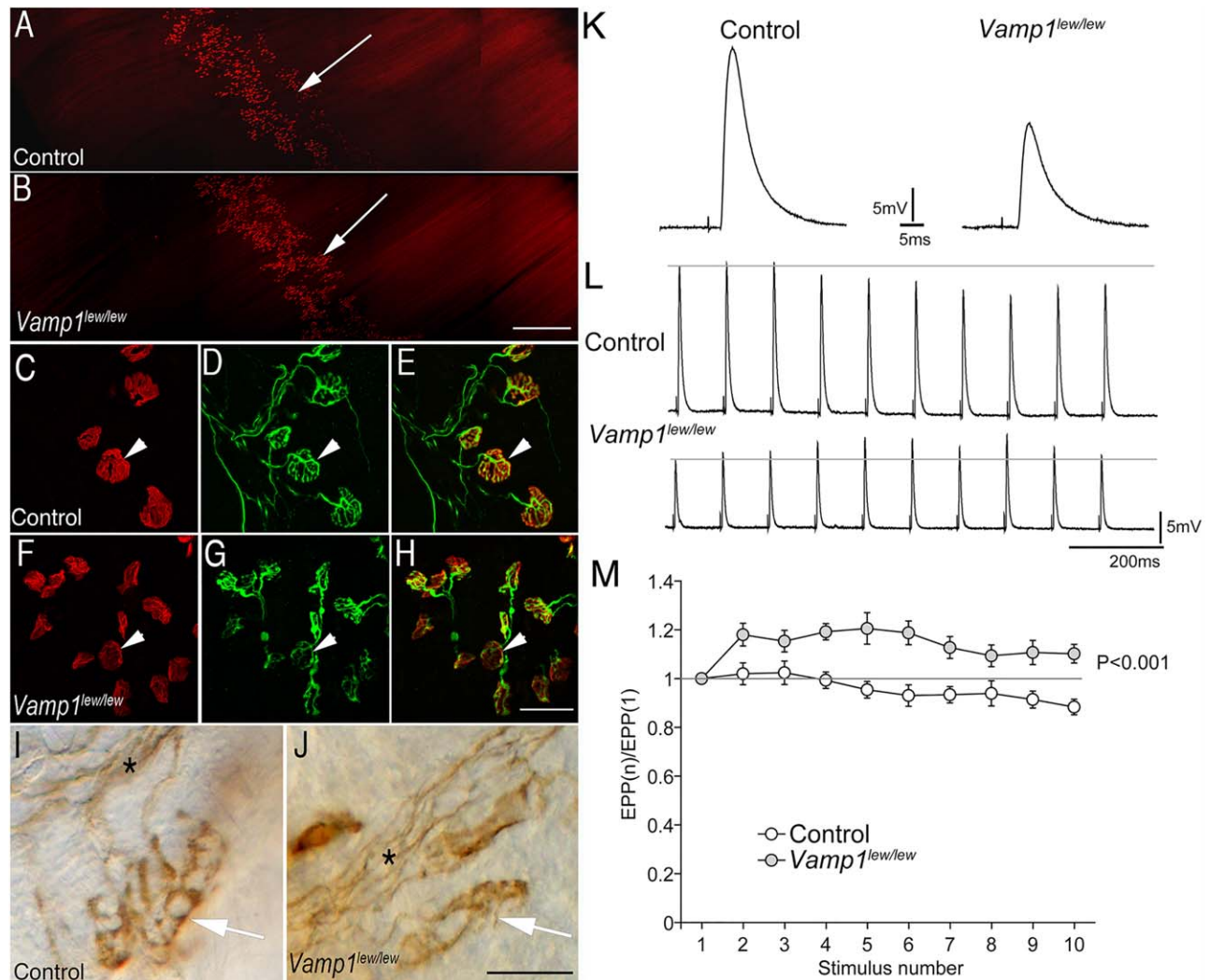


**FIGURE 2:** Synaptic defects at the neuromuscular junctions in *Vamp1<sup>lew/lew</sup>* mice. (A, B) Low-power images of the whole-mount diaphragm muscles (P14) labeled by Texas Red—conjugated  $\alpha$ -bungarotoxin. The endplate band (arrow) is similarly localized along the central regions of the muscle in both control (A) and *Vamp1<sup>lew/lew</sup>* mice (B). (C–H) High-power confocal images of individual neuromuscular synapses in triangularis sterni muscles, labeled by Texas Red—conjugated  $\alpha$ -bungarotoxin (arrowheads in C and F) and antineurofilament NF150 and antisynaptotagmin2 antibodies (arrowheads in D and G point to the nerve terminals). Merged images are shown in E and H, for control and *Vamp1<sup>lew/lew</sup>* mice, respectively. (I, J) Individual neuromuscular synapses (arrows) in triangularis sterni muscles labeled by antisyntaxin1 antibodies. The synapses are markedly smaller in *Vamp1<sup>lew/lew</sup>* mice compared with the control. Asterisks indicate nerve bundles. (K) An example of endplate potentials (EPPs) recorded in the diaphragm muscle in control and *Vamp1<sup>lew/lew</sup>* mice. (L) EPP traces responding to a low-frequency, repetitive nerve stimulation (10Hz). (M) Quantitative measurement of the ratios of EPP amplitudes: EPP(n) to the first EPP amplitude, (EPP1). A low-frequency, repetitive stimulation (10Hz) led to a run-down of EPPs in control, but synaptic facilitation in (*Vamp1<sup>lew/lew</sup>*) mice.

homozygous mutation identified in Family 2 consists of a substitution of a highly conserved arginine (Gerp++ score = 5.77) by a proline within the v-SNARE domain. The mutated arginine residue in position 49 corresponds to the arginine in position 47 of the better-studied SNARE homolog *VAMP2*, encoding another synaptobrevin with similar functions to *VAMP1*.<sup>20</sup>

Interestingly, it has been shown that disruption of this specific site in *VAMP2* interferes with SNARE complex assembly, impairing neurotransmission, likely due to lack of association with other proteins involved in vesicle

fusion.<sup>21–23</sup> The Arg49Pro mutation is predicted as deleterious by SIFT, PolyPhen, and Mutation Taster and is carried in the heterozygous state by only 1 individual in the ExAC database (<http://exac.broadinstitute.org>, last accessed January 2017). Of note, in the ExAC database of 60,706 individuals there are only 17 individuals with heterozygous nonsynonymous single nucleotide substitutions within the v-SNARE domain and 4 individuals in total carrying heterozygous truncating variants in *VAMP1*. None of these variants is present as homozygous, providing supportive evidence of pathogenicity for

biallelic *VAMP1* variants, either resulting in changes of the gene reading frame or affecting conserved active sites crucial to v-SNARE domain function.

Interestingly, we also showed that the electrodiagnostic anomalies recorded in *VAMP1*-associated CMS are consistent with the abnormal features of presynaptic transmission we recorded in the *VAMP1* null mutant mice (including the incremental response to RNS; see Fig 2). These animals, of a model called *lethal wasting* (carrying a homozygous mutation that causes the truncation of half of the protein), lack movement because of an impaired NMJ transmission and die within 3 weeks of birth.<sup>11,12</sup>

To date, biallelic variants in *VAMP1* have never been reported, but heterozygous mutations in this gene have been described by a single study in association with a phenotype of autosomal dominant spastic ataxia.<sup>23</sup> However, we have not observed any neurological phenotype in the heterozygous carriers from the 2 families.

In conclusion, the identification of biallelic variants in *VAMP1* as a novel cause of CMS, in addition to other genes (eg, *SNAP25B*, *SYT2*) previously associated with similar presynaptic abnormalities of neuromuscular transmission,<sup>5,6</sup> highlights the crucial role of different SNAREs in NMJ physiology. Intriguingly, the relatively mild phenotype showed by our patients compared to the mouse model, which dies prematurely, suggests the possible existence of species-specific compensation of vesicle fusion and release at the nerve terminal, perhaps through genetic modifiers in humans but not in mice or fruit flies. This highlights a promising area of future research aimed at the pathways involved in physiological presynaptic vesicle exocytosis at the motor endplate.

## Acknowledgment

This study was supported by the Wellcome Trust (WT093205MA, WT104033AIA), Medical Research Council (H.H.), European Community's Seventh Framework Programme (FP7/2007-2013, under grant agreement No. 2012-305121; B.W., H.H.), National Institute for Health Research University College London Hospitals Biomedical Research Centre (H.H. and National Institutes of Health (NIH, NS-055028; W.L.).

We thank the families for enthusiastic collaboration in this study.

## Author Contributions

Study concept and design: W.L., J.E.R., B.W., H.H. Data acquisition and analysis: A.M., A.S., K.M., L.B.-V., M.W.H., S.A., M.P., S.E., S.W., A.Y.M., M.S., O.B.,

S.S.K. Drafting the manuscript and figures: V.S., A.D.V., Y.L., Q.Y.

## Potential Conflicts of Interest

Nothing to report.

## References

- Engel AG, Shen XM, Selcen D, Sine SM. Congenital myasthenic syndromes: pathogenesis, diagnosis, and treatment. *Lancet Neurol* 2015;14:420–434.
- Beeson D. Congenital myasthenic syndromes: recent advances. *Curr Opin Neurol* 2016;29:565–571.
- Schaaf CP. Nicotinic acetylcholine receptors in human genetic disease. *Genet Med* 2014;16:649–656.
- O'Grady GL, Verschuuren C, Yuen M, et al. Variants in *SLC18A3*, vesicular acetylcholine transporter, cause congenital myasthenic syndrome. *Neurology* 2016;87:1442–1448.
- Herrmann DN, Horvath R, Sowden JE, et al. Synaptotagmin 2 mutations cause an autosomal-dominant form of Lambert-Eaton myasthenic syndrome and nonprogressive motor neuropathy. *Am J Hum Genet* 2014;95:332–339.
- Shen XM, Selcen D, Brengman J, Engel AG. Mutant *SNAP25B* causes myasthenia, cortical hyperexcitability, ataxia, and intellectual disability. *Neurology* 2014;83:2247–2255.
- Pitt M. Neurophysiological strategies for the diagnosis of disorders of the neuromuscular junction in children. *Dev Med Child Neurol* 2008;50:328–333.
- Aharoni S, Sadeh M, Shapira Y, et al. Congenital myasthenic syndrome in Israel: genetic and clinical characterization. *Neuromuscul Disord* 2017;27:136–140.
- Mencacci NE, Kamsteeg EJ, Nakashima K, et al. De novo mutations in *PDE10A* cause childhood-onset chorea with bilateral striatal lesions. *Am J Hum Genet* 2016;98:763–771.
- Delle Vedove A, Storbeck M, Heller R, et al. Biallelic loss of proprioception-related *PIEZO2* causes muscular atrophy with perinatal respiratory distress, arthrogryposis, and scoliosis. *Am J Hum Genet* 2016;99:1406–1408.
- Nystuen AM, Schwendinger JK, Sachs AJ, et al. A null mutation in *VAMP1/synaptobrevin* is associated with neurological defects and prewean mortality in the lethal-wasting mouse mutant. *Neurogenetics* 2007;8:1–10.
- Liu Y, Sugiura Y, Lin W. The role of synaptobrevin1/*VAMP1* in Ca<sup>2+</sup>-triggered neurotransmitter release at the mouse neuromuscular junction. *J Physiol* 2011;589(pt 7):1603–1618.
- Richards S, Aziz N, Bale S, et al. Standards and guidelines for the interpretation of sequence variants: a joint consensus recommendation of the American College of Medical Genetics and Genomics and the Association for Molecular Pathology. *Genet Med* 2015;17:405–424.
- Sutton RB, Fasshauer D, Jahn R, Brunger AT. Crystal structure of a SNARE complex involved in synaptic exocytosis at 2.4 Å resolution. *Nature* 1998;395:347–353.
- Cupertino RB, Kappel DB, Bandeira CE, et al. SNARE complex in developmental psychiatry: neurotransmitter exocytosis and beyond. *J Neural Transm (Vienna)* 2016;123:867–883.
- Kittel RJ, Heckmann M. Synaptic vesicle proteins and active zone plasticity. *Front Synaptic Neurosci* 2016;8:8.
- Weimbs T, Low SH, Chapin SJ, et al. A conserved domain is present in different families of vesicular fusion proteins: a new superfamily. *Proc Natl Acad Sci U S A* 1997;94:3046–3051.

18. Hong W. SNAREs and traffic. *Biochim Biophys Acta* 2005;1744:120–144.
19. Rothman JE. The principle of membrane fusion in the cell (Nobel lecture). *Angew Chem Int Ed Engl* 2014;53:12676–12694.
20. Zimmermann J, Trimbuch T, Rosenmund C. Synaptobrevin 1 mediates vesicle priming and evoked release in a subpopulation of hippocampal neurons. *J Neurophysiol* 2014;112:1559–1565.
21. Hao JC, Salem N, Peng XR, et al. Effect of mutations in vesicle-associated membrane protein (VAMP) on the assembly of multimeric protein complexes. *J Neurosci* 1997;17:1596–1603.
22. Trimbuch T, Xu J, Flaherty D, et al. Re-examining how complexin inhibits neurotransmitter release. *Elife* 2014;3:e02391.
23. Trimbuch T, Rosenmund C. Should I stop or should I go? The role of complexin in neurotransmitter release. *Nat Rev Neurosci* 2016;17:118–125.



### 7.3 Appendix C

**Delle Vedove A**, Natarajan J, Zanni G, Eckenweiler M, Muiños-Bühl A, Storbeck M, Guillén Boixet J, Barresi S, Pizzi S, Hölker I, Körber F, Franzmann TM, Bertini ES, Kirschner J, Alberti S, Tartaglia M, Wirth B. CAPRIN1<sup>P512L</sup> causes aberrant protein aggregation and associates with early-onset ataxia. *Cell Mol Life Sci.* 2022 Sep 22;79(10):526. doi: 10.1007/s00018-022-04544-3. PMID: 36136249; PMCID: PMC9499908.

This work was published by Springer Nature and is appended under the Publisher's permission.





# CAPRIN1<sup>P512L</sup> causes aberrant protein aggregation and associates with early-onset ataxia

Andrea Delle Vedove<sup>1,2,3</sup> · Janani Natarajan<sup>4</sup> · Ginevra Zanni<sup>5</sup> · Matthias Eckenweiler<sup>6</sup> · Anixa Muiños-Bühl<sup>1,2,3</sup> · Markus Storbeck<sup>1,2,3</sup> · Jordina Guillén Boixet<sup>4</sup> · Sabina Barresi<sup>5</sup> · Simone Pizzi<sup>5</sup> · Irmgard Hölker<sup>1,2,3</sup> · Friederike Körber<sup>7</sup> · Titus M. Franzmann<sup>4</sup> · Enrico S. Bertini<sup>5</sup> · Janbernd Kirschner<sup>6</sup> · Simon Alberti<sup>4</sup> · Marco Tartaglia<sup>5</sup> · Brunhilde Wirth<sup>1,2,3,8</sup>

Received: 8 July 2022 / Revised: 15 August 2022 / Accepted: 31 August 2022  
© The Author(s) 2022

## Abstract

CAPRIN1 is a ubiquitously expressed protein, abundant in the brain, where it regulates the transport and translation of mRNAs of genes involved in synaptic plasticity. Here we describe two unrelated children, who developed early-onset ataxia, dysarthria, cognitive decline and muscle weakness. Trio exome sequencing unraveled the identical de novo c.1535C > T (p.Pro512Leu) missense variant in *CAPRIN1*, affecting a highly conserved residue. In silico analyses predict an increased aggregation propensity of the mutated protein. Indeed, overexpressed CAPRIN1<sup>P512L</sup> forms insoluble ubiquitinated aggregates, sequestering proteins associated with neurodegenerative disorders (ATXN2, GEMIN5, SNRNP200 and SNCA). Moreover, the CAPRIN1<sup>P512L</sup> mutation in isogenic iPSC-derived cortical neurons causes reduced neuronal activity and altered stress granule dynamics. Furthermore, nano-differential scanning fluorimetry reveals that CAPRIN1<sup>P512L</sup> aggregation is strongly enhanced by RNA in vitro. These findings associate the gain-of-function Pro512Leu mutation to early-onset ataxia and neurodegeneration, unveiling a critical residue of CAPRIN1 and a key role of RNA–protein interactions.

**Keywords** Neurodegeneration · Prion-like domain · Protein misfolding · De novo variant · CRISPR/Cas9

✉ Brunhilde Wirth  
brunhilde.wirth@uk-koeln.de

<sup>1</sup> Institute of Human Genetics, University Hospital of Cologne, University Cologne, 50931 Cologne, Germany

<sup>2</sup> Center for Molecular Medicine Cologne, University of Cologne, 50931 Cologne, Germany

<sup>3</sup> Institute for Genetics, University of Cologne, 50674 Cologne, Germany

<sup>4</sup> Center for Molecular and Cellular Bioengineering, Biotechnology Center, Technische Universität Dresden, 01307 Dresden, Germany

<sup>5</sup> Genetics and Rare Diseases Research Division and Unit of Muscular and Neurodegenerative Disorders - the Department of Neurosciences of the Bambino Gesù Childrens' Hospital, IRCCS, Rome, Italy

<sup>6</sup> Department of Neuropediatrics and Muscle Disorders, Faculty of Medicine, Medical Center—University of Freiburg, University of Freiburg, 79106 Freiburg, Germany

<sup>7</sup> Institute of Diagnostic and Interventional Radiology, 50937 Cologne, Germany

<sup>8</sup> Center for Rare Diseases, University Hospital of Cologne, 50931 Cologne, Germany

## Abbreviations

ADHS	Attention deficite/hyperactivity disorder
ALS	Amyotrophic lateral sclerosis
ASD	Autism spectrum disorder
CAPRIN1	Cell cycle associated protein 1
BSA	Bovine serum albumin
crRNA	CRISPR RNA
DLS	Dynamic light scattering
FBS	Fetal bovine serum
FCS	Fluorescence correlation spectroscopy
FTLD	Frontotemporal lobar degeneration
FXTAS	Fragile X tremor/ataxia syndrome
HD	Huntington's disease
iPSC	Induced pluripotent stem cell
gRNA	Guide RNA
LBD	Lewy bodies dementia
MEA	Microelectrode array
MRI	Magnetic resonance imaging
nanoDSF	Nano-differential scanning fluorimetry
ND	Neurodegenerative disorder
PD	Parkinson's disease
PEI	Polyethylenimine

PFA	Paraformaldehyde
PQC	Protein quality control
PrLD	Prion-like domain
PBS-T	PBS + 0,2% tween20
RBP	RNA-binding protein
SCA2	Spinocerebellar ataxia 2
SG	Stress Granule
SSEP	Somatosensory evoked potential
ssODN	Single-stranded oligodeoxynucleotides
ssRNA	Single stranded RNA
UPS	Ubiquitin–proteasome system
TBS-T	TBS + 0.2% tween20
tracrRNA	Transactivating CRISPR RNA
UTR	Untranslated region
WES	Whole exome sequencing
WT	Wild-type

## Introduction

Cell Cycle-Associated Protein 1 (*CAPRIN1* [MIM: 601178]) is a ubiquitously expressed protein, whose levels are high in tissues characterized by an elevated cell turnover, but is also abundant in the brain [1–4]. There, it plays a crucial role as an RNA-binding protein (RBP), which regulates the transport and translation of mRNAs of synaptic proteins [2, 5]. *CAPRIN1* binds to mRNAs via C-terminal RGG motifs and contains a prion-like domain (PrLD) [6, 7]. PrLDs are characterized by the lack of a defined three-dimensional structure and a low complexity sequence composition [8, 9]. They interact dynamically with other proteins and RNAs, and these interactions can trigger phase transitions as well as protein aggregation [10]. Indeed, *CAPRIN1* is a component of stress granules (SGs), cytoplasmic assemblies of RBPs and stalled mRNAs that form under stress conditions [6, 11]. The N-terminal part of *CAPRIN1* harbors a dimerization domain and the binding sites for the RBPs G3BP1 and FMR1 [6, 12, 13].

Interestingly, many PrLD-containing RBPs (ATXN2, TARDBP, FUS, TIA1, HNRNPA1 and HNRNPA2B1) have been associated with neurodegenerative disorders (NDs) [7]. However, missense mutations in *CAPRIN1* have not been linked to neurodegeneration so far. Constitutive *Caprin1* knockout in mice causes perinatal death and impairs the formation and maintenance of synapses and neuronal network [5], while *CAPRIN1* deficiency has been associated with autism spectrum disorders (ASD) and long-term memory impairment [3, 14–17].

Here we describe a novel early-onset ataxia and neurodegenerative disorder caused by a single recurrent missense variant in *CAPRIN1*. We propose a gain-of-function mechanism mediated by increased protein aggregation propensity

and highlight the crucial role of RNA–protein interactions in its pathophysiology.

## Materials and methods

### Genetic studies

Genetic studies were performed as part of clinical and/or research investigations dependent on clinical presentation and family history. DNA was extracted from blood. DNA samples from A-I.1, A-I.2, A-II.3, B-I.1, B-I.2 and B-II.2 were prepared for whole exome sequencing (WES) and analyzed as described in detail in Note S1. *CAPRIN1* exon 14 genomic region was amplified by PCR following the manufacturer's protocol (Multiplex PCR Kit—QIAGEN) with specific primers (*CAPRIN1*-E14, Table S1).

### In silico *CAPRIN1*<sup>P512L</sup> modeling

Human *CAPRIN1* (Q14444-1) and *CAPRIN1*<sup>P512L</sup> FASTA protein sequences were pasted in PLAAC [18]. The Relative weighting of background probabilities ( $\alpha$ ) was set to 0 and *Homo Sapiens* was selected as organism background frequency.

The CamSol intrinsic solubility profile was obtained from the CamSol web server using the same FASTA sequences [19].

### Cell culture

HEK293T cells were cultured in DMEM (ThermoFisher Scientific) supplemented with 10% FBS (SIGMA), 1% Pen Strep (ThermoFisher Scientific), 0.7  $\mu$ g/ml Amphotericin B (ThermoFisher Scientific). SH-SY5Y cells were cultured in DMEM/F-12, GlutaMAX (ThermoFisher Scientific) supplemented with 10% FBS, 1% Pen Strep. All cells were cultured at 37 °C with 5% CO<sub>2</sub>.

iPSCs were cultured in Matrigel-coated plates (Corning) in mTeSR1 or mTeSR Plus medium (StemCell Technologies). All cells were cultured at 37 °C with 5% CO<sub>2</sub>.

### Constructs cloning

Total RNA was extracted from HEK293T (RNeasy Kit—QIAGEN) and reversely transcribed to cDNA (QuantiTect Reverse Transcription Kit—QIAGEN) following the manufacturer's protocol. *CAPRIN1* [GenBank: NM\_005898.5] cDNA was amplified with specific primers (*CAPRIN1*\_cl, Table S1) and cloned into pcDNA-3.1/V5-His following the manufacturer's protocol (pcDNA3.1/V5-His TOPO TA

Expression Kit—Invitrogen). The c.1535C>T variant was introduced using site-directed mutagenesis with specific primers (CAPRIN1\_P512L\_SDM, Table S1) following the manufacturer's protocol (QuikChange II XL Site-Directed Mutagenesis Kit—Agilent Technologies). The cDNAs were then subcloned into a pEGFP-C2 vector using XhoI and BamHI restriction sites.

For the experiments in insect cells, *CAPRIN1* open reading frame optimized for insect cell expression was subcloned into pOCC468 or pOCC305 vector [20]. pOCC468-CAPRIN1 contains Twinstrep-MBP-Prescission-mGFP at the 5' end of CAPRIN1 and Prescission-6xHIS at the 3' end. pOCC305-CAPRIN1 contains Twinstrep-MBP-Prescission- at the 5' of CAPRIN1 and Prescission-6xHIS at the 3'. The P512L substitution was introduced with the Q5R Site-Directed Mutagenesis Kit (New England BioLabs) using specific primers (CAPRIN1-P512L\_MG, Table S1).

For the gRNA insertion in the Cas9 expression vector (pX330-hCas9-long-chimeric-grna-g2p; Leo Kurian's laboratory), the plasmid was digested with BbsI (NEB) and annealed oligos (CAPRIN1-P512L\_gRNA, Table S1) were ligated to it.

### Protein expression in HEK293T/SH-SY5Y cells

HEK293T cells were transfected with pcDNA-3.1/V5-His harboring CAPRIN1 (1–709, WT or P512L) using Lipofectamine 2000 Transfection Reagent (ThermoFisher Scientific) and samples were further processed for Solubility analysis.

SH-SY5Y cells were seeded on glass coverslips (VWR), transfected with pEGFP-C2 harboring CAPRIN1 (1–709, WT or P512L) using FuGENE HD Transfection Reagent (Promega) and processed for immunofluorescence.

### Solubility analysis

Sequential extraction of proteins from the different soluble fractions was performed following a published protocol [21]. Briefly, 24 h post transfection, cells were washed twice with PBS, lysed in cold RIPA buffer (SIGMA), and sonicated. Cell lysates were centrifuged at 100,000 g for 30 min at 4 °C to generate RIPA-soluble samples. Pellets were washed, sonicated and centrifuged twice with PBS. RIPA-insoluble pellets were then extracted with urea buffer (8 M urea, 4% CHAPS, 30 mM Tris, pH 8.5), sonicated, and centrifuged at 100,000 g for 30 min at 22 °C. Protease inhibitors were added to all buffers before use. Protein concentration was determined with the Bradford method.

### Immunoblotting

Protein lysates (10 µg) in Laemmli Buffer were heated at 95 °C for 5 min, then separated on 12% polyacrylamide gels and transferred onto nitrocellulose membranes (Merck Millipore). Membranes were blocked for 1 h in 5% BSA in TBS-T, incubated overnight with primary antibodies (Table S2) in 2.5% BSA in TBS-T at 4 °C, washed three times in TBS-T and incubated with HRP-conjugated secondary antibodies (Table S2) for 1 h at room temperature. Proteins were visualized using the Immobilon Western chemiluminescent HRP substrate (Merck Millipore). Quantification was performed with ImageLab (Bio-Rad).

### Immunofluorescence

Coverslips were washed in PBS and fixed in 4% PFA for 10 min. They were then washed three times in PBS, permeabilized in PBS-T for 10 min and blocked for 1 h at room temperature in 5% BSA in PBS-T. Coverslips were then incubated overnight with primary antibodies (Table S2) in 5% BSA in PBS-T at 4 °C, washed three times in PBS-T, incubated with conjugated secondary antibodies (Table S2) for 1 h at room temperature, washed three times in PBS-T, rinsed in water and mounted with ProLong Gold antifade reagent with DAPI (Invitrogen) on Polylysine slides (ThermoFisher Scientific). Images were acquired with a Zeiss AxioImager M2 microscope equipped with ApoTome2 system and processed using ZEN software (Zeiss). Pearson's colocalization coefficient was obtained using the Coloc 2 tool in ImageJ. Stress granules were quantified with a self-compiled macro in ImageJ, which uses the Weka Trainable Segmentation plugin on the G3BP1 signal. A cell was considered positive if  $\geq 3$  signals were detected.

### CRISPR/Cas9 P512L knock-in in iPSCs

#### Homozygous CAPRIN1<sup>P512L/P512L</sup> cell line

HUVEC iPSCs were CRISPR/Cas9 genetically edited into homozygous CAPRIN1<sup>P512L/P512L</sup> based on a published protocol [22, 23]. Briefly, cells were seeded in mTeSR1 medium (StemCell Technologies) supplemented with 10 µM Y-27632 (Selleckchem) in a 6-wells plate at a confluency of  $1.8 \times 10^4$  cells/cm<sup>2</sup>. After 24 h cells were transfected with a Cas9 expression vector harboring a gRNA targeting CAPRIN1 exon 14 and a 400 bp ssODN (CAPRIN1-ssODN1, Table S1) using Lipofectamine 3000 Reagent (ThermoFisher Scientific). Starting 24 h post-transfection, cells were selected for 72 h with 1.5 µg/ml Puromycin (ThermoFisher Scientific). Afterwards they were split with Accutase (ThermoFisher Scientific) and seeded in mTeSR1 medium with 10 µM Y-27632 into a 96 wells plate at

single-cell density. The day after, the medium was changed to mTeSR1 medium. After 12 days, colonies were split into 6-well plates and further expanded. After DNA extraction using QuickExtract DNA Extraction Solution (Lucigen), a 326 bp region targeted by the gRNA was amplified by PCR (CAPRIN1-SA, Table S1) and genome editing was screened by T7 Endonuclease (NEB) assay. In the case of a positive result, a 901 bp region (CAPRIN1-E14, Table S1) was sequenced by Sanger sequencing.

### Heterozygous CAPRIN1<sup>WT/P512L</sup> cell line

HUVEC iPSCs were CRISPR/Cas9 genetically edited into heterozygous CAPRIN1<sup>WT/P512L</sup> iPSC lines following the manufacturer's protocol [24]. One hour before nucleofection, mTeSR Plus medium (StemCell Technologies) was changed with medium supplemented with 10  $\mu$ M Y-27632. After detachment with Accutase, 10<sup>6</sup> HUVEC iPSCs were resuspended in OptiMEM (ThermoFisher Scientific), mixed with a crRNA, tracrRNA-ATTO550, Cas9:dCas9 1:4, Electroporation enhancer, 150 bp ssODN (IDT) (CAPRIN1-ssODN2, Table S1) and nucleofected using Nucleofector 2b Device (Lonza). Cells were plated in mTeSR Plus medium with HDR enhancer (IDT). After 24 h, single cells were sorted in 96-well plates and the remaining cells in 6-well plates in mTeSR Plus medium with CloneR (StemCell Technologies) and Y-27632. Since no colonies were observed in the 96-well plates, after 5 days colonies from the 6-well plates were split again at single-cell density in a 96-well plate and subsequently expanded. Screening of the colonies was performed using an allele-specific PCR (CAPRIN1-P512L-ASP, Table S1). In the case of a positive result, a 901 bp region was sequenced by Sanger sequencing (CAPRIN1-E14, Table S1).

Off-targets for both CAPRIN1<sup>WT/P512L</sup> and CAPRIN1<sup>P512L/P512L</sup> lines were excluded by Sanger sequencing in the first five gRNA off-targets sites predicted using CRISPOR. Expression of pluripotency markers was confirmed by immunofluorescence.

### Neuronal differentiation

Neurons of cortical layer V and VI were generated according to a published protocol with minimal modifications [25]. In brief, iPSCs were dissociated with Accutase (ThermoFisher Scientific) and seeded on matrigel-coated (Corning) wells at a density of 3  $\times$  10<sup>5</sup>/cm<sup>2</sup> in mTeSR Plus medium (StemCell Technologies) supplemented with 10  $\mu$ M Y-27632 (Selleckchem) (day 0–D0). On D1, the medium was replaced daily by a neural induction medium [N2/B27 (ThermoFisher Scientific), 0.5  $\mu$ M LDN-193189 (Selleckchem) and 10  $\mu$ M SB431542 (StemCell Technologies)]. On D8, NIM was supplemented with 20 ng/ml FGF2 (Sigma). On D9, cultures

were split with Accutase and seeded in N2/B27 medium with 20 ng/ml FGF2 and 10  $\mu$ M Y-27632 onto Matrigel-coated wells. On D10, N2/B27 medium with 20 ng/ml FGF2 was added. On D11, cells were cultured in N2/B27 medium with a change of medium every other day. On D19, neural precursors were dissociated and frozen. For maturation, frozen precursors were thawed and seeded in N2/B27 medium with 10  $\mu$ M Y-27632, with a change of medium every other day. On D26, cells were detached with Accutase and reseeded at 5  $\times$  10<sup>4</sup>/cm<sup>2</sup> density on 0.05% PEI (Sigma-Aldrich) and 20  $\mu$ g/ml Laminin (Sigma) coated wells/coverlips. On D27 and D29, the medium was changed to N2/B27 supplemented with 10  $\mu$ M PD0325901 (Tocris) and 10  $\mu$ M DAPT (Tocris). From D31 the cells were cultured in N2/B27 medium with medium changes every other day.

### Microelectrode array recordings

On D26, 7.5  $\times$  10<sup>4</sup> cells / well were seeded in a 24-well epoxy plate with a microelectrode array (MEA) (Multi Channel Systems). Cells were recorded with a Multiwell-MEA-System (Multi Channel Systems) for 3 min at 37 °C between D29 and D57 using the Multiwell-Screen software (Multi Channel Systems) and analyzed with the Multiwell-Analyser software (Multi Channel Systems). When no activity was recorded, the parameter was set to 0. The following parameters were used: 2nd order low-pass filter frequency: 3500 Hz; 2nd order high-pass filter frequency: 100 Hz; rising/falling edge of the automatic threshold estimation: 5.5/– 5.5 SD; minimum spike count in burst: 3; minimum channels participating in a network burst: 5; minimum simultaneous channels for a network burst; minimum spikes per minute: 5; minimum amplitude: 10  $\mu$ V.

### SG dynamics study

On D36, iPSC-derived neurons plated onto coverslips were treated for 1 h with 0.5 mM Sodium Arsenite (SA, NaAsO<sub>2</sub>, Sigma-Aldrich), then washed in PBS and incubated in N2/B27 medium for 0–240 min to study SG resolution. Coverslips were then processed for Immunofluorescence.

### Recombinant protein expression and purification

mGFP-CAPRIN1 WT and P512L, as well as CAPRIN1 WT were purified from Sf9 insect cells using a baculovirus expression system [26, 27]. Cells expressing recombinant TwinstrepII-MBP-mGFP-CAPRIN1-6xHis were lysed in 50 mM Tris–HCl pH 7.5, 300 mM KCl, 150 mM Arginine-HCl, 1 mM DTT and 1  $\times$  EDTA-free protease inhibitor cocktail (Roche Applied Sciences) using a LM10 Microfluidizer (Microfluidics) at 5000 psi. The lysate was cleared by centrifugation at a maximum speed for 1 h at 4 °C. The

supernatant was applied to a 5 ml Strep-Tactin®XT 4Flow® column (IBA Lifesciences GmbH) using an ÄKTA pure 25 (GE Healthcare). The column was washed with 10 column volumes (CV) of 50 mM Tris–HCl pH 7.5, 300 mM KCl, 150 mM Arginine-HCl and 1 mM DTT and the protein was eluted with 3 CV of 50 mM Tris–HCl pH 7.5, 300 mM KCl, 1 mM DTT and 50 mM biotin. The eluted protein was applied to a 5 mL HiTrap Q HP column (GE Healthcare). The column was washed with 20 CV of 50 mM Tris–HCl pH 7.5, 50 mM KCl and 1 mM DTT. Elution was achieved with a linear gradient of 20 CV of 50 mM Tris–HCl pH 7.5, 1000 mM KCl and 1 mM DTT. The elution fractions containing MBP-mGFP-CAPRIN1-6xHis were pooled and incubated 6 h at RT with 6xHis-Prescission protease (1:300 w/w) to cleave off the MBP and 6xHis tags. The sample was then applied to a HiLoad 16/600 Superdex 200 pg column (GE Healthcare) equilibrated in 50 mM Tris–HCl pH 7.5, 300 mM KCl and 1 mM DTT. mGFP-CAPRIN1 fractions were pooled, concentrated to ~100 µM with Amicon Ultra centrifugal 30 kDa MWCO filters (Merck Millipore), flash-frozen with liquid nitrogen and stored at –80 °C. Purified proteins were quality controlled by SDS-PAGE and Coomassie staining. The homogeneity of GFP-tagged proteins was determined by imaging the gels using the Amersham typhoon scanner.

### Nano-differential scanning fluorimetry (nanoDSF)

mGFP-CAPRIN1 (WT or P512L) was diluted to a final protein concentration of 5 µM in 50 mM Tris/KOH pH 7.5 and 75 mM KCl. Unfolding transitions were recorded with a Prometheus Panta (Nanotemper) in high sensitivity capillaries (Nanotemper) at 0.3 °C min<sup>-1</sup>. Data analysis and plotting were with the R/RStudio software package.

### Total RNA and mRNA isolation

Total RNA was isolated from HeLa cells using the RNeasy Mini Kit (QIAGEN). mRNA was isolated from total RNA using the Dynabeads™ mRNA purification Kit (ThermoFisher). The tangled total RNA was prepared according to published work [20]. Poly(A) (Sigma-Aldrich, Cat#10108626001), Poly(C) (Sigma-Aldrich, Cat#P4903), Poly(G) (Sigma-Aldrich, Cat#P4404), Poly(U) (Sigma-Aldrich, Cat#P9528), and Ribosomal RNA (Bioworld, Cat#11020001-2) were all purchased. The 5' UTR-KpnB1-nanoLUC mRNA was transcribed with an mMESSAGE T7 kit (Invitrogen).

### RNA-induced aggregation of CAPRIN1

5 µM mGFP-CAPRIN1 (WT or P512L) were incubated for 4 h at RT in 25 mM HEPES/KOH pH 7.5, 75 mM,

2 mM MgCl<sub>2</sub>, 1% PEG-20 K with and without 50 ng/µl of RNA. When indicated, KCl concentration was increased to 500 mM or 100 µg/µl RNase A was added. Samples were mounted in 384-well plates (Greiner bio-one, #781000-06) with custom attached pegylated glass coverslips [28]. Samples were imaged with a Nikon Eclipse Ti2 inverted microscope, equipped with a Prime 95B 25 mm camera (Photometrics) and a 60x/1.2 Plan Apo Lambda water objective. Images were analyzed with Fiji.

### Fluorescence anisotropy measurements

100 nM of ATTO590-labelled RNA were mixed with increasing concentrations of the mGFP-CAPRIN1 or mGFP-CAPRIN1<sup>P512L</sup>, in 25 mM HEPES–KOH, pH 7.5, 75 mM KCl and incubated for 10 min at 25 °C. Fluorescence anisotropy was measured with a Tecan Spark plate reader in 384-well plates (Greiner bio-one). Fluorescent excitation was at 598 nm/20 slit width and emission was recorded at 664 nm/30 slit width. Fluorescence anisotropy was calculated using the manufacturer's software. For RNA competition assay, x100 nM of ATTO590-labelled RNA and 3 µM of mGFP-CAPRIN1 was preincubated for 10 min at 25 °C and then competed for with an increasing concentration of unlabeled long homopolymeric polyA RNA. The complex then competed with an increasing concentration of unlabeled long homopolymeric polyA RNA. Fluorescence anisotropy data were fitted to Eq. (1), where  $r$  is the determined fluorescence anisotropy at a given protein concentration ( $c$ ),  $L_t$  is the ligand concentration,  $K_D$  is the apparent dissociation constant and  $r_{\text{free}}$  and  $r_{\text{bound}}$  the fluorescence anisotropy of the free and protein-complexed ATTO590-labelled RNA, respectively. Data analysis and plotting were carried out with R/RStudio software package.

$$r = r_{\text{free}} + (r_{\text{free}} - r_{\text{bound}}) \cdot \frac{\frac{(K_D + c + L_t)}{2} - \sqrt{\left(\frac{(K_D + c + L_t)}{2}\right)^2 - 4cL_t}}{L_t} \quad (1)$$

### FCS measurements

FCS measurements were carried out using a LSM780 (Zeiss) confocal microscope. The system and measurements were calibrated using ATTO488 ( $D = 4.0 \pm 0.1 \times 10^{-6} \text{ cm}^2 \text{ s}^{-1}$  at 25 °C) [29]. Diffusion times were recorded using a 488 nm argon laser for excitation and a 495–555 nm bandpass filter for emission, at 3.5 µW laser power, AOTF dampening factor of 10% with 15 rep for 10 s. The diffusion coefficients were calculated using Eq. (2).

$$D = \omega^2 / 4\tau_D \quad (2)$$

The radius of the proteins was then calculated using the Stokes–Einstein Eq. (3).

$$D = k_b T / 6\pi\eta R_h \quad (3)$$

All FCS measurements were carried out with 50 nM of mGFP-CAPRIN1 WT or P512L or mGFP in 25 mM Tris-KOH, pH 7.5, 75 mM KCl and 1 mM DTT at 22 °C. For oligomerization experiments 50 nM mGFP-CAPRIN1 WT were mixed with either 100 or 2000 nM unlabelled CAPRIN1. ATTO488 dye and mGFP were used as standards to calculate the diffusion volume and the number of GFP molecules in the diffusion volume respectively. Data analysis and plotting were carried out with R/RStudio software package.

### Statistical analysis

All statistical analyses were performed using the software Prism 9 (GraphPad). Unpaired *t* test were used for the comparison of two groups (solubility analysis, aggregates number/size, circularity, colocalization, biochemical properties), while one-way ANOVA was used for the comparison of three groups. Chi-square test was applied to compare frequencies of aggregates in transfected SH-SY5Y cells.

## Results

### Two independent ataxic individuals carry the same de novo Pro512Leu mutation in CAPRIN1

Affected individual II.3 of family A was referred for genetic counseling at the age of 10 years because of the development of gait abnormalities and predominantly proximal muscle weakness (positive Gower's sign). She was born to non-consanguineous parents of Turkish descent and had two older healthy siblings (Fig. 1a). Her symptoms worsened over the following years, with increased muscle weakness and the development of ataxia with light tremor and dysdiadochokinesis. The progressive trunk instability and scoliosis lead her to be first confined to a wheelchair and later to a bed. The motor deficits were accompanied by bulbar symptoms (dysphagia and dysarthria), deficits in sustained attention, social withdrawal and cognitive decline. She attended a mainstream school but later changed to a special needs school. Formal testing revealed an intelligence quotient of 64. Standard laboratory and metabolic tests were negative. Electromyography and nerve conduction studies identified a sensorimotor axonal neuropathy. Muscle biopsy revealed neurogenic fiber atrophy and suralis nerve biopsy uncovered a chronic axonal neuropathy with loss of small- and big-caliber nerve fibers. Magnetic resonance imaging (MRI) at

16 years of age displayed cerebral and cerebellar atrophy (Fig. 1b). Deletions of *SMN1* were excluded and no causative variant was found using an in-house NGS gene panel covering 62 genes associated with lower motor neuron disorders [30].

Affected individual II.2 of family B was born to non-consanguineous parents of Italian descent and had a healthy sister (Fig. 1a). He articulated his first words with slight phonetic problems and presented with dysarthria at the age of 4 years. At the age of 7 years, he developed slowly progressive ataxia and learning difficulties (IQ: 77). By the age of 11 years, his trunk stability worsened and standing up became more difficult. At the age of 12 years, MRI showed global cerebellar atrophy (Fig. 1b). At the age of 13 years, he showed increased muscle fatigue and muscle hypotrophy, with absent deep tendon reflexes in all four limbs. He also became increasingly anxious but improved with psychotherapy. Standard laboratory and metabolic tests were negative. Somatosensory evoked potentials (SSEPs) were reduced in the lower limbs.

Both affected individuals and the respective parents (A-I.1, A-I.2, A-II.3, B-I.1, B-I.2, B-II.2) were subjected to trio whole exome sequencing. Variant filtering followed standard metrics (quality, allele frequency < 0.01 in gnomAD; Note S1). Variants were prioritized assuming an autosomal recessive model of inheritance or a de novo mutation occurrence. The c.1535C > T (NC\_000011.10:g.34090659C > T, exon 14, p.Pro512Leu) *CAPRIN1* (GenBank: NM\_005898.5) variant resulted as the most likely candidate in both families: this variant was absent in gnomAD [31], affects a highly conserved residue and was predicted to be deleterious by multiple scores (CADD PHRED score: 29.8; SIFT: 0 [deleterious]; PolyPhen-2: 0.993 [probably damaging]) (Fig. 1c–e) [32, 33]. In addition, the likelihood that the same de novo variant occurs in two independent individuals is extremely rare (1 in 154 million, Note S2).

Several other characteristics support the involvement of *CAPRIN1* as a neurodegeneration-causing gene: (i) *CAPRIN1* is highly expressed in the human and murine central nervous system, and in particular in the cortex and cerebellum [3, 4]; (ii) *CAPRIN1* is an RBP harboring a PrLD (Fig. 1f and g) [2, 7], feature shared by many ND-linked genes [10]; (iii) *CAPRIN1* is a component of SGs [6], whose role in NDs is well documented [34]; *CAPRIN1* is an interacting partner of ATXN2 and GEMIN5 [35, 36], whose pathogenic variants are associated with ataxia [37, 38], and FMR1 (Fig. 1f) [13], a protein associated with fragile X tremor/ataxia syndrome (FXTAS) [39].

Note added in proof: Just after the acceptance of our manuscript, we were notified by GeneMatcher of a patient identified at NINDS, NIH (female, 14 yrs old) with exactly the same de-novo variant and an identical phenotype (cerebellar



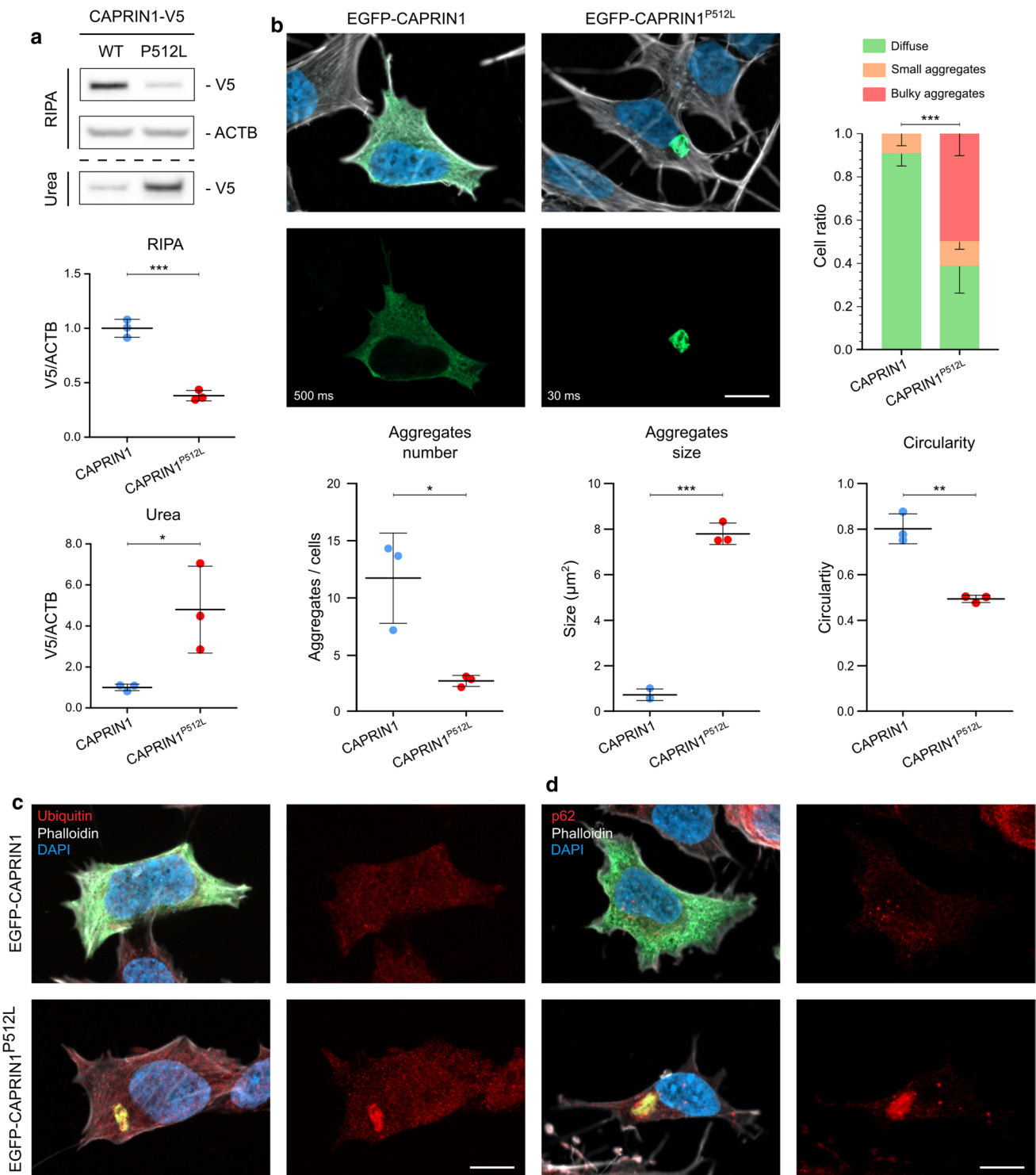


**Fig. 2** CAPRIN1<sup>P512L</sup> is less soluble than CAPRIN1. **a** Immunoblot from sequential protein extraction with RIPA and urea buffers in HEK293T transfected cells. While CAPRIN1-V5 is mostly eluted in the RIPA fraction, CAPRIN1<sup>P512L</sup>-V5 is more insoluble and is eluted in the urea fraction (Bars: mean  $\pm$  SD;  $n=3$ ; unpaired  $t$  test: \*\*\* $p < 0.001$ , \* $p < 0.05$ ). **b** CAPRIN1<sup>P512L</sup> forms aggregates. SH-SY5Y cells transiently expressing EGFP, EGFP-CAPRIN1

and EGFP-CAPRIN1<sup>P512L</sup>. While EGFP-CAPRIN1 mostly shows a diffuse cytoplasmatic distribution, EGFP-CAPRIN1<sup>P512L</sup> forms few, bulky aggregates. The exposure time for the green channel is reported in the panel. (Scale bar: 10  $\mu$ m. Bars: mean  $\pm$  SD;  $n \geq 3$ ;  $\chi^2$  test: \*\*\* $p < 0.0001$ ; unpaired  $t$  test: \* $p < 0.05$ ; \*\* $p < 0.01$ ; \*\*\* $p < 0.001$ ). **c** CAPRIN1<sup>P512L</sup> aggregates are positive for Ubiquitin. **d** CAPRIN1<sup>P512L</sup> aggregates are positive for p62. (Scale bar: 10  $\mu$ m)

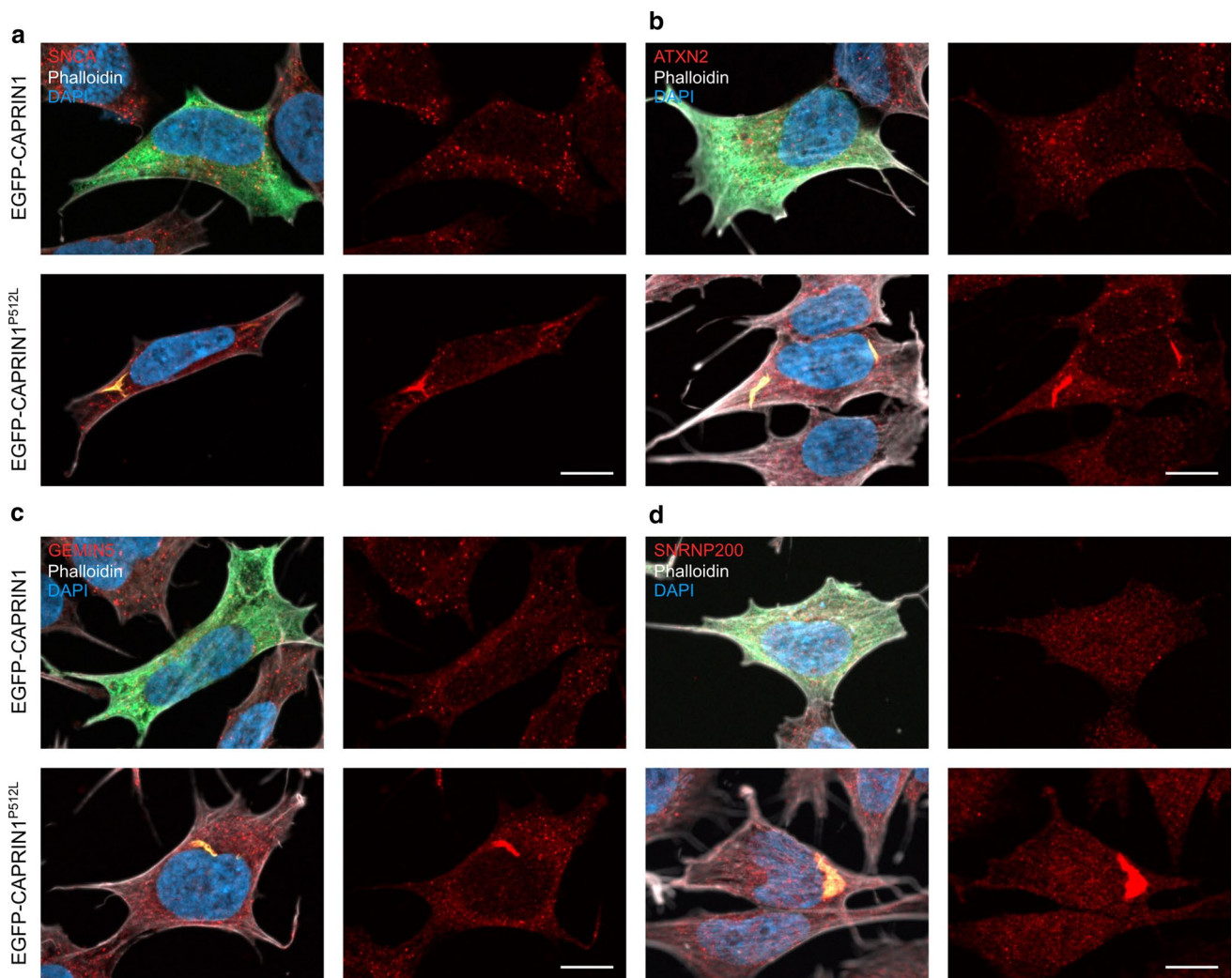


**Fig. 3** CAPRIN1<sup>P512L</sup> aggregates are positive for NDs-related proteins. **a** EGFP-CAPRIN1<sup>P512L</sup> aggregates are positive for SNCA. **b** EGFP-CAPRIN1<sup>P512L</sup> aggregates are positive for ATXN2. **c** EGFP-

CAPRIN1<sup>P512L</sup> aggregates are positive for GEMIN5. **d** EGFP-CAPRIN1<sup>P512L</sup> aggregates are positive for SNRNP200. (Scale bar: 10  $\mu$ m)

**Table 1** Pearson's correlation coefficients for colocalization

	CAPRIN1	CAPRIN1 <sup>P512L</sup>	<i>p</i> value
Ubiquitin	0.07 ± 0.09	0.71 ± 0.17	***
p62	0.39 ± 0.09	0.69 ± 0.17	**
SNCA	0.34 ± 0.14	0.89 ± 0.12	***
ATXN2	0.43 ± 0.07	0.75 ± 0.02	***
GEMIN5	0.40 ± 0.07	0.81 ± 0.22	**
SNRNP200	0.11 ± 0.06	0.94 ± 0.03	***

\**p* < 0.05, \*\**p* < 0.01, \*\*\**p* < 0.001

**Table 2** Biochemical properties of mGFP-CAPRIN1 and mGFP-CAPRIN1<sup>P512L</sup>

	CAPRIN1	CAPRIN1 <sup>P512L</sup>	<i>p</i> value
Ratio, 20 °C (F350/330) <sup>a</sup>	0.84 ± 0.006	0.86 ± 0.009	**
<i>T</i> <sub>m</sub> (°C) <sup>b</sup>	47.8 ± 0.1	48.4 ± 0.1	***
Radius (FCS, nM)	4.8 ± 0.5	5.8 ± 0.2	*

\**p* < 0.05, \*\**p* < 0.01, \*\*\**p* < 0.001

<sup>a</sup>F350/F330 fluorescence ratio at 20 °C

<sup>b</sup>Unfolding temperature

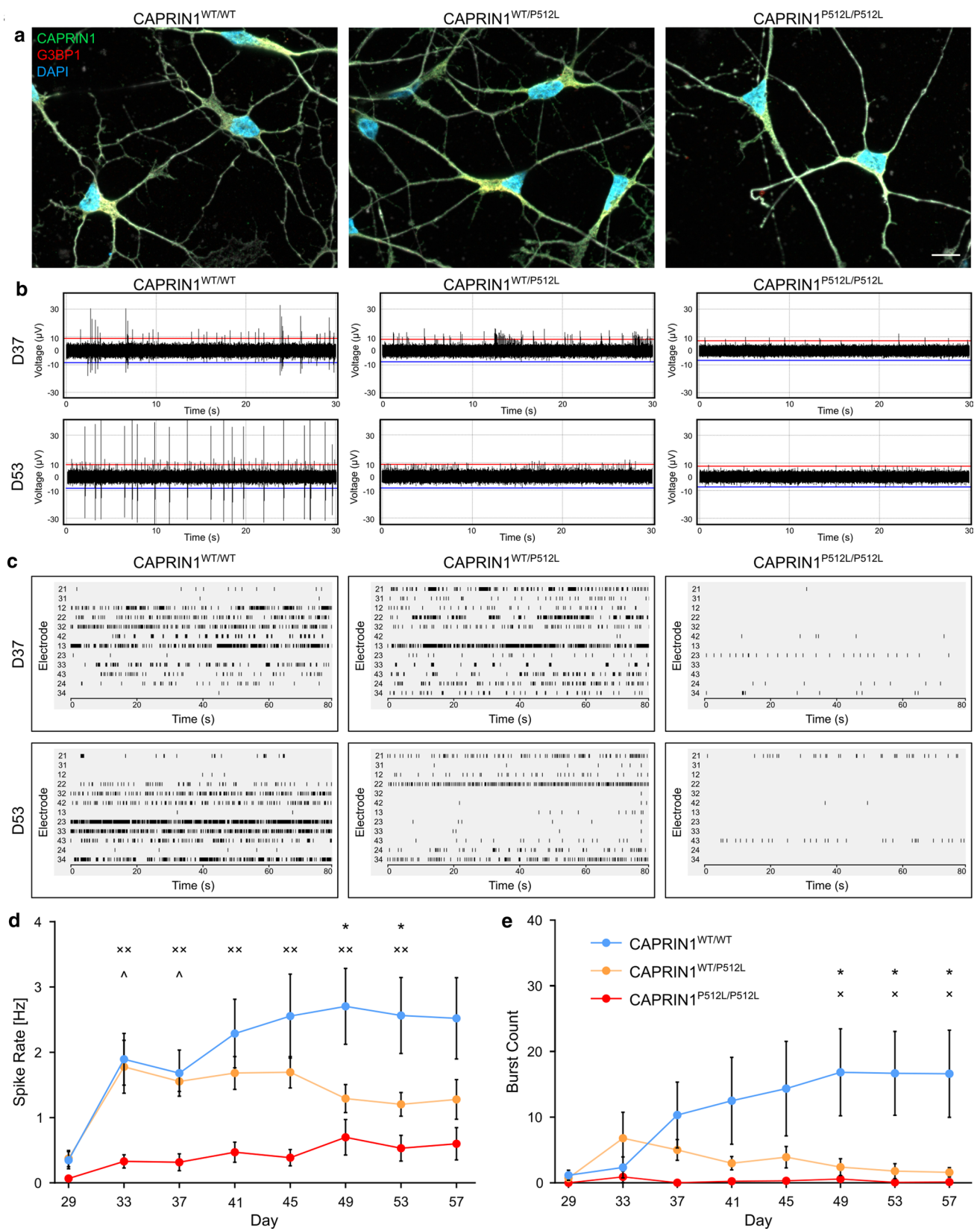


**Fig. 4** CAPRIN1<sup>P512L</sup> neurons show reduced neuronal activity. **a** At maturation (D36), CAPRIN1<sup>WT/P512L</sup> and CAPRIN1<sup>P512L/P512L</sup> do not show overt protein aggregation. **b** Representative traces from a MEA electrode at day 37 (D37) and 53 (D53). **c** Representative activity plots of a MEA well at day 37 (D37) and 53 (D53). **d** CAPRIN1<sup>WT/P512L</sup> and CAPRIN1<sup>P512L/P512L</sup> iPSC-derived neurons show reduced spike rate in comparison with CAPRIN1<sup>WT/WT</sup> ones (Bars: mean ± SEM; n = 3; one-way ANOVA: \*CAPRIN1<sup>WT/WT</sup> vs CAPRIN1<sup>WT/P512L</sup>, \*CAPRIN1<sup>WT/WT</sup> vs CAPRIN1<sup>P512L/P512L</sup>, ^CAPRIN1<sup>WT/P512L</sup> vs CAPRIN1<sup>P512L/P512L</sup>, \*/^p < 0.05, \*\*p < 0.01). **e** CAPRIN1<sup>WT/P512L</sup> and CAPRIN1<sup>P512L/P512L</sup> iPSC-derived neurons show reduced burst counts in comparison with CAPRIN1<sup>WT/WT</sup> ones (Bars: mean ± SEM; n = 3; one-way ANOVA: \*CAPRIN1<sup>WT/WT</sup> vs CAPRIN1<sup>WT/P512L</sup>, \*CAPRIN1<sup>WT/WT</sup> vs CAPRIN1<sup>P512L/P512L</sup>, ^CAPRIN1<sup>WT/P512L</sup> vs CAPRIN1<sup>P512L/P512L</sup>, \*/^p < 0.05)

atrophy, ataxia and motor > sensory axonal neuropathy) as the other two patients (S. Donkervoort and C.G. Bönne-mann, direct communication).

### In silico CAPRIN1<sup>P512L</sup> modeling predicts increased aggregation propensity

Since mutations linked to NDs in PrLD-containing proteins cause increased protein misfolding and the P512L substitution occurs close to the PrLD (Fig. 1f) (residues 537–709) [20, 40–43], we hypothesized that it would render CAPRIN1 prone to misfolding and aggregation. Indeed, in silico analysis of CAPRIN1 and CAPRIN1<sup>P512L</sup> using the PLAAC, CamSol and ZipperDB tools predicted an increase in aggregation propensity and an increase in protein insolubility for CAPRIN1<sup>P512L</sup> (Fig. 1h, i and S1a) [18, 19, 44].

### CAPRIN1<sup>P512L</sup> forms insoluble aggregates

To investigate the potentially increased aggregation propensity of CAPRIN1<sup>P512L</sup>, we overexpressed V5-tagged CAPRIN1 and CAPRIN1<sup>P512L</sup> in HEK293T cells and sequentially extracted proteins from a more soluble (RIPA) and less soluble (urea) fraction. CAPRIN1-V5 was mainly eluted in the RIPA-soluble fraction, while CAPRIN1<sup>P512L</sup>-V5 exhibited reduced solubility and was recovered in the urea-soluble fraction (Fig. 2a), a behavior found in other mutant PrLD-containing proteins related with degenerative disorders [21].

Remarkably, in SH-SY5Y cells, overexpression of EGFP-tagged CAPRIN1 mostly revealed diffuse cytoplasmic localization and coalesces in small round clusters (Fig. 2b and S1b), compatible with the induction stress granules, as previously reported [2, 6]. On the contrary, EGFP-CAPRIN1<sup>P512L</sup> mostly formed a few, large aggregates (Fig. 2b–d, 3a–d and S1b–d).

### CAPRIN1<sup>P512L</sup> aggregates are positive for typical NDs markers

Since protein misfolding and impairment of the protein quality control (PQC) are widely recognized pathomechanism of NDs [45], we investigated protein homeostasis markers, such as ubiquitin and p62. Under physiological conditions, the formation of aggregates is prevented by the activity of molecular chaperons of the PQC, which are also able to unfold misfolded proteins. When folding is not possible, misfolded proteins are ubiquitinated by E3 ubiquitin ligases and directed to proteasomal degradation via the ubiquitin–proteasome system (UPS) [46, 47]. Indeed, bulky CAPRIN1<sup>P512L</sup> aggregates were positive for ubiquitin (Fig. 2c). Moreover, since insoluble aggregates can inhibit the 26S proteasome and be targeted for lysosomal degradation by macroautophagy [48, 49], we stained CAPRIN1<sup>P512L</sup> aggregates for p62/SQSTM1 positivity and we could indeed detect a strong signal, as reported for other NDs (Fig. 2d) [50]. Taken together, these results suggest that CAPRIN1<sup>P512L</sup> misfolds and becomes targeted for degradation.

### CAPRIN1<sup>P512L</sup> aggregates sequester ataxia-related proteins

We next investigated if CAPRIN1<sup>P512L</sup> inclusions sequester other proteins, resembling the pathophysiology of other age-related neurodegenerative disorders: for example, α-synuclein (SNCA) inclusions (Lewy bodies) can be found in Parkinson's disease (PD) and Lewy bodies dementia (LBD) [51]. Likewise, TARDBP aggregates are a common feature in both amyotrophic lateral sclerosis (ALS) and frontotemporal lobar degeneration (FTLD) pathology despite their genetic heterogeneity [52, 53]. CAPRIN1 has also been detected in aggregates in TARDBP or FUS-positive ALS spinal cord motor neurons [35, 54, 55]. We detected a strong SNCA positivity for CAPRIN1<sup>P512L</sup> aggregates (Fig. 3a, Table 1), but no colocalization with TARDBP and FUS (Fig. S1c and S1d).

We next examined whether CAPRIN1<sup>P512L</sup> aggregates would sequester other known CAPRIN1 binding partners. We focused on specific candidates: ATXN2, whose polyQ expansions cause spinocerebellar ataxia 2 (SCA2) [37], and GEMIN5, whose biallelic mutations cause neurodevelopmental delay and ataxia [38]. Indeed, both proteins were present in the CAPRIN1<sup>P512L</sup> inclusions (Fig. 3b and c; Table 1).

Due to the progressive muscle atrophy of the affected individuals, we additionally investigated if the aggregates contained SNRNP200, another CAPRIN1 interacting partner that has been reported in the cortical and spinal motor neurons of ALS cases and indeed we could detect it (Fig. 3d;

Table 1) [36]. Taken together, these results indicate that CAPRIN1<sup>P512L</sup> inclusions are able to sequester multiple ND and ataxia-related proteins.

### CAPRIN1<sup>P512L</sup> iPSC-derived neurons show reduced neuronal activity

To study the effects of the P512L substitution in a human neuronal cell model, we generated the heterozygous CAPRIN1<sup>WT/P512L</sup> and the homozygous CAPRIN1<sup>P512L/P512L</sup> isogenic cell lines from the CAPRIN1<sup>WT/WT</sup> HUVEC iPSC line using CRISPR/Cas9 genome editing (Fig. S2a). We

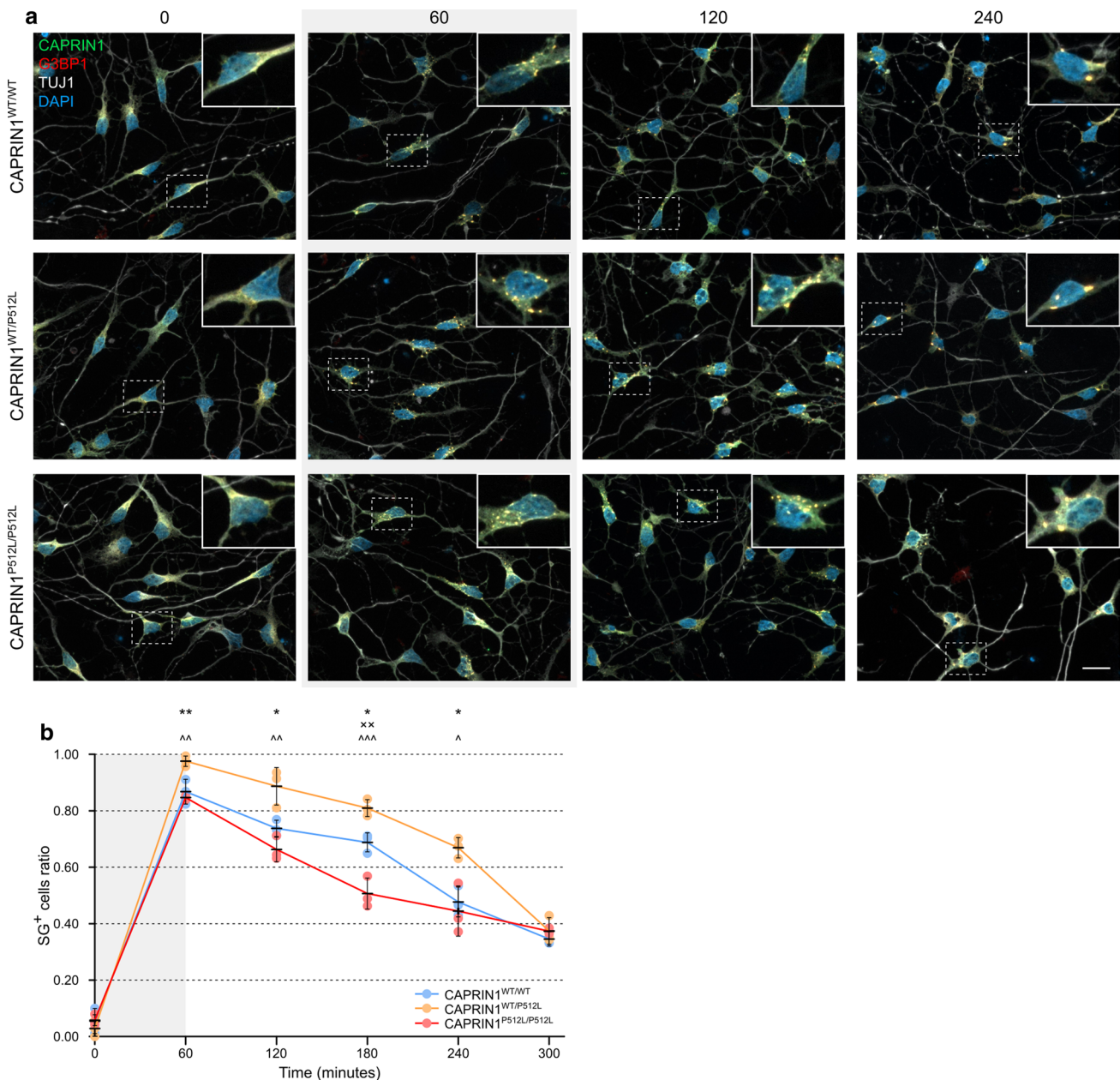


**Fig. 5** CAPRIN1<sup>P512L</sup> neurons show impaired stress granules dynamics. **a** Representative pictures of the neurons. iPSC-derived neurons were treated for 60 min with 0.5 mM NaAsO<sub>2</sub>. Medium was then exchanged with normal medium and cells were incubated at different time points and fixed. The number on top indicate the time in

minutes. **b** Quantification of the SG<sup>+</sup> cell ratio (Bars: mean ± SEM; n=3; one-way ANOVA: \*CAPRIN1<sup>WT/WT</sup> vs CAPRIN1<sup>WT/P512L</sup>, \*CAPRIN1<sup>WT/WT</sup> vs CAPRIN1<sup>P512L/P512L</sup>, ^CAPRIN1<sup>WT/P512L</sup> vs CAPRIN1<sup>P512L/P512L</sup>, \*/^p < 0.05; \*\*/\*^/^^p < 0.01; ^^p < 0.001. Scale bar: 20 μm)

then differentiated them in cortical neurons using the protocol from Schuster et al. 2020 (Fig. S2b and S2c). These iPSC-derived neurons do not show any significant change in CAPRIN1 levels at neuronal maturation (D36), nor any overt morphological alteration of the cell soma or the neurites (Fig. 4a).

In particular, both iPSCs and iPSC-derived neurons harboring the CAPRIN1<sup>P512L</sup> mutation did not display any protein aggregates, even upon proteasomal inhibition (Fig. S3a-b and S4a). Their absence, however, is reported for many other iPSC-derived neuronal cell lines that harbor mutations associated with protein aggregation in tissue sections from individuals suffering of ataxia, Parkinson's disease or Huntington's disease (HD) [56–58].

Since in several disease models electrophysiological changes in neurons precede neuronal loss [59], we recorded the spontaneous neuronal activity using a microelectrode array system. Interestingly, while CAPRIN1<sup>WT/WT</sup> and CAPRIN1<sup>WT/P512L</sup> neurons increased their firing rate upon maturation, CAPRIN1<sup>P512L/P512L</sup> neurons showed a clearly reduced spike rate and almost no bursting throughout the whole recording period (Fig. 4b–e). On the other hand, after an initial overlap, also the activity of CAPRIN1<sup>WT/P512L</sup> neurons progressively decreased (Fig. 4b–e).

### CAPRIN1<sup>P512L</sup> iPSC-derived neurons show impaired stress granules dynamics

Since CAPRIN1 represents one of the main components of SGs [6, 11], and disease-linked mutations in TARDBP, FUS or C9ORF72 cause an increase of cells presenting SGs upon stress [60–62], we hypothesized that the CAPRIN1<sup>P512L</sup> mutation could alter their dynamics. Therefore, we treated the iPSC-derived neurons with sodium arsenite (SA), a common SG inducer [6], and studied their resolution at different time points. Intriguingly, upon SA treatment, a higher fraction of CAPRIN1<sup>WT/P512L</sup> neurons showed SGs in comparison to both CAPRIN1<sup>WT/WT</sup> and CAPRIN1<sup>P512L/P512L</sup> neurons (Fig. 5a and b). Moreover, in CAPRIN1<sup>WT/P512L</sup> neurons the resolution of the SGs occurred slower than in the other cell lines, resulting in the persistence of SG for a longer time after stress removal. Strikingly, this difference could not be observed in CAPRIN1<sup>P512L/P512L</sup> neurons, where the SGs resolution tended to be even faster than in the CAPRIN1<sup>WT/WT</sup> neurons, suggesting a more complex scenario where the CAPRIN1 properties and interactions might play a major role.

### CAPRIN1<sup>P512L</sup> adopts an extended conformation

To investigate whether the P512L mutation influences CAPRIN1 structure, we characterized recombinantly produced and purified mGFP-CAPRIN1 and

mGFP-CAPRIN1<sup>P512L</sup> (Fig. 6a). We used nano-differential scanning fluorimetry (nanoDSF) to monitor the tertiary structure and unfolding transitions of CAPRIN1. This revealed significant differences in the fluorescence ratio (F350/F330) at 20 °C and increased stability of mGFP-CAPRIN1<sup>P512L</sup> in comparison to mGFP-CAPRIN1 (Fig. 6b, Table 2). These data suggest that the mutation does not cause a substantial destabilization of the protein and that the two proteins have a similar tertiary structure. Dynamic light scattering (DLS) and fluorescence correlation spectroscopy (FCS) measurements showed that mGFP-CAPRIN1<sup>P512L</sup> exhibits an increased hydrodynamic radius compared to that of mGFP-CAPRIN1 (Fig. 6c, Table 2). Taken together, the data suggest that CAPRIN1<sup>P512L</sup> adopts an extended yet near-native conformation.

### The P512L mutation does not impair CAPRIN1 dimerization

Given the differences in hydrodynamic radius between CAPRIN1 and CAPRIN1<sup>P512L</sup> and the ability of CAPRIN1 to form dimers [12], we used FCS to test for changes in CAPRIN1 oligomerization. We measured the brightness of mGFP-CAPRIN1 and mGFP-CAPRIN1<sup>P512L</sup> and compared it to the brightness of free GFP. Both proteins were shown to associate into dimers in solution even at concentrations as low as 50 nM (Fig. 6d). Consistent with the formation of CAPRIN1 dimers, the GFP brightness decreased when mGFP-CAPRIN1 was mixed with an excess of unlabeled CAPRIN1, demonstrating the formation of spectroscopic heterodimers (Fig. S5a). In accordance with the distance between the mutated residue and the annotated dimerization domain (residues 132–251) [12], our data demonstrate that the P512L mutation does not affect dimerization, but rather results in an expanded conformation of the protein.

### CAPRIN1<sup>P512L</sup> aggregation is enhanced by RNA

Since CAPRIN1 is an RBP, we examined whether this conformational change would alter its affinity for RNA. To this end, we incubated CAPRIN1 with ATTO590-labelled single-stranded RNA (ssRNA). CAPRIN1<sup>P512L</sup> showed reduced RNA affinity ( $K_D^{CAPRIN1}$ :  $\sim 506 \pm 223$  nM;  $K_D^{CAPRIN1-P512L}$ :  $\sim 947 \pm 239$  nM; Fig. 6e). We then tested the reversibility of the CAPRIN1-RNA interaction by adding unlabeled long homopolymeric polyA RNA as a competitor. In accordance with the previous data, CAPRIN1 binds ssRNA  $\sim$  twofold tighter than CAPRIN1<sup>P512L</sup> ( $K_I^{CAPRIN1}$ :  $60.5 \pm 0.7$  ng/ $\mu$ l;  $K_I^{CAPRIN1-P512L}$ :  $33.5 \pm 12$  ng/ $\mu$ l; Fig. 6f).

To further investigate CAPRIN1<sup>P512L</sup> properties, we observed mGFP-CAPRIN1 and mGFP-CAPRIN1<sup>P512L</sup> by fluorescence microscopy. While mGFP-CAPRIN1 displayed a diffuse signal, mGFP-CAPRIN1<sup>P512L</sup> formed

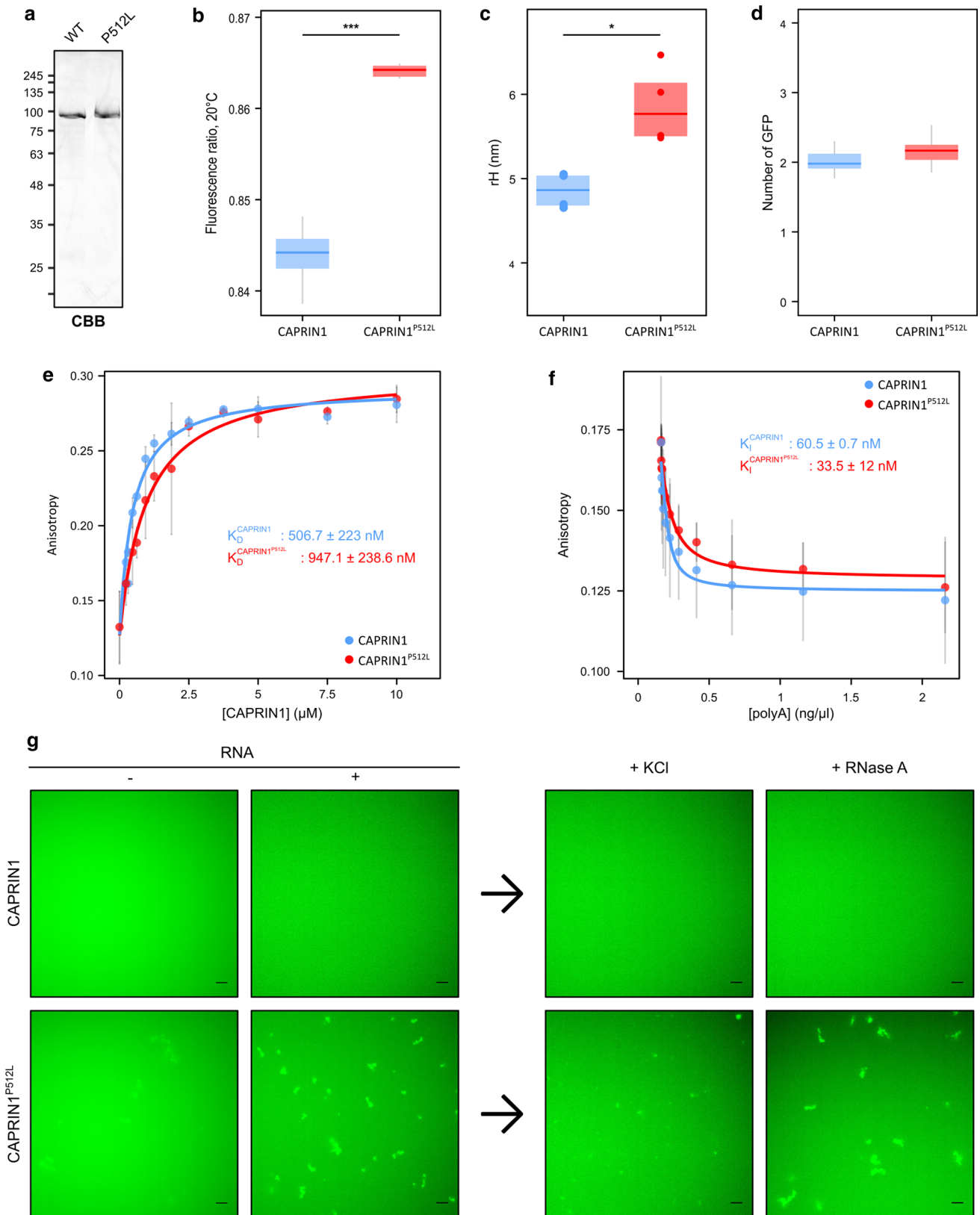


**Fig. 6** Dynamics of CAPRIN1<sup>P512L</sup> and RNA. **a** Purified mGFP-CAPRIN1 and mGFP-CAPRIN1<sup>P512L</sup> stained with Coomassie (CBB) on SDS-PAGE. **b** CAPRIN1<sup>P512L</sup> adopts a more extended conformation than CAPRIN1. The fluorescence ratio (F350/F330) at 20 °C of the two proteins is shown (mGFP-CAPRIN1:  $0.845 \pm 0.006$ ; mGFP-CAPRIN1<sup>P512L</sup>:  $0.864 \pm 0.009$ ;  $n=9$ ; unpaired  $t$  test:  $***p < 0.001$ ). **c** CAPRIN1<sup>P512L</sup> adopts a more extended conformation than CAPRIN1. Hydrodynamic radii (rH) were calculated using FCS (mGFP-CAPRIN1<sup>P512L</sup>:  $4.8 \pm 0.5$  nm; mGFP-CAPRIN1<sup>P512L</sup>:  $5.8 \pm 0.2$  nm;  $n=3$ ; unpaired  $t$  test:  $p < 0.05$ ). **d** CAPRIN1<sup>P512L</sup> dimerization is not impaired. The GFP brightness comparison of 50 nM mGFP-CAPRIN1 and mGFP-CAPRIN1<sup>P512L</sup> to mGFP indicate that both proteins form dimers. **e** CAPRIN1<sup>P512L</sup> has a reduced RNA affinity. Fluorescence anisotropy measured the binding affinity of CAPRIN1 and CAPRIN1<sup>P512L</sup> using <sup>ATTO590</sup>ssRNA. ( $K_D^{\text{CAPRIN1}}$ :  $506 \pm 223$  nM;  $K_D^{\text{CAPRIN1-P512L}}$ :  $\sim 947 \pm 238.6$  nM;  $n=3$ ). **f** CAPRIN1<sup>P512L</sup> has a reduced RNA affinity. An increasing amount of unlabeled polyA was added to <sup>ATTO590</sup>ssRNA-bound mGFP-CAPRIN1 or mGFP-CAPRIN1<sup>P512L</sup> and changes in anisotropy were measured ( $K_I^{\text{CAPRIN1}}$ :  $60.5 \pm 0.7$  ng/ $\mu$ l;  $K_I^{\text{CAPRIN1-P512L}}$ :  $33.5 \pm 12$  ng/ $\mu$ l;  $n=2$ ). **g** CAPRIN1<sup>P512L</sup> aggregation is enhanced by RNA incubation. Upon RNA addition, mGFP-CAPRIN1<sup>P512L</sup> aggregates while mGFP-CAPRIN1 remains soluble. KCL or RNase A were added to check the reversibility of the interaction (Scale bar: 10  $\mu$ m)

small agglomerates, confirming the increased aggregation propensity seen in our cell models (Fig. 6g). Since CAPRIN1 is an RBP and recent studies demonstrated the pivotal role of RNA in the modulation of protein aggregation [63, 64], we next incubated the purified proteins with RNA. Strikingly, while mGFP-CAPRIN1 remained soluble, mGFP-CAPRIN1<sup>P512L</sup> formed large, microscopically visible aggregates (Fig. 6g). This effect was independent of the RNA type, and all RNA types tested caused aggregation of mGFP-CAPRIN1<sup>P512L</sup> (Fig. S5b). Since the association of RBPs with nucleic acids is often driven and stabilized through electrostatic interactions, we increased the salinity after complex formation to distinguish weaker (reversible) from stronger (irreversible, indicative of aggregates) interactions. Increasing the salinity reduced the degree of aggregation only to some extent, and the addition of RNase A did not dissolve the aggregates (Fig. 6g). This suggests that CAPRIN1<sup>P512L</sup> misfolding might be triggered by RNA, but that RNA is not necessary for aggregate persistence. Consistent with this, our FISH analysis in CAPRIN1<sup>P512L</sup> transfected cells showed that the formed aggregates do not contain polyA RNA (Fig. S5c).

Taken together, these data indicate that the Pro512Leu mutation alters the dynamics of binding to RNA which might influence the aggregation propensity of CAPRIN1.

## Discussion

To date, *CAPRIN1* has been associated with two conditions: increased *CAPRIN1* expression has been connected to certain cancers [65], while its reduction has been linked with

autism spectrum disorders and speech delay [14–17]. In contrast, we identify the recurrent de novo CAPRIN1<sup>P512L</sup> mutation in two independent individuals with early onset progressive ataxia and intellectual disability, which increases the protein propensity to aggregate and causes electrophysiological alterations in iPSC-derived neurons.

Strikingly, both affected individuals carry the identical de novo c.1535C > T variant, an event which is per se highly unlikely to occur by chance (Note S2). This variant is not reported in gnomAD, where *CAPRIN1* constraint metrics indicate that the gene has a reduced tolerance for missense mutations ( $Z=1.69$ ;  $o/e: 0.76$  (95% CI 0.69–0.84)) and missense SNVs in the  $\pm 100$  bp range from the variant have all very rare frequencies ( $< 0.0001$ ).

The P512L substitution affects the highly conserved proline residue exchanging a secondary structure breaker for a non-polar, aliphatic leucine (Fig. 1d and e) [65]. Although this amino acid substitution affects a residue close to CAPRIN1 PrLD (residues 537–709) and its surrounding region is enriched for residues found in prion-like domains, such as serine and glutamine, the proline-surrounding sequence is highly conserved. This suggests that this region is not disordered but adopts a specific fold that is most probably disrupted by the introduction of the leucine residue. In particular, the fact that the P512L substitution lead to an increase in the hydrodynamic radius of the protein, suggests that this proline is in the *cis* configuration in the wild-type protein and generates a kink in the polypeptide chain [66]. We hypothesize that this kink is absent in CAPRIN1<sup>P512L</sup>, causing the observed extended conformation. Moreover, due to the distance of this residue from potential post-translational modifications sites, this substitution is unlikely to influence them [67].

Our data suggest that the leucine substitution renders the protein prone to misfolding and aggregation, which is accelerated by the presence of RNA. Therefore, it is highly likely that the P512L acts in a gain-of-function manner. Furthermore, the gain-of-function model is in accordance with the increasing evidence that, conversely, CAPRIN1 reduction (e.g. haploinsufficiency) causes a different phenotype, characterized by language impairment, attention-deficit/hyperactivity disorder

(ADHD) and ASD [14–17]. This suggests an intriguing parallel between CAPRIN1 and FMR1: FMR1 loss-of-function mutations are linked to Fragile X syndrome, a neurodevelopmental disorder characterized by intellectual disability due to hypermethylation of long CGG repeats ( $> 200$ ) [68], while FMR1 gain-of-function mutations are linked to FXTAS, a neurodegenerative disorder where shorter CGG expansions (50–200) lead to increase in FMR1 expression [39, 69]. An important difference between the CAPRIN1 neurodegenerative disorder and FXTAS is the different disease onset: while the former

occurs during childhood, the latter affects individuals older than 50 years of age [39]. This suggests that the protein quality control machinery is unable to control the aggregation properties of CAPRIN1<sup>P512L</sup> and it could be related to the importance of the other proteins sequestered in the aggregates.

Intriguingly, we observed that CAPRIN1<sup>P512L</sup> inclusions contain ATXN2 and GEMIN5. This is interesting because ATXN2 polyQ repeats cause autosomal dominant SCA2 ( $\geq 33$  repeats) or increase ALS risk (31–32 repeats) through neuronal ATXN2 aggregation [10] and the affected individuals show both progressive ataxia and muscle weakness and atrophy. On the other side, biallelic mutations in GEMIN5 have recently been linked to early-onset neurodevelopmental delay and ataxia [38]. This suggests that sequestration of ATXN2 and GEMIN5 in CAPRIN1<sup>P512L</sup> inclusions could at least in part be responsible for the observed gain-of-function phenotypes. In fact, CAPRIN1 and many other stress granule proteins are embedded in a dense network of protein–protein interactions even before they assemble into stress granules [70–72]. The fact that mutant CAPRIN1 is in a near-native state, suggests that many of these interactions will remain intact during misfolding and aggregation. Accordingly, CAPRIN1 aggregation may inactivate many associated proteins, providing an explanation for the severity of the disease phenotype.

Given the importance of the cell-specific environment in investigating a phenotype [25], we prioritized a neuronal model over patient-derived cell lines. Therefore, we generated the heterozygous CAPRIN1<sup>WT/P512L</sup> and the homozygous CAPRIN1<sup>P512L/P512L</sup> isogenic iPSC lines using CRISPR/Cas9 technology and differentiated them in cortical neurons, since both affected individuals suffered also from intellectual disability and even showed cortical atrophy and to avoid the considerable limitations of iPSC-derived cerebellar neurons, such as low cellular yield, need of coculture with mice-derived progenitors or long differentiation duration of the available protocols [73]. At neuronal maturation (D36), we did not observe marked differences in differentiation efficiency (Fig. S2b and S2c), which would indicate a correct neuronal maturation and confirm the neurodegenerative nature of the disorder. We did not observe the formation of CAPRIN1 aggregates, even after proteasomal inhibition in both iPSCs and iPSC-derived neurons (Fig. S3a, S3b and S4a). One possible justification is a caveat of the disease model per se: iPSC-derived neurons usually lack the maturity of postnatally differentiated neurons and this acquires particular relevance when investigating a neurodegenerative disorder, where neuronal ageing plays a crucial role in the development of a phenotype [58]. In fact, iPSC-derived neurons used to study diseases characterized by protein aggregation like Alzheimer's disease, Parkinson's disease or Huntington's disease mostly failed to detect

amyloid beta,  $\alpha$ -synuclein or HTT aggregation, respectively [56–58]. Based on the characterization of the iPSC-derived neurons conducted in the protocol's original paper [25], it is reasonable to expect that the iPSC-derived neurons used in this study are not mature enough. Indeed, studies have shown that bypassing the iPSC state through direct reprogramming of somatic cells maintained aging hallmarks and recapitulated some disease phenotypes that are not present in iPSC-derived neurons [74]. This alternative approach was not pursued because of reproducibility concerns. However, it is important to note that iPSC-derived neurons could exhibit disease-specific alterations even in the absence of overt protein aggregation [58]. Interestingly, the activity of the iPSC-derived neurons decreases with the number of mutated CAPRIN1 alleles: while the spike rate and burst number of CAPRIN1<sup>WT/P512L</sup> neurons is initially comparable to the one of CAPRIN1<sup>WT/WT</sup> neurons, that of CAPRIN1<sup>P512L/P512L</sup> neurons is always low: this suggests that pathophysiological changes in the neurons precede the formation of aggregates. This is in agreement with many NDs characterized by protein aggregation, where alterations in several cellular processes are found in neurons without inclusions, even in animal models [59, 75]. In CAPRIN1<sup>WT/P512L</sup> neurons, the mutation causes an increase in the SG formation and a reduction in their resolution, in line with disease-linked mutations in other ND-related genes (*TARDBP*, *FUS* or *C9ORF72*) [60–62]. However, the homozygous mutation does not cause an increase in their formation, but even a slightly faster resolution. A possible explanation of this phenomenon is that the increased aggregation propensity of CAPRIN1<sup>P512L</sup> might be counterbalanced by its reduced affinity for RNA. In homozygous CAPRIN1<sup>P512L</sup> neurons, the protein's low affinity for RNA tends to hinder the formation of SGs, compensating its increased aggregation. By contrast, in heterozygous neurons, the aggregation-prone but low-RNA-binding CAPRIN1<sup>P512L</sup> can still form dimers with the wild-type CAPRIN1, and its aggregation propensity might increase SGs formation. These data suggest differences in the assembly of SGs that could be due altered RNA binding affinity, but whether SGs promote the formation of pathological CAPRIN aggregates or whether CAPRIN1 aggregates independently of SGs remains to be investigated.

Indeed, the pivotal role of protein-RNA interactions in aggregation is becoming increasingly clear: while for some mutations of ALS-related genes, such as *TARDBP*, *FUS*, *HNRNPA2B1* and *HNRNPA1*, the purified mutated proteins alone were often sufficient to enhance its aggregation propensity [20, 40–42], recent studies demonstrated the RNA ability to hinder or promote aggregation [63, 64, 76]. For example, RNA is able to antagonize *TARDBP* aggregation and disease-associated mutations would promote aberrant phase transitions of RNA-deficient *TARDBP* proteins [77]. Conversely, RNA increases the aggregation propensity of

CAPRIN1<sup>P512L</sup> and RNA removal does not revert the conformational change; this indicates that the misfolding might be irreversible. Interestingly, polyG RNA is able to trigger not only CAPRIN1<sup>P512L</sup> aggregation but the one of CAPRIN1 too. A possible explanation for this phenomenon could be the intrinsic ability of polyG RNA to undergo phase separation due to the formation of G-quadruplex structures [78].

In conclusion, we identify with the P512L mutation a highly critical domain in CAPRIN1, the alteration of which associates with early-onset ataxia and intellectual disability, thereby associating another PrLD-containing protein to a novel neurodegenerative disorder. Moreover, we provide further evidence for the pivotal role of protein-RNA interactions in the assembly of aggregates.

**Supplementary Information** The online version contains supplementary material available at <https://doi.org/10.1007/s00018-022-04544-3>.

**Acknowledgements** We are grateful to the patients and family members for taking part in this study. We thank Dr. Leo Kurian for providing the HUVEC iPSC line and the Cas9 expression vector pX330-hCas9-long-chimeric-grna-g2p. We thank Dr. Valentina Piano for critical reading and commenting the manuscript.

**Author contributions** ADV conceptualization; investigation; writing—original draft; writing—review & editing. JN conceptualization; investigation; writing—original draft; writing – review & editing. GZ resources; ME resources; AMB investigation. MS investigation. JGB investigation. SB investigation. SP investigation. IH resources. FK resources. TMF conceptualization; supervision; writing—review & editing. ESB resources. JK resources. SA conceptualization; supervision; writing—review & editing. MT resources. BW conceptualization; supervision; writing—review & editing.

**Funding** Open Access funding enabled and organized by Projekt DEAL. G. Z. and E. S. B. are members of the European Reference Network for Rare Neurological Diseases (ERN-RND) (Project ID No 739510). This work was supported by the Light Microscopy Facility, a Core Facility of the CMCB Technology Platform at TU Dresden. This work was supported by the German Research Foundation [Wi 945/17-1 (project-ID 398410809); Wi 945/18-1 (project ID 384170921); Wi 945/19-1 (project-ID 417989143); SFB1451 (project-ID 431549029 – A01), and GRK1960 (project ID 233886668)], the European Community's Seventh Framework Programme (FP7/2007-2013) under grant agreement no. 2012-305121 "Integrated European –omics research project for diagnosis and therapy in rare neuromuscular and neurodegenerative diseases (NEUROMICS)" and the European Research Council (ERC) under the European Union's Horizon 2020 research and innovation program under the Marie Skłodowska-Curie grant agreement No 956185 (SMABEYOND) and No 725836 (PhaseAge), the Center for Molecular Medicine Cologne (project No C18), the Italian Ministry of Health (CCR-2017-23669081, RCR-2020-23670068\_001, Ricerca 5 × 1000), Italian Ministry of Research (FOE 2019) and Fondazione Bambino Gesù (Vite Coraggiose).

**Data availability** The exome data of family A are stored in the EGA database under the access numbers EGAN00001366922, EGAN00001366923, EGAN00001366924. Request should be addressed to the NeurOmics data sharing committee. The exome data for family B can be made available upon reasonable request.

## Declarations

**Conflict of interest** The authors have no relevant financial or non-financial interests to disclose.

**Ethical approval and informed consent** This study conformed to standards outlined in the Declaration of Helsinki and was approved by the Ethics Committee of the University of Cologne (Reference Number 13-022) and Ospedale Pediatrico Bambino Gesù (Reference Number 1702\_OPBG\_2018). Informed written consent for the collection of human material, for the participation in the study and for publication purposes was obtained from the respective subjects or their legal guardians following the regulations of the Ethics Committees of the University of Cologne and Ospedale Pediatrico Bambino Gesù.

**Open Access** This article is licensed under a Creative Commons Attribution 4.0 International License, which permits use, sharing, adaptation, distribution and reproduction in any medium or format, as long as you give appropriate credit to the original author(s) and the source, provide a link to the Creative Commons licence, and indicate if changes were made. The images or other third party material in this article are included in the article's Creative Commons licence, unless indicated otherwise in a credit line to the material. If material is not included in the article's Creative Commons licence and your intended use is not permitted by statutory regulation or exceeds the permitted use, you will need to obtain permission directly from the copyright holder. To view a copy of this licence, visit <http://creativecommons.org/licenses/by/4.0/>.

## References

1. Grill B, Wilson GM, Zhang KX et al (2004) Activation/division of lymphocytes results in increased levels of cytoplasmic activation/proliferation-associated protein-1: prototype of a new family of proteins. *J Immunol* 172:2389–2400. <https://doi.org/10.4049/jimmunol.172.4.2389>
2. Shiina N, Shinkura K, Tokunaga M (2005) A novel RNA-binding protein in neuronal RNA granules: regulatory machinery for local translation. *J Neurosci* 25:4420–4434. <https://doi.org/10.1523/JNEUROSCI.0382-05.2005>
3. Nakayama K, Ohashi R, Shinoda Y et al (2017) RNG105/caprin1, an RNA granule protein for dendritic mRNA localization, is essential for long-term memory formation. *Elife*. <https://doi.org/10.7554/eLife.29677>
4. GTE Portal. dbGaP Accession phs000424.v8.p2. <https://gteportal.org/home/gene/CAPRIN1>. Accessed 21 Jan 2022
5. Shiina N, Yamaguchi K, Tokunaga M (2010) RNG105 deficiency impairs the dendritic localization of mRNAs for Na<sup>+</sup>/K<sup>+</sup> ATPase subunit isoforms and leads to the degeneration of neuronal networks. *J Neurosci* 30:12816–12830. <https://doi.org/10.1523/jneurosci.6386-09.2010>
6. Solomon S, Xu Y, Wang B et al (2007) Distinct structural features of caprin-1 mediate its interaction with G3BP-1 and its induction of phosphorylation of eukaryotic translation initiation factor 2alpha, entry to cytoplasmic stress granules, and selective interaction with a subset of mRNAs. *Mol Cell Biol* 27:2324–2342. <https://doi.org/10.1128/MCB.02300-06>
7. March ZM, King OD, Shorter J (2016) Prion-like domains as epigenetic regulators, scaffolds for subcellular organization, and drivers of neurodegenerative disease. *Brain Res* 1647:9–18. <https://doi.org/10.1016/j.brainres.2016.02.037>

8. King OD, Gitler AD, Shorter J (2012) The tip of the iceberg: RNA-binding proteins with prion-like domains in neurodegenerative disease. *Brain Res* 1462:61–80. <https://doi.org/10.1016/j.brainres.2012.01.016>
9. Candelise N, Scaricamazza S, Salvatori I et al (2021) Protein aggregation landscape in neurodegenerative diseases: clinical relevance and future applications. *Int J Mol Sci*. <https://doi.org/10.3390/ijms22116016>
10. Harrison AF, Shorter J (2017) RNA-binding proteins with prion-like domains in health and disease. *Biochem J* 474:1417–1438. <https://doi.org/10.1042/BCJ20160499>
11. Kedersha N, Panas MD, Achorn CA et al (2016) G3BP-Caprin1-USP10 complexes mediate stress granule condensation and associate with 40S subunits. *J Cell Biol* 212:845–860. <https://doi.org/10.1083/jcb.201508028>
12. Wu Y, Zhu J, Huang X et al (2016) Crystal structure of a dimerization domain of human Caprin-1: insights into the assembly of an evolutionarily conserved ribonucleoprotein complex consisting of Caprin-1, FMRP and G3BP1. *Acta Crystallogr D Struct Biol* 72:718–727. <https://doi.org/10.1107/S2059798316004903>
13. El Fatimy R, Tremblay S, Dury AY et al (2012) Fragile X mental retardation protein interacts with the RNA-binding protein Caprin1 in neuronal RiboNucleoProtein complexes [corrected]. *PLoS ONE* 7:e39338. <https://doi.org/10.1371/journal.pone.0039338>
14. Jiang YH, Yuen RK, Jin X et al (2013) Detection of clinically relevant genetic variants in autism spectrum disorder by whole-genome sequencing. *Am J Hum Genet* 93:249–263. <https://doi.org/10.1016/j.ajhg.2013.06.012>
15. Du Y, Li Z, Liu Z et al (2020) Nonrandom occurrence of multiple de novo coding variants in a proband indicates the existence of an oligogenic model in autism. *Genet Med* 22:170–180. <https://doi.org/10.1038/s41436-019-0610-2>
16. Ohashi R, Takao K, Miyakawa T et al (2016) Comprehensive behavioral analysis of RNG105 (Caprin1) heterozygous mice: reduced social interaction and attenuated response to novelty. *Sci Rep* 6:20775. <https://doi.org/10.1038/srep20775>
17. Pavinato L, Delle Vedove A, Carli D et al (2022) CAPRIN1 haploinsufficiency causes a neurodevelopmental disorder with language impairment, ADHD and ASD. *Brain*. <https://doi.org/10.1093/brain/awac278>
18. Lancaster AK, Nutter-Upham A, Lindquist S et al (2014) PLAAC: a web and command-line application to identify proteins with prion-like amino acid composition. *Bioinformatics* 30:2501–2502. <https://doi.org/10.1093/bioinformatics/btu310>
19. Sormanni P, Aprile FA, Vendruscolo M (2015) The CamSol method of rational design of protein mutants with enhanced solubility. *J Mol Biol* 427:478–490. <https://doi.org/10.1016/j.jmb.2014.09.026>
20. Guillen-Boixet J, Kopach A, Holehouse AS et al (2020) RNA-induced conformational switching and clustering of G3BP drive stress granule assembly by condensation. *Cell* 181(346–361):e17. <https://doi.org/10.1016/j.cell.2020.03.049>
21. Kim HJ, Kim NC, Wang YD et al (2013) Mutations in prion-like domains in hnRNP A2B1 and hnRNP A1 cause multisystem proteinopathy and ALS. *Nature* 495:467–473. <https://doi.org/10.1038/nature11922>
22. Panopoulos AD, Ruiz S, Yi F et al (2011) Rapid and highly efficient generation of induced pluripotent stem cells from human umbilical vein endothelial cells. *PLoS ONE* 6:e19743. <https://doi.org/10.1371/journal.pone.0019743>
23. Frank S, Ahuja G, Bartsch D et al (2019) yIncT defines a class of divergently transcribed lncRNAs and safeguards the T-mediated mesodermal commitment of human PSCs. *Cell Stem Cell* 24(318–327):e8. <https://doi.org/10.1016/j.stem.2018.11.005>
24. Homology-directed repair using the Alt-R CRISPR-Cas9 System and HDR Donor Oligos. Version 2. <https://eu.idtdna.com/pages/products/crispr-genome-editing/alt-rcrispr-cas9-system>. Accessed 10 Nov 2020
25. Schuster S, Heuten E, Velic A et al (2020) CHIP mutations affect the heat shock response differently in human fibroblasts and iPSC-derived neurons. *Dis Model Mech*. <https://doi.org/10.1242/dmm.045096>
26. Hoell JI, Larsson E, Runge S et al (2011) RNA targets of wild-type and mutant FET family proteins. *Nat Struct Mol Biol* 18:1428–1431. <https://doi.org/10.1038/nsmb.2163>
27. Jarvis DL (2014) Recombinant protein expression in baculovirus-infected insect cells. *Methods Enzymol* 536:149–163. <https://doi.org/10.1016/B978-0-12-420070-8.00013-1>
28. Alberti S, Saha S, Woodruff JB et al (2018) A user's guide for phase separation assays with purified proteins. *J Mol Biol* 430:4806–4820. <https://doi.org/10.1016/j.jmb.2018.06.038>
29. Absolute Diffusion Coefficients: Compilation of Reference Data for FCS Calibration. [https://www.picoquant.com/scientific/technical-and-application-notes/category/technical\\_notes\\_techniques\\_and\\_methods/details/absolutediffusion-coefficients-compilation-reference-fcs-data](https://www.picoquant.com/scientific/technical-and-application-notes/category/technical_notes_techniques_and_methods/details/absolutediffusion-coefficients-compilation-reference-fcs-data). Accessed 11 Feb 2022
30. Karakaya M, Storbeck M, Strathmann EA et al (2018) Targeted sequencing with expanded gene profile enables high diagnostic yield in non-5q-spinal muscular atrophies. *Hum Mutat* 39:1284–1298. <https://doi.org/10.1002/humu.23560>
31. Genome Aggregation Database. <https://gnomad.broadinstitute.org/>. Accessed 02 Feb 2022
32. Schuster-Bockler B, Schultz J, Rahmann S (2004) HMM Logos for visualization of protein families. *BMC Bioinform* 5:7. <https://doi.org/10.1186/1471-2105-5-7>
33. Wheeler TJ, Clements J, Finn RD (2014) Skyline: a tool for creating informative, interactive logos representing sequence alignments and profile hidden Markov models. *BMC Bioinform* 15:7. <https://doi.org/10.1186/1471-2105-15-7>
34. Wolozin B, Ivanov P (2019) Stress granules and neurodegeneration. *Nat Rev Neurosci* 20:649–666. <https://doi.org/10.1038/s41583-019-0222-5>
35. Blokhuis AM, Koppers M, Groen EJM et al (2016) Comparative interactomics analysis of different ALS-associated proteins identifies converging molecular pathways. *Acta Neuropathol* 132:175–196. <https://doi.org/10.1007/s00401-016-1575-8>
36. Vu L, Ghosh A, Tran C et al (2021) Defining the Caprin-1 interactome in unstressed and stressed conditions. *J Proteome Res* 20:3165–3178. <https://doi.org/10.1021/acs.jproteome.1c00016>
37. Pulst SM, Nechiporuk A, Nechiporuk T et al (1996) Moderate expansion of a normally biallelic trinucleotide repeat in spinocerebellar ataxia type 2. *Nat Genet* 14:269–276. <https://doi.org/10.1038/ng1196-269>
38. Kour S, Rajan DS, Fortuna TR et al (2021) Loss of function mutations in GEMIN5 cause a neurodevelopmental disorder. *Nat Commun* 12:2558. <https://doi.org/10.1038/s41467-021-22627-w>
39. Jacquemont S, Hagerman RJ, Leehey M et al (2003) Fragile X premutation tremor/ataxia syndrome: molecular, clinical, and neuroimaging correlates. *Am J Hum Genet* 72:869–878. <https://doi.org/10.1086/374321>
40. Johnson BS, Snead D, Lee JJ et al (2009) TDP-43 is intrinsically aggregation-prone, and amyotrophic lateral sclerosis-linked mutations accelerate aggregation and increase toxicity. *J Biol Chem* 284:20329–20339. <https://doi.org/10.1074/jbc.M109.010264>
41. Murakami T, Qamar S, Lin JQ et al (2015) ALS/FTD mutation-induced phase transition of FUS liquid droplets and reversible

- hydrogels into irreversible hydrogels impairs RNP granule function. *Neuron* 88:678–690. <https://doi.org/10.1016/j.neuron.2015.10.030>
42. Patel A, Lee HO, Jawerth L et al (2015) A liquid-to-solid phase transition of the ALS protein FUS accelerated by disease mutation. *Cell* 162:1066–1077. <https://doi.org/10.1016/j.cell.2015.07.047>
  43. Conicella AE, Zerze GH, Mittal J et al (2016) ALS mutations disrupt phase separation mediated by alpha-helical structure in the TDP-43 low-complexity C-terminal domain. *Structure* 24:1537–1549. <https://doi.org/10.1016/j.str.2016.07.007>
  44. Goldschmidt L, Teng PK, Riek R et al (2010) Identifying the amyloids, proteins capable of forming amyloid-like fibrils. *Proc Natl Acad Sci U S A* 107:3487–3492. <https://doi.org/10.1073/pnas.0915166107>
  45. Ross CA, Poirier MA (2004) Protein aggregation and neurodegenerative disease. *Nat Med* 10(Suppl):S10–S17. <https://doi.org/10.1038/nm1066>
  46. Lowe J, Blanchard A, Morrell K et al (1988) Ubiquitin is a common factor in intermediate filament inclusion bodies of diverse type in man, including those of Parkinson's disease, Pick's disease, and Alzheimer's disease, as well as Rosenthal fibres in cerebellar astrocytomas, cytoplasmic bodies in muscle, and mallory bodies in alcoholic liver disease. *J Pathol* 155:9–15. <https://doi.org/10.1002/path.1711550105>
  47. Ciechanover A, Kwon YT (2017) Protein quality control by molecular chaperones in neurodegeneration. *Front Neurosci* 11:185. <https://doi.org/10.3389/fnins.2017.00185>
  48. Bence NF, Sampat RM, Kopito RR (2001) Impairment of the ubiquitin-proteasome system by protein aggregation. *Science* 292:1552–1555. <https://doi.org/10.1126/science.292.5521.1552>
  49. Verhoef LG, Lindsten K, Masucci MG et al (2002) Aggregate formation inhibits proteasomal degradation of polyglutamine proteins. *Hum Mol Genet* 11:2689–2700. <https://doi.org/10.1093/hmg/11.22.2689>
  50. Kuusisto E, Salminen A, Alafuzoff I (2001) Ubiquitin-binding protein p62 is present in neuronal and glial inclusions in human tauopathies and synucleinopathies. *NeuroReport* 12:2085–2090. <https://doi.org/10.1097/00001756-200107200-00009>
  51. Spillantini MG, Schmidt ML, Lee VM et al (1997) Alpha-synuclein in Lewy bodies. *Nature* 388:839–840. <https://doi.org/10.1038/42166>
  52. Arai T, Hasegawa M, Akiyama H et al (2006) TDP-43 is a component of ubiquitin-positive tau-negative inclusions in frontotemporal lobar degeneration and amyotrophic lateral sclerosis. *Biochem Biophys Res Commun* 351:602–611. <https://doi.org/10.1016/j.bbrc.2006.10.093>
  53. Neumann M, Sampathu DM, Kwong LK et al (2006) Ubiquitinated TDP-43 in frontotemporal lobar degeneration and amyotrophic lateral sclerosis. *Science* 314:130–133. <https://doi.org/10.1126/science.1134108>
  54. Bakkar N, Kovalik T, Lorenzini I et al (2018) Artificial intelligence in neurodegenerative disease research: use of IBM Watson to identify additional RNA-binding proteins altered in amyotrophic lateral sclerosis. *Acta Neuropathol* 135:227–247. <https://doi.org/10.1007/s00401-017-1785-8>
  55. de Boer EMJ, Orié VK, Williams T et al (2020) TDP-43 proteinopathies: a new wave of neurodegenerative diseases. *J Neurol Neurosurg Psychiatry*. <https://doi.org/10.1136/jnnp-2020-322983>
  56. Consortium HDi (2012) Induced pluripotent stem cells from patients with Huntington's disease show CAG-repeat-expansion-associated phenotypes. *Cell Stem Cell* 11:264–278. <https://doi.org/10.1016/j.stem.2012.04.027>
  57. Jeon I, Lee N, Li JY et al (2012) Neuronal properties, in vivo effects, and pathology of a Huntington's disease patient-derived induced pluripotent stem cells. *Stem Cells* 30:2054–2062. <https://doi.org/10.1002/stem.1135>
  58. Logan S, Arzua T, Canfield SG et al (2019) Studying human neurological disorders using induced pluripotent stem cells: from 2D monolayer to 3D organoid and blood brain barrier models. *Compr Physiol* 9:565–611. <https://doi.org/10.1002/cphy.c180025>
  59. Chopra R, Shakkottai VG (2014) The role for alterations in neuronal activity in the pathogenesis of polyglutamine repeat disorders. *Neurotherapeutics* 11:751–763. <https://doi.org/10.1007/s13311-014-0289-7>
  60. Liu-Yesucevitz L, Bilgutay A, Zhang YJ et al (2010) Tar DNA binding protein-43 (TDP-43) associates with stress granules: analysis of cultured cells and pathological brain tissue. *PLoS ONE* 5:e13250. <https://doi.org/10.1371/journal.pone.0013250>
  61. Lo Bello M, Di Fini F, Notaro A et al (2017) ALS-related mutant FUS protein is mislocalized to cytoplasm and is recruited into stress granules of fibroblasts from asymptomatic FUS P525L mutation carriers. *Neurodegener Dis* 17:292–303. <https://doi.org/10.1159/000480085>
  62. Dafinca R, Scaber J, Ababneh N et al (2016) C9orf72 hexanucleotide expansions are associated with altered endoplasmic reticulum calcium homeostasis and stress granule formation in induced pluripotent stem cell-derived neurons from patients with amyotrophic lateral sclerosis and frontotemporal dementia. *Stem Cells* 34:2063–2078. <https://doi.org/10.1002/stem.2388>
  63. Maharana S, Wang J, Papadopoulos DK et al (2018) RNA buffers the phase separation behavior of prion-like RNA binding proteins. *Science* 360:918–921. <https://doi.org/10.1126/science.aar7366>
  64. Kovachev PS, Gomes MPB, Cordeiro Y et al (2019) RNA modulates aggregation of the recombinant mammalian prion protein by direct interaction. *Sci Rep* 9:12406. <https://doi.org/10.1038/s41598-019-48883-x>
  65. Yang ZS, Qing H, Gui H et al (2019) Role of caprin-1 in carcinogenesis. *Oncol Lett* 18:15–21. <https://doi.org/10.3892/ol.2019.10295>
  66. Chou PY, Fasman GD (1978) Prediction of the secondary structure of proteins from their amino acid sequence. *Adv Enzymol Relat Areas Mol Biol* 47:45–148. <https://doi.org/10.1002/9780470122921.ch2>
  67. Hornbeck PV, Zhang B, Murray B et al (2015) PhosphoSitePlus, 2014: mutations, PTMs and recalibrations. *Nucleic Acids Res* 43:D512–D520. <https://doi.org/10.1093/nar/gku1267>
  68. Hagerman RJ, Berry-Kravis E, Hazlett HC et al (2017) Fragile X syndrome. *Nat Rev Dis Primers* 3:17065. <https://doi.org/10.1038/nrdp.2017.65>
  69. Hagerman R, Hagerman P (2021) Fragile X-associated tremor/ataxia syndrome: pathophysiology and management. *Curr Opin Neurol* 34:541–546. <https://doi.org/10.1097/WCO.0000000000000954>
  70. Markmiller S, Soltanieh S, Server KL et al (2018) Context-dependent and disease-specific diversity in protein interactions within stress granules. *Cell* 172(590–604):e13. <https://doi.org/10.1016/j.cell.2017.12.032>
  71. Youn JY, Dunham WH, Hong SJ et al (2018) High-density proximity mapping reveals the subcellular organization of mRNA-associated granules and bodies. *Mol Cell* 69(517–532):e11. <https://doi.org/10.1016/j.molcel.2017.12.020>
  72. Youn JY, Dyakov BJA, Zhang J et al (2019) Properties of stress granule and P-body proteomes. *Mol Cell* 76:286–294. <https://doi.org/10.1016/j.molcel.2019.09.014>

73. Silva TP, Bekman EP, Fernandes TG et al (2020) Maturation of human pluripotent stem cell-derived cerebellar neurons in the absence of co-culture. *Front Bioeng Biotechnol* 8:70. <https://doi.org/10.3389/fbioe.2020.00070>
74. Tang Y, Liu ML, Zang T et al (2017) Direct reprogramming rather than iPSC-based reprogramming maintains aging hallmarks in human motor neurons. *Front Mol Neurosci* 10:359. <https://doi.org/10.3389/fnmol.2017.00359>
75. Arnold ES, Ling SC, Huelga SC et al (2013) ALS-linked TDP-43 mutations produce aberrant RNA splicing and adult-onset motor neuron disease without aggregation or loss of nuclear TDP-43. *Proc Natl Acad Sci U S A* 110:E736–E745. <https://doi.org/10.1073/pnas.1222809110>
76. Zacco E, Grana-Montes R, Martin SR et al (2019) RNA as a key factor in driving or preventing self-assembly of the TAR DNA-binding protein 43. *J Mol Biol* 431:1671–1688. <https://doi.org/10.1016/j.jmb.2019.01.028>
77. Mann JR, Gleixner AM, Mauna JC et al (2019) RNA binding antagonizes neurotoxic phase transitions of TDP-43. *Neuron* 102(321–338):e8. <https://doi.org/10.1016/j.neuron.2019.01.048>
78. Zhang Y, Yang M, Duncan S et al (2019) G-quadruplex structures trigger RNA phase separation. *Nucleic Acids Res* 47:11746–11754. <https://doi.org/10.1093/nar/gkz978>

**Publisher's Note** Springer Nature remains neutral with regard to jurisdictional claims in published maps and institutional affiliations.

# Supplementary Information

## Supplementary Notes

### Note S1. WES and data analysis

For Family A, DNA was prepared using the Nextera Exome Enrichment method from Illumina. In short, 50 ng of genomic DNA was “tagmented” using the Nextera transposome complex, generating adaptor-ligated DNA fragments ready for enrichment. All samples were barcode/index-labelled via index primers during the enrichment PCR. Samples were quantified using Picogreen measurements and the quality of each sample was assessed using the Agilent BioAnalyzer. Up to 12 samples were pooled together in equal quantities before capture. A bait library of >340,000, 95-mer biotinylated probes was used to enrich a 62 Mb region of the genome containing 201,121 coding exons (20,794 genes), UTRs, and non coding RNA regions. The biotinylated probes were used to hybridize to the target sequences, followed by capture using streptavidin beads. The captured DNA was further amplified by PCR and the quality of the pooled, enriched sequencing libraries was determined on the BioAnalyzer. Further, quality control was done by sequencing each 12-sample pool on the Illumina MiSeq instrument, assessing optimal cluster densities, distribution of reads from each sample within the pool, and other quality metrics such as insert size. WES samples were sequenced on Illumina HiSeq 2500 instruments (four lanes per pool), using TruSeq v4 cluster and SBS kits, respectively. Variants were analyzed using the Clinical Sequence Miner application (DeCODE Genetics, Iceland). Low-quality variants, variants with call ratios of less than 20%, and variants with global allele frequencies higher than 0.01 were excluded from analysis. Variants were prioritized based on pathogenicity predictions by multiple scores (CADD, SIFT, PolyPhen-2). The analysis for homozygous or compound heterozygous variants did not produce any likely candidate.

For Family B, DNA was extracted from circulating leukocytes and enriched by means of IDT Exome Research v1.0 kit for parallel sequencing. Raw data were processed and analyzed using an in-house pipeline based on the GATK Best Practices [1]. The UCSC GRCh37/hg19 version of genome assembly was used as reference for reads alignment by means of BWA-MEM aligner [2]. Germline variant calling was performed giving BAM files as input to HaplotypeCaller algorithm [1]. SnpEff v.4.3 and dbNSFP v.3.5 tools was used for known disease variants annotation (ClinVar) [3, 4], variant functional annotation, as well as for *in silico* prediction of impact by means of Combined Annotation Dependent Depletion (CADD) v.1.4 [5], Mendelian Clinically Applicable Pathogenicity (M-CAP) v.1.3 and Intervar v.2.0.1 [6, 7]. Population frequencies were annotated from both gnomAD database and in-house database including ~2500 exomes. Filters were applied in order to extract high-quality variants (GATK hard-filtering, QUAL>100), low-frequency (gnomAD MAF<0.1%, in-house exomes database<1%) non-synonymous SNV and INDELS within coding exons and splice regions. Functional impact evaluation of variants was made assigning a higher priority to variants with CADD score>20, M-CAP score>0.025, tagged as pathogenic/likely-pathogenic by InterVar, as well as relying on Phenolyzer score [8], a tool for gene/phenotype associations. The exome enrichment evaluation showed 150x average coverage and 20x depth at least for 95% of

the target regions. Among 78,877 high-quality variants, 14,329 affected either CDS or splice sites, whereas 444 had low or unknown frequencies according to the aforesaid frequency thresholds.

**Note S2. Probability calculation for occurrence of identical *de novo* variants in individuals with similar phenotype**

These calculations were based on Marbach et al, 2019.

In humans, the germline SNV *de novo* mutation (DNM) rate averages  $1.29 \times 10^{-8}$  (95%CI:  $1.02 \times 10^{-8}$  -  $1.56 \times 10^{-8}$ ) per base pair per generation [9]. Therefore, for an average 45 Mb exome, the highest expected SNV DNM number is 0.72.

The  $p$  likelihood for a second individual to carry the variant in the same nucleotide is  $1.12 \times 10^{-8}$  or about 1 in 89 million, based on the formula (1).

$$p = 1 - (1 - r)^n \quad (1)$$

where  $r$  is the *de novo* mutation rate and  $n$  the number of expected DNMs per individual.

Since the non-CpG C>T transition likelihood is 58% [10], the probability of the occurrence of the C>T transition at the same position is  $0.65 \times 10^{-8}$ , or about 1 in 154 million).

This calculation assumes no multiple testing. Even though the two variants were independently discovered, in the hypothesis of a cohort of 100 phenotypically similar ataxic individuals in a database (e.g. GeneMatcher), all of them recruited through trio-WES, the adjusted probability of finding an additional occurrence of the identical *de novo* would be  $0.65 \times 10^{-6}$  (1 in 1,5 million).

## Supplementary Figures and Legends

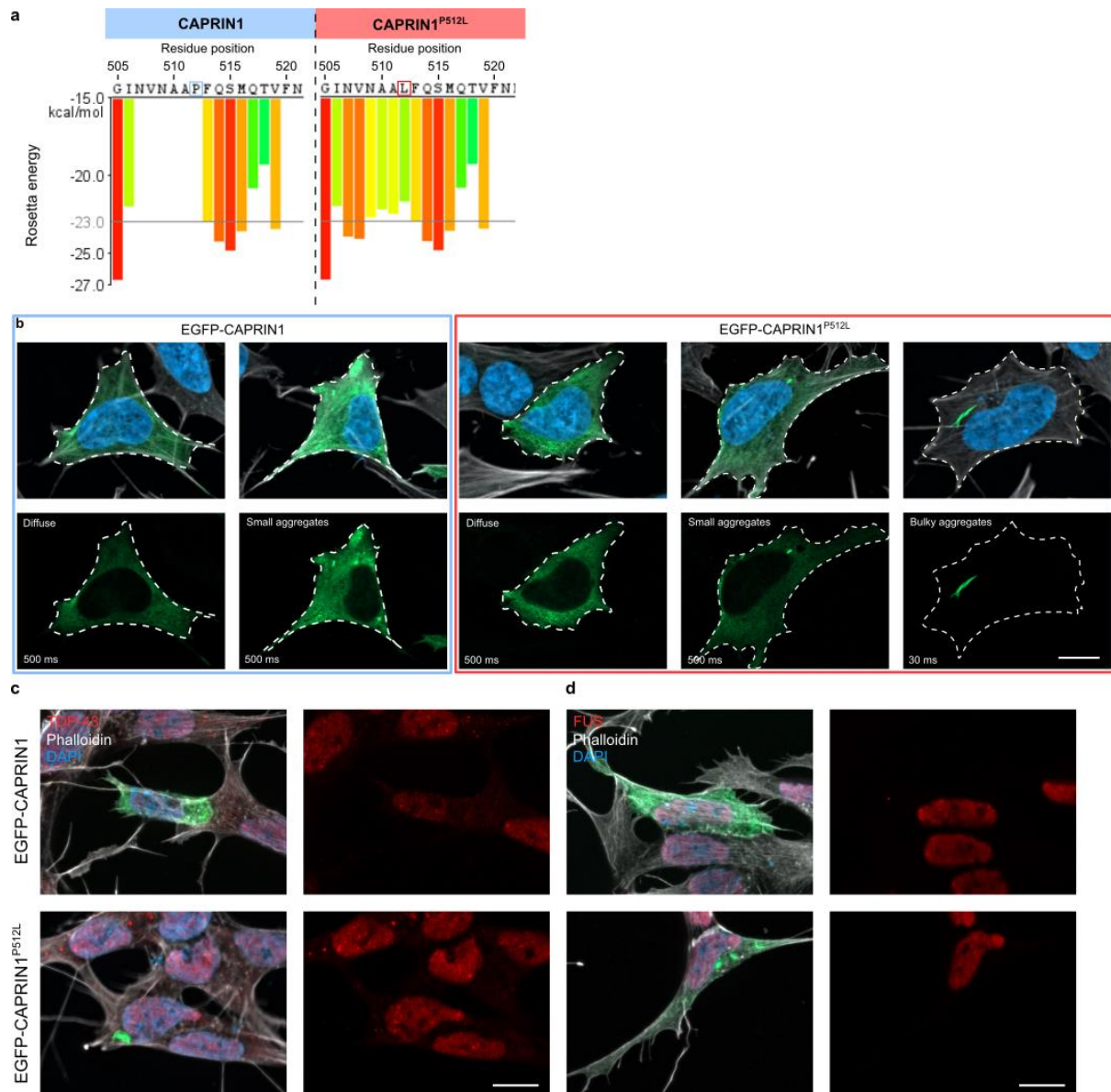


**Figure S1. CAPRIN1<sup>P512L</sup> aggregates characteristics**

- ZipperDB predicts an increase in the amyloid fibril-forming potential of CAPRIN1<sup>P512L</sup>.
- Representative images of CAPRIN1 and CAPRIN1<sup>P512L</sup> in SH-SY5Y cells (cell contour marked by the dashed white line) (Scale bar: 10  $\mu$ m).
- CAPRIN1<sup>P512L</sup> aggregates are TDP-43<sup>-</sup> and FUS<sup>-</sup> (Scale bar: 10  $\mu$ m).

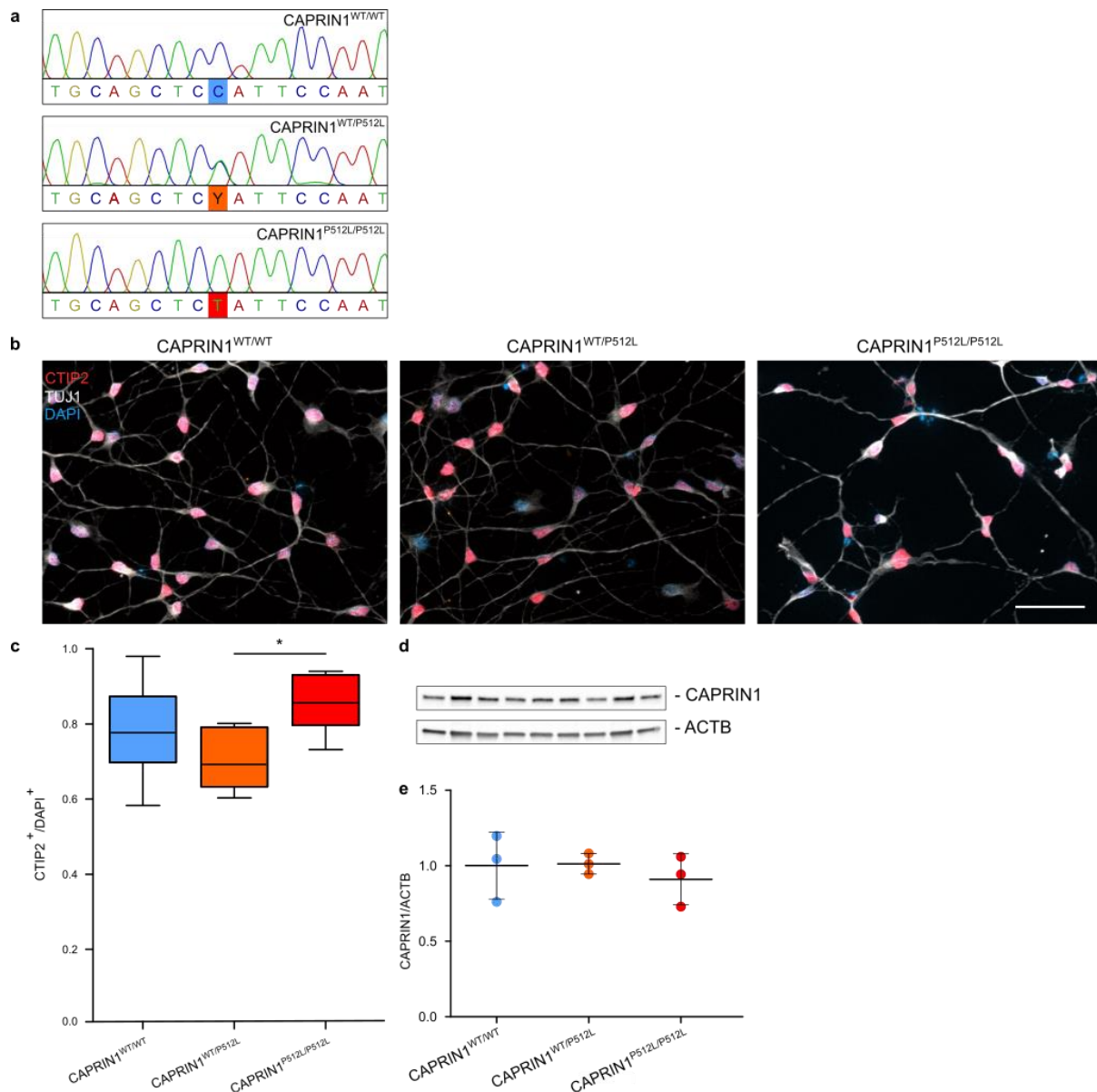


**Figure S2. Characterization of iPSC lines and iPSC-derived neurons**

- Pherograms from Sanger sequencing of the CAPRIN1<sup>WT/WT</sup>, CAPRIN1<sup>WT/P512L</sup> and CAPRIN1<sup>P512L/P512L</sup> iPSC lines confirm the correct editing of the c.1535C>T variant in CAPRIN1 (NM\_005898.5).
- CTIP2 staining confirms the differentiation of the iPSCs in cortical layer V and VI neurons according to Schuster et al, 2020 [11] (Scale bar: 50  $\mu$ m).
- Quantification of CTIP2<sup>+</sup> neurons (\*: p<0.05).
- Immunoblotting showing that CAPRIN1 levels are not changed in CAPRIN1<sup>P512L</sup>-harboring cell lines.
- Quantification of the immunoblot data in Figure S2D.

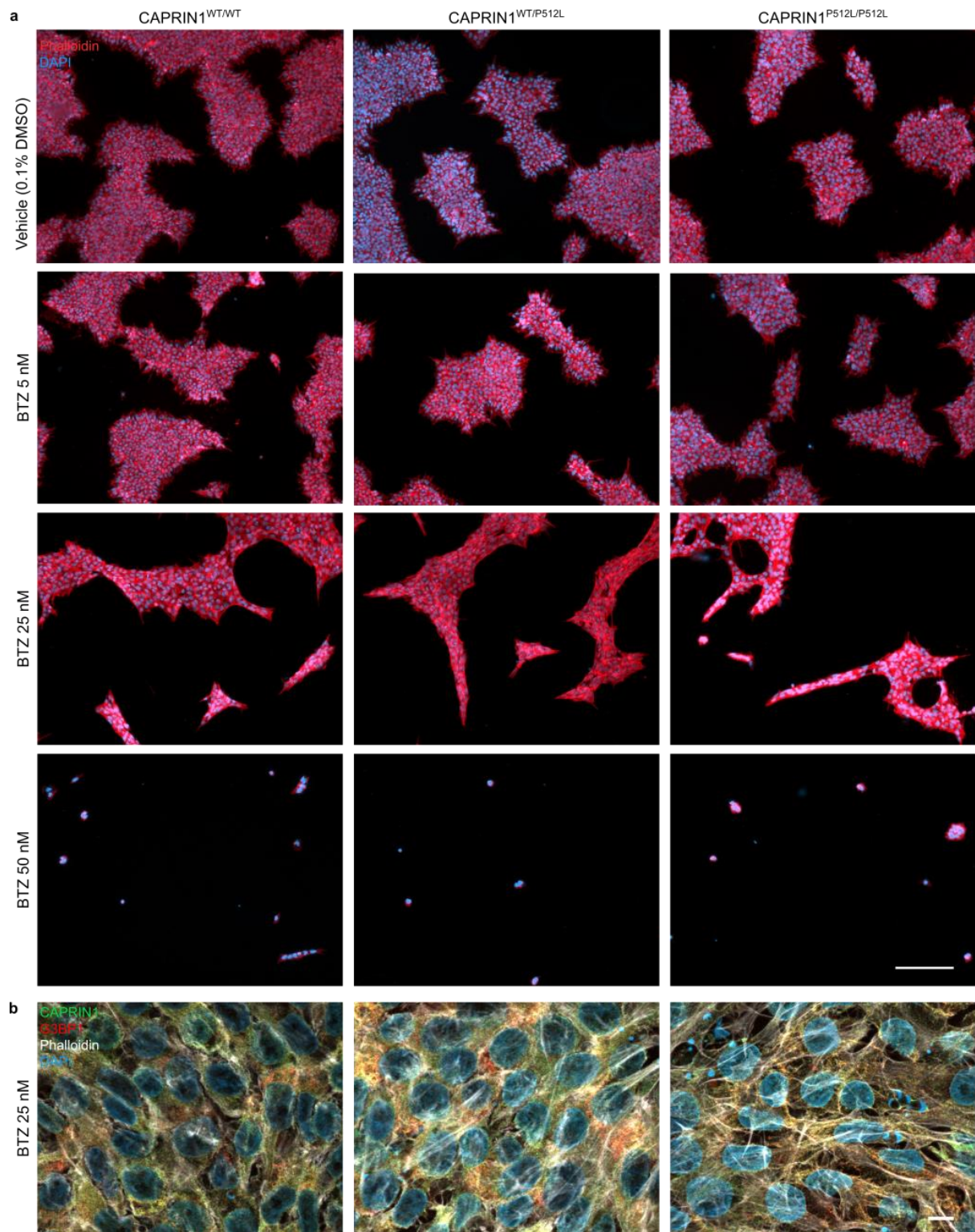


**Figure S3. Proteasomal inhibition does not lead to aggregates formation in iPSCs**

- a) iPSCs treated with the proteasomal inhibitor Bortezomib (BTZ) for 24 h show colony shrinkage at 25 nM and almost complete cell death at 50 nM (Scale bar: 200  $\mu$ m).
- b) iPSC treated with 25 nM for 24 h do not show aggregation (Scale bar: 10  $\mu$ m).

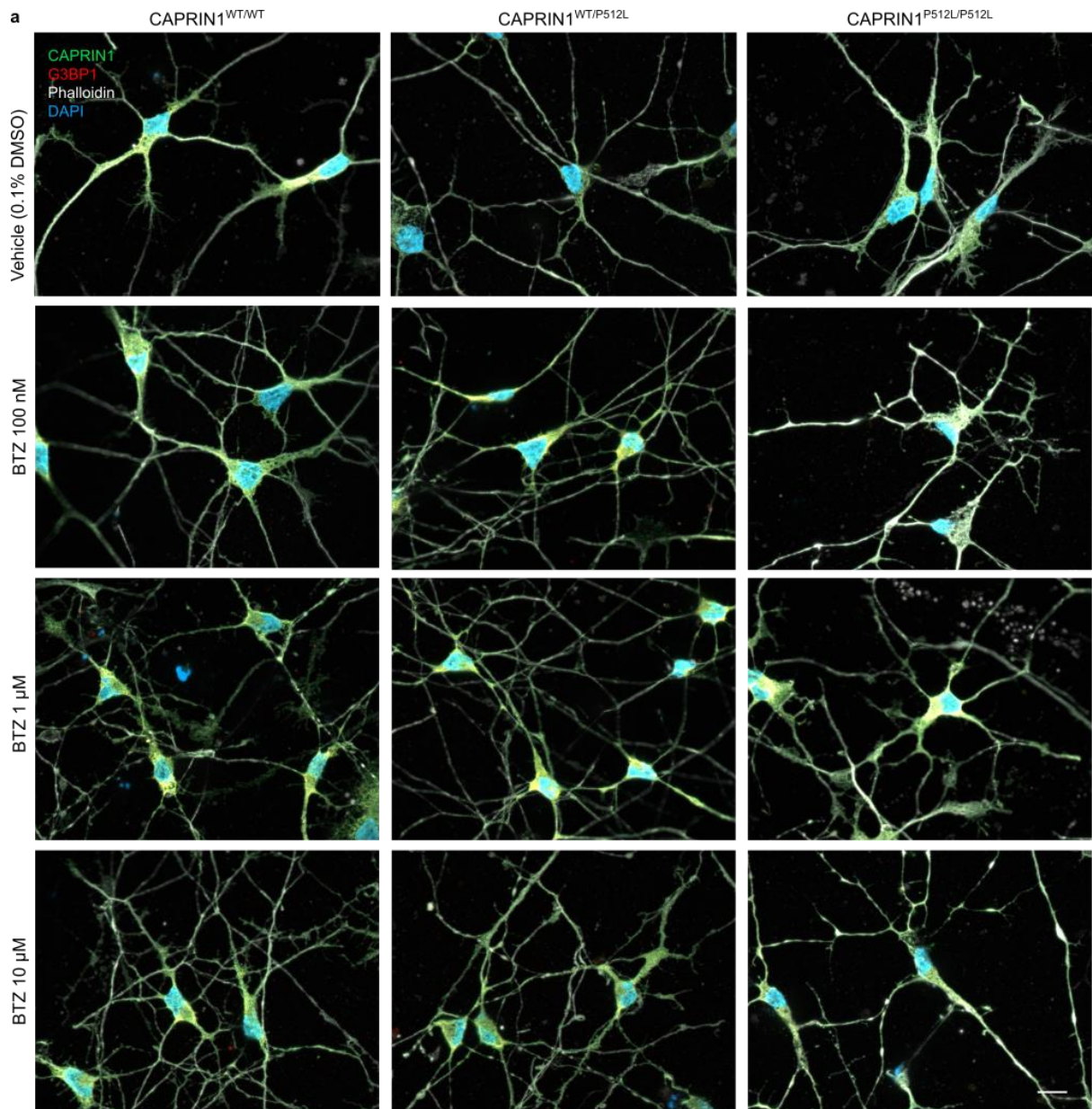


**Figure S4. Proteasomal inhibition does not lead to aggregates formation in iPSC-derived neurons**

- a) iPSC-derived neurons treated with up to 10  $\mu\text{M}$  of the proteasomal inhibitor Bortezomib (BTZ) for 24 h do not show aggregation (Scale bar: 10  $\mu\text{m}$ ).

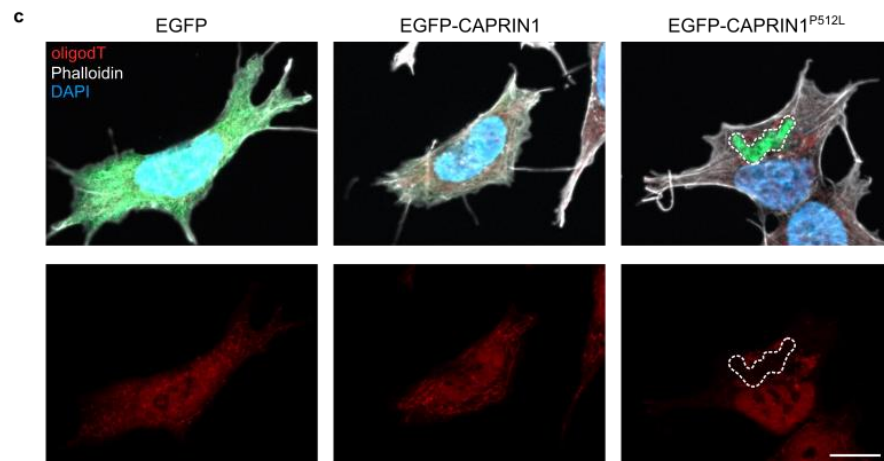
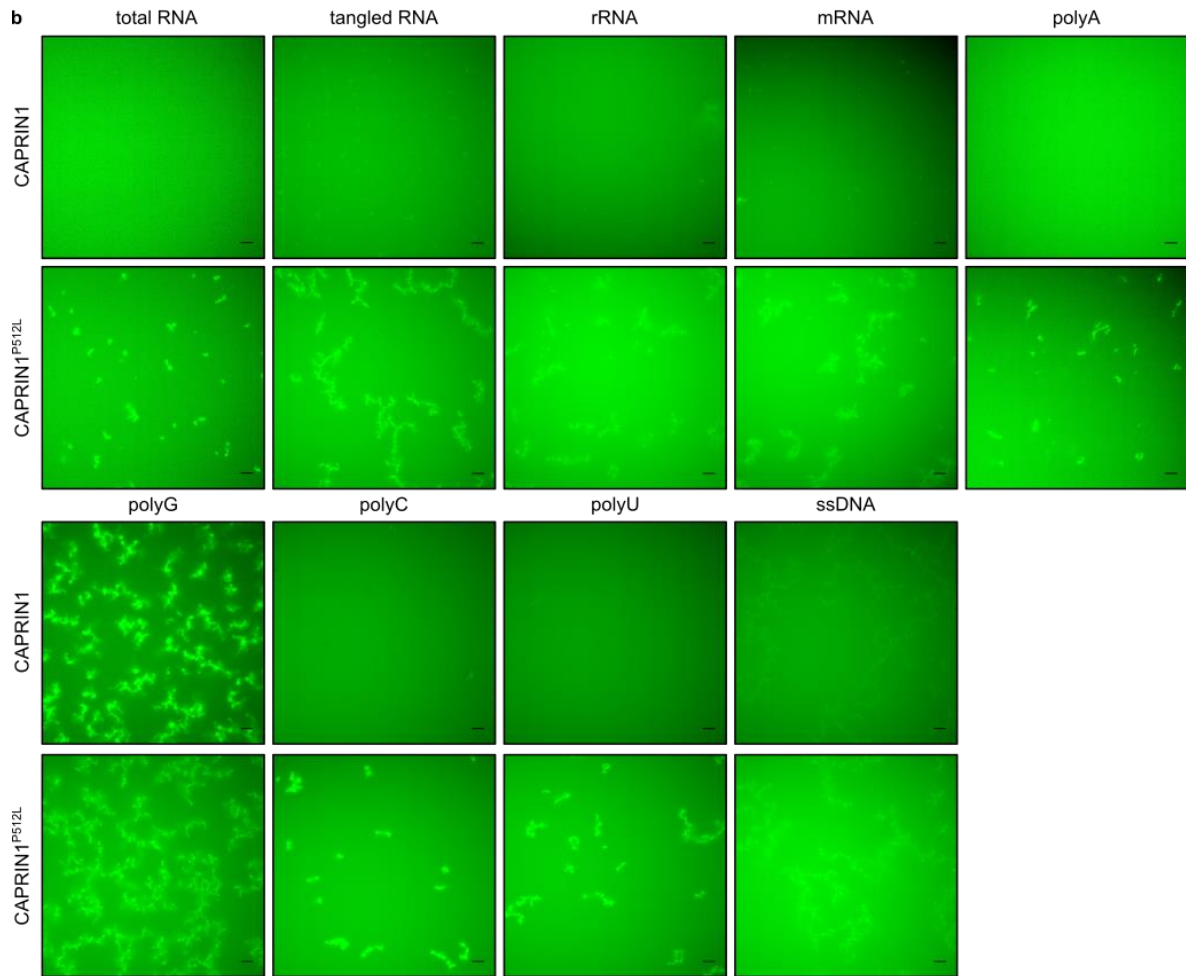
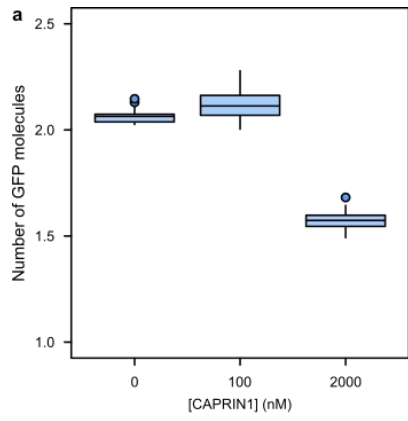


**Figure S5. CAPRIN1<sup>P512L</sup> dimerizes and its aggregation is triggered by RNA.**

- a) Upon mixing mGFP-CAPRIN1 with an excess of unlabeled CAPRIN1, the reduction in GFP brightness shows that CAPRIN1 forms dimers.
- b) CAPRIN1<sup>P512L</sup> aggregates independently of the RNA type. Several RNA types were added to mGFP-CAPRIN1 and mGFP-CAPRIN1<sup>P512L</sup>. While only polyG RNA was able to form overt mGFP-CAPRIN1 aggregates, mGFP-CAPRIN1<sup>P512L</sup> formed aggregates with all RNA types (Scale bar: 10  $\mu$ m).
- c) CAPRIN1<sup>P512L</sup> aggregates do not contain RNA in SH-SY5Y cells. polyA FISH showing the lack of polyadenylated RNAs in CAPRIN1<sup>P512L</sup> aggregates (aggregate contour marked by the dashed white line) (Scale bar: 10  $\mu$ m).

## Supplementary Methods

### Bortezomib treatment

iPSC and iPSC-derived neurons (D35) were treated with several concentrations of the proteasomal inhibitor Bortezomib (BTZ) (Selleckchem S1013) or its vehicle (0.1% DMSO) for 24 h.

### PolyA FISH

Transfected SH-SY5Y cells were fixed with 4% PFA for 10 minutes, washed with PBS and permeabilized with 0.2% Triton X-100 diluted in PBS for 10 min. Afterwards, cells were washed with 2× SSC and hybridized by incubation for 2 h at 37°C in 4× SSC containing 10% formamide, 5% dextran sulfate, 1% BSA, 0.5 mM EDTA, and 100 nM biotinylated oligo-dT probe (23-mer, IDT). They were then washed three times in 2× SSC and blocked in 3% BSA diluted in 4× SSC for 1 h at room temperature. Then, they were incubated with an anti-biotin antibody (Sigma-Aldrich, B3640) diluted in 1% BSA (in 4× SSC) for 1 h. Cells were then washed in 4× SSC and incubated with secondary antibodies conjugated with secondary antibodies/probes (see Table S2) diluted in 1% BSA (in 4× SSC) for 1 h. Finally, they were washed in 4× SSC, then 2× SSC, and mounted with ProLong Gold antifade reagent with DAPI (Invitrogen) on Polylysine slides (ThermoFisher Scientific). They were then imaged as described in the 'Immunofluorescence' section of 'Material and methods'.

## Supplementary Tables

**Table S1. Nucleotide sequences of oligos and ssODNs**

Name	Sequence (5' → 3')
CAPRIN1_cl_F	ACGATGCCCTCGGCCACCAG
CAPRIN1_cl_R	ATTCACTTGCTGAGTGTTTCATTTGCGGC
CAPRIN1_P512L_SDM_F	AATCAATGTAAATGCAGCTCTATTCCAATCCATGCAAACGG
CAPRIN1_P512L_SDM_R	CCGTTTGCATGGATTGGAATAGAGCTGCATTTACATTGATT
CAPRIN1-P512L_MG_s	GTTAATGCAGCTCTATTTCAGAGCATGC
CAPRIN1-P512L_MG_as	ATTAATGCCGGAGCTGTGGAGTGGC
CAPRIN1-P512L_gRNA_F	CACCGACCGTTTGCATGGATTGGAA
CAPRIN1-P512L_gRNA_R	AAACTTCCAATCCATGCAAACGGTC
CAPRIN1-SA_F1	TCCCTTCTGCTGCGTCTCA
CAPRIN1-SA_R1	ACAGGCACATCACTCATAAGGCTAA
CAPRIN1-E14_F1	TCATCCACAAGTGAGGGGTACACA
CAPRIN1-E14_R1	AGGTGCTTGCTCAAGAATCAAGGTA
CAPRIN1-ssODN1	CCGCTAAAGTGCATCTATTCACTTTGTGTTTAGGCAACAATCTCTTTAAATAC AGACCAGACTACAGCATCATCCCTTCCTGCTGCGTCTCAGCCTCAAGTA TTTCAGGCTGGGACAAGCAAACCTTTACATAGCAGTGGAATCAATGTAAAT GCAGCTCTATTCCAATCCATGCAAACGGTAAGCAAATTAACCTAACATTAATT GCCTAGTATGTAATATGAATCATGGTAGATTTTCTTTCTTTGTTAAAGGTCT TCATTTAACTGTGCTTGAGTCTGCATCTTTCATTAAGTGTAGGGTATATTTAA TTGAACATAAACTGATTATTCAGAGATTAAGTATAACTGATACTAACGGATATTCTA GAGATAAATTTAGCCTTATGAGTGTATGTCCTG
CAPRIN1-ssODN2	TCCTGCTGCGTCTCAGCCTCAAGTATTTTCAGGCTGGGACAAGCAAACCTTTA CATAGCAGTGAATCAATGTAAATGCAGCTCTATTCCAATCCATGCAAACGG TAAGCAAATTAACCTAACATTAATTGCCTAGTATGTAATATGAATCA
CAPRIN1-P512L-ASP_F	GTTTACCGCTAAAGTGCATC
CAPRIN1-P512L-ASP_MUT_R	CGTTTGCATGGATTGGAAGA
CAPRIN1-P512L-ASP_WT_R	CGTTTGCATGGATTGGAAGG

**Table S2. Antibodies**

<b>Target Antigen</b>	<b>Species</b>	<b>Manufacturer</b>	<b>Reference</b>
ACTB	mouse	Proteintech	HRP-60008 RRID:AB_2819183
ATXN2	mouse	Santa Cruz Biotechnology	sc-515602 SAMPLE
CAPRIN1	rabbit	Proteintech	15112-1-AP RRID:AB_2070016
CTIP2	rabbit	Abcam	ab240636
FUS	mouse	Santa Cruz Biotechnology	sc-47711 RRID:AB_2105208
GEMIN5	rabbit	Proteintech	24897-1-AP RRID:AB_2879784
G3BP1	mouse	Santa Cruz Biotechnology	sc-365338 RRID:AB_10846950
p62	mouse	Abcam	ab56416 RRID:AB_945626
SNCA	mouse	Santa Cruz Biotechnology	sc-12767 SAMPLE RRID:AB_628318
SNRNP200	mouse	Santa Cruz Biotechnology	sc-393170
TDP-43	rabbit	Proteintech	10782-2-AP RRID:AB_615042
TUJ1	chicken	Novus Biologicals	NB100-1612 RRID:AB_10000548
Ubiquitin	mouse	Santa Cruz Biotechnology	sc-8017 RRID:AB_628423
V5	rabbit	Abcam	ab9116 RRID:AB_307024
Biotin	goat	Sigma-Aldrich	B3640 RRID:AB_258552
<b>Probe</b>	<b>Species</b>	<b>Manufacturer</b>	<b>Reference</b>
Alexa Fluor 488 donkey anti-rabbit IgG (H+L)	donkey	Invitrogen	A21206 RRID:AB_2535792
Alexa Fluor 568 donkey anti-rabbit IgG (H+L)	donkey	Invitrogen	A10042 RRID:AB_2534017
Alexa Fluor 568 F(ab') <sub>2</sub> fragment of goat anti-mouse IgG (H+L)	goat	Invitrogen	A11019 RRID:AB_143162
Alexa Fluor 568 donkey anti-goat IgG (H+L)	donkey	Invitrogen	A11057 RRID:AB_142581
Alexa Fluor 647 goat anti-chicken IgG (H+L)	goat	Invitrogen	A21449 RRID:AB_2535866
Alexa Fluor™ 647 Phalloidin		Invitrogen	A22287
Anti-rabbit IgG, HRP-linked	goat	Cell Signaling Technology	7074S RRID:AB_2099233

## References

- [1] Van der Auwera GA, Carneiro MO, Hartl C et al (2013) From FastQ data to high confidence variant calls: the Genome Analysis Toolkit best practices pipeline. *Curr Protoc Bioinformatics* 43:11 10 1-11 10 33. <https://doi.org/10.1002/0471250953.bi1110s43>
- [2] Li H *Aligning sequence reads, clone sequences and assembly contigs with BWA-MEM*. 2013. arXiv:1303.3997.
- [3] Cingolani P, Platts A, Wang le L et al (2012) A program for annotating and predicting the effects of single nucleotide polymorphisms, SnpEff: SNPs in the genome of *Drosophila melanogaster* strain w1118; iso-2; iso-3. *Fly (Austin)* 6:80-92. <https://doi.org/10.4161/fly.19695>
- [4] Liu X, Jian X, Boerwinkle E (2013) dbNSFP v2.0: a database of human non-synonymous SNVs and their functional predictions and annotations. *Hum Mutat* 34:E2393-402. <https://doi.org/10.1002/humu.22376>
- [5] Kircher M, Witten DM, Jain P et al (2014) A general framework for estimating the relative pathogenicity of human genetic variants. *Nat Genet* 46:310-5. <https://doi.org/10.1038/ng.2892>
- [6] Jagadeesh KA, Wenger AM, Berger MJ et al (2016) M-CAP eliminates a majority of variants of uncertain significance in clinical exomes at high sensitivity. *Nat Genet* 48:1581-1586. <https://doi.org/10.1038/ng.3703>
- [7] Li Q, Wang K (2017) InterVar: Clinical Interpretation of Genetic Variants by the 2015 ACMG-AMP Guidelines. *Am J Hum Genet* 100:267-280. <https://doi.org/10.1016/j.ajhg.2017.01.004>
- [8] Yang H, Robinson PN, Wang K (2015) Phenolyzer: phenotype-based prioritization of candidate genes for human diseases. *Nat Methods* 12:841-3. <https://doi.org/10.1038/nmeth.3484>
- [9] Tian X, Browning BL, Browning SR (2019) Estimating the Genome-wide Mutation Rate with Three-Way Identity by Descent. *Am J Hum Genet* 105:883-893. <https://doi.org/10.1016/j.ajhg.2019.09.012>
- [10] Marbach F, Rustad CF, Riess A et al (2019) The Discovery of a LEMD2-Associated Nuclear Envelopathy with Early Progeroid Appearance Suggests Advanced Applications for AI-Driven Facial Phenotyping. *Am J Hum Genet* 104:749-757. <https://doi.org/10.1016/j.ajhg.2019.02.021>
- [11] Schuster S, Heuten E, Velic A et al (2020) CHIP mutations affect the heat shock response differently in human fibroblasts and iPSC-derived neurons. *Dis Model Mech* 13. <https://doi.org/10.1242/dmm.045096>



## 8 Acknowledgements

First and foremost, I want to thank my supervisor, Prof. Dr. Brunhilde Wirth, for giving me the opportunity to work in her research group on such a fascinating project. I'm grateful for her support, her continuous availability and her input during all these years. I thank her for having encouraged my scientific and personal growth, allowing me to attend numerous courses and conferences. Her passion and dedication for science are admirable.

I'd also like to extend my thanks to my tutors, Prof. Dr. Andreas Beyer and Prof. Dr. Kay Hofmann, for their scientific advice. I cannot forget to thank Dr. Min Jeong Kye for the scientific – and non – discussions.

Thanks to all the members of the research groups Wirth, Kye, Zempel and Piano for the time we spent together. Thanks in particular to Markus Storbeck, who chaperoned me during my first steps in science. A special thank goes to Anixa, who rapidly became a friend, and not only a colleague. Thanks for bringing your bubbly personality to the lab and outside of it and for sharing with me the good and less good moments of these years. Thanks to all the friends who work with me: Tamás, Eleonora, Jorge and Çağla: how much I will miss our coffees at Oliveri and the meals together! Thank you Lisa P. for all the fun we had in the lab investigating *CAPRIN1*. Thanks to all the other current or former AG Wirth members that I got to know during these years: Markus R., Ludwig, Laura, Mohsen, Miriam, Anna, Lilian, Natalia, Svenja, Aaradhita, Janine, Eva, Bryony, Eike, Nur, Ilka, Lisa W., Sofia, Marlen and Mert.

Thanks to our current and former TAs: Irmgard, who introduced me to cell culture and has always the best suggestions for places to see and things to do around, then Sebastian, Roman, Jenny, Vanessa, Kristina, Andrea and Theresa. Thanks to the other current and former AG Kye members: Inês, Wiebke, Max, Johanna. Thanks to the other AG Zempel members: Hans, Sarah, Michael, Aghyad, and Felix. Thanks to AG Piano members: Valentina and Çağlar. Thanks also to all the colleagues of AG Beck, AG Netzer, AG Hänsel-Hertsch, and the diagnostics team.

Thanks to Uwe, who always helps with the small and the big administrative issues and to Radu, who I call for all the IT problems.

A big thank goes to my parents, Luciano and Lucina, my sisters Martina e Chiara and their respective partners Patrik and Flavio: you always supported me in my choice of embarking on this unusual venture, and welcomed me back at home at every occasion.

Thanks to all the friends that I got to know here in Cologne and are still here or already moved on to the next adventure in another part of the world. Thanks Tanio, for having been my first friend in Germany, and having watched over me during the out-of-the-lab adventures in Cologne. Thanks Simone, for being my reference point here. Thanks Francesco for all our gym and party hours together. Thanks Andrea and Stefan for the exquisite hospitality that you always offer me.

Thank you to all my friends in Italy: Daniela, Andrea, Alessio, Geetha, Giangi, Cristina,... and also to the "GROP" members: Cecilia, Davide, Elisa, Jenny and Maura... Thank you for our traditional get-togethers when I'm back visiting. Thank you Elisa, for always being there for me after all these years, after all the distances and the up and downs of our lives. Thanks for your continuous support, all the past and future memories and continuing growing "wiser" together.

## 9 Curriculum Vitae

### 9.1 Personal Information

Surname: Delle Vedove  
Name: Andrea  
Date of Birth: 10.12.1988  
Place of Birth: Cividale del Friuli, Italy  
Nationality: Italian

### 9.2 Education

2015 - 2022 **Interdisciplinary Program Molecular Medicine**  
Institute of Human Genetics, University of Cologne – Cologne (Germany)  
2013 - 2014 **Qualification Certificate in Medicine and Surgery**  
University of Udine – Udine (Italy)  
2007 - 2013 **Single-cycle Master's Degree Program in Medicine and Surgery**  
University of Udine – Udine (Italy)  
2002 - 2007 **Secondary School**  
Scientific High School "G. Marinelli" – Udine (Italy)

### 9.3 Work Experience

2015 - 2022 **Scientific Researcher**  
Institute of Human Genetics, University of Cologne – Cologne (Germany)  
2014 **Medical Locum**  
Health Authority n° 4 „Medio Friuli“ – Udine (Italy)  
2014 **Attending Physician**  
Institute of Medical Genetics, University Hospital „S. Maria della Misericordia“ – Udine (Italy)



## 10 Eidesstattliche Erklärung

Ich versichere, dass ich die von mir vorgelegte Dissertation selbstständig angefertigt, die benutzten Quellen und Hilfsmittel vollständig angegeben und die Stellen der Arbeit – einschließlich Tabellen, Karten und Abbildungen –, die anderen Werken im Wortlaut oder dem Sinn nach entnommen sind, in jedem Einzelfall als Entlehnung kenntlich gemacht habe; dass diese Dissertation noch keiner anderen Fakultät oder Universität zur Prüfung vorgelegen hat; dass sie – abgesehen von unten angegebenen Teilpublikationen – noch nicht veröffentlicht worden ist sowie, dass ich eine solche Veröffentlichung vor Abschluss des Promotionsverfahrens nicht vornehmen werde. Die Bestimmungen dieser Promotionsordnung sind mir bekannt. Die von mir vorgelegte Dissertation ist von Prof. Dr. Brunhilde Wirth betreut worden.

Eine Übersicht der Publikationen folgt:

**Delle Vedove A\***, Storbeck M\*, Heller R, et al. Biallelic Loss of Proprioception-Related *PIEZO2* Causes Muscular Atrophy with Perinatal Respiratory Distress, Arthrogryposis, and Scoliosis. Am J Hum Genet. 2016 Nov 3;99(5):1206-1216. doi: 10.1016/j.ajhg.2016.09.019. Erratum in: Am J Hum Genet. 2016 Dec 1;99(6):1406-1408.

Salpietro V\*, Lin W\*, **Delle Vedove A\***, et al. Homozygous mutations in *VAMP1* cause a presynaptic congenital myasthenic syndrome. Ann Neurol. 2017 Apr;81(4):597-603. doi: 10.1002/ana.24905.

Eisenberger T, Di Donato N, ... **Delle Vedove A**, et al. A C-terminal nonsense mutation links PTPRQ with autosomal-dominant hearing loss, DFNA73. Genet Med. 2018 Jun;20(6):614-621. doi: 10.1038/gim.2017.155.

Karakaya M, Storbeck M, ... **Delle Vedove A**, et al. Targeted sequencing with expanded gene profile enables high diagnostic yield in non-5q-spinal muscular atrophies. Hum Mutat. 2018 Sep;39(9):1284-1298. doi: 10.1002/humu.23560.

Janzen E, Wolff L, ... **Delle Vedove A**, et al. *PLS3* Overexpression Delays Ataxia in *Chp1* Mutant Mice. Front Neurosci. 2019 Sep 19;13:993. doi: 10.3389/fnins.2019.00993.

Pavinato L, **Delle Vedove A**, Carli D, et al. *CAPRIN1* haploinsufficiency causes a neurodevelopmental disorder with language impairment, ADHD and ASD. Brain. 2022;awac278. doi: 10.1093/brain/awac278. In press.

**Delle Vedove A**, Natarajan J, Zanni G, et al. *CAPRIN1*<sup>P512L</sup> causes aberrant protein aggregation and associates with early-onset ataxia. Cell Mol Life Sci. 2022 Sep 22;79(10):526. doi: 10.1007/s00018-022-04544-3.

Overhoff M, Tellkamp F, ... **Delle Vedove A**, et al. Autophagy regulates neuronal excitability by controlling cAMP/protein kinase A signaling at the synapse. EMBO J. 2022 Oct 11:e110963. doi: 10.15252/embj.2022110963. Epub ahead of print. PMID: 36217825.

\* The authors contributed equally to this work

Ich versichere, dass ich alle Angaben wahrheitsgemäß nach bestem Wissen und Gewissen gemacht habe und verpflichte mich, jedmögliche, die obigen Angaben betreffenden Veränderungen, dem Promotionsausschuss unverzüglich mitzuteilen.

Köln, 11.01.2023

Andrea Delle Vedove

